GROUNDWATER RECHARGE ESTIMATION IN TABLE MOUNTAIN GROUP AQUIFER SYSTEMS WITH A CASE STUDY OF KAMMANASSIE AREA

by

Yong Wu

Submitted in the fulfillment of the requirements for the degree of

Doctor of Philosophy

in the

Department of Earth Sciences
Faculty of Natural Sciences
University of the Western Cape
Cape Town

Supervisor: Prof. Yongxin Xu
Co-supervisor: Dr. Rian Titus

August 2005

DECLARATION

I declare that ***GROUNDWATER RECHARGE ESTIMATION IN TABLE MOUNTAIN GROUP AQUIFER SYSTEMS WITH A CASE STUDY OF KAMMANASSIE AREA*** is my own work, that it has not been submitted for any degree or examination in any other university, and that all the sources I have used or quoted have been indicated and acknowledge by complete references.

Full name: Yong Wu Date: August 2005

Signed…….

Abstract

Groundwater Recharge Estimation in Table Mountain Group Aquifer Systems with a case study of Kammanassie Area

Y. Wu

PhD Thesis

Department of Earth Sciences

Key words: Hydrogeology, hydrogeochemistry, topography, Table Mountain Group, Kammanassie area, groundwater recharge processes, recharge estimation, mixing model, chloride mass balance, water balance, cumulative rainfall departure

The Table Mountain Group (TMG) sandstone is a regional fractured rock aquifer system with the potential to become the major source of future bulk water supply to meet both agricultural and urban requirements in the Western and Eastern Cape Provinces, South Africa. The TMG aquifer including Peninsula and Nardouw formations comprises approximately 4000m thick sequence of quartz arenite with outcrop area of 37,000 km^2. Groundwater in the TMG aquifer is characterized by its low TDS and excellent quality.

Based on the elements of the TMG hydrodynamic system including boundary conditions of groundwater flow, geology, geomorphology and hydrology, nineteen hydrogeological units were identified, covering the area of 248,000km^2. Limited studies focused on recharge have been carried out in the TMG area in the past 10 years. The results were estimated as high as up to 55% of precipitation. These high estimates of TMG recharge recently postulated by some groundwater specialists raised huge media coverage on the groundwater potential of TMG.

In order to estimate realistic recharge rates of the TMG aquifers and to understand the impacts of climatic changes on recharge and large scale groundwater development, six conceptual recharge models were developed; three major groups of topographic features identified, in which different recharge processes and groundwater regimes occur. The tendency, periodicity and anomalous events of climate were analysed in the Kammanassie area.

After a detailed discussion of influences of time lag, actual recharge area and storativity of the aquifer in question, the recharge rates were estimated in the Kammanassie area from 1994 to 2002 using mixing model of chloride mass balance, cumulative water level departure versus cumulative rainfall departure, regression of cumulative spring flux and water balance methods. In this study, much lower recharge estimates are obtained. The estimated recharge rates are 1.18-2.03%, 0.24-7.56%, 3.29-4.01% and 2.32-4.4 % of the precipitation, respectively. Even in the same area, the results are largely different using different methods. To fill the gaps in the different results, the estimated recharge rates from each method were integrated in order to qualify the recharge rates using the weights of the different methods. The integrated rates indicated 1.63%-4.75% of the precipitation as recharging the aquifer in the Kammanassie Mountain area from 1994 to 2003. For the Peninsula Aquifer in the Vermaaks River, the budget of 3-D numeric simulation model confirmed that the recharge rate could not exceed 1.96% of the rainfall at steady state. The results were further corroborated by the 1.65%-3.30% of the annual precipitation for 95% confidence interval. This has significant implication on the water supply strategy for the Kammanassie area.

Water balance approach to the spatial distribution of recharge in the TMG area is adopted based on evapotranspiration and runoff models. The average recharge rate is 29.74mm·a^{-1} in the TMG area. The highest recharge rate is 137.4mm·a^{-1} related to Mean Annual Precipitation (MAP) of 1842.06 mm·a^{-1}; the lowest recharge rate is 0.72mm·a^{-1} related to MAP of 163.51mm·a^{-1}. The regions of the recharge rate more than 35mm·a^{-1} occur in the hydrogeological unit 5, 6, 8 and part of the hydrogeological unit 17. The other areas are smaller than 35mm·a^{-1}. The recharge rate is a non-linear positively proportional to the MAP. Most high recharge percentages are related to rainfall of 300 to 1100mm·a^{-1}. The recharge percentage would be less if precipitation is greater than 1100mm·a^{-1} or less than 300mm·a^{-1}. Lower recharge estimates for the TMG suggest that the caution must be taken when a water supply strategy is formulated for the TMG area.

ACKNOWLEDGEMENTS

It was 1997 when Dr. Xu visited China I expressed my wish to go overseas for my PhD. Four years later he visited China again and gave me the good news that I had been offered an opportunity to make my dream come true. Early in the year 2002, I became a PhD student of the University of the Western Cape.

This thesis was only made possible with the co-operation of many individuals and institutions. The author therefore wishes to record his sincere thanks to the following:

- Prof. Yongxin Xu for all his assistance and useful advice in the research.
- The Council for Geoscience in Pretoria, in particular Dr. Rian Titus, for his useful suggestions.
- The Department of Water Affairs and Forestry in Bellville, in particular Mr. Mike Smart and Ms Rossida Peter for their kind help with collecting chemical data and sampling programs.
- Overberg Water, in particular Shahied Solomon, Deon Haasbroek and Johan Uys, for all their assistance during the sampling programs, steering committee meetings and for providing data sets and information on request.
- Reginald Domoney, Browen Honigwachs, secretary of Department of Earth Sciences; Dr. Shafick Adams and Braun Lawrence for their assistance during research in South Africa.
- Caroline Barnard for her kind help during the recharge project.
- The postgraduate students: An Eijkelenburg, Segun Adelana, Lixiang Lin, Haili Jia, Humberto Antonio Saeze (PhD students), Vuyolwethu Sigonyela, Riyaz Nakhwa Ignatius, Mokete Seboko, Joubert Bulasigobo and Fortress Netili (MSc students) in Groundwater Group at UWC are thanked for their friendship and support.
- Finally, to my wife, Xianfeng Sun, my son, Zhenghao, my parents and family, a **big** and **special** thank you for all your immense support and patience.

Abbreviations and Notations

Notation in literatures

$\bar{c}_g$ average chloride concentration of the groundwater

$\overline{m}$ chloride mass flux

$?$ total water potential

A recharge area or area of catchment

a thermal diffusivity of the aquifer

A_b total area of drainage

A_b total area of the basin

A_f area of basin floor

b rate of increase in surface temperature

C pore water chloride concentration

$c_0 q_0$ heat capacity of the water

c_g concentration of chloride in the groundwater

Ck_p chloride concentration in precipitation

Cl_{gw} chloride concentration in groundwater

Cl_{gw} chloride concentration in groundwater at the water table

Cl_{ib} average chloride concentration in interstitial flow below the basin floor

Cl_{ir} average chloride concentration in regional interstitial flow between basin floors

Cl_p precipitation weighted chloride concentration

Cl_r chloride concentration of the runoff

Cl_r chloride concentration of the runoff water to the basin floor

Cl_{sm} chloride concentration in soil moisture

Cl_t average chloride concentration in the ground water

Cl_{uz} chloride concentration in the unsaturated zone

cq heat capacity of the aquifer

C_R recession constant controlling the rate of decline of the groundwater level

D dry chloride deposition

D average depth of the aquifer

D hydrodynamic dispersion coefficient

D rate of addition within the aquifer

DS current depth of soil water

E evaporation

$E_t(t)$ evapotranspiration

ET_{gw} evapotranspiration

ET_{unsat} evaporation from the unsaturated zone

F volume of the *i th* flow path within the sample divided by the total volume of the sample

FC field capacity

F_w a vector in a plane

h sampling depth of the water

h total depth of the aquifer

H total thickness of the aquifer

K hydraulic conductivity of the soil matrix

$K(?)$ the unsaturated hydraulic conductivity

LINRES Linear reservoir Module

Maxil maximum intercept loss

n aquifer porosity

P annual precipitation

P precipitation

P(t) precipitation

P_{av} representing an open aquifer system

P_e effective precipitation

P_i rainfall for month i

P_t a threshold value representing aquifer boundary conditions

q interstitial ground water recharge flux rate

q volumetric water flux

q_{CMB} is the water flux calculated using CMB

Q is the deposition of airborne chloride

$Q(t)$ runoff

$Q_{(x,y,t)}$ the pumpage from the element

Q_a net discharge or abstraction from the groundwater system

Q_d surface flow

$Q_{gi-1}*D$ a summation of the decay of previous groundwater contribution

q_i water flux of the *i th* flow path

q_i actual water flux of the sample

Q_{i-1}*i rainfall induced flow increment

Q_{ib} recharge through interstitial pores in the basin floor

Q_{loss} seepage

Q_{mb} recharge through macropores in or near the basin floor

Q_{out} natural outflow

Q_p groundwater abstraction

Q_s flux of spring in catchment

Q_{tb} total recharge through the basin floor

r runoff

r fraction of a CRD which contributes to recharge

r run-on flux from the catchment area

R recharge rate

RE groundwater recharge to the aquifer system

RE recharge

$R_e(t)$ recharge

$RE_{(x,y,t)}$ recharge per element, which could either be from rainfall, from a river crossing the element, or from irrigation

RE_{eff} effective recharge

RE_S recharge upstream of the measuring point

RE_{tot} represents the total recharge

R_f rainfall

R_{ib} recharge ratio in interstitial flow below the basin floor

R_{ir} recharge ratio concentration in regional interstitial flow between basin floors

R_{mb} recharge ratio in macropore flow in the basin floor

RO run-off

R_p percolation of soil moisture

R_{sm} moisture flux ($mm \cdot yr^{-1}$)

R_{sm} moisture flux ($mm \cdot yr^{-1}$)

R_t total recharge ratio

R_T a total recharge rate

R_T total recharge

S aquifer storativity

S surface run-off

SATFLOW Saturated Flow Module

SMD soil moisture deficit

SOMOS soil moisture Module

$S_{x,y}$ aquifer storativity, which also indicates spatial variation

S_y specific yield

t time

T aquifer transmissivity

T_0 surface temperature before surface warming

t_a average age

T_C total chloride content

T_D total atmospheric chloride Deposition

TG the natural thermal gradient

TM total moisture content

T_M total moisture content

T_s time since the water infiltrated

T_x and T_y aquifer transmissivity in the x and ? direction

v vertical groundwater flux

W width of the cross section

x, y refers to the spatial distribution

z depth (taken as positive when measured downward)

z depth co-ordinate

z vertical space coordinate

a_0 porosity of the aquifer at the water level

? h change in water level in the aquifer

? h_i water level change during month i

? t time increment over which the water balance is executed

? V change in saturated volume of the aquifer

? ?(t) change in volumetric water content

? volumetric water content;

$?_i$ volumetric water content of the *i th* flow path within the sample.

? radioactive decay constant

? correlation coefficient

? filtration velocity vector (actual mean velocity times porosity)

$\overline{u}$ average value of u

? matrix potential

?(?) matrix potential

? 1$_{mb}$ average chloride concentration in macropore flow in the basin floor

Notation in this study

$\overline{X}$ arithmetic mean

$X_{interval}$ confidence interval

$GM_{\bar{y}}$ geometric mean

Δh average drawdown related influence radius [L]

A recharge area or catchment area [L^2]

B groundwater catchment area [L^2]

C_{in} chloride concentration of interflow [ML^{-3}, $mg\cdot\ell^{-1}$]

c chloride concentration [ML^{-3}, $mg\cdot\ell^{-1}$]

c_0 regression constant [no dimension]

C_{01} chloride concentration of runoff [ML^{-3}, $mg\cdot\ell^{-1}$]

C_1 chloride concentration of hypodermic runoff [ML^{-3}, $mg\cdot\ell^{-1}$]

C_2 illuvial (salt deposit) zone [ML^{-3}, $mg\cdot\ell^{-1}$]

C_{21} interflow from illuvial zone [ML^{-3}, $mg\cdot\ell^{-1}$]

C_{22} chloride concentration of infiltrating water [ML^{-3}, $mg\cdot\ell^{-1}$]

C_e chloride concentration of sheet flow [ML^{-3}, $mg\cdot\ell^{-1}$]

C_s concentration of chloride values of aquifer storage [ML^{-3}, $mg\cdot\ell^{-1}$]

C_g chloride concentration of groundwater [ML^{-3}, $mg\cdot\ell^{-1}$]

C_{g0} chloride concentration of old storage water in aquifer [ML^{-3}, $mg\cdot\ell^{-1}$]

CN curve number

C_p concentration of chloride values of abstraction from pumping [ML^{-3}, $mg\cdot\ell^{-1}$]

C_r chloride concentration of rainfall [ML^{-3}, $mg\cdot\ell^{-1}$]

C_r concentration of chloride values of rainfall [ML^{-3}, $mg\cdot\ell^{-1}$]

CRD cumulative rainfall departure [L]

C_s chloride concentration of surface water [ML^{-3}, $mg\cdot\ell^{-1}$]

C_v concentration of chloride values of indirect recharge [ML^{-3}, $mg \cdot \ell^{-1}$]

r density of water [ML^{-3}]

$E(t)$ actual evapotranspiration [L]

f_c coverage of vegetation

f_i factor of intensity of rainfall $C_i = h_r / T_t$

f_s soil factor

f_v vegetation factor

$\overline{H}_y$ Harmonic mean

h_r rainfall lasting time [T]

P precipitation [L]

$P(t)$ precipitation [L]

$p_d(t)$ periodicity item

Q abstraction [L^3]

q_{rfi} special flow of spring [L^3T^{-1}]

Q_{Eti} evapotranspiration of subsurface flow [L^3T^{-1}]

Q_f amount of regional water [L^3T^{-1}]

Q_{infi} total infiltration to the unsaturated zone [L^3T^{-1}]

Q_{outi} total outflow such as spring flow [L^3T^{-1}]

Q_p monthly abstraction [L^3T^{-1}]

Q_r amount of rainwater [L^3T^{-1}]

Q_{Rei} recharge to the deep aquifer [L^3T^{-1}]

Q_v indirect recharge volume [L^3T^{-1}]

r coefficient of slope, recharge rate [LT^{-1}]

R influence radius, R? t [L]

$R(t)$ direct runoff [L]

R_A extraterrestrial radiation [MT^{-3}, MJ m^{-2} d^{-1})

$R_E(t)$ Groundwater recharge [LT^{-1}]

s storativity

Abbreviations

^{13}C Carbon-13

^{14}C Carbon-14

^{18}O Oxygen-18

^{2}H Deuterium

^{36}Cl Chloride-36

^{3}H Tritium

a.s.m.l above sea mean level

C/S Cedarberg Shale

CFC Chlorofluorocarbon

CMB Chloride mass balance

CNC Cape nature Reserve

CRD Cumulative rainfall departure

CWB Channel Water Budget

CWB Channel Water Budget

CWD Cumulative water level departure

DRASTIC model name is derived from depth-to-water table, net recharge, aquifer media, soil media, topography, impact of vadose zone and conductivity (hydraulic).

DWAF Department of Water Affairs and Forestry

EARTH Extended model for Aquifer Recharge and moisture Transport through unsaturated Hardrock

EV-SF Equal volume-Spring Flow

GD Groundwater dating

GIS Geographical Information Systems

GM Groundwater Modelling

GMWL Global Meteoric Water Line

KKRWSS Klein Karoo Rural Water Supply Scheme

Klein Karoo namely Little Karoo

MAP Mean annual precipitation

MAR Mean annual runoff

MWL Meteoric Water Line

NGDB National Groundwater Database

pmC Percent modern carbon

REGIS Water Resources and Geographical Information Systems database in

Department of Water Affairs and Forestry

SAWS South Africa Weather Service

SVF Saturated Volume Fluctuation

TMG Table Mountain Group

UFM Unsaturated Flow Model

UFM unsaturated flow modeling

WB Water Balance

WM watershed modeling

WR90 Water Research Commission Flow data in 1990 (published in 1994)

WRC Water Research Commission

WTF Water Table Fluctuation

WTF Water Table Fluctuation

ZFP Zero Flux Plane

Notation of strata

C-Pd Dwyka: Tillite, sandstone, mudstone, shale

Dbi Bidouw: Shale, siltstone, sandstone

Dc Ceres: Shale, sandstone

Dl Lake Mentz; Shale, sandstone, diamictite

Dt Traka: Shale, siltstone, sandstone

Dw Witpoort: Quartzitic sandstone, siltstone, shale

Je Enon: Conglomerate, sandstone

J-K Kirkwood: Mudstone, sandstone, conglomerate

Kb Conglomerate: sandstone

Ks Sundays River: Sandstone, mudstone, shale

N-? Cape Granite Suite: Biotite granite, porphyritic granite

N-?g Biotite granite: granodiorite

Nbi Bridgetown Suite: Altered igneous rocks

Nbr Brandwacht, Greywacke

Nf Franschhoek: Quartzite, conglomerate, slate

Ng Grootderm Suite: See Ns, Nh, Nnu, Nho

Nga Gamtoos: Limestone, phyllite, granulestone, quartzite

Nk Kango: Sandstone, shale, conglomerate, limestone

Nka Kaaimans: Quartzite,phyllite, schist

Nkl Klipplaat: Schist

Nno Phyllite, greywacke, quartzite, dolomite

Np Piketberg, Phyllitic shale, greywacke, limestone

Npo Porterville: Phyllitic shale, greywacke, limestone, arenite

Nty Shale, greywacke, quartzite

Ny Diorite, gabbro

N-? k Kuboos Granite: Porphyritic granite

N-? m Porphyritic biotite granite

N-? s Porphyritic biotite granite

N-? w Porphyritic granite

Op Graafwater, Piekenierskloof : Quartzitic sandstone, shale

Ope Peninsula Skiereiland: Quartzitic sandstone

P a Adelaide & Estcourt: Mudstone, sandstone

Pf Fort Brownn: Shale

Ppw Whitehill, Prince Albert, Prins Albert: See Ppr, Pw

Pr Laingsnurg, Ripon, Vischkuil, Collingham, Whitehill and Prince Albert:

Sandstone, shale

Pt Tierberg: Shale

Pwa Waterford:Sandstone, shale

Qsc Quaternary aeolian sand

Qst Quaternary Aeolian sand

Sn Nardouw, Cedarberg, Sederberg and Pakhuis: Quartzitic sandstone, shale, tillite

Tg Grahamstown: Silcrete

T-Qb Bredasdorp: Limestone, sandstone, conglomerate

Tra-Tra Shale, siltstone

? cc Malmesbury Group

? g Biotite granite, granodiorite

? k Sandstone, conglomerate, shale

? kn Shale, siltstone, sandstone, limestone

Contents

SUBMITTED IN THE FULFILLMENT OF THE REQUIREMENTS FOR THE DEGREE OF 1
NOTATION IN LITERATURES IV
NOTATION IN THIS STUDY VIII
ABBREVIATIONS X
NOTATION OF STRATA XI
LISTS OF TABLES XXV

SUBMITTED IN THE FUL FILLMENT OF THE REQUIREMENTS FOR THE DEGREE OF 1
NOTATION IN LITERATURES IV
NOTATION IN THIS STUDY VIII
ABBREVIATIONS X
NOTATION OF STRATA XI
LISTS OF TABLES XXV

Submitted in the fulfillment of the requirements for the degree of 1
AUGUST 2005 1
ABBREVIATIONS AND NOTATIONS IV
Notation in literatures iv
Notation in this study viii
Abbreviations x
Notation of strata xi
LISTS OF TABLES xxv

AUGUST 2005 1
ABBREVIATIONS AND NOTATIONS IV
LISTS OF FIGURES XXIV

AUGUST 2005 1
ABBREVIATIONS AND NOTATIONS IV
LISTS OF FIGURES XXIV

Yong Wu *1*

Submitted in the fulfillment of the requirements for the degree of 1

Doctor of Philosophy..... *1*

AUGUST 2005 ..... **1**

DECLARATION **2**

Abstract i

ABBREVIATIONS AND NOTATIONS ..... **IV**

Notation in literatures iv

Notation in this study..... viii

c_0 regression constant [no dimension]..... viii

Abbreviations x

Notation of strata..... xi

Contents xiii

LISTS OF TABLES xxv

Yong Wu *1*

Submitted in the fulfillment of the requirements for the degree of 1

Doctor of Philosophy..... *1*

AUGUST 2005 ..... **1**

DECLARATION **2**

Abstract i

ABBREVIATIONS AND NOTATIONS ..... **IV**

Notation in literatures iv

Notation in this study..... viii

c_0 regression constant [no dimension]..... viii

Abbreviations x

Notation of strata..... xi

Contents xiii

LISTS OF TABLES xxv

Yong Wu *1*

Submitted in the fulfillment of the requirements for the degree of 1

Doctor of Philosophy..... *1*

AUGUST 2005 ..... **1**

DECLARATION **2**

Abstract i

ABBREVIATIONS AND NOTATIONS ..... **IV**

Notation in literatures iv

Notation in this study viii

c_0 regression constant [no dimension] viii

Abbreviations x

Notation of strata xi

Contents xiii

LISTS OF TABLES xxv

Yong Wu *1*

Submitted in the fulfillment of the requirements for the degree of 1

Doctor of Philosophy *1*

AUGUST 2005 ..... **1**

DECLARATION **2**

Abstract i

ABBREVIATIONS AND NOTATIONS ..... **IV**

Notation in literatures iv

Notation in this study viii

c_0 regression constant [no dimension] viii

Abbreviations x

Notation of strata xi

Contents xiii

LISTS OF TABLES xxv

5.6 SUMMARY **66**

Yong Wu *1*

Submitted in the fulfillment of the requirements for the degree of 1

Doctor of Philosophy *1*

AUGUST 2005 ..... **1**

DECLARATION **2**

Abstract i

ABBREVIATIONS AND NOTATIONS ..... **IV**

Notation in literatures iv
Notation in this study..... viii
c_0 regression constant [no dimension]..... viii
Abbreviations x
Notation of strata..... xi
Contents xiii
LISTS OF TABLES xxv

Yong Wu *1*
Submitted in the fulfillment of the requirements for the degree of 1
Doctor of Philosophy..... *1*
AUGUST 2005 ..... **1**
DECLARATION **2**
Abstract i
ABBREVIATIONS AND NOTATIONS ..... **IV**
Notation in literatures iv
Notation in this study..... viii
c_0 regression constant [no dimension]..... viii
Abbreviations x
Notation of strata..... xi
Contents xiii
LISTS OF TABLES xxv

Yong Wu *1*
Submitted in the fulfillment of the requirements for the degree of 1
Doctor of Philosophy..... *1*
AUGUST 2005 ..... **1**
ABBREVIATIONS AND NOTATIONS ..... **IV**
Notation in literatures iv
Notation in this study..... viii
c_0 regression constant [no dimension]..... viii
Abbreviations x
Notation of strata..... xi
LISTS OF TABLES xxv

Yong Wu *1*

Submitted in the fulfillment of the requirements for the degree of 1

Doctor of Philosophy..... *1*

AUGUST 2005 ..... **1**

DECLARATION **2**

Abstract i

ABBREVIATIONS AND NOTATIONS ..... **IV**

Notation in literatures iv

Notation in this study..... viii

c_0 regression constant [no dimension]..... viii

Abbreviations x

Notation of strata..... xi

Contents xiii

LISTS OF TABLES xxv

Yong Wu *1*

Submitted in the fulfillment of the requirements for the degree of 1

Doctor of Philosophy..... *1*

AUGUST 2005 ..... **1**

DECLARATION **2**

Abstract i

ABBREVIATIONS AND NOTATIONS ..... **IV**

Notation in literatures iv

Notation in this study..... viii

c_0 regression constant [no dimension]..... viii

Abbreviations x

Notation of strata..... xi

Contents xiii

LISTS OF TABLES xxv

DECLARATION **2**

Abstract i

c_0 regression constant [no dimension]..... viii

Contents xiii

Appendix III Information of unsuccessful production boreholes of the KKRWSS

Yong Wu *1*

Submitted in the fulfillment of the requirements for the degree of 1

Doctor of Philosophy *1*

AUGUST 2005 ..... **1**

ABBREVIATIONS AND NOTATIONS ..... **IV**

Notation in literatures iv

Notation in this study viii

c_0 regression constant [no dimension] viii

Abbreviations x

Notation of strata xi

LISTS OF TABLES xxv

Appendix IV Information of some monitoring boreholes: Eastern Section

Yong Wu *1*

Submitted in the fulfillment of the requirements for the degree of 1

Doctor of Philosophy *1*

AUGUST 2005 ..... **1**

ABBREVIATIONS AND NOTATIONS ..... **IV**

Notation in literatures iv

Notation in this study viii

c_0 regression constant [no dimension] viii

Abbreviations x

Notation of strata xi

LISTS OF TABLES xxv

Appendix V Summary of water quality in the Vermaaks area

Yong Wu *1*

Submitted in the fulfillment of the requirements for the degree of 1

Doctor of Philosophy *1*

AUGUST 2005 ..... **1**

ABBREVIATIONS AND NOTATIONS ..... **IV**

Notation in literatures iv

Notation in this study viii

c_0 regression constant [no dimension] viii

Abbreviations x

Notation of strata xi
LISTS OF TABLES xxv
Appendix VI Constitutes of isotopes in the Kammanassie area
Yong Wu *1*
Submitted in the fulfillment of the requirements for the degree of 1
Doctor of Philosophy *1*
AUGUST 2005 ..... **1**
ABBREVIATIONS AND NOTATIONS ..... **IV**
Notation in literatures iv
Notation in this study viii
c_0 regression constant [no dimension] viii
Abbreviations x
Notation of strata xi
LISTS OF TABLES xxv
Appendix VII (a) Recharge in m^3 based on two-component mixing model
Yong Wu *1*
Submitted in the fulfillment of the requirements for the degree of 1
Doctor of Philosophy *1*
AUGUST 2005 ..... **1**
ABBREVIATIONS AND NOTATIONS ..... **IV**
Notation in literatures iv
Notation in this study viii
c_0 regression constant [no dimension] viii
Abbreviations x
Notation of strata xi
LISTS OF TABLES xxv
Appendix VII (b) Recharge proportions of the scenarios from two-component model
Yong Wu *1*
Submitted in the fulfillment of the requirements for the degree of 1
Doctor of Philosophy *1*
AUGUST 2005 ..... **1**
ABBREVIATIONS AND NOTATIONS ..... **IV**
Notation in literatures iv
Notation in this study viii

c_0 regression constant [no dimension]..... viii
Abbreviations x
Notation of strata..... xi
LISTS OF TABLES xxv
Appendix VIII Recharge volumes (m^3) based on two-component model
Yong Wu *1*
Submitted in the fulfillment of the requirements for the degree of 1
Doctor of Philosophy..... *1*
AUGUST 2005 ..... **1**
ABBREVIATIONS AND NOTATIONS ..... **IV**
Notation in literatures iv
Notation in this study..... viii
c_0 regression constant [no dimension]..... viii
Abbreviations x
Notation of strata..... xi
LISTS OF TABLES xxv
Appendix IX Recharge proportions from three-component model
Yong Wu *1*
Submitted in the fulfillment of the requirements for the degree of 1
Doctor of Philosophy..... *1*
AUGUST 2005 ..... **1**
ABBREVIATIONS AND NOTATIONS ..... **IV**
Notation in literatures iv
Notation in this study..... viii
c_0 regression constant [no dimension]..... viii
Abbreviations x
Notation of strata..... xi
LISTS OF TABLES xxv
Appendix X Recharge in m^3 from three-component model
Yong Wu *1*
Submitted in the fulfillment of the requirements for the degree of 1
Doctor of Philosophy..... *1*
AUGUST 2005 ..... **1**
ABBREVIATIONS AND NOTATIONS ..... **IV**

Notation in literatures iv
Notation in this study..... viii
c_0 regression constant [no dimension]..... viii
Abbreviations x
Notation of strata..... xi
LISTS OF TABLES xxv
Appendix XI Recharge rates of the scenarios based on two-component model
Yong Wu *1*
Submitted in the fulfillment of the requirements for the degree of 1
Doctor of Philosophy..... *1*
AUGUST 2005 ..... **1**
ABBREVIATIONS AND NOTATIONS ..... **IV**
Notation in literatures iv
Notation in this study..... viii
c_0 regression constant [no dimension]..... viii
Abbreviations x
Notation of strata..... xi
LISTS OF TABLES xxv
Appendix XII (a) Recharge estimates of the scenario 1 based on three-component model in the Vermaaks River Wellfield from 1994 to 2003
Yong Wu *1*
Submitted in the fulfillment of the requirements for the degree of 1
Doctor of Philosophy..... *1*
AUGUST 2005 ..... **1**
ABBREVIATIONS AND NOTATIONS ..... **IV**
Notation in literatures iv
Notation in this study..... viii
c_0 regression constant [no dimension]..... viii
Abbreviations x
Notation of strata..... xi
LISTS OF TABLES xxv
Appendix XIII Genetic types of groundwater regime
Yong Wu *1*
Submitted in the fulfillment of the requirements for the degree of 1
Doctor of Philosophy..... *1*

AUGUST 2005 ..... **1**

ABBREVIATIONS AND NOTATIONS ..... **IV**

Notation in literatures iv

Notation in this study viii

c_0 regression constant [no dimension] viii

Abbreviations x

Notation of strata xi

LISTS OF TABLES xxv

Appendix XIV (a) Recharge rate from the impact of preceding rainfall

Yong Wu *1*

Submitted in the fulfillment of the requirements for the degree of 1

Doctor of Philosophy *1*

AUGUST 2005 ..... **1**

ABBREVIATIONS AND NOTATIONS ..... **IV**

Notation in literatures iv

Notation in this study viii

c_0 regression constant [no dimension] viii

Abbreviations x

Notation of strata xi

LISTS OF TABLES xxv

Appendix XV The estimated recharge rate in the Kammanassie area

Yong Wu *1*

Submitted in the fulfillment of the requirements for the degree of 1

Doctor of Philosophy *1*

AUGUST 2005 ..... **1**

ABBREVIATIONS AND NOTATIONS ..... **IV**

Notation in literatures iv

Notation in this study viii

c_0 regression constant [no dimension] viii

Abbreviations x

Notation of strata xi

LISTS OF TABLES xxv

Appendix XVI Results based on water balance approach

Yong Wu *1*

Submitted in the fulfillment of the requirements for the degree of 1
Doctor of Philosophy..... *1*
AUGUST 2005..... **1**
ABBREVIATIONS AND NOTATIONS..... **IV**
Notation in literatures iv
Notation in this study..... viii
c_0 regression constant [no dimension]..... viii
Abbreviations x
Notation of strata..... xi
LISTS OF TABLES xxv
Appendix XVII Recharge rates for the quaternary catchment in the outcrop of the TMG
Yong Wu *1*
Submitted in the fulfillment of the requirements for the degree of 1
Doctor of Philosophy..... *1*
AUGUST 2005..... **1**
ABBREVIATIONS AND NOTATIONS..... **IV**
Notation in literatures iv
Notation in this study..... viii
c_0 regression constant [no dimension]..... viii
Abbreviations x
Notation of strata..... xi
LISTS OF TABLES xxv

LISTS OF FIGURES

ERROR! NO TABLE OF FIGURES ENTRIES FOUND.Figure 3.3 Sketch of the rainfall infiltration breakthrough process 35
Figure 3.4 Time lag scenarios a-c. 35
Error! No table of figures entries found.
Figure 5.1 Groundwater regions in the TMG area (After vegter, 2001) 50
Error! No table of figures entries found. Figure 5.12 Contour of chloride concentration of rainfall in the Kammanassie area 65

Error! No table of figures entries found.
Error! No table of figures entries found.
Error! No table of figures entries found. Figure 8.18 Relation between interflow, local flow and regional flow.....126

Error! No table of figures entries found.
Error! No table of figures entries found.
Error! No table of figures entries found. Figure 10.25 Hydrographs of the Vermaaks and Marnewicks Rivers. 184
Figure 10.26 Regression based on flow in the V-notch and rainfall in the Parshall against the catchment area 186
Figure 10.27 Regression based on flow in the M-notch and rainfall in the Wildebeesvlakte against the catchment area 187
Figure 10.28 Relationship between recharge rates and recharge area.....188
Figure 10.29 Regression based on total flow in the two catchments and rainfall in the Wildebeesvlakte rainfall station.....188
Figure 10.30 Model grids of the Peninsula Formation Window 190
Figure 10.31 Four patterns of recharge estimates. 193
Figure 10.32 A 95% and 90% confidence interval for the population median amount of recharge estimates. 197

Error! No table of figures entries found.

LISTS OF TABLES

Error! No table of figures entries found.
Error! No table of figures entries found.
Error! No table of figures entries found.
Error! No table of figures entries found.
Table 7.1 Seasonal rainfall patterns at the Kammanassie Dam rainfall station (1925-2001).. 97
Table 7.2 Seasonal tendencies in the Kammanassie Dam rainfall station..... 98
Error! No table of figures entries found.
Error! No table of figures entries found.
Error! No table of figures entries found.
Error! No table of figures entries found. Table 10.20 Outline of the recharge estimates ...196

Table 11.1 Soil factor and coverage percentages of vegetation.....207
Table 11.2 Factors of vegetation in the outcrop of the TMG.....207
Table 11.3 Model of temperature in the TMG area.....208
Table 11.4 Outline of the annual recharge estimates in the TMG area.....213
Table 11.5 Ranges of the recharge estimates related to the precipitation in the TMG area..218
Table 11.6 Sensitivity of the factors.....222
Table 11.7 Estimated errors of estimates in the Wildebeesvlakte rainfall station.....224

Chapter 1
Introduction

1.1 BACKGROUND

The Table Mountain Group (TMG) sandstone is a regional fractured rock aquifer with the potential to be major source of future bulk water supply to meet both agricultural and urban requirements in the Western and Eastern Cape Provinces in South Africa. The TMG aquifer mainly consists of sandstone, shale and quartz arenite that are exploited extensively for agricultural purposes. The largest groundwater supply from a fractured rock aquifer system in South Africa is taken from Kammanassie Mountain region found in the TMG aquifer systems (Cleaver et al., 2003). There has been limited research into the aquifer systems, especially with respect to recharge estimation, until now.

Although groundwater recharge is widely recognised as the key factor in determining the sustainable management of groundwater resources, less comprehensive study of groundwater recharge of the TMG aquifer systems has been undertaken yet. The ultimate aim of this study is to improve the understanding of the recharge processes and to quantify recharge rates, which is one of the critical issues regarding the sustainable development of the TMG aquifer systems. The understanding of factors influencing recharge, such as climatic, geomorphological and hydrogeological settings, is of paramount importance to accomplish the aims of the current study.

In order to estimate realistic recharge rates of the TMG aquifers and to understand the climatic impacts on recharge, conceptual recharge models need to be developed. These models should account for an improved understanding of recharge mechanisms and processes at the various geomorphological settings and under changing climatic conditions.

1.2. OBJECTIVES OF THE RESEARCH

The study has the following three objectives:

- Quantification of realistic recharge rates and the processes of recharge in the TMG aquifer system in the Kammanassie area;
- Evaluation of the sensitivity of recharge rates to rainfall patterns (spatial and temporal patterns) with a focus on understanding the impacts of climatic changes on groundwater recharge; and
- The use and development of innovative techniques to assist in recharge estimation in the TMG aquifer systems.

To achieve the aims, the TMG aquifer systems were subdivided into hydrogeological units based on climate, geology and hydrogeological characteristics. For confirming the hydrogeological conceptual model within the hydrogeological units, a hydrogeochemical conceptual model was used to quantify and qualify the relationship between rainfall, surface water, springs and the water in shallow, local and regional aquifers. The focus of the study is on recharge mechanisms and recharge estimation within the TMG area. The study evaluates recharge processes and recharge estimation methods in the TMG aquifer systems. The recharge estimation was illustrated with case studies. In particular, the study addressed the following issues:

1) Cross-calibration of recharge estimation techniques;
2) Spatial and temporal variability of recharge;
3) Impact of climatic change on recharge in the Kammanassie area.

The results of the study attempts to improve our understanding of the functioning of the TMG aquifer systems. In this way, it contributes to the sustainable development of a potential bulk water supply source in the Western and Eastern Cape Provinces.

1.3 SITE SELECTION

The study includes the TMG area, with special emphasis on the Kammanassie area. The Kammanassie area was selected for the following reasons:

a) It represents a typical area with tectonic characteristics, hydrogeologic settings and climatic regimes;
b) Availability of relatively comprehensive data sets; and
c) A relatively well-documented conceptual hydrogeological model for the area.

Several previous studies in the region have provided a good source of background information (Kotze, 2000, 2001 and 2002). The outcrops of the TMG in the study area generally occur in mountainous terrain and valleys. The cold and hot springs occurred in the Kammanassie area did assist in constructing a hydrogeological conceptual model.

Several management problems have occurred during the abstraction from the Klein Karoo Rural Water Supply Scheme (KKRWSS) since 1984. These included over-abstraction, decline in borehole efficiency and iron-oxidizing bacteriological clogging of some of the borehole screens. The main concern was that the production capacity of boreholes would decrease and nearby springs at the Cedarberg Shale (C/S) band in the Kammanassie Mountains would run dry, even the ecosystem would be shifted. It is important that the hydrogeological conceptual model and water balance are better understood in order to answer most or all of the following questions:

- How much information about flow and recharge can be revealed from hydrogeochemistry and groundwater level fluctuation in the production boreholes?
- What are the recharge processes and the realistic groundwater recharge rates in the study area?

Chapter 2

Approach and Methodology

A comprehensive approach to understanding the TMG recharge was adopted. The research dealt with both temporal and spatial variability of groundwater recharge. Existing recharge estimation methods were reviewed in light of their applicability to the TMG aquifers.

The study incorporated the following main steps in the research approach:

- Desk study
- Data collation
- Fieldwork
- Interpretation of hydrogeological and hydrogeochemical data
- Conceptualisation and classification of recharge processes at different scales
- Identification of appropriate estimation methods
- Calculation of recharge rates and comparison of results within a case study

2.1 DESK STUDY

2.1.1 Review

The desk study involved a review of all relevant available information, including:

- A literature review on recharge mechanisms and estimations in fractured rock aquifer.
- A literature review of previous studies of the TMG aquifer includes geological and hydrogeological maps and reports, remote sensing images, recharge researches and other databases, which are Department of Water Affairs and Forestry (DWAF), South Africa National Groundwater Database (NGDB) and REGIS Database, Geographical Information Systems (GIS) of Cape Nature Reserve (CNC) and Water Research Commission (WRC) WR90 Flow data.

2.1.2 Data collection

Time series data were captured from National Groundwater Database (NGDB) and REGIS Database at Department of Water Affair and Forestry (DWAF), South Africa; Geographical Information Systems of Cape Nature Conservation (CNC) and Water Research Commission (WRC) WR90 Flow data.

The rainfall samples for chloride concentrations from 2003 to 2004 were collected from three new monitoring stations at the Purification Works in Dysselsdorp. The samples of borehole water, surface water, interflow, spring flow and soil were collected from the field study. The chemical constituents of the samples were analysed by Bemlab located in Somerset West, Western Cape Province of South Africa.

2.1.3 Data collation and analysis

During the data collection, it was noted that data sets, such as rainfall data, spring flow data and monthly chemical data, were often incomplete, which must be patched up for scientific calculation. Some data were incorrect due to unclear print or decimal missing, which must be estimated scientifically. The format of the data sets is different in the different database, which must be harmonized.

2.1.3.1 Treatment of missing data

The missing data were interpolated and an analogy was conducted as follows:

Interpolated method

If a time series is incomplete in a period, the data have occasion to estimate intermediate values between the available data. The most common method used for this purpose is polynomial interpolation including (a) first-order (linear connecting two points, (b) second-order (quadratic or parabolic) connecting three points, and (c) third-order (cubic) connecting four point (Chapra and Canale, 1998). In this study, the first-order version is used to estimate the missing data in a time series. The simplest

form of interpolation is to connect two data points with a straight line. This technique, called linear interpolation, is depicted graphically in Figure 2.1. Using triangles (Chapra and Canale, 1998),

$$\frac{f_1(x) - f(x_0)}{x - x_0} = \frac{f(x_1) - f(x_0)}{x - x_0}$$

which can be rearranged to yield

$$f_1(x) = f(x_0) + \frac{f(x_1) - f(x_0)}{x - x_0}(x - x_0) \tag{2.1}$$

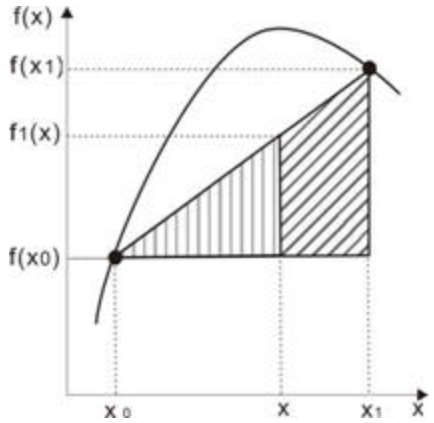

The shaded areas indicate the similar triangles used to derive the linear-interpolation formula [equation (2.1)] (After Chapra and Canale, 1998)

Figure 2.1 Graphical depiction of linear interpolation

Analogy analysis and linear regression interpolation method

Suppose a time series: $t_1, t_2, t_3, t_4, t_5, t_6, \ldots, t_{n-1}, t_n$,

There is monogamy observation (measured) value here:

Station A: $f_{11}, f_{12}, f_{13}, f_{14}, f_{15}, f_{16}, \ldots, f_{1,n-1}, f_{1n}$,

Station B: f_{21} (unknown), f_{22}(unknown), $f_{23}, f_{24}, f_{25}, f_{26}, \ldots, f_{2,n-1}$(unknown), f_{2n}(unknown).

The analogy analysis is depicted graphically in Figure 2.2. The shaded areas are the plots of the observation value. The fit line (solid line) is derived by regression analysis from t_2 to t_{n-1}, and there is significant correlation by F-Test. The data on the dash line need to be estimated. The equation of fit line is written as:

$$f_2(t)=kf_1(t)+c \tag{2.2}$$

hence, the missing value of f_{21}, f_{22} , $f_{2,n-1}$ and f_{2n} may be estimated as:

$f_{21}=kf_{11}+c$, $f_{22}=kf_{12}+c$, and
$f_{2,n-1}=kf_{1,n-1}+c$, $f_{2n}=kf_{1n}+c$.

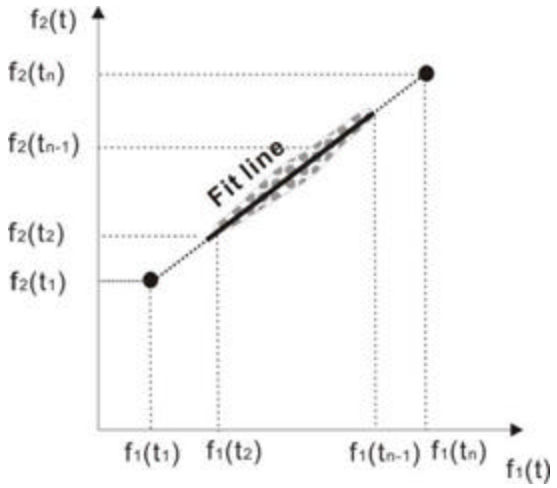

The shaded areas indicate the measured data plots used to derive the linear regression interpolation formula [equation (2.2)]. The solid line is fit line. The data on the dash line need to be estimated.

Figure 2.2 Graphical depiction of linear regression interpolation

2.1.3.2 Statistical analysis

The statistical analysis methods used in the study include the arithmetic, geometrical and harmonic mean, standard deviation and coefficient of variation (refer to Neter et al., 1988).

Arithmetic mean

The equation for the Arithmetic mean($\overline{X}$) is:

$$\overline{X} = \frac{1}{N}\sum_{i=1}^{n} X_i \tag{2.3}$$

The mean has a number of unique properties including

(a) the sum of the values of a set of items is equal to the mean multiplied by the number of items:

$$\sum_{i=1}^{n} X_i = n\overline{X}$$

(b) the sum of the deviations of the X_i values from their mean $\overline{X}$ is zero:

$$\sum_{i=1}^{n} (X_i - \overline{X}) = 0$$

(c) the sum of these squared deviations is a minimum when A= $\overline{X}$:

$\sum_{i=1}^{n} (X_i - A)^2$ is a minimum when A=$\overline{A}$

Geometric mean

The equation for the geometric mean is:

$$GM_{\overline{y}} = \sqrt[n]{y_1 y_2 y_3 \cdots y_n} \tag{2.4}$$

The harmonic mean is undefined for a data set that contains zero or negative value.

Harmonic mean

The equation for the harmonic mean (H_y) is:

$$\frac{1}{H_y} = \frac{1}{n}\sum\frac{1}{y_1} \tag{2.5}$$

The harmonic mean is undefined for a data set that contains zero or negative value.

Standard deviation

The most commonly used measure of variability in statistical analysis is called the variance. It is a measure that takes into account all the values in a set of items.
The variance s^2 of a set of values $x_1, x_2, \ldots, x_n$ is defined:

$$s^2 = \frac{\sum_{i=1}^{n}(x_i - \overline{X})^2}{n-1} \tag{2.6}$$

The standard deviation is a measure of absolute variability in a set of items. Frequently, the relative variability is a more significant measure. The most commonly used measure of relative variability is the coefficient of variation. The positive square root of the variance is called the standard deviation and is denoted as by s:

$$s = \sqrt{s^2} \tag{2.7}$$

Coefficient of variation is the ratio of the standard deviation to the mean expressed as a percentage:

$$C = 100\frac{s}{\overline{X}} \tag{2.8}$$

Therefore the error would be introduced in the recharge estimation using different mean value. There are large errors when the concentrations of chloride are between x' +s to x'+3s , so the chloride mass balance method is unfit to calculate the recharge rate under the conditions.

2.1.3.3 Analysis of confidence

The confidence interval is a range on either side of a sample mean. Confidence is a function of alpha, standard deviation and size. Alpha is the significance level used to compute the confidence level. The confidence level equals 100 (1 - alpha)%, or in other words, an alpha of 0.05 indicates a 95 percent confidence level.

Population standard deviation for the data range is assumed to be known. Size (n) is the sample size. If we assume alpha equals 0.05, we need to calculate the area under the standard normal curve that equals (1 - alpha), or 95%. This value is ± 1.96. The confidence interval is therefore:

$$X_{interval} = \overline{X} \pm 1.96(\frac{s}{\sqrt{n}}) \tag{2.9}$$

When the sample size n exceeds 15, for a desired 1-α confidence interval $L_r \le h \le U_r$, select the largest integer r that does not exceed (Neter et al., 1988):

$$0.5\,[n+1-z(1-\alpha/2)\sqrt{n}\,] \tag{2.10}$$

2.1.3.4 Error analysis

The relationships between time series of rainfall data and time series of water level fluctuation, spring flow and chloride concentrations of the borehole water were analysed statistically using correlation analysis, regression analysis, auto-regression and trend analysis. An F-Test was carried out in cross-correlation analysis.

The error analysis was conducted according to the influence factors of recharge rate. For example, the chloride mass balance mixing model method is dependent on the recharge areas. The errors are discussed in comparison with different recharge areas, such as the catchment area, the area related to the hydrogeological boundary, the area affected by pumping and an assumed elongated area. The recharge estimates from method of cumulative water level departure versus cumulative rainfall departure are

dependent on storativity. Therefore, the error analysis concentrated on the variation of storativity including its confidence.

Recharge estimates with water balance approach are dependent on multiple factors (i.e. temperature, soil parameters, vegetation type, cover rate and rainfall parameters). The error analysis of the estimates is made according to the interval analysis (Moore, 1966) as follows:

Suppose $I(R)$ is aggregate of recharge estimates for an interval, the classical intervals set is

$$I(R) = \{ [a,b] \quad | \ a \le b, a, b \in R \}$$

If **a**=**b**

a=[**a, a**] is called as point interval

Suppose two intervals $I, J \in I(R)$,

$$I = [a,b], \ J = [c,d]$$

then, arithmetic operation

$$[a,b] + [c,d] = [a + c, b + d],$$

$$[a,b] - [c,d] = [a - c, b - d],$$

$$[a,b] \cdot [c,d] = [\min(ac, ad, bc, bd), \max(ac, ad, bc, bd)]$$

$$[a,b] / [c,d] = [a,b] \cdot \left[\frac{1}{d}, \frac{1}{c} \right], \quad 0 \notin [c,d]$$

For $I, J, K \in I(R)$,

$$I \cdot (j + K) \subset I \cdot J + I.K$$

The recharge rate range can be calculated following the above steps.

2.2 FIELD WORK

A detailed list of the fieldwork performed in this study is presented in Appendix I. It can be categorised as follows:

- Geomorphological investigations using satellite images
- Hydrogeological surveys
- Borehole water, surface water, spring sampling in the Vermaaks River Wellfield
- Soil sampling
- Setting up monitoring rainfall stations
- Rain water collection

2.3 CONSTRUCTION OF CONCEPTUAL MODELS OF RECHARGE PROCESSES

At different scales, the structural geology and topography play a significant role in understanding the recharge processes and mechanisms. A framework for assessing recharge processes in the study area is illustrated in Figure 2.3.

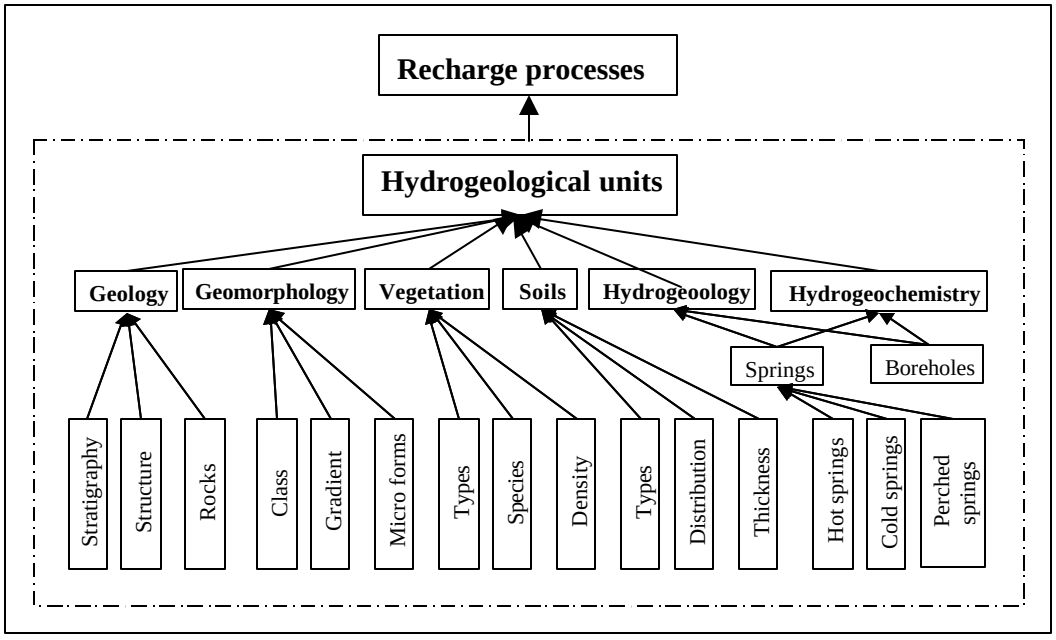

Figure 2.3 A framework for study of recharge processes

2.4 RECHARGE ESTIMATION

An approach of cross-calibration of the following set of methods was adopted to quantify groundwater recharge rates:

- Tracer techniques: Chloride Mass Balance (CMB) method;
- Catchment Water Balance techniques, e.g. the Spring Volume Fluctuation (SVF) method; and
- The Cumulative Rainfall Departure (CRD) method by Bredenkamp et al. (1995) and Xu and Van Tonder (2001) and the Extended model called Rainfall Infiltration Breakthrough (RIB) by Xu and Beekman (2003).
- Verification of a numeric model simulation

A comparative study in the case study area enabled the testing of various methods and approaches to recharge estimation. A framework for the recharge estimation is illustrated in Figure 2.4. In this study, the CMB method is discussed in detail because the method has been widely applied to estimate groundwater recharge in semi-arid regions, especially in South Africa.

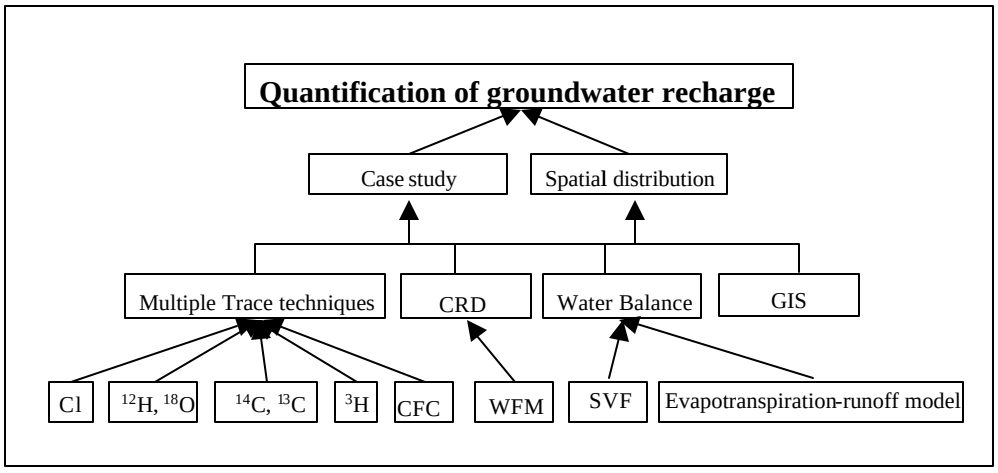

Figure 2.4 A framework for study of recharge estimation

A mixing model based on the CMB method was constructed for estimating recharge rate. Figure 2.5 shows the framework for the mixing model based on the study of

hydrogeochemistry. The framework includes four steps, which are literature study, field study, interpretation of chemical data and constructing conceptual model and modelling.

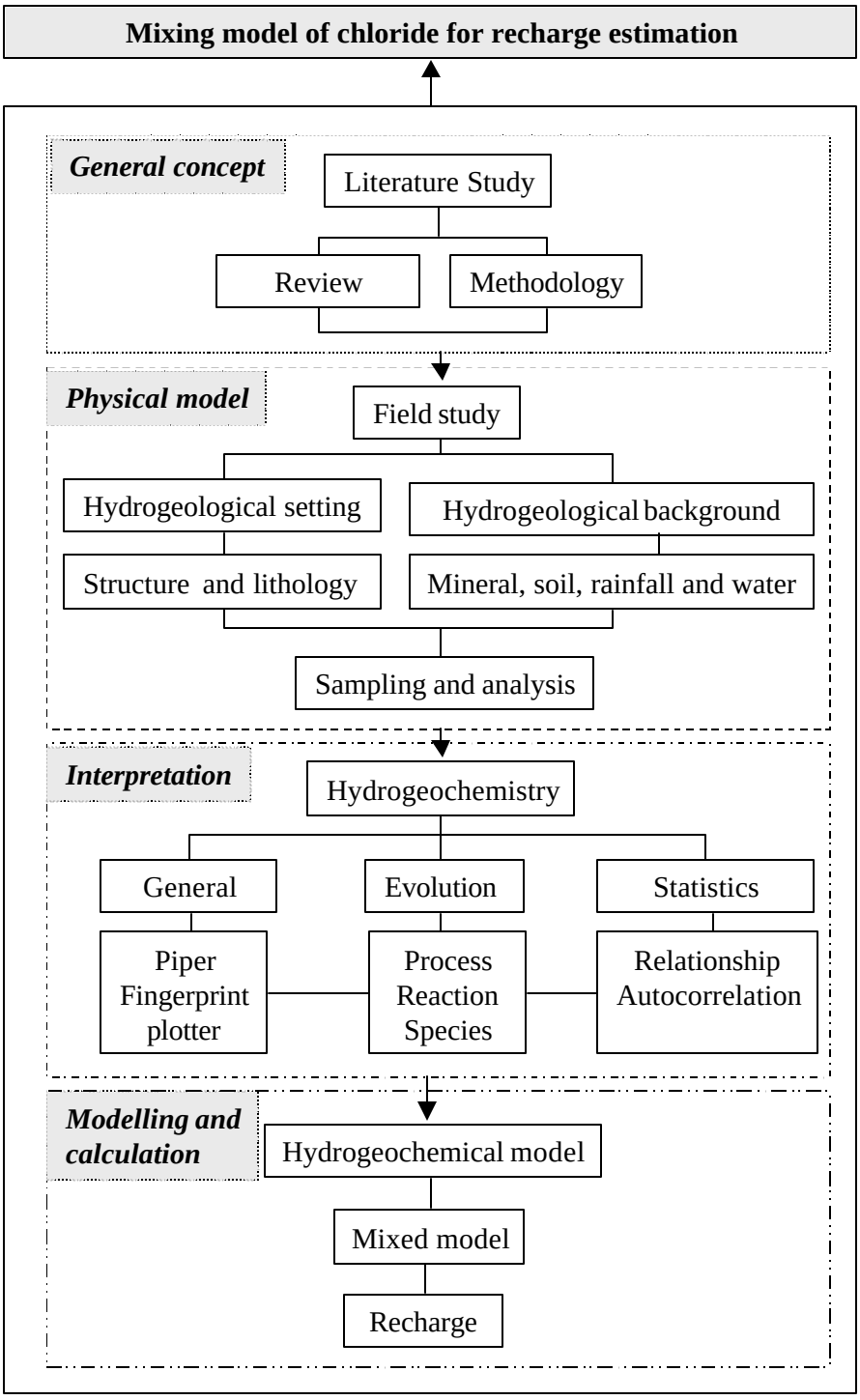

Figure 2.5 A framework for study of mixing model

2.5 SENSITIVITY OF RECHARGE ESTIMATES

A research methodology was developed to address the impact of climatic change in areas with various geomorphological characteristics, in the Kammanassie area. Geomorphological characteristics, relevant to groundwater recharge, of different areas of the TMG aquifer systems was classified within a GIS framework. Changes in climate and rainfall patterns and frequencies were related to aquifer recharge within the Kammanassie region. Influence factors of recharge such as temperature, soil, vegetation and rainfall intensity were examined and analysed. A framework for the sensitivity analysis of the recharge estimates is illustrated in Figure 2.6.

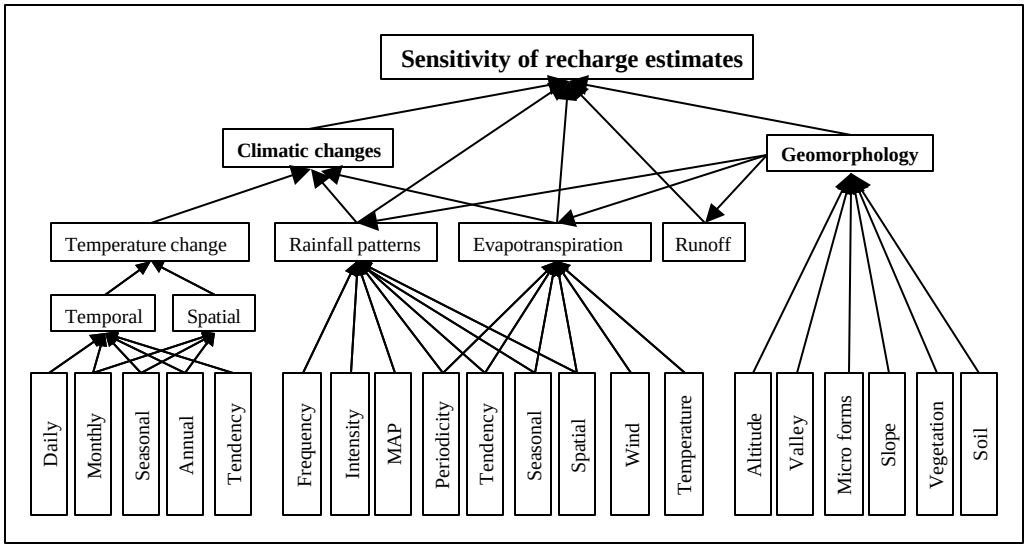

Figure 2.6 A framework of approach to sensitivity analysis of recharge estimates

Chapter 3

Literature Review

Quantification of recharge is prerequisite for the assessment of groundwater resources. Yet it is impossible to measure recharge directly at a catchment and regional scale, especially in hard rock areas. Although there are various well-established methods for the recharge estimation (Lerner et al., 1990), few can be applied successfully to the TMG area. Assessment of groundwater recharge is one of the key challenges in determining the sustainable yield of TMG aquifers, especially in the Kammanassie where people are concern about negative impact on the National Park. The recharge rates are generally low in comparison with annual rainfall or evapotranspiration, hence research efforts are still needed to determine them precisely. This review focuses on the recharge estimation methods; the relevant literature related to the subtopic was incorporated in the each subtopic. Here is not given unnecessary details.

3.1 REVIEW OF RECHARGE ESTIMATION METHODS

3.1.1 Overview of recharge estimation

Most of the classification methods focus on the unsaturated and saturated zones and approach to the recharge, including direct measurement and indirect estimation, which are constructed by Darcy's Law or water balance. Beekman and Xu (2003) classified the recharge estimation methods based on spatial scale and technique method as follows:

- Hydrogeological provinces: regions of similar climate and geology with similar geomorphic history. For example, alluvial fans and riverbeds, sand and sandstone and volcanic areas (Lerner et al., 1990);

- Hydrological zones: atmosphere, surface water; and unsaturated and saturated zones (Bredenkamp et al., 1995; Beekman et al., 1999 and Scanlon et al., 2002); or

- Physical and Tracer approaches: direct versus indirect, water balance and Darcyan physical methods; and chemical, isotopic and gaseous tracer methods (Lerner et al., 1990; and Kinzelbach et al., 2002).

An overview of commonly used recharge estimation methods is given in Table 3.1. The methods were grouped according to hydrological zones. A brief description of the principles, formulae, limitations and references is given for each method. Methods referring to surface water and the unsaturated zone estimate d the potential recharge, whereas methods referrin g to the saturated zone estimated the actual recharge. A review about choosing appropriate technique for quantify groundwater recharge, including the applicable space and time scales, the range of recharge rates that have been estimated with each technique, the reliability of the recharge estimates, and important factors that promote or limit the use of a particular technique was presented (Scanlon et al., 2002). Methods that have great potential to forecast recharge are those which have established relationships between rainfall, abstraction and water level fluctuations, such as the CRD, EARTH, Auto Regression Moving Averages and empirical methods. Critical in reliable forecasting of recharge is the accuracy of forecasting rainfall in terms of frequency of events, quantity and intensity. Note that the accuracy of forecasting recharge is further complicated by the non-linearity of groundwater resources in their response to rainfall (Beekman and Xu, 2003).

A review of commonly used methods in semi-arid Southern Africa is presented in Table 3.2. Methods were evaluated in terms of applicability and ratings (Beekman and Xu, 2003). The ratings themselves are mainly based on the authors' experience. They should be treated with caution since they are subjective by nature. Table 3.2 highlights the following:

- All methods can be used in large ranges of flux. Most methods are only applicable at small scales. Some methods are used for short periods of time, which may not reflect the groundwater regime related to recharge.
- The CMB method can be used in the unsaturated and saturated zones at scale with a range from $0.1m^2$ to $10\ 000m^2$ from years to thousands of years (spatial scales range from ~200 m to several kilometres, Scanlon et al., 2002).

Table 3.1 Outline of estimation methods of recharge in literature

Zone	Method	Principle	Formula[1)]	Limitations	Ref.
Surface water	Hydrograph separation	Stream hydrograph separation: outflow balances recharge minus evapotranspiration and abstraction	Groundwater recharge (Q_{gi}) is function of input (I) and output (O), the general form is $Q_{gi}=f(I, O)$	Ephemeral rivers, related to numerical model. Storativity is sensitive. Water table contour is not easy to obtain. O and I values are difficult to control.	11, 31, 32
	Channel Water Budget (CWB)	Recharge derived from difference in flow upstream and downstream accounting for evapotranspiration, in and outflow and channel storage change	$RE_{eff} = R_f - RO_{eff} - ET_{tot}$	Flow measurements are inaccurate.	7
Unsaturated zone	Lysimeter	Difference in flux between rainfall and seepage proportional to recharge	R=DS-FC; R=DPF*(DS-FC); R=CREC*(S-FC)*DS/SC; R=C**{b (DS-FC)}; R=C (DS -FC)**b; $R = I_c\left\{1-\frac{sc-DS}{sc-fc}\right\}^3$; IHACRES model: R=P*(DS-FC)**C-Q; R=CRAK*(P-Q-E)*DS/SC; GSFB model; ARBM model; R=BFI/(1-BFI)*Q.	Many estimation models must be compared. It is difficult to control data quality and their spatial variability. This is ineffective for hard rock area.	13-29
	Unsat. Flow Mod. (UFM) / Richards' Equation	Unsaturated flow simulation e.g. by using numerical solutions to Richards equation	$\frac{dq}{dt}=\left[K(q)\left(\frac{dy}{dz}-1\right)\right]$	Poorly known relationship between hydraulic conductivity -moisture content	2,4
	Zero Flux Plane (ZFP)	Changes in soil moisture storage below Zero Flux Plane (=zero vertical hydraulic gradient) proportional to recharge	$F(z)=\int_{t1}^{t2} q(z)dt=\int_{z0}^{t2}\|q(t1)-(q(t2)\|dz$	Subsurface heterogeneity; periods of high infiltration; there is a problem when flux is low. Poorly known hydraulic conductivity of soil.	2, 8, 9

Table 3.1 continued

Unsaturated zone	Environmental (CMB)	Chloride Mass Balance – Profiling: drainage inversely proportional to Cl in pore water	$R_{sm(c)} = \frac{TD * TM}{TC}$	Long-term atmospheric deposition unknown. Chlorine recycling in biosphere and atmosphere is not known.	1,2,8,9, 35
	Historical: Tritium profiles	Vertical distribution of tracer as a result of activities in the past (^{3}H, ^{36}Cl)	$RE(\%) = \frac{^3H_{pr}}{^3H_{rf}} \cdot 100$	Present ^{3}H levels are almost undetectable, ^{3}H is lost in other ways or ^{3}H water has penetrated beyond the soil.	1,2, 8,9
Saturated-unsaturated zone	Cum ulative rainfall departure (CRD)	Water level response proportional to cumulative rainfall departure	$R_T = rCRD_i = S_y(\Delta h_i + (Q_{pi} + Q_{outi})/(AS_y))$ *with* $CRD_i = \sum_{i=1}^{N} P_i - \left(2 - \frac{1}{P_{av}i} \sum_{i=1}^{N} P_i\right) iP_t$	Deep (multi-layer) aquifer; sensitive to S_y	2, 3
	Water Balance (WB)	Based hydrologic cycle water balance and climate elements	$\mathrm{Re}(t) = P(t) - Et(t) - Q(t) - \Delta q(t)$	Et and Qt are theoretical; $\Delta q(t)$ should be equal to zero.	30
	EARTH	Lumped distributed model simulating water level fluctuations by coupling climatic, soil moisture and groundwater level data for estimating recharge	RE=f (Maxil, SOMOS, LINRES, Satflow) $RE = S(h_t - c_R h_{t-1})$ $p_e + R_p + RE + Q_d = P$	11 parameters are required. Poorly known S_y.	5, 8
	Water Table Fluctuation (WTF)	Water level response proportional to recharge/discharge	$RE = \mathrm{a}.Rf + b$	In/outflow and S_y usually unknown	2

Table 3.1 continued

Saturated-unsaturated zone	Environmental (CMB)	Chloride mass balance: amount of Cl into the system balanced by amount of Cl out of the system for negligible surface runoff/runon	$R_t = \frac{T_d}{Cl_{gw}}$, $\frac{dF_s}{dx} = Q + D$, $\nabla \cdot F_w = \frac{dF_w}{dx} = R$ $\nabla \cdot F_w = \frac{\partial F_w}{\partial x} + \frac{\partial F w}{\partial y} = P - E - S = R$, $F_s = \int_0^h u c_g dz$	Long-term atmospheric deposition unknown. Chlorine recycling in biosphere and atmosphere is not known.	1,2,6,8 ,9, 32
Saturated zone	Groundwater Modelling (GM)	Recharge inversely derived from numerical modelling groundwater flow and calibrating on hydraulic heads / groundwater ages	$RE_{average} = T \cdot \frac{W}{A} \cdot \frac{dh}{dl} \times 365 \times 1000 \quad mm/a$	Time consuming; poorly known transmissivity; sensitive to boundaries. T and S values are usually derived by assuming steady state conditions.	2, 8
	Inverse of the dynamic model (Model flow)		$S_{x,y} \frac{\partial h}{\partial t} = \frac{\partial}{\partial x}\left(T_x \frac{\partial h}{\partial x}\right) + \frac{\partial}{\partial y}\left(T_y \frac{\partial h}{\partial y}\right) - RE_{(x,y,t)} + Q_{(x,y,t)}$		
	Sat. Volume Fluctuation (SVF)	Water balance over time based on averaged groundwater levels from monitoring boreholes	$S.\frac{\Delta V}{\Delta t} = I - O + RE - Q_a$	S is not easy to decide. I value is often assumed equal to O value. Flow-through region; multi-layer aquifers	2
	Water balance:EV-SF	Water balance at catchment scale	$RE = \frac{Q_S}{A}$	Shallow groundwater, regional flow cannot be considered.	2
	Groundwater dating (GD)	Age gradient derived from tracers, inversely proportional to recharge; Recharge unconfined aquifer based on vertical age gradient (^{3}H, CFCs, ^{3}H/^{3}He).	$t_S = \frac{nH}{RE_S} \ln\left(\frac{H}{h}\right)$, $t_a = \frac{1}{l} \ln\left(1 + \frac{n_0 D}{RE_S} l\right)$	^{14}C, ^{3}H/^{3}He, CFC: poorly known porosity / correction for dead carbon contribution. Poorly known porosity. Recharge confined aquifer based on horizontal age gradient (^{14}C and ^{36}Cl)	1, 4, 9, 33,34, 36

Table 3.1 continued

Saturated zone	Stable isotopes	$^{18}O, ^{2}H$	$Q_g = Q_w\left(\frac{d\ ^{18}O_w - d\ ^{18}O_g}{d\ ^{18}O_g - d\ ^{18}O_R}\right)$	There is no monogamous relationship between rainfall, rivers and groundwater. Flow paths are not easily known. Various mixing ratios could yield the same final isotopic value, lack of a distinct signature.	12
	Groundwater temperature	T	$T(z,t) = T_0 + T_G(z - Ut) + \{(b + T_G U)/2U\}[(z + Ut)e^{Uz/a} \times erfc\{(z + Ut)/2(at)^{1/2}\} + (Ut - z)erfc\{z - Ut)/2(at)^{1/2}\}]$ $U = vc_0 r_0 / cr$	The thermal diffusivity and the heat capacity of the aquifer are not easy to obtain.	

1Beekman et al., 1996	7 Lerner et al., 1990	13 Chapman and Malone, 1999	19 Boughton, 1993b	25 Chiew et al., 1993	31 White et al., 2003
2 Bredenkamp et al., 1995	8 Gieske, 1992	14 Aston and Dunin, 1997	20 Fleming, 1975	26 Lopes et al., 1982	32 Cook et al., 2001
3 Xu & van Tonder, 2001	9 Selaolo, 1998	15 AWRC, 1969	21 Chapman and Malone, 1999	27 Dawdy and O'Donnell, 1965	33 Cook and Solomon, 1997
4 Weaver & Talma, 2002	10 Sami & Hughes, 1996	16 Black et al., 1969	22 Huggins and Monke, 1967	28 Ye et al., 1997	34 Cook et al., 1998
5 Lee and Gehrels, 1997	11 Xu et al., 2002	17 Boughton, 1993 a, b	23 Chapman, 1999	29 Evans and Jakeman, 1998	35 Cook et al., 1994
6 Beekman and Sunguro, 2002	12 Fritz et al. 1976	18 Boughton, 1993b	24 Jakeman and Hornberger, 1993	30 Tyner et al., 2000	36 Cook and Solomon, 1995

1) Symbols are designated in general notation

Table 3.2 Review of common recharge estimation methods used for semi-arid Southern Africa (Beekman and Xu, 2003)

Zone	Method	Applicability[2]			Rating[3]		
		Flux ($mm \cdot yr^{-1}$)	Area (km^2)	Time (yrs)	Acc.	Ease	Cost
SW	Baseflow	400-4000 (0.1-1000)	10^{-4}-1300 (10-1000)	0.3-50 (1-100)	2	2	1-2
	CWB	100-5000	10^{-3}-10	1d-1yr	2-3	2	3
	WM	1-400	10^{-1}-5×10^5	1d-10yr	2	2-3	3
Unsaturated[1]	Lysimeter	1-500	0.1-30m^2	0.1-6	1-2	3	3
	UFM	20-500	0.1-1m^2	0.1-400	3	2	2
	ZFP	30-500	0.1-1m^2	0.1-6	3	2	2
	CMB	0.1-300 (0.6-300)	0.1-1m^2	5-10000	2	1	1
	Historical	10-50 (10-80)	0.1-1m^2	1.5-50	2-3	2-3	3
Saturated - Unsaturated	CRD	(0.1-1000)	(1-1000)	(0.1-20)	1-2	1-2	1
	EARTH	(1-80)	(1-10m^2)	(1-5)	1-2	2	1
	WTF	5-500	5×10^{-5}->10^{-3}	0.1-5	2	1	1
	CMB	0.1-500	2×10^{-6} – >10^{-2}	5->10000	2	1	1
Saturated	GM	(0.1-1000)	(10^{-6}-10^9)	(1d–20yr)	2	3	2-3
	SVF	(0.1-1000)	(1-1000)	(0.1-20)	1-2	1-2	1
	EV-SF	(0.1-1000)	(1-100)	(1-100)	1-2	1-2	1-2
	GD	^{14}C: 1-100 $^3H/^3He$, CFC: 30-1000	^{14}C, $^3H/He^3$, CFC: $2*10^{-6}$->10^{-3}	^{14}C: 200-200000 $^3H/He^3$, CFC: 2-40	3	2-3	3

HS:	Hydrograph Separation – Baseflow	**EARTH**:	Extended model for Aquifer Recharge and Moisture Transport through Unsaturated Hardrock
CWB:	Channel Water Budget		
WM:	Watershed Modelling	**WTF**:	Water Table Fluctuation
UFM:	Unsaturated Flow Modelling	**GM**:	Groundwater modelling
ZFP:	Zero Flux Plane	**SVF**:	Saturated Volume Fluctuation
CMB:	Chloride Mass Balance	**EV-SF**:	Equal Volume - Spring Flow
CRD:	Cumulative Rainfall Departure	**GD**:	Groundwater Dating

[1]All methods for estimating fluxes through the unsaturated zone assume diffuse vertical flow whereas in reality flow along preferred pathways is the rule rather than the exception. These methods therefore tend to overestimate the diffuse flux.

[2]Data in brackets are estimates from Southern Africa; Rainfall may be up to 2000 $mm \cdot yr^{-1}$.

[3]Ratings for methods applied to semi-arid southern Africa.

3.1.2 Recharge forecast

Forecasting groundwater recharge has become increasingly important, particularly with regard to the envisaged impacts of climatic change in short and long term on the limited water resources in the TMG area. Some guidelines for recharge estimation are given in Lerner et al. (1990) and Scanlon et al. (2002). The combined chemical and

isotopic mass balance approach is based on dating moisture and groundwater using the CMB Balance and ^{14}C groundwater dating methods.

Some methods can be applied with greater certainty in the arid and semi-arid region of Southern Africa, such as CMB, CRD, EARTH, WTF, GM and SVF (Xu and Beekman, 2003). Three of these methods: WB, CRD and CMB are widely applied and will be discussed in more detail. They represent an increasing complexity in their use and data requirements. It is worth mentioning that the approach based on integrating spatial climatic and hydrogeological datasets in a GIS environment, namely DRASTIC approach (Aller et al., 1982), may have the potential to become quantitative once it is combined with recharge estimation methods given in Table 3.1.

3.2 RECHARGE STUDIES IN THE TMG AREA

The first systematic recharge studies carried out in South Africa date back to the early 1970's and were undertaken in the Western Transvaal (Bredenkamp and Vogel, 1970 and Bredenkamp et al., 1974) and the Northern Cape (Smit, 1978). Recharge studies were mostly carried out on a local scale and as part of a larger groundwater resource assessment project. A manual, namely "Preparation of a Manual on Quantitative Estimation of Groundwater Recharge and Aquifer Storativity" (Bredenkamp et al., 1995), presents a great variety of well-tested (semi-empirical) methods that are widely employed in South Africa. In addition, it contains a wealth of recharge case studies and data covering the last 30 years. Of particular interest is that a first attempt was made to rate the different estimation techniques in terms of ease of application, reliability and availability of data.

In the last 10 years, some recharge studies were conducted in the TMG area. The results are listed in Table 3.3. The following becomes clear:

- CMB is the most independent method to estimate recharge in the TMG area. There are large differences in the recharge estimates using different methods by different researcher in the same area. A typical example is the Vermaaks River area.

- High recharge rates were obtained by using GIS but no detailed algorithm documented.

Table 3.3 Review of recharge estimates in the TMG area

Place		Method	Aquifer	MAP	RE %	Source
Vermaaks River		Base flow	Peninsula	560	8.9	Bredenkamp, 1995
		Unknown	Peninsula	299-714	17	
		CMB	Nardouw / Peninsula		43.5 /11.1	Kotze, 2000 and 2002
		SVF			3.1 /19.7	
		SVF (fit)			3.4 /16.4	
		CRD			3.2 /14.4	
		Base flow			21.4 /12.5	
		EARTH			2.9 /23.9	
		^{2}H displacemen			0.3 /2.7	
		^{14}C age			1.8 /2.0	
		GIS raster	TMG		2.5-4.8	Woodford, 2002
		CMB			5	Weaver et al., 2002
Langebaan Road Field		CMB	Bredas-dorp	396.4-648.9	9.7	Weaver and Talma, 2002
		CMB			11.2	
		CMB			13.5	
		CMB			11.5	
Greater Oudtshoorn Districts		Empirical	Peninsula	165-1049	14	Hartnady and Hay, 2002
		Empirical	Nardouw		7	
Struibaai		CMB	TMG	436	17.4	Weaver and Talma, 1999, 2002
Agter Witzenberg		CMB	Nardouw	579-777	50, 44	
Botriver			Nardouw	477.2-1546.2	20	
Hermanus		^{14}C		635	22 (20-24)	Rosewarne and Kotze, 1996
Uitenhage Artesian Basin		Spring flow		298.2-1202.6	10	Kok, 1992
		CMB	Groot Winterhoek		25	Maclear, 1996
		CMB			55	R Parson, 2002
Whole TMG (within a radius of 200km from Cape Town)		GIS	13200km^2 outcrop	600-2,020	33	Weaver and Tama, 2002
CAGE	Low rainfall	GIS	Low lying	285.8-371.2	8	Hartnady and Hay, 2000 and 2002
	High mountain		TMG		23	
	Mountain area				30-40	
		Isotopes			50	Weaver et al., 1999
Uitenhage, Coega aquifers		WB	TMG	460	83	Kok, 1992
		CMB	TMG	250-850	24-55	Maclear, 1996
		WB			11	Bredenkamp, 2000; Xu and Maclear, 2003

3.3 CHLORIDE MASS BALANCE METHOD

The CMB method has been extensively applied to estimate groundwater recharge in arid regions (Erisson and Khunakasem, 1969; Allison et al., 1985; Johnston, 1987; Phillips, 1994; Wood and Sanford, 1995; Sami and Hughes, 1996; Tyner et al., 1998 and Cook et al., 1994 and 2001). It equates the mass flux of chloride at the ground surface to that of chloride beneath the depth at which evapotranspiration takes place. At the soil surface chloride occurs naturally from precipitation and dry fallout. Slightly higher recharge rates can be estimated using Cl in groundwater than in soil water because extraction of water from the soil generally requires additional dilution (Scanlon et al., 2002). The uses of the CMB method that involves chemical tracers provide more accurate estimates of groundwater recharge in arid to semi-arid regions (Bazuhair and Wood, 1996). The method is applicable in areas of high evapotranspiration where the infiltrating water becomes concentrated (Johansson, 1987).

The CMB is often used as a first approximation of recharge due to its simplicity and cost effectiveness. Preferably, results should be verified with other methods. There are three approaches to estimate recharge using the CMB method:

- The first approach involves the chloride concentration of rain and soil moisture (unsaturated zone) and gives an estimate of the moisture flux.
- The second approach involves the chloride concentrations of groundwater (saturated zone), whereby the total average recharge is estimated.
- The third approach involves the comparison of the first two approaches to define the recharge mechanism.

3.3.1 Theoretical aspects

3.3.1.1 Unsaturated zone

Chloride concentrations generally increase through the root zone as a result of evapotranspiration and then remain constant below this depth (Scanlon et al., 2002). Three conceptual chloride concentration profiles are shown in Figure 3.1. Bulge-

shaped Cl profiles at some sites have been attributed to paleoclimatic variations or to diffusion to a shallow water table (Scanlon 1991, Cook et al., 1989).

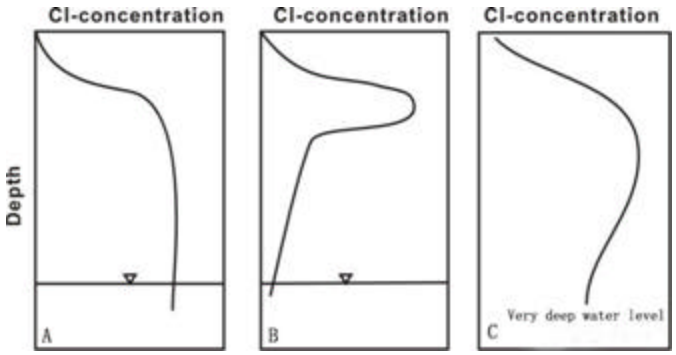

A. Piston flow with abstraction of water by roots. B. Abstraction of water by roots, but with either preferred flow of water to beneath the root zone, or diffuse loss of chloride to the water table. C. Profile that may reflect the recharge history of a site.

Figure 3.1 Conceptual depth profiles for the chloride tracer

(After Allison, 1988)

The CMB method is applied to the unsaturated zone between the deepest zero flux plane and the water table. The method yields a recharge flux for a specific locality and should ideally be integrated with area weights to estimate areal recharge. Most plant species do not take up significant quantities of chloride from soil water, thus chloride is mainly concentrated by evapotranspiration in the root zone (Allison et al., 1994). Edmunds and Gaye (1994) correlated recharge with the chloride concentrations in soils. High chloride concentrations are generally associated with lower rates of recharge and vice versa. If a steady state is attained between the chloride flux at the surface and the chloride flux beneath the evapotranspiration and mixing zones, the following mass balance can be defined (Eriksson and Khunakasem, 1969, quoted from a secondary source: Beekman and Xu Y, 2003):

$$R_{sm} = \frac{P \cdot Ck_p + D}{Cl_{sm}} = \frac{T_d}{Cl_{sm}} \qquad (3.1)$$

where R_{sm} is moisture flux ($mm \cdot yr^{-1}$), P is precipitation ($mm \cdot yr^{-1}$), Ck_p is chloride concentration in precipitation ($mg \cdot \ell^{-1}$), Cl_{sm} is chloride concentration in soil moisture ($mg \cdot \ell^{-1}$), and D is dry chloride deposition ($mg \cdot m^{-2} \cdot yr^{-1}$). The sum of $P \cdot Cl_p$ and D is

also referred to as "Total atmospheric chloride Deposition" (T_D) and originates from both precipitation and dry fall out.

A better estimate of the moisture flux is obtained from a mass balance, which integrates chloride and moisture contents cumulatively (c) over a specific depth interval (Gieske, 1992):

$$R_{sm\ (c)} = \frac{T_d \times T_M}{T_c} \tag{3.2}$$

where T_M is total moisture content ($mm \cdot m^{-2}$), and T_C is total chloride content ($mg \cdot m^{-2}$). Three potential problems have been identified with the above calculation methods (Wood, 1999):

- It is difficult to quantify the mass flux of chloride that is due to run on, or of the topographic features present at the sampling sites.
- The system may not be at a steady state with respect to the input mass flux.
- This method cannot measure total recharge if any unmeasured recharge takes place through macropores in the system.

To incorporate the additional mass resulting from run-on, Wood and Sanford (1995) have suggested the following equation for a closed depression:

$$R_{sm} = \left(\frac{T_D}{Cl_{sm}}\right) + r\left(\frac{A_b Cl_r}{A_f Cl_{sm}}\right) \tag{3.3}$$

where r is run-on flux from the catchment area, A_b is total area of the basin, Cl_r is chloride concentration of the runoff water to the basin floor, and A_f is area of the basin floor.

If recharge takes place through macropores, equation (3.3) is inappropriate. Total recharge is a combination of macropore and interstitial (matrix) recharge. Macropore recharge occurs through cracks, fractures, solution holes, natural pipes, animal

burrows, root tubes and other macro-scale openings, while interstitial flow moves largely between individual grains or a fine mesh of fractures. Macropore flow allows solutes to reach the water table faster because of greater permeability and with less surface area, thus, less opportunity for sorption and kinetically controlled reactions to mitigate constituents, which are concerned (Wood et al., 1997). Macropore flow is addressed in many studies (Bouma et al., 1977; Beven and Germann, 1982; Thorburn and Rose, 1990; Watson and Luxrnoore, 1986 and Germann, 1990). From contaminant hydrology point of view, it is typified by the work reported by Sharma and Hughes (1985), Pettyjohn (1987), Hess and Parks (1988), Germann and Gupte (1988), Hornberger et al. (1990) and Mathieu and Bariac (1996).

Based on the equation (3.3), interstitial recharge is rewritten as (Wood et al., 1997):

$$q = \frac{PCl_p}{Cl_{uz}} + r\frac{A_b Cl_r}{A_f Cl_{uz}} \tag{3.4}$$

where q is interstitial groundwater recharge flux rate ($L \cdot T^{-1}$). Cl_{un} is chloride concentration in the unsaturated zone ($M \cdot L^{-3}$); the other notations are same as equation (3.3).

The ratio of average chloride content in precipitation (wet and dry deposition) to that in groundwater can be used to calculate recharge rates. The input flux is the product of the chloride concentration in precipitation multiplied by the amount of precipitation over the study area. The input flux is divided by the chloride concentration in groundwater. Total recharge is estimated using the following equation (Adams, 2002; Beekman and Xu, 2003):

$$R_T = \frac{T_D}{Cl_{gw}} \tag{3.5}$$

where R_T is total recharge, T_D is total deposition, and Cl_{gw} is chloride concentration in groundwater. The Cl_{gw} originates from various flow components in the unsaturated zone. For an areal R_T, Cl_{gw} represents the harmonic mean of chloride concentrations in groundwater.

3.3.1.2 Saturated zone

The computations of recharge rates are based on the chloride balance and water balance at a steady state. They are similar except that the evaporation term for chloride is zero. The general formulation has been given by Eriksson and Khunakasem (1969) and can be presented as follows. The integral ground water flow of water F_w, which is a vector, is defined as

$$F_w = \int_0^h u\,dz \tag{3.6}$$

where ? is the so-called filtration velocity vector (actual mean velocity times porosity), z the depth co-ordinate and h the total depth of the aquifer. F_w is thus a vector in a plane. In a similar way, the integral ground water flow of salinity, F_s (measured by chloride) is defined as

$$F_s = \int_0^h u\,c_g\,dz \tag{3.7}$$

where c_g is the concentration of chloride in the groundwater, and is like u , which is a function of depth. The divergence of the integral flow of water is related to precipitation and evaporation by

$$\nabla \cdot F_w = \frac{\partial F_w}{\partial x} + \frac{\partial F w}{\partial y} = P - E - S = R \tag{3.8}$$

where P is precipitation, E evaporation, S surface run-off and R recharge rate. If the average $\bar{c}_g$ can be estimated, the relation above can be utilized for further derivations. It is not at all evident that the chloride concentrations determined are averages of the vertical distribution. If a great number of samples are taken at different points and varying depths and the results are smoothed by constructing isolines of c_g, this will be a fair representation of the true average $\bar{c}_g$. Assuming this to be the case then:

$$\frac{dF_s}{dx} = \frac{d}{dx}(\overline{c_g} F_w) = Q \tag{3.9}$$

or

$$\overline{c}_g F_w = \int_0^x Q dx \tag{3.10}$$

The integration, beginning at the upstream boundary (water shed) is carried out along the general direction of groundwater flow, the recharge rate(R) can be computed as follows:

$$F_w = \frac{1}{\overline{c}_g} \int_0^x Q dx \tag{3.11}$$

and since

$$F_w = \int_0^x R dx \tag{3.12}$$

Under steady state, 1-D flow, the chloride mass flux at any depth will equal the chloride mass flux at the surface. The chloride mass flux under steady-state conditions as defined as (Scanlon, 1991):

$$\overline{m} = -D \frac{dC}{dz} + Cq \tag{3.13}$$

Solving for q yields the volumetric water flux:

$$q = \frac{1}{C}\left[\overline{m} + D \frac{dC}{dZ}\right] \tag{3.14}$$

where q is the volumetric water flux, C is the pore water chloride concentration, $\overline{m}$ is the chloride mass flux, D is the hydrodynamic dispersion coefficient, and z is the vertical space coordinate.

As water moves downward through the soil profile, some of it is removed by evapotranspiration, reducing the water flux and causing the remaining pore water chloride to become increasingly concentrated with chloride (Scanlon, 1991). In arid regions, it is often assumed that D is negligible (Allison et al., 1985, Phillips, 1994), and equation (3. 14) simplifies to:

$$q = \overline{m} / c \tag{3.15}$$

The pore water age at a given depth can be calculated by dividing the mass of chloride in the profile above that depth by the surface chloride mass flux (Phillips, 1994):

$$t_z = \frac{\int_0^z q\, C dz}{\overline{m}} \tag{3.16}$$

where t_z is the pore water age at a depth of z, and $?$ is the volumetric moisture content.

3.3.1.3 Combined method

The chemistry of groundwater at the water table may be further enriched in chloride due to the uptake of evaporative salts or formation water in the saturated or unsaturated zone, leading to the underestimation of recharge. Similarly, lateral flow from different recharge areas in non-homogenous porous media may give rise to salinities different from that found in the unsaturated zone. Edmunds and Gaye (1994) suggested that the combined use of unsaturated and saturated zone data for determining recharge, avoids the uncertainties derived from using the water table data alone. In a bimodal flow regime, it is assumed that R_T originates from only two flow components in the unsaturated zone, which are fully mixed in the groundwater: a (slow) diffuse (R_{sm}) and a (quick) preferential (R_{pr}) flow component. As $Cl_{pr} \ll Cl_{gw} < Cl_{sm}$, the relative contribution of either R_{sm} or R_{pr} to R_T expressed as a fraction, is calculated as (Sharma and Hughes, 1985):

$$f(R_{pr}) = 1 - f(R_{sm}) \approx \left(\frac{Cl_{sm} - Cl_{gw}}{Cl_{sm}} \right) \tag{3.17}$$

3.3.2 CMB assumptions

The CMB of unsaturated zone assumptions are summarised as follows (Tyner et al., 2000):

1) Vertical downward piston displacement adequately represents the chloride transport (that is little to no preferential flow);
2) Chloride is not retarded by adsorption nor accelerated by anion exclusion;
3) Chloride is conservative;
4) Chloride application rate is constant and known;
5) There is no appreciable runon or runoff from the sampling sites; and
6) Steady-state conditions prevail in the soil column (Johnston, 1987; Dettinger, 1989; Scanlon 1992; USGS, 1994; and Ginn and Murphy, 1997).

Any changes as stated above, should derive an error of the estimated recharge rate. Large errors or mistakes would be produced if the conditions did not satisfy the presupposition. This is also the process of error propagation. It is well known that preferential recharge processes occur in the outcrop of the TMG, therefore if the method is used, there should be large discrepancy in the recharge estimates.

3.3.3 Applicability and application

Based on the above discussion of CMB method, the following comments should be noted:

- These formulae can be used for 1-D flow at steady state;
- The changes of soil moisture are ignored; no recharge occurs across the catchment boundary.
- Recharge is not unidirectional in most realistic recharge scenarios;
- The deposition of airborne chloride related to precipitation and evapotranspiration is not constant;
- The chloride concentration along the flow path is not easy to measure. In order to obtain spatial and temporal recharge rather than point recharge, long network monitoring runs are also needed at different scales.

Walker et al. (1991) demonstrated non-steady state conditions in cases where changes in land use occurred. The main source of uncertainty in applying the CMB method is the rainfall chemistry for the preceding periods (Edmunds and Gaye, 1994). Ideally, the method requires a minimum of three to four years of chloride input data and undisturbed soil samples up to the water table (Sukhija et al., 1988). Other important sources that need to be considered are applied fertilisers and the biological activity of the soils.

The method can be used to estimate recharge ranging from 0.05 mm to 300 mm per year over temporal scales ranging from a few decades to thousands of years. The CMB method gives site-specific estimates (up to $1m^2$) in the unsaturated zone (Scanlon et al., 2002). The most reliable estimates of site-specific moisture fluxes may be obtained through a multiple tracer profiling approach (Simmers et al., 1997). Cook et al. (1989) used the CMB method with the electromagnetic geophysical technique to identify the spatial variability of groundwater recharge in a semi-arid region. Wood and Sanford (1995) found that in semi-arid areas recharge rates obtained using the CMB method is comparable to recharge rates obtained by physically based methods. The method is independent of whether recharge is focused or diffused (Bazuhair and Wood, 1996). The spatial scales of recharge increase significantly when the saturated zone is used to estimate recharge and similar temporal scales and fluxes are observed as with the unsaturated zone profiling techniques as shown in Figure 3.2.

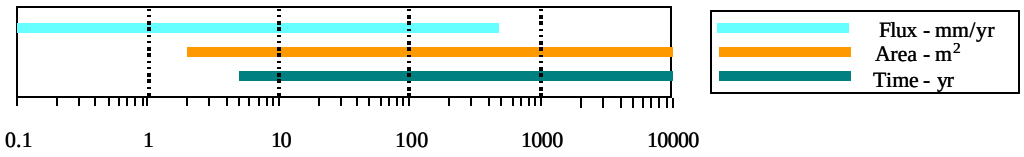

Figure 3.2 Range of fluxes that can be estimated in the saturated zone
(After Scanlon et al., 2002)

3.3.4 Data requirements and accuracy of method

The following data is required in the CMB method, namely, precipitation, precipitation chemistry, dry chloride deposition, soil moisture chloride concentration and groundwater chloride concentration related to rainfall events. Uncertainties in the

rainfall chloride concentrations, as a result of measurement errors and other contributing sources, and the validity of assumptions, are the main factors that influence the accuracy of the method.

3.4 GROUNDWATER LEVEL FLUCTUATION METHOD

Hydrographs are charts that display the change of a hydrologic variable over time. Although they are from a stream, hydrographs can also be made for lakes, water wells, springs and other bodies of water. A hydrograph provides a way of seeing seasonal and yearly changes in the water level of an aquifer related to rainfall. The Water-table Fluctuation Method (WFM) may be the most widely used technique for estimating recharge. The advantages of the WFM include its simplicity and insensitivity to the mechanism by which water moves through the unsaturated zone. Uncertainty in estimates may be generated by the limitation of specific yield (Healy and Cook, 2002).

The Cumulative Rainfall Departure (CRD) method is based on the premise that water level fluctuations are caused by rainfall events (Bredenkamp et al., 1995). The method is applied extensively in South Africa. The method was revised to accommodate for trends in rainfall time series (Xu and Van Tonder, 2001, Xu and Beekman, 2003). It would be used to obtain the variability of recharge even without a recharge coefficient or storativity. The method cannot be applied in areas without groundwater level fluctuations or water levels not responding well to rainfall. In the above form it should only be applied to unconfined aquifers. Groundwater levels of fractured aquifers with small storativity are particularly sensitive to estimates resulted from the method.

A method, namely Rainfall Infiltration Breakthrough (RIB or recharge) was used to estimate recharge, which only part of infiltrated rainfall breaks through the zone where evapotranspiration occurs and percolates to the groundwater table (Xu and Beekman, 2003). The arrival time of this water at the water table is delayed due to the 3-dimensional spreading of moisture (Figure 3.3). The records of rainfall events are expressed as a time series: P_1, P_2, P_3, … P_m, P_{m+1}, P_{m+2} … P_n, P_{n+1}, P_{n+2}, … P_i (Figure 3.4), scenario a (a combination of point and diffuse recharge): recharge is the cumulative result of all previous rainfall. Scenario b (quick infiltration process):

recharge results from the previous n rainfall events immediately before the current rainfall event. Scenario c (a piston flow in unconsolidated aquifers): recharge results from a limited rainfall series between m and n.

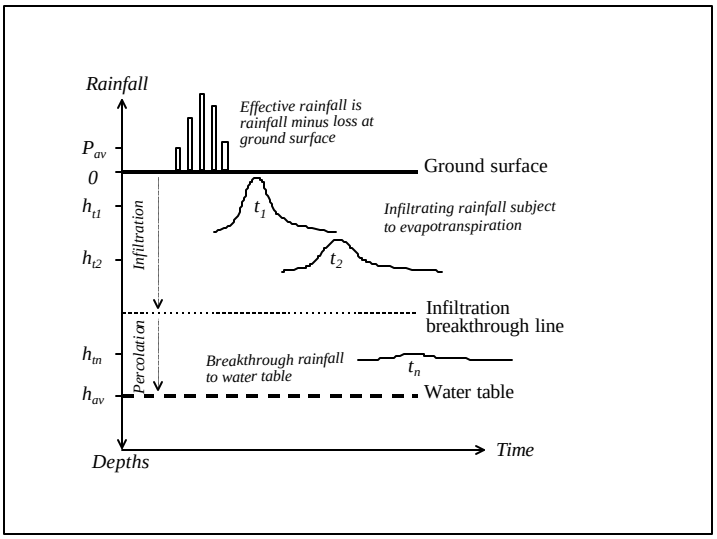

Figure 3.3 Sketch of the Rainfall Infiltration Breakthrough process
(After Xu and Beekman, 2003)

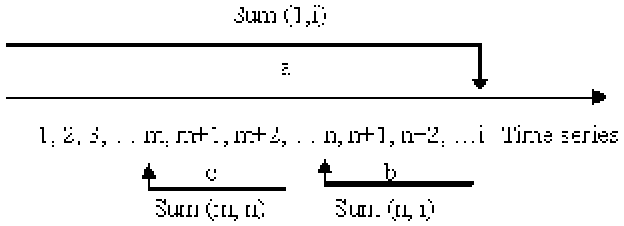

Figure 3.4 Time lag scenarios a-c (adapted from Xu and Beekman, 2003)

A RIB is defined as follows (Xu and Beekman, 2003):

$$RIB\,(i)_m^n = r\left(\sum_{i=m}^{n} P_i - \left(2 - \frac{\overline{p}_{mn}}{P_{av}}\right)\sum_{i=m}^{n} P_t\right) \quad (3.18)$$

$(i = 1, 2, 3, \ldots I)$
$(n = i, i-1, i-2, \ldots N)$
$(m = i, i-1, i-2, \ldots M)$
$M < N < I$

where r is that fraction of CRD which contributes to the RIB (recharge percentage); P_{av} is average rainfall over the entire rainfall time series; $\overline{p}_{mn}$ is the average value

from m-*th* to n-*th* month; P_t is a threshold value representing aquifer boundary conditions, and P_{av} representing an open aquifer system); the symbol *i* represents a sequential number of a rainfall record, while parameters m and n, introduced as memory markers, represent the start and end of a time series length, during which period rainfall events contribute to the RIB(*i*).

The groundwater table fluctuation ?h is is a function of aquifer storativity S and recharge fluctuation ? RIB (Haijtema, 1995; Xu et al., 2001):

$$\Delta h_i = (1/S) \cdot \left(RIB(i)_m^n - 2Th_{av} / L^2 \right) \tag{3.19}$$

where h_{av} is the average saturated aquifer thickness, T is aquifer transmissivity, and L is average distance of groundwater flow away from the groundwater mound.

3.5 WATER BALANCE APPROACH TO RECHARGE

The hydrological water balance for an area can be defined as:

$$R_e(t) = P(t) - E_t(t) - Q(t) - \Delta q(t) \tag{3.20}$$

where $R_e(t)$ is recharge, P(t) is precipitation, $E_t(t)$ is evapotranspiration, Q(t) is runoff, and ??(t) is change in volumetric water content. The term (t) designates that the terms are distributed through time. A common approach for approximating $E_t(t)$ involves first, the estimation of a reference crop, evapotranspiration as a crop coefficient, soil and rocks types. A common method to estimate Q(t) is to apply the SCS runoff equation (USDA-SCS, 1985). $E_t(t)$ and Q(t) were initially estimated based on meteorological and site-specific. Assuming ??(t) is negligible between subsequent years, an annual estimate of Re(t) can be calculated The method can be applied in most recharge scenarios. The accuracy is related to the recharge process and impact of soils and vegetation. Monthly or daily rainfall and temperature data, together with coefficients of soil and vegetation are required.

3.6 SUMMARY

A wealth of recharge estimation methods for (semi-)arid areas is currently available with each method having its own limitations. Whereas one method may be applied in specific site studies, another method may be suited for regional studies. Whereas one method may represent a short time scale, such as from event-based recharge to daily/monthly/yearly recharge, another may represent a much longer time scale, ranging from decades to thousands of years. Clarity on the aim of the recharge study is crucial in choosing appropriate methods for recharge estimation. Confidence in the recharge estimation improves when applying a multitude of methods.

An extraordinary concern in application of the methods is the difficulty in assessing the uncertainty associated with any given estimate. Uncertainties and inaccuracies of the estimates arise from spatial and temporal variability in processes and parameter values, measurement errors, and the validity of assumptions, which different methods are based on. The recharge estimates with statistical confidence levels would be better presented in a range of integrated values, which are combined with the results of variety of method.

In South Africa, experience in recharge estimation covers a time span of at least three decades. In comparison to the various techniques, including the range, space/time scales, and reliability of recharge estimates, the following methods based on different recharge processes can be applied with greater certainty in the TMG area: the CMB, CRD, WB, and Regression of spring flux, as data required for application of these methods are readily available in most cases. Of course, recharge estimation goes forward one by one, and it posses an iterative process that includes refinement of estimates as additional data are gathered.

Chapter 4

Geological Background

4.1 INTRODUCTION

The sediments of the Cape Supergroup were deposited in a shallow marine environment under tidal, wave and storm influences, as well as in a non-marine, braided-fluvial environment from early Ordovician to early Carboniferous. This predominantly siliclastic sequence is exposed along the entire length of the Cape Fold Belt (CFB), the 280-220 million year old Orogenic belt straddling the west and south coasts of South Africa. The succession of quartz arenites, shales and siltstone, with minor conglomerate and a thin diamictite unit, has been subdivided into the Table Mountain, Bokkeveld and Witteberg Group (Du Toit, 1954; Rust, 1967; Theron, 1962; Theron and loock, 1988; Broquet, 1992). For the western and Eastern Cape, maximum thickness of the Cape Super group amounts to 5, 300m and 9, 600 m respectively (SACS, 1980). The medium to coarse grain sizes and relative purity of some of the quartz arenites, together with their well indurated nature and fracturing due to folding and faulting in the fold belt, enhance both the quality of the groundwater and its exploitation potential.

The presently exposed structure and thickness of the Table Mountain Group (TMG) rocks are the result of initial deposition within an east-trending basin (Rust, 1973) along the Southern and Southwestern Cape regions, which was modified by two major tectonic events, namely the Permo-Triassic Cape Orogeny and the fragmentation of Southwestern Gondwana during the Mesozoic. The Cape Orogeny had the effect of tectonically thickening the sequence in areas of high strain like the Southern Cape. The CFB consists of two branches forming a mountain chain of about 1 200 km along the south coast and part of the west coast (De Villiers, 1944; Söhnge and Hälbich, 1983). The Cape Orogeny resulted in further deformation of

the metamorphosed Neoproterozic rocks, the Cape Granite Suite, together with its cover sequence of Ordovician to Triassic rocks (Cape Super Group and part of the Karoo Sequence). The outcrop of the southern branch is about 200km, and of the western branch, about 150km. Both branches are arcuate in plan view and convex towards the Karoo Basin merging with northeast-trending folds in the syntaxis of the Southwestern Cape.

4.2 STRATIGRAPHY

The CFB is a largely east-west striking feature located roughly south of 33°S. It consists predominantly of sedimentary and metamorphic rocks. The entire geological succession in the study areas includes the basement rocks, Cape Supergroup and part of the Karoo. The succession with their associated thickness and lithological compositions were summarised in Figure 4.1. All the Cape Supergroup rocks namely the TMG, Bokkeveld and Witteberg Groups are presented in the study area. Of the above, only the TMG is of relevance in this study. A stratigraphical outline of the study area is presented in Figure 4.2.

The TMG comprises of an approximately 4 000 m thick sequence of quartz arenite and minor shale layers deposited in a shallow, but extensive, predominantly east-west striking basin, changing to a northwest orientation near Worcester. The maximum thickness in the east section (Port Elizabeth) is approximately 3010 m (Rust, 1973, Figure 4.3). The TMG comprises of the Piekenierskloof Formation, Graafwater Formation, Peninsula Formation, Parkhuis Formation, Cederberg Formation and Nardouw Subgroup.

The bottom of the TMG is the Piekenierskloof Formation or Graafwater Formation. The Piekenierskloof Formation is quartzitic sandstone with coarse-grained to gritty zones, 10-150m. The Graafwater Formation has thickness of 25-65m and comprises of thin-bedded sandstone, siltstone, shale and mudstone.

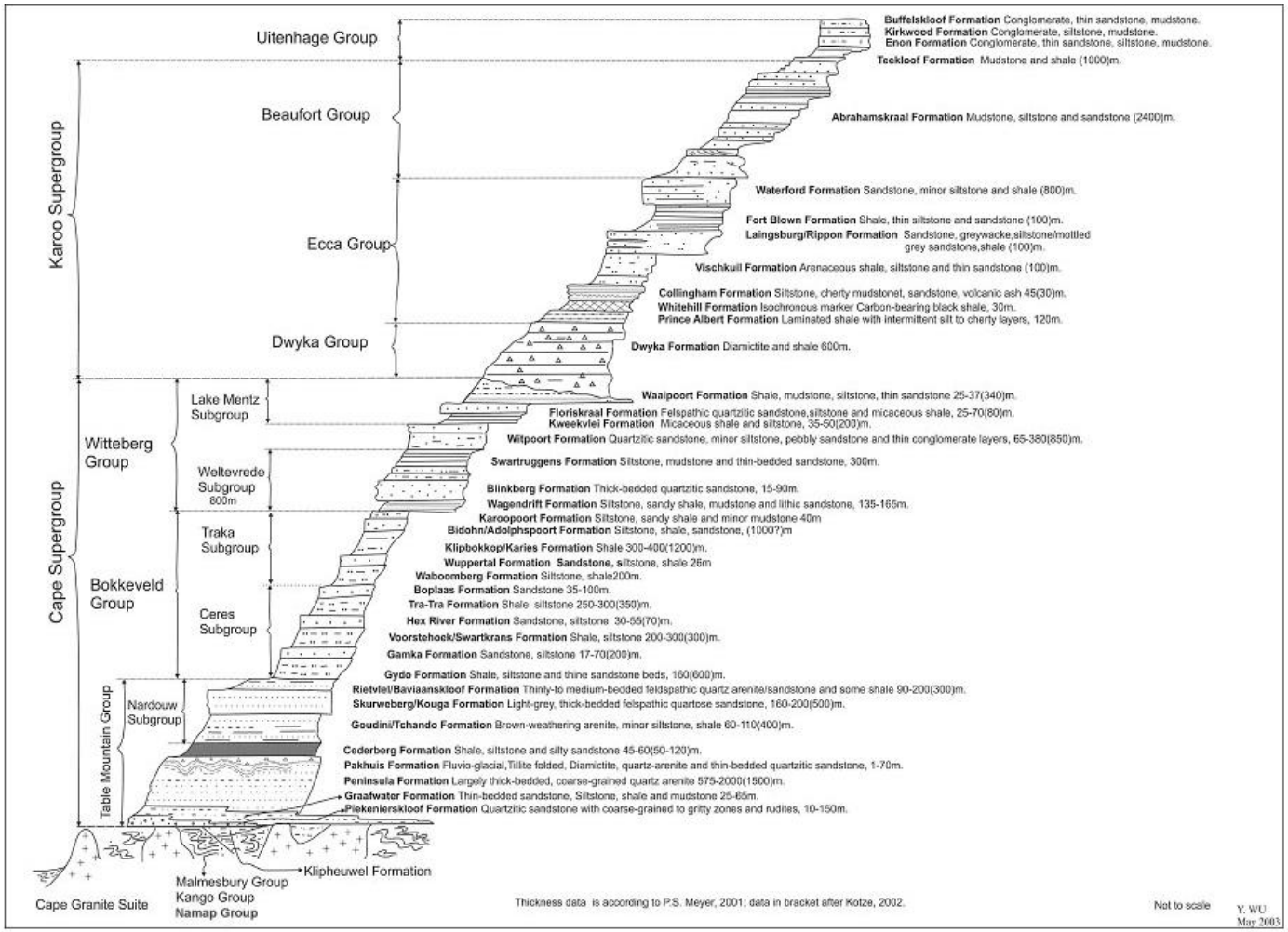

Figure 4.1 Geological sequences in the study area

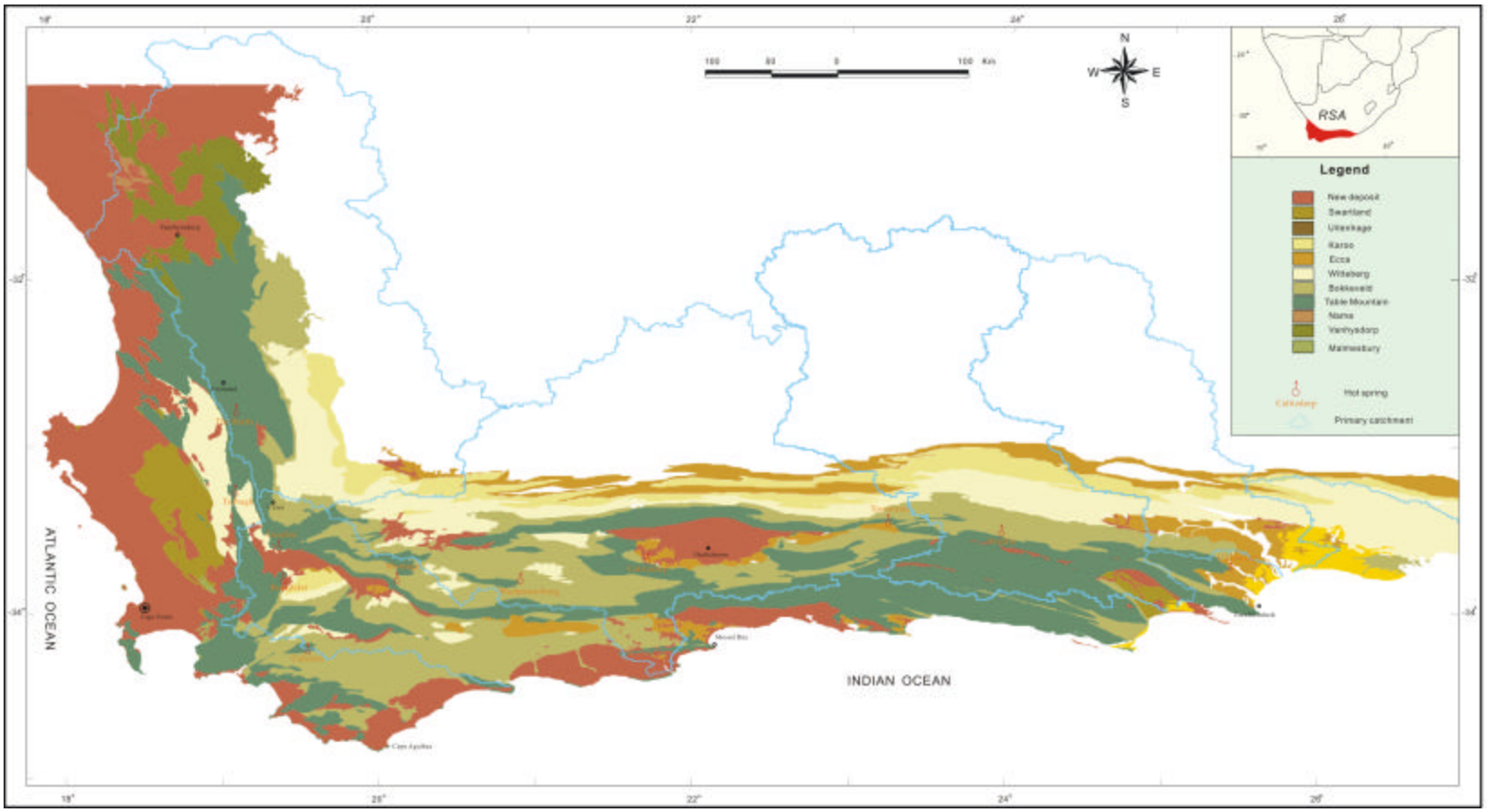

Figure 4.2 Stratigraphy in the study area

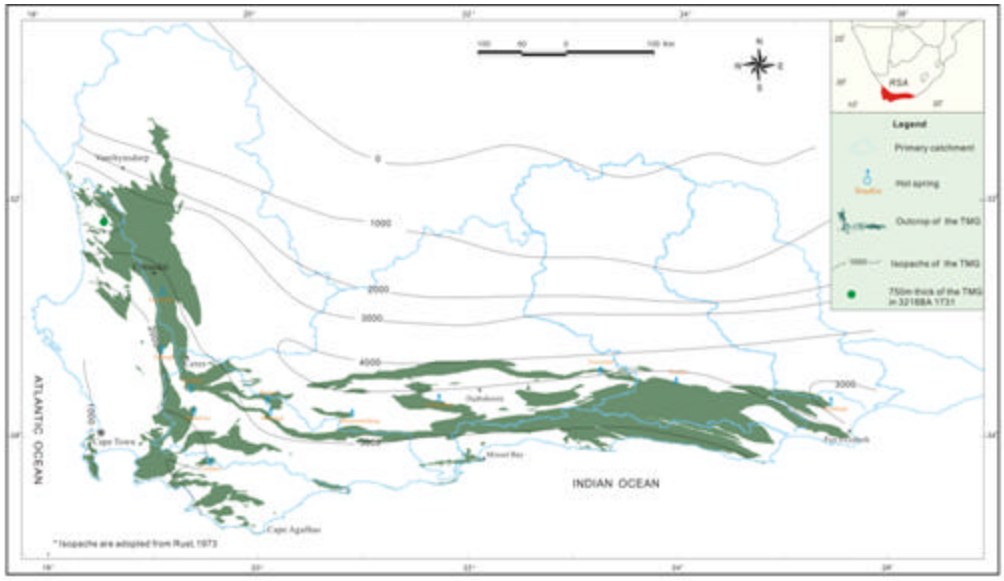

Figure 4.3 Isopach of the Table Mountain Group

The name of the Peninsula Formation is derived from the Cape Peninsula (Rust, 1967), where the full succession (550m) is exposed against Table Mountain. It comprises a succession of coarse-grained, white quartz arenite with scattered small pebbles and discrete thin beds of a matrix-supported conglomerate. The formation reaches a thickness of about 1800m at Clanwilliam in the west (Rust, 1967), but is reportedly much thicker (Rust, 1973; Johnson, 1991) in the Eastern Cape. The exact thickness is difficult to measure due to the severe folding and unknown amounts of thickening due to thrusting (Booth and Shone, 1992) within the formation. It is noticed that the residual thickness of the TMG (as stated above) is very different from borehole to borehole. The determination of formation thickness is also impeded by the general lack of marker beds. In the Cape Peninsula, Fuller and Broquet (1990) identified two informal members within the formation that are separated by a meter of clast-supported conglomerate (probably equating with the Slanghoek Member of Rust, 1967). The Pakhuis Formation occurs above the Peninsula Formation and comprises a 40m which succession of glacially derived sediments, but is restricted to the Southwestern Cape (Broquet, 1992; Rust, 1967).

The Cederberg Formation with a thickness of 50-120m comprises shale, siltstone and silty sandstone. It is prominently a marker band between the Peninsula Formation and the Nardouw Subgroup. It is a hydrodynamic and recharge boundary.

The Nardouw Subgroup, with its three subdivisions, the Goudini, Skurweberg and Rietvlei (Baviaanskloof in the Eastern Cape) Formations, is another thick (maximum 1200m) unit of sandstone that varies between quartz arenite, silty and feldspathic arenites, accompanied by minor inter-bedded conglomerate and shale. This lithological diversity, together with textural, grain size and bedding thickness differences, lead to pronounced differences in weathering, structural and hydrogeological characteristics. The basal unit, the Goudini Formation, is characterised by reddish weathering, thin sandstone beds with common shale intercalations. The Skurweberg Formation is thick-bedded arenite. The topmost unit, the Rietvlei Formation contains more feldspar and is characterised in the field by a vegetation growing on it. The contact with the overlying dark shale of the Bokkeveld Group is usually abrupt.

Basement rocks are comprised of the Maalgaten Granite and a variety of sedimentary and metamorphic rocks, respectively belonging largely to the Cango and Kaaimans Groups. Basement rocks are exposed south of the Outeniqua Mountains and north of the Cango Fault Zone in the south and north, respectively (Figure 4.3). The cratonic sheet sandstones (Rust, 1967; Tankard et al., 1982) of the TMG in the lowest part of the Cape Supergroup form the backbone of CFB from Vanrhynsdorp in the west to Port Elizabeth in the east.

Alluvial valley deposits are associated with the larger river channels, while colluvial (slope) deposits produced by sheet-wash, occur on gently sloping surfaces away from the river channels.

4.3 REGIONAL STRUCTURE

The entire geological succession of the CFB was subjected to severe north-south orientated compressive stresses during the Cape Orogeny. This resulted in a variety of geological features and structures. Figure 4.4 shows the tectonic pattern and outline of structures. The CFB consists of two branches, namely western branch and southern branch, which form the characteristic mountain chain along the southern and part of the western coasts of South Africa. The western and southern branches of the CFB meet in a 100 km wide syntaxis area, comprising NE-trending folds situated between Ceres and Gansbaai (approximately 200 km to the west of the study area).

In the Southern Cape and Klein Karoo, the southern branch of the CFB comprises a 900 km long gently arcuate belt. The more resistant strata of the group form prominent E-W trending mountain ranges, that is Swartberg, Rooiberg, Gamkaberg, Kammanassie and Outeniqua Mountains.

The above-mentioned mountain ranges are separated by synclinal intermountane basins. The resistant quartzites are exposed in the cores of anticlinal mountains and form a rugged topography. The valleys are broad and due to the underlying less resistant Bokkeveld Group sediments.

The compressional deformation during the Cape Orogeny was followed by extensional tectonic, during which the Uitenhage Group was deposited within a number of fault-bounded basins, reaching a thickness of > 2000m in places. The examples of the extensional tectonics include the following (Duvenhage et al., 1993):

- Reverse faults associated with over-folding, during the Cape Orogeny;
- The Cango Fault (CF), a reverse fault on a previous thrust fault plane; and
- Several normal faults of the post-Cretaceous age.

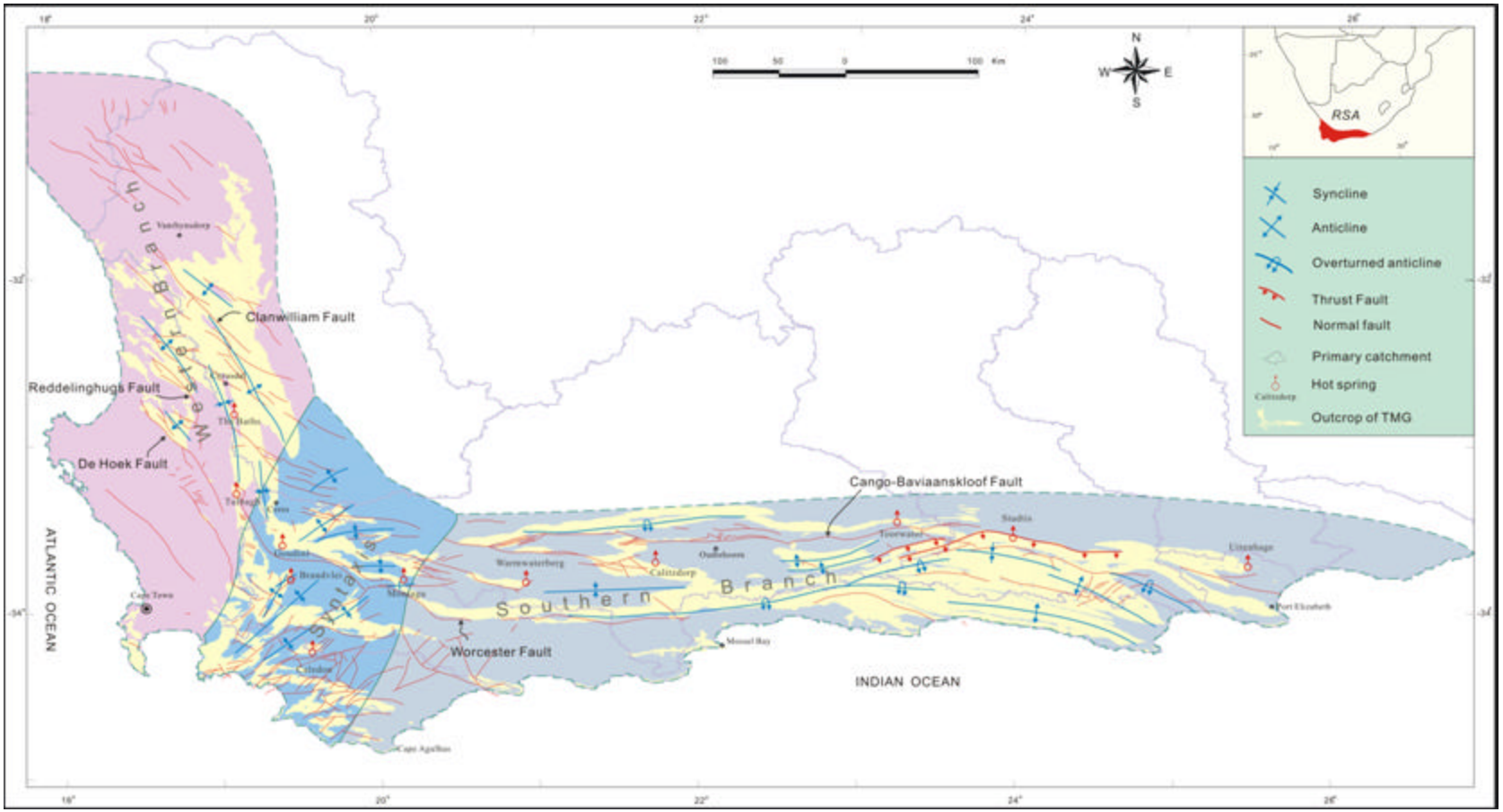

Figure 4.4 Sketch of the structure in the study area

(Faults are adapted from Council for Geoscience, 1997)

Several examples of recent tectonic activity (neotectonics) exist in the south-eastern Cape (Andreoli et al, 1989; Hill, 1988; Hattingh and Goedhart, 1997; Hartnady, 1998) and Karoo (Woodford and Chevallier, 1998). The tectonic activity suggests that an extensional tectonic regime continues to prevail, with an extension in a NNE-SSW direction and compression in a WNW-ESE direction. These were associated with the following events:

- Cape Orogeny: N-S, NW-SE, NE-SW, E-W (thrusting) systems.
- Gondwana break-up (extensional tectonics): development of E-W oblique shears.
- Extension with a right-lateral shear component and reactivation of earlier fractures (E-W, WNW, and N-S).
- Tertiary to present time: continuation of the extensional stress regime in a NNE-SSW direction.

The E-W striking system consists of long, continuous E-W and WNW trending faults extending across the entire study area, of which only the most prominent faults, with large displacements, are shown on the 1: 250 000 scale geological maps. The satellite lineament map, therefore, provides a much more complete representation of the most predominant fracture sets, which are E-W, WNW and ENE trending fracture sets (more fractures and longer extent) in the east section of the TMG.

The N-S trending fracture system consisted of shorter, more discontinuous fractures, which generally corresponded to a dense network of NNW-SSE, NNE-SSW trending joints (forming a conjugate) and less prominent N-S trending joints, often not showing any displacements on geological maps or satellite images. These fractures or joints can be very penetrative and form prominent morphotectonic features.

The observed fracture pattern is the combined result of at least two major tectonic events, that is the Cape Orogeny (280-220 million years ago) and the fragmentation of

Gondwanaland (200-123 million years ago). Most of the E-W trending fractures represent normal faults, with variable components of oblique, often right lateral movement, associated with continental break-up. WNW trending fractures may represent Riedel-shears, while ENE trending fractures may represent the P-shear direction.

However, the orientation of thrust faults formed during the Cape Orogeny were also E-W trending or parallel and curvilinear with respect to the general trend of the CFB. Extensive field mapping and construction of balanced cross-sections was the only way to determine the abundance of thrust faulting relative to normal faulting. Normal faulting seemed to have controlled the emplacement of dolerite dykes in the Western Karoo and deposition of the Uitenhage Group and even high-level terrace deposits.

North-south trending fractures display large variations in geographic distribution. The Kammanassie and Rooiberg Anticlines have by far the highest density of fractures and joints, of which the majority were most probably related to the Cape Orogeny. The NNW, NNE and NS trending fractures have left a strong overprint over the CFB structures. Some of the lineaments crossing the Uitenhage Group outcrops were older than the fractures. Some regional faults, with more than 50km in length related to hydrodynamic system and recharge boundary, are listed in Table 4.1.

Table 4.1 General characteristics of mega faults in the CFB

Name	Characteristics
Clanwilliam Fault	Normal fault NE/SE, extends more than 90km.
Leipoldtville Fault	>50km, through Piekenierskloof Formation.
Redelinghuge Fault	>50km, NW strike in northwest and NS in south section.
Theerivier Fault	>50km, NW-SE strike, near anticline axis.
De Hoek Fault	>90km, NW-SE strike, inflexion point locates nearby De Hoek.
Touwsriver Fault	>70km, NWW-SSE,
Worcester Fault	>100km, Thrust fault.
Cango-Baviaanskloof Fault	The Cango Fault Zone (CFZ), previously known as the Swartbergverskuiwing (Du Preez, 1965), is a prominent east west striking regional structure, dipping approximately 70º to the south. The CFZ starts east of Ladismith and continues past Uniondale (the eastern and western boundaries of the study area) over a distance of more than 220 km. The CFZ has a span of almost 7000 m and has exposed pre-Cape rocks to the north. This block of pre-Cape rocks, bounded by the Swartberg in the north and Enon Formation in the south, is known as the Cango Inlier.
Olifants Fault System	NW/SE-striking faults crossing the area, form a sub-parallel, continuous, intercontinuous, interconnected system, extending over distances of more than 100 km. Together these systems constitute four megafault zones, i.e. Saron-Aurora Megafault (SAM), Gydo-Verlorevlei Megafault(GVM), Twee Riviere-Liepoldtville Megafault(TLM), Krakadouw-Klawer Megafault(KKM).
Suurbraak Fault	>100km, EW, wave strike, normal fault.
Outeniqua Mountains Fault	>100km, arch fault, strata reverse.
Genadendal Fault	>100km, arch fault, NW-SE strike in West section, EW strike in middle section, NEE in east section, wave.
Hawston - Middleton Fault Zone	>70km, NE to NEE strike fault group.

Chapter 5

Aquifer Settings

5.1 INTRODUCTION

Approximately outcrop areas of 37 000 km^2 of the TMG distribute within an area of 248 000km^2 in the Western and Eastern Cape Provinces, South Africa. The TMG comprises about 4 000m thick sequence of quartz arenite, which form the TMG Super Aquifer. Information of climate, hydrology, geomorphology and geology are used to develop conceptual models of recharge in the TMG system.

The TMG area has been subdivided into groundwater regions on the basis of both lithostratigraphy and physiography, namely crystalline metamorphic and igneous, intrusive, extrusive, sedimentary and composite (Vegter, 2001). There are twenty one groundwater regions shown in Figure 5.1, in which six groundwater regions in the north of the TMG may have hydraulic connectivity at depth, namely to Bushmanland Pan Belt (35), Hantam (36), Tanqua Karoo (37), Western Great Karoo (41), Southern Highland (40) and Eastern Great Karoo (42).

In earlier studies, four sections of the entire TMG Super Aquifer were outlined, based on different thickness of geological successions or their positions in the CFB and on associated tectonic regimes present (Figure 5.2):

A. The Western TMG Section (A), the CAGE study – Hartnady and Hay (2000).
B. The Agter-Witzenberg and Ceres-Hex River (B) – Central TMG Section, Rosewarne (1984), Kotze and Rosewarne (1997) and Weaver et al. (1999).
C. The TMG Aquifer in the Klein Karoo Section (C), Kotze (2001).
D. The Eastern TMG Section, Murray (1996).

The above-mentioned case studies have indicated that significant differences in fracturing and faulting styles, lithological sequences, recharge and natural discharge (springs) prevail in each section of the TMG Aquifer. Informally named aquizones were made for outside or apart from the formal hydrogeological hierarchy (Al-Aswad and Al-Bassam, 1997; Kotze, 2002).

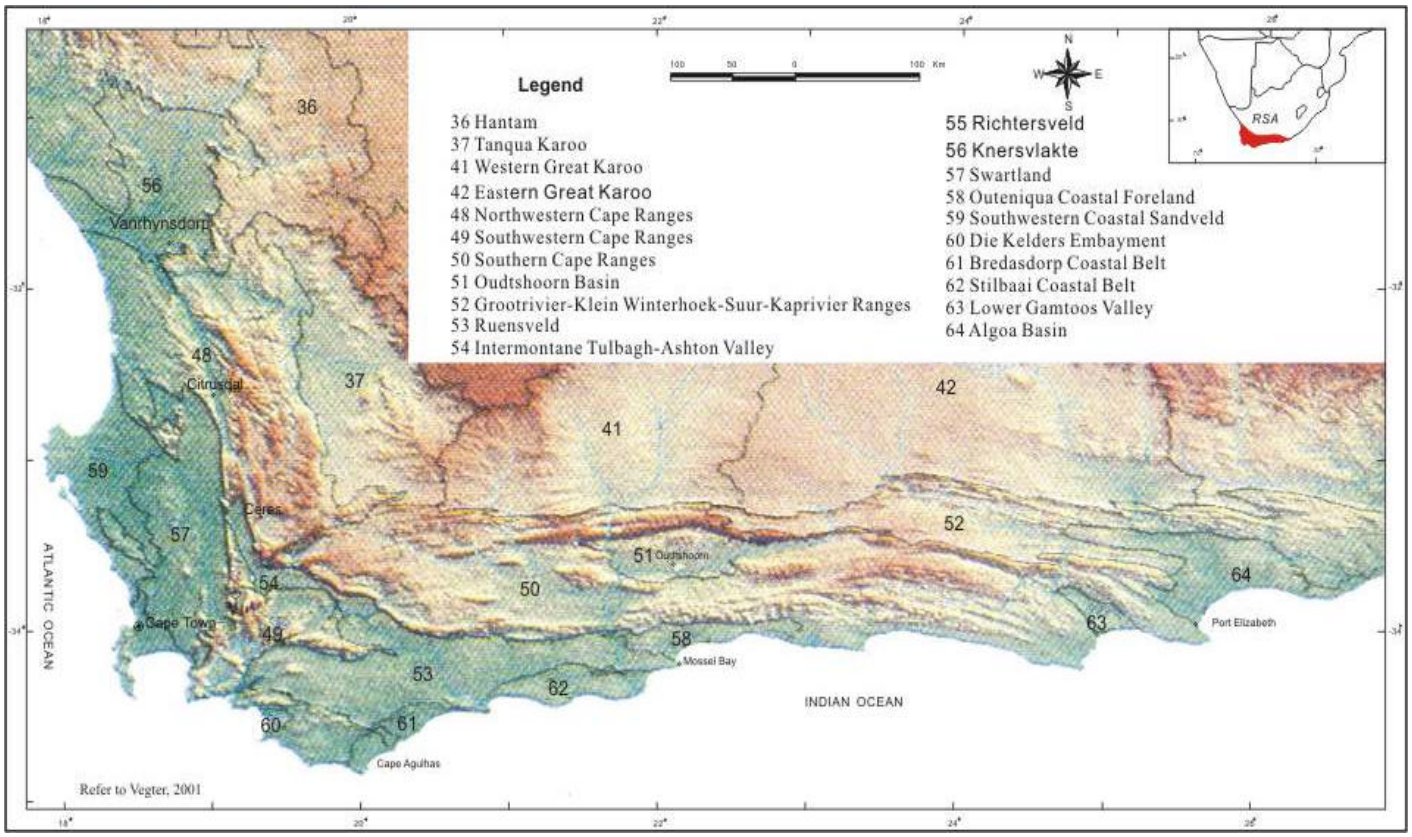

Figure 5.1 Groundwater regions in the TMG area (After Vegter, 2001)

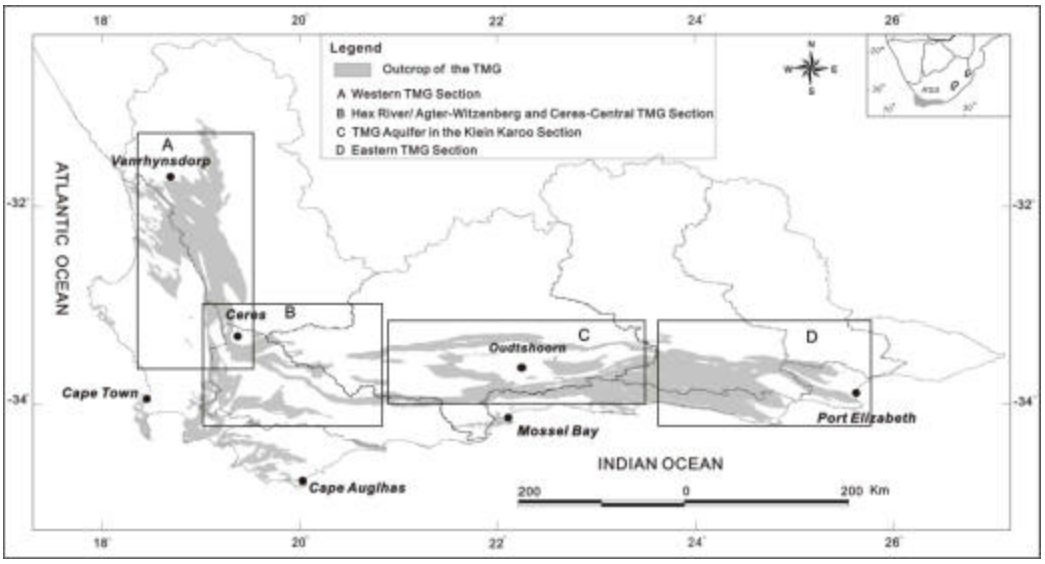

Figure 5.2 Four sections of the TMG aquifer in early studies

The interpretation of satellite imagery, structural, hydrochemistry and hydrogeological data were collated to define the conceptual hydrogeological model for the Klein Karoo Section of the TMG aquifer. For delineation of fractured rock aquifer at a local scale, a term, namely Keystone Block was put forward by Kotze (2002).

This chapter aims to study the hydrogeological outline including the type of aquifer system, hydrogeological boundary, identification of the hydrogeological unit and hydrogeochemical characteristics of the aquifer systems.

5. 2 AQUIFER SYSTEMS OF THE TMG

5.2.1 Generic model

Generally a hydrodynamic aquifer system has three elements, namely aquifer, aquitard and hydraulically impermeable boundaries, and possesses a recharge area, a flow area and a discharge area as well (Figure 5.3). In some cases, the discharge area is very close to the recharge area or even overlap, so the flow path is short.

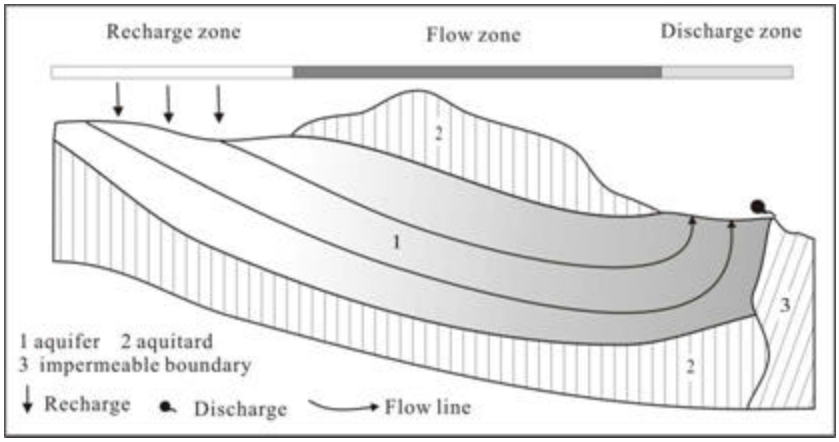

Figure 5.3 Elements of the hydrodynamic system

5.2.2 Types of the TMG aquifer

Folded and fractured rock aquifer systems are domination in the TMG area. The TMG aquifers, i.e. geological units with economically exploitable groundwater quantities, are classified as secondary aquifers. Extensive folding and faulting gave rise to the secondary porosity during several tectonic events. The style of fracturing and folding depends on the matrix and regional tectonics of the fracture pattern. The following TMG aquifer systems are presented in the TMG area:

- Horizontal terrane aquifer system
- Inclined strata aquifer system
- Folded strata aquifer system
  - Syncline aquifer sub system
  - Anticline aquifer sub system

- Fracture zone aquifer system
- Weathered rock (crust) aquifer system (not discussed here)

5.2.2.1 Horizontal terrane aquifer

Two types of aquifer occur in a horizontal terrane, namely perched and unconfined aquifers. An example is Platteklip Gorge Spring as can be seen in Figure 5.4. The issue point of the spring is on an interface of the Peninsula and Graafwater Formation.

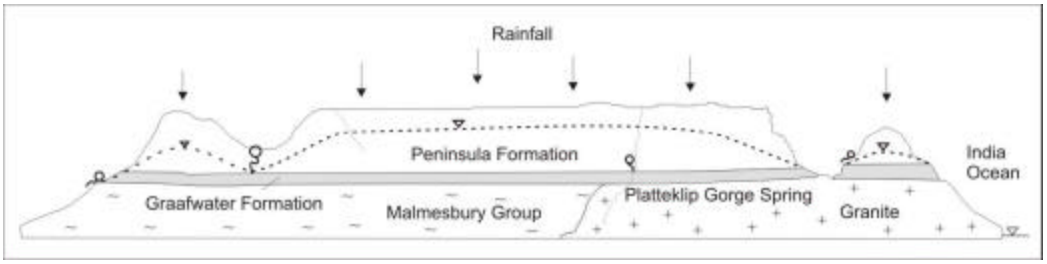

Figure 5.4 Horizontal terrane aquifer in the Table Mountain

5.2.2.2 Folded strata aquifer system

The folded TMG aquifer system includes syncline and anticline sub systems. The syncline sub system located in basin area is a permeable rock layer within low permeable rock layers. Four typical configurations, namely fault-fold-lithology controlled, fold-lithology controlled, leakage and overflow system, are shown in Figure 5.5. The anticline aquifer sub system distributes a core of the anticline with wide-open fractures, such as the Kammanassie mega-fold (refer to Figure 8.6).

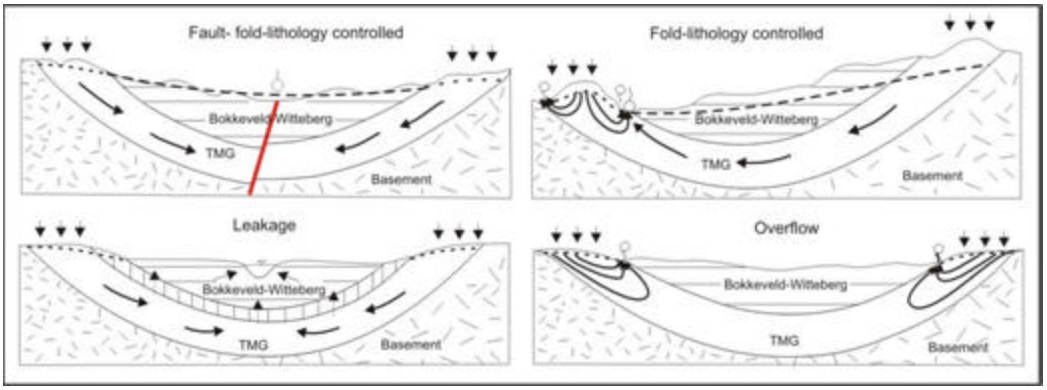

Figure 5.5 Models of syncline aquifer systems

5.2.2.3 Fracture zone aquifer system

According to the hydrogeological function of a fracture, five types are classified as follows (Sheng et al., 1985):

- Fracture: Tensile, the permeability of this fault is larger than the hanging wall and footwall.
- Fracture conduit: Connecting different aquifers or aquifer system, for example the Brandvlei Fault.
- Impermeable fracture, such as Wemmershoek Fault, Worcester Fault, Cango Fault. The permeability of the faults is much smaller than that of the hanging wall and footwall.
- Storage fracture is defined as a closed storage space in a fault zone.
- No water fracture, which a fault with no water-runs where there is no storage space and very low permeability in these fault zones.

The heterogenous and anisotropic fractured rock aquifer system comprises an open fracture, conduit and hydraulic boundary (impermeable fault) as can be seen in Figure 5.6. The following points are illustrated:

1) Fractures are divided into open, closed and infilled fractures.
2) Fracture density is related to the thickness of the layer of lithology.
3) Conduits, storage as well as exclusion of groundwater can be present in a fracture.
4) There are weathered and tectonic fractured rock aquifer systems.
5) Hydraulically connected aquifers occur in different aquifers by conduit fractures.
6) In a fracture zone aquifer system, groundwater can be obtained at another side of the mountain and the opposite bank of the river as well.
7) Cool water occurs in local flow, but thermal water can occur in regional flow, which may flow along the TMG buried by thick younger formations in basin area.

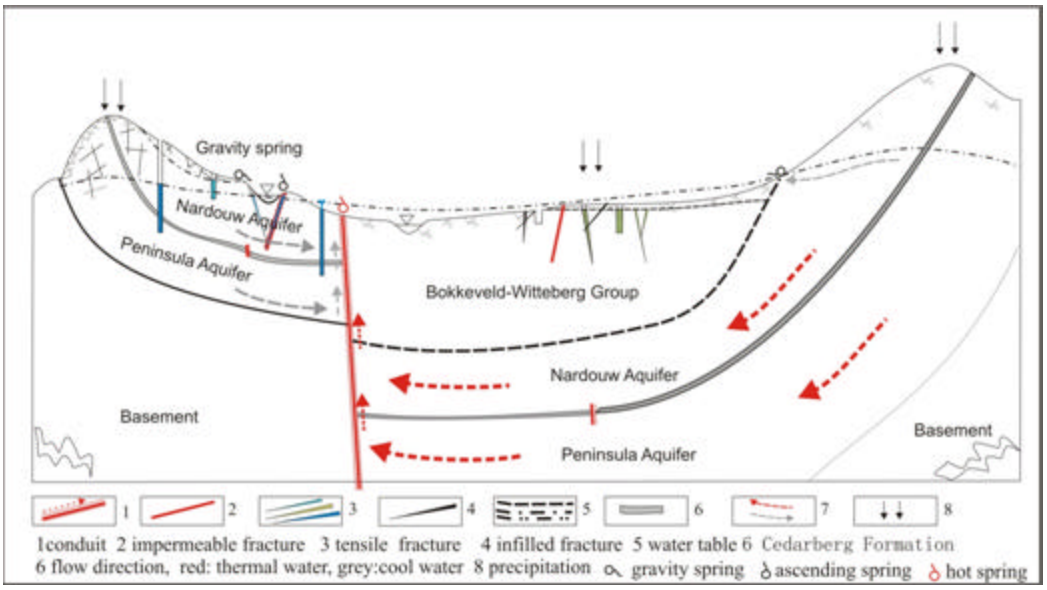

Figure 5.6 A model of the TMG fractured rock aquifer system

5.2.3 Composite aquifer system

An independent aquifer system usually occurs locally, but regional aquifer systems are always complex and synthetically produced. Different aquifer systems may connect to each other through the faults or leakage layers. The composite aquifer systems are

1) The monocline -fault aquifer system [Cape Peninsula]
2) The syncline-fault aquifer system [Montagu, Witzenberg]
3) The anticline-fault aquifer system [Vermaaks River Valley]
4) The syncline-anticline-fault (fold-fault) aquifer system [Brandvlei]

5.3 HYDROGEOLOGICAL BOUNDARY OF THE TMGAQUIFER

5.3.1 Lithology

Lithology may control springs occurrences due to the impedance or presence of impermeable layers. Springs discharge at contact zones with interbeds and lithological boundaries, such as the Bokkeveld, the Malmesbury, the Kango and the Namap Group and the Cedarberg Formation. There are a few well-known Cedarberg Formation

related springs, such as Hoeksberg Spring (south of McGregor), Vermaaks Spring, Marnewicks Spring, the Meirings, the Swartberg Spring (feeding the Dorps River at Price Albert) and the Humansdorp Spring.

5.3.2 Faults

A regional fault is normally a structural boundary as well as a hydrogeological boundary. Most of the regional faults are impermeable boundaries, but fault branches are tensile faults, which are excellent infiltration paths.

There are fault-controlled hot springs, occurring from Citrusdal in the west to Uitenhage in the east. The alignment of these springs follows a remarkable imagining curved line, which appears to mimic the shape of CFB (refer to Figure 4.4). The alignment of these springs may be meaningful in terms of the deeper CFB structure (Meyer, 2002). The major fault controlled springs have the following characteristics:

- They all come out of conduits in competent, fractured and fissured quartzitic-sandstone of the TMG, which are in all instances faulted against, or are in contact with the incompetent Cedarberg Formation and Bokkeveld and Uitenhage Groups aquicludes.
- They are hypothermal springs, with water temperatures in excess of 20°C. They are thus all relatively deep circulating springs. The yields range from 9 to 127 $\ell \cdot s^{-1}$ with limited seasonal fluctuations.
- The ECs of the groundwater do not exceed 35 $mS \cdot m^{-1}$. The dominant chemical determinants of the groundwater are sodium and chloride. Hydroxides of iron and/or manganese, ranging between 0.1 and 2.0 $mg \cdot \ell^{-1}$, have been recorded in most of them.

5.3.3 Drainage system

A watershed is usually a groundwater recharge boundary, but groundwater recharge can be obtained from vicinity catchments through fracture networks. In most cases, primary and secondary catchment boundaries are related to structures or are one of hydrodynamic boundaries in the TMG area (Figure 5.7). The main river, which is a very active hydrogeological boundary, is not only a discharge area but also a source of recharge. Most of the perennial rivers occur in the discharge areas of the TMG aquifer, such as the Olifants River (Olifants Doorn area), Great Berg River, Breede River, Gourits River (Figure 5.7). The Indian and Atlantic Oceans are important groundwater discharge zones for the TMG aquifer. Groundwater discharges directly into the oceans in most of the southern coast from Strand to Port Elizabeth.

Some important hydrogeological boundaries are used in identifying of hydrogeological units, namely fault, lithologies, rivers and oceans, are listed in Table 5.1.

Table 5.1 Types of hydrogeological boundary in the TMG area

Boundary	Class	Name / Characteristics
Fault	Regional, >50km,	Clanwilliam Fault, Leipoldtville fault, Redelinghuis Fault, Theerivier faults, De Hoek Fault, Touwsriver fault, Worcester Fault, Cango-Baviaanskloof Fault, Olifants fault system, Suurbraak fault, Outeniqua mountains fault, Genadendal fault, Hawston - Middleton fault Zone, Baviaanskloof Mountains thrust fault etc.
Lithology/ Stratigraphy	Group, Formation	Group: Malmesbury, Kango, Namap, Bokkeveld, Witteberg, Dwyka, Ecca, Beaufort, Uitenhage Formation: Cedarberg
River	Main branch, perennial	Olifans (Western coast), Great Berg, Breede River, Sonderend, Touws, Groot, Gourits, Gamka, Olifans (Calitzsdorp), Kammanassie, Gamtoos, Swartkops.
Drainage Oceans	Primary catchment	E, F, G, H, L, M, N Atlantic Ocean and India Ocean

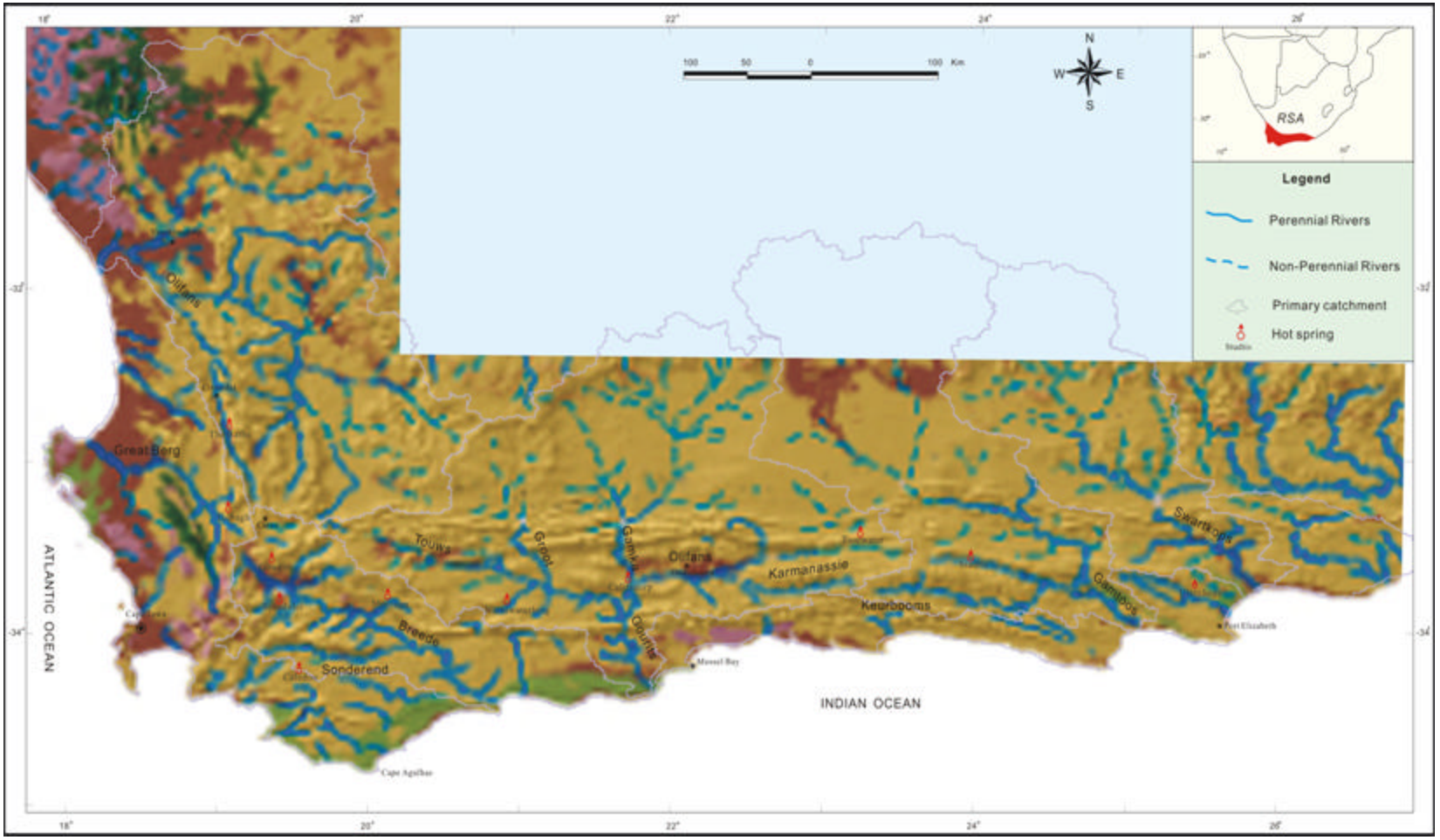

Figure 5.7 Drainage systems in the TMG area

5.4 HYDROGEOLOGICAL UNITS

According to the similarity of hydrogeological properties of the TMG, nineteen hydrogeological units were identified, covering the area of 248 000km^2 in the Western and Eastern Cape provinces (Figure5.8). The general characteristics of the hydrogeological units are listed in Table 5.2.

Table 5.2 Hydrogeological units in the TMG area

Unit no	Name	Boundary	Characteristics and Stratigraphy
0	Karoo	North: Zero deposit boundary of the TMG, South: End of the outcrop of the TMG	The TMG aquifers are covered by younger Formations. Recharge comes from an outcrop of the TMG in the southern area. Stratigraphy involved: Dl, Dbi, C-Pd, Pt, Ppw, Pr, Pa, Pf, Pwa; Ope, Sn.
1	Vanrhynsdorp	North: End of outcrop of the TMG; South: Clanwilliam Fault. Cango-Baviaanskloof Fault, Baviaanskl thrust Fault.	Anticline is dominant. Stratigraphy involved: C-P, Dc, Dw, Tra-Tra; Ope, Sn.
2	Clanwilliam	North: Clanwilliam Fault; South: Leipoldtville Fault	Anticline–syncline-anticline –Fault system. The strata are NW-SE trend. Stratigraphy involved: Ng, ?kn, Dc, Dbi, Tra-Tra, Op, Ope, Sn.
3	Piketberg	North: Leipoldtville Fault (NW-SE); South: De Hoek Fault (NW-SE)	Anticline -Fault fracture aquifer system. Stratigraphy involved: Np, Npo, Nbi, ?k, Op, Ope, Sn
4	Wellington	North, De Hoek Fault (NW-SE), Worcester Fault (NE-SE to E-W) South: Mooreesburg-Wellington ((NW-SE)-Paarl-Franschhoek (NWW-SEE) East: Brandvlei (NE-SW)	Fault-anticline aquifer system. Stratigraphy involved: Nno, Nbi, Ny, Nki, N-?w, N-? m and Ope, Sn
5	Stellenbosch	North: Mooreesburg-Wellington ((NW-SE)-Paarl-Franschhoek (NWW-SEE); South: Table Mountain East: Franschhoek-Stellenbosch Fault (NE-SW).	Fault aquifer system. Stratigraphy involved: ? g, N-?k, N-?s, Nf, ?k, Nty; Ope
6	Cape Peninsula	Cape Peninsula, Atlant ic Ocean	Monocline aquifer system, TMG is located on top of Malmesbury Group (?cc) and granite.
7	Ceres	North: Theeriver Fault (NW-SE) and Touwsriver Fault (E-W); South: Worcester Fault (NE-SE to E-W); East: Hex River Fault (NE-SW)	Fault controlled aquifer system. Stratigraphy involved: Npo, Nbr, C-Pd, Dbi, Dc, Dw; Ope, Sn

Table 5.2 Hydrogeological units in the TMG (continued)

Unit No	Name	Boundary	Characteristics and Stratigraphy
8	Worcester	North: Worcester Fault (NE-SE to E-W) West: Brandvlei Fault (NE-SW) and Franschhoek-Stellenbosch Fault (NE-SW). East: Betty's Bay-Botriver-Berea Fault Zone (NE-SW) and Robertson Fault (NE-SW)	An anticline-syncline-fault aquifer system. Stratigraphy involved: N-?, Nf, Ppw, C-Pd; Ope, Sn
9	Montagu	North: Touwsriver - Herbertsdale Fault Zone (NW-SE) South: Worcester- Swellendam - Herbertsdale Fault Zone West: Hex River Fault (NE-SW)	Fault-syncline aquifer system. Stratigraphy involved: N - ? Dbi, Dc, Dl, Dw; Ope, Sn
10	Bonnievale	North: Worcester- Swellendam Fault South: Berea-Greyton-Stormsvlei Fault (E-W) and Wydgelee Fault. East: Bontebok Fault (NW-SE) West: Robertson Fault (NE-SW)	Fault-syncline aquifer system. Stratigraphy involved: N- ?, Nf, Dbi, Dw, Je, Ope, Sn
11	Caledon	North: Berea-Greyton - Stormsvlei Fault (E-W) and Wydgelee Fault (NW-SE). East: Bontebok Fault (NW-SE) West: Betty's Bay-Botriver-Berea Fault Zone (NE-SW) South: Coast line	Fault controlled aquifer systems. Stratigraphy involved: N- ?, Nty, Dbi, Dc, Je, T-Qb, Qst; Ope, Sn
12	Riversdale	North: Worcester- Swellendam - Herbertsdale Fault Zone South: Coast line West: Bontebok Fault (NW-SE) East: drainage boundary	Fault aquifer system and monocline aquifer system. Stratigraphy involved: Dc, Dbi, Dc, Dw, Je, J-K, T-Qb; Ope, Sn
13	Swartberg	North: End of outcrop of the TMG; South: Ladismith Fault (E-W) and Cango Fault (E-W)	Fault – overturned anticline aquifer system. Stratigraphy involved: Nk, Dt, Je; Ope, Sn
14	Oudtshoorn	North: Ladismith Fault (E-W) and Cango Fault (E-W); Northwest: Touws Fault zones Northeast: Baviaanskloof Fault zone South: watershed.	Fault- fold aquifer system. Stratigraphy involved: Dbi, Dc, Dt, Dw, J-K, Kb; Ope, Sn
15	George	North: Watershed; South: Coast line; West: Drainage; East: Outeniqua Fault zone	Fault-monocline aquifer system Stratigraphy involved: N- ? g, Nka, Tg, T-Qb, J-K, Ope, Sn
16	Studis	North: End of the outcrop of the TMG (Baviaanskloof Trust Fault); South: Kouga Fault zone	Fault- syncline aquifer system. Stratigraphy involved: Nk, Je; Ope, Sn
17	Humansdorp	North: Kouga Fault zone South: Coast line	Fault-anticline aquifer system. Stratigraphy involved: Dc, Je, J-K; Ope, Sn
18	Uitenhage	North: End of the outcrop of the TMG; South: Coast line	Fault-anticline aquifer system. Stratigraphy involved: Nga, Ks, Qsc; Ope, Sn

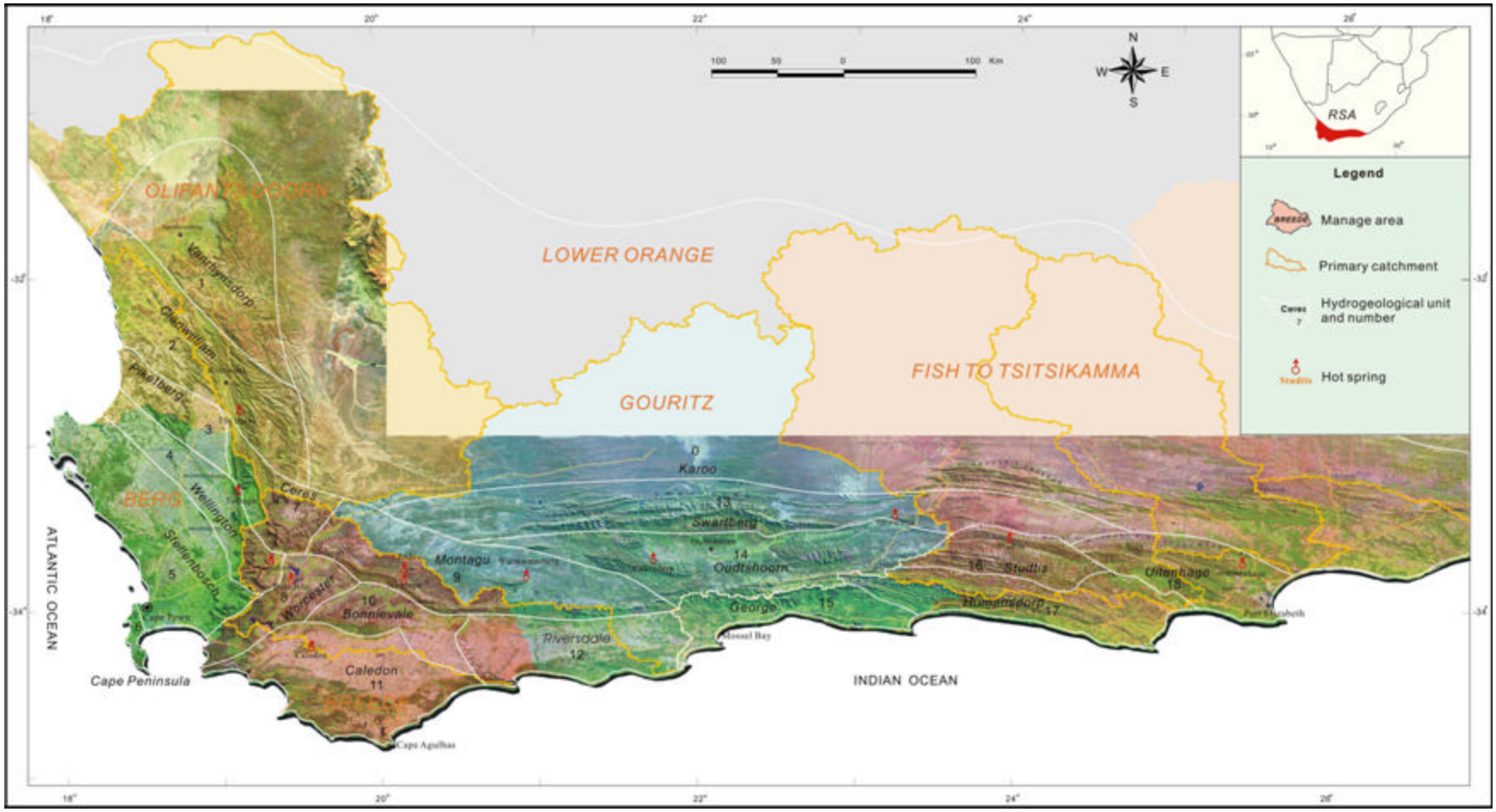

Figure 5.8 Hydro geological units in the TMG area

5.5 HYDROGEOCHEMICAL CHARACTERISTICS OF THE TMG AQUIFER

The statistical analysis was based on chemical data of 98 samples distributed throughout the whole TMG area (collected from NGDB and Vegter, 1995 a, b), in which 89 samples were taken from the Peninsula Aquifer. The major ion patterns in the groundwater are predominately (Table 5.3). A Cl-Na type water occurs based on Durov's hydrogeochemical classification system (Figure 5.9).

Table 5.3 Water qualities in the TMG aquifer (unit: $mg \cdot \ell^{-1}$; EC: $mS \cdot m^{-1}$)

Item	EC	TDS	pH	K^+	Na^+	Ca^{2+}	Mg^{2+}	F^-	Cl^-	HCO_3^-	NO_3^--N	SO_4^{2-}	PO_4^{3-}	SiO_2
Minimum	5.0	21.0	4.2	0.1	3.9	0.5	0.7	0.01	7.4	0.4	0.01	0.2	0.01	4.9
Average	14.8	83.4	6.0	2.0	16.8	3.8	2.6	0.15	28.6	16.140	1.88	5.4	0.03	13.4
Maximum	53.0	189.0	7.6	10.0	46.0	18.0	7.1	0.49	82.0	85.440	17.90	18.9	0.16	37.9
Stand. dev	8.4	42.6	0.8	2.5	9.6	4.0	1.5	0.13	17.1	17.9	3.42	4.5	0.03	8.4

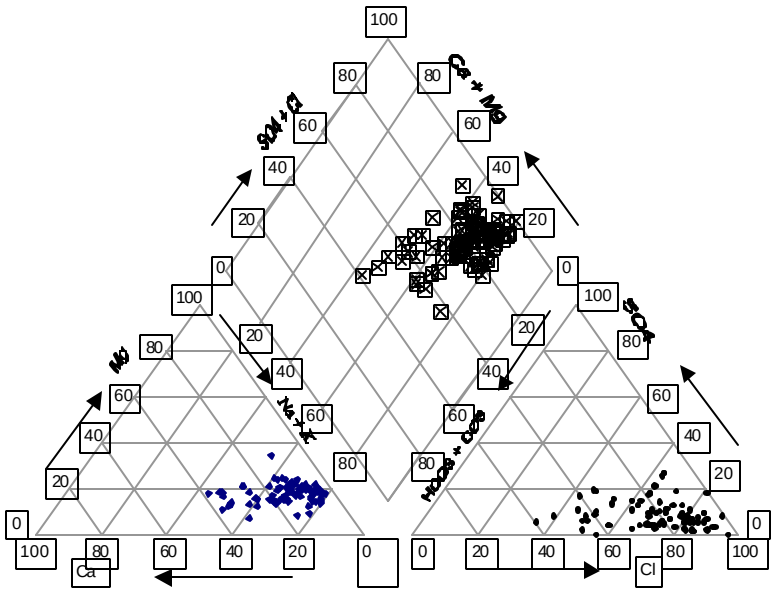

Figure 5.9 Piper diagram of hydrochemistry in the TMG aquifer

5.5.1 Chloride concentration in the TMG aquifer

The analysis results of the 98 samples were used to calculate the background value of

chloride in the TMG aquifer. Figure 5.10 shows the characteristics of chloride concentration. Most of them are less than 40mg·ℓ^{-1}. The distribution of the concentration is shown in Figure 5.11. The frequency is 32.7%, 24.5%, 15.3% for concentrations of 10-20mg·ℓ^{-1}, 20-30mg·ℓ^{-1} and 30-40mg·ℓ^{-1}, respectively. The frequency is 8.2% in 50-60mg·ℓ^{-1} and 60-70mg·ℓ^{-1}. The concentration can be divided into two levels, which are 10-40 mg·ℓ^{-1} and 50-70mg·ℓ^{-1}.

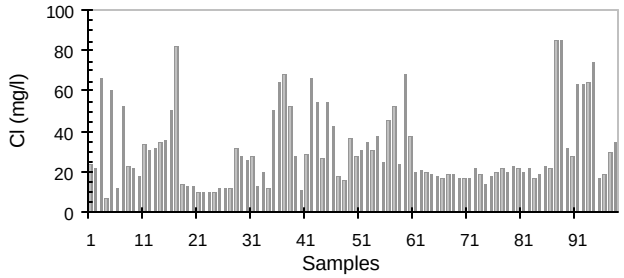

Figure 5.10 Chloride concentrations in the TMG aquifer

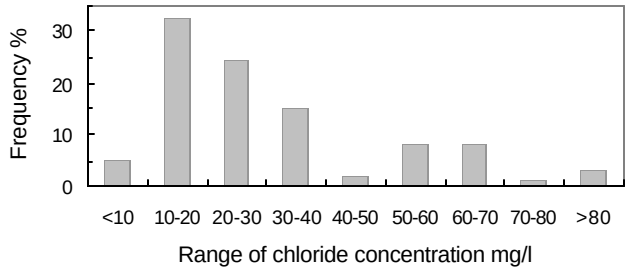

Figure 5.11 Frequency of chloride concentrations in the TMG aquifer

The statistical analysis results of the 98 chloride concentrations are listed in Table 5.4. The discrepancies between arithmetic and harmonic and geometrical are 38%, and 18%, respectively. Therefore the error would be introduced in the recharge estimation using different mean value. There are large errors when the resultant concentration lies between x' +s to x'+3s, so the chloride mass balance method cannot be used to estimated the recharge rate under these conditions.

Table 5.4 Chloride concentrations of the TMG aquifer (mg·ℓ^{-1})

Type	Mean	x' +s [1)]	x'+2s	x'+3s	x'-s
Arithmetic	30.9	50.1	69.1	88.1	7.12
Geometrical	26.2	45.2	64.3	83.4	11.9
Harmonic	22.5	41.6	60.6	79.7	3.43

[1)] s - standard deviation

The population mean and the interval of the chloride concentration for 95% and 90% confidence are listed in Table 5.5. The confidence of the samples indicated that the interval of chloride concentration increases with decreasing sample size. For instance, the interval is 22.4-29.9mg·ℓ^{-1} for 100 sample sizes, but 4.56- 47.8mg·ℓ^{-1} for 3 sizes. In other words, the error [(max-min)/max] is 25% when the sample size is 100; but the error is 90% when the sample size is 3.

Table 5.5 Confidence of the chloride concentration

Conditions	a=0.05,s=19.1, mean=30.9						a=0.1,s=19.1, mean=30.9					
Sample size	100	50	20	10	5	3	100	50	20	10	5	3
Confidence	3.74	5.29	8.37	11.8	16.7	21.6	3.14	4.44	7.02	9.93	14	15.9
Maximum (mg·ℓ^{-1})	29.9	31.5	34.5	38	42.9	47.8	29.3	30.6	33.2	36.1	40.2	42.1
Minimum (mg·ℓ^{-1})	22.4	20.9	17.8	14.3	9.44	4.56	23	21.7	19.2	16.2	12.1	10.3

5.5.2 Chloride in the other aquifers of the study area

In comparison to chloride concentration in the TMG aquifer, the chloride concentrations in the other aquifers of the study area are illustrated in Table 5. 6. Large differences of the concentration occur between the TMG aquifer and the aquifers around the TMG due to lithology. A very low recharge rate would be produced based on the chloride concentration presented in Table 5.6 if equation (3.1) is adopted. This may be the reason why the CMB method cannot be used to estimate the recharge rate in the aquifer with high background concentration values of chloride, which comes from multiple sources. A contour map of chloride concentration of rainfall is constructed as shown in Figure 5.12. If the chloride concentration of rainfall is taken

from the map and the concentration of groundwater taken from the Table 5.6, large difference in recharge rate should occur in the same contour of chloride concentration due to different chloride concentration of groundwater in the aquifers. It is worth mentioning that the contour of chloride concentration of rainfall is not accurate, this is beyond the study, and this is left for future work.

Table 5.6 Chloride concentrations in the surrounding aquifers of the TMG

Aquifer (Group or Formation)	Maximum ($mg \cdot \ell^{-1}$)	Minimum ($mg \cdot \ell^{-1}$)	Mean ($mg \cdot \ell^{-1}$)	Sample size
Malmesbury	3196.0	37.0	636.6	9
Cape Granite	688.0	86.0	365.6	5
Bokkeveld	4393.0	112.0	1092.7	9
Witteberg	1638.0	71.0	595.4	7
Dwyka	1984.0	53.0	673.0	7
Ecca	1550.0	104.0	519.2	6
Beaufort	394.0	67.6	249.3	6
Suurberg	864.0	829.0	846.5	2
Uitenhage	2537.0	336.0	1497.3	6
Algoa	856.0	615.0	735.5	2
De Hoopvlei	150.0	140.0	145.0	4
Coastal sand	745.0	106.4	431.4	4
Alluvial	2400.0	16.0	656.7	7

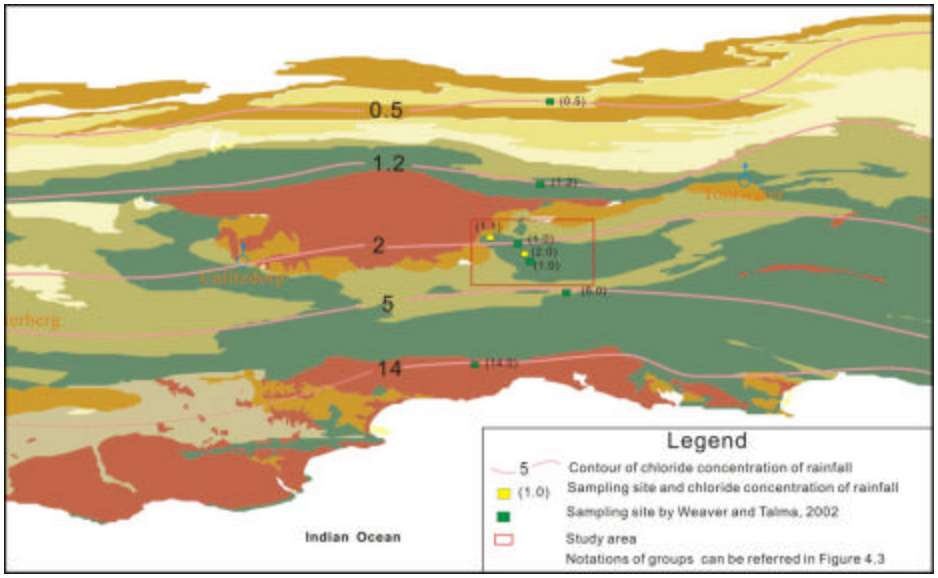

Figure 5.12 Contour of chloride concentration of rainfall in the Kammanassie area

5.6 SUMMARY

According to the occurrence of aquifer, five types of aquifer systems, namely the horizontal terrane aquifer system, incline strata aquifer system, folded strata aquifer system, fractured rock aquifer system and weathered rock (crust) aquifer system, are classified. Based on geological and hydrodynamic characteristics, namely, geomorphology and boundary conditions of groundwater flow, nineteen hydrogeological units in the TMG area have been identified, covering the area of 248,000km^2.

Groundwater in the TMG aquifer with Cl-Na type of water is characterised by its low TDS. Chloride and sodium are main ions, as all other major ions are very low concentrations. Based on the 98 samples distributed in the TMG area, the frequency is 32.7%, 24.5%, 15.3% for concentrations of 10-20mg·ℓ^{-1}, 20-30mg·ℓ^{-1} and 30-40mg·ℓ^{-1}, respectively. The frequency is 8.2% each for concentrations of 50-60mg·ℓ^{-1} and 60-70mg·ℓ^{-1}. The errors between arithmetic and harmonic and geometrical are 38%, and 18%, respectively. Therefore the error would be introduced in the recharge estimation using different mean value. Large differences of the chloride concentration occur between the TMG aquifer and the aquifers around the TMG due to lithology. These would be the limitation of the application of chloride mass balance because of multiple sources of chloride.

Chapter 6

Role of Geomorphology in Recharge Processes

6.1 INTRODUCTION

Geomorphology plays a vital role in the formulation of groundwater recharge. The recharge areas of the TMG aquifer lie primarily in the rugged mountainous areas with altitudes ranging from 200m to 2 250m. To the northeast of the mountains lies the relatively high altitude plateau of the Karoo at an elevation of between 800m and 2 000m. In the west section, the NW-SE trend of the mountains runs parallel to the coastline and consists of the Bokkeveld, Piketberg, Cedarberg, Skurweberg, Cold Bokkeveld and Witsenberg Mountains. In the syntaxis area, the ranges strike northeast, such as the Hex River Mountains, Riversonderend and Overberg Mountains. The Swartberg Mountains lie in the north, and the Langeberg Range and Outeniqua Mountains in the southern E-W striking range, which runs parallel to the coastline with the Kammanassie Mountain range, lying in the east between them (refer to Figure 7.1). The topography of the eastern section is, to a large extent, characterised by a number of northwest-southeast striking mountain ranges and ridges, such as the Kouga, Tsitsikamma-Kareedouw, Baviaanskloof, Grootrivier Mountain and Great Winterhoek Mountains.

The influence of lithology and geomorphology in semi-arid areas is illustrated in Botswana by differences between the Kalahari sands and adjoining Precambrian hard-rock area (Gieske 1992; De Vries 1997; Selaolo 1998; De Vries et al. 2000). The impact of topography on local and regional groundwater flow paths was demonstrated by Tóth (1963). Water runs off steeper slopes more quickly with less infiltration into the ground, and thus produces less recharge than flatter areas where water has more time to soak into the ground (Sophocleous and Buchanan, 2003). The texture of the soil became heavier the recharge decreased (Kennett-Smith et al., 1994). The rate of evapotranspiration increases as the vegetative cover increases. Evapotranspiration losses may range from 38.1 cm per year for barren rocky areas to 89 cm per year for heavily forested areas (Wisler and Brater, 1963). Recharge is generally much greater in nonvegetated than in vegetated regions (Gee et al., 1994) and greater in areas of

annual crops and grasses than in areas of trees and shrubs (Prych 1998). Plants, especially exotics consume amount of water from soils (Le Maitre et al., 2002). A poor vegetation cover on a permeable soil or a fractured porous bed-rock near the surface, together with high-intensity rainfall, create favourable conditions for recharge (De Vries and Simmers, 2002). Preferential flow contributes on average ~50% of the estimated total recharge, though values as high as 70–90% are known (De Vries and Simmers, 2002). Gieske et al. (1990) observed horizontally concentrated infiltration into rills and lateral soil-water movement toward intervening ridges.

The interaction of climate, geology, morphology, soil condition, and vegetation determines the recharge process. Recharge induced by minor topographic variations is also important at a local scale (De Vries and Simmers, 2002). An understanding of the geomorphology contributes to a better delineation of the recharge processes of the TMG aquifer system and an improved appreciation of recharge estimation. This chapter aims to conceptualise models of recharge processes in the TMG area through field investigation.

6.2 TOPOGRAPHY

The topography of recharge areas of the TMG aquifer is controlled by lithology and structure. The mountain ranges are consistent with the orientation of structures. Gentle slope topography is characterized in southern Grabouw. Gorge topography predominates along river valley in the outcrop of the TMG area. Fault controlled topography is typified by a mega fault, such as the De Hoek Fault, Worcester Fault and Cango Fault.

Four types of topography controlling different recharge processes are identified in the TMG area, namely mesa (Figure 6.1), cuesta (Figure 6.2), fold-controlled topography (Figure 6.3) and fault-controlled topography (Figure 6.4). Vertical infiltration controls the recharge process in the mesa area. Percolation occurs along the bedding fractures and recharges vicinity catchment in the cuesta area. Recharge processes are more complex in the folded and faulted rock area where more effective recharge may occur in the area with high density of fractures and percolate to local or other catchment via fracture networks.

Figure 6.1 Horizontal topography (mesa) in the Table Mountain

Figure 6.2 Cuesta (incline) topography in the Rooiels Bay

Figure 6.3 Fold controlled topography in Montagu

Figure 6.4 Fault controlled topography in Rawsonville

6.3 A ROLE OF FRACTURE ON RECHARGE

The processes of recharge are specifically associated with open fractures. These fractures, when near the surface, are often totally or semi-infilled by soil with vegetation. An open fracture can be identified using Radon technique (Wu et al., 2003). A typical example is the fractures in the Table Mountain (Figure 6.5). In this figure the ongoing infiltration process is observed through bubble formation on the water surface. If the infiltration rate is smaller than the intensity of rainfall, surface flow occurs.

High infiltration rate may occur in unfilled fracture. The infiltration may be influenced by soils due to reducing aperture of fractures and vegetation due to increasing evapotransporation in semi filled-in fracture. A good example is the Blikhuis area shown in Figure 6.6.

The outcrop rocks are highly fractured in most area of the TMG. Stress relief fractures are often seen in the near land surface, especially in steep slopes. Rainfall can produce as high as 100% infiltration rate near land surface, but the fractures trend to close at depths, therefore, most of rainfall infiltration comes out as interflow. An example is the Vermaaks Valley (Figure 6.7).

The fractures without displacement are one type of preferential fractures. These fractures can link to the aquifer directly. Some paleo-fractures are sealed but some subsequent fractures are not cemented. These fractures in Rooiels Bay are typical examples (Figure 6.8). The fractures at Dunn's Castle are the typical examples (Figure 6.9). The tectonic fractures together with weathering and stress relief fractures can form the preferential fracture zones, in which effective recharge will be increased. This type is characterized at Platteklip Gorge (Figure 6.10). The open fracture density near the surface is the key factor controlling the infiltration rate, but recharge is constrained by characteristics of fractures at depth. The wide-open fractures not only enhance rainfall infiltration but also form preferential recharge.

Figure 6.5 Fractures clogged with infillings near the surface in the Table Mountain

Figure 6.6 Open and semi infilled fractures in the Blikhuis

Figure 6.7 Stress-relief fractures in the Vermaaks valley

Figure 6.8 Fissure without displacement in the Rooiels Bay

Figure 6.9 Preferential fractures at Dunn's Castle

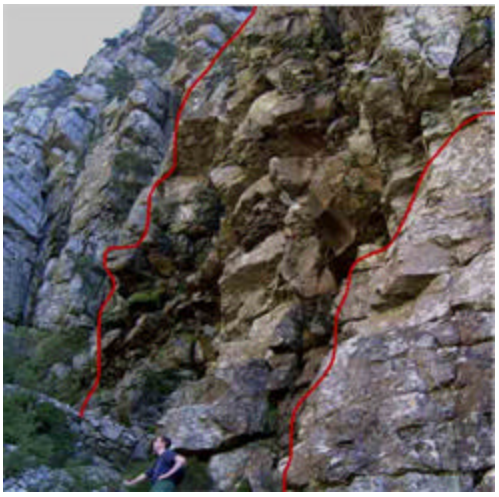

Figure 6.10 Preferential fracture zone at Platte klip Gorge, Cape Town

6.4 IMPACT OF SLOPE ON RECHARGE

6.4.1 Slope type

Recharge is related to the slope gradient of mountains. For instance, rainfall has sufficient time to infiltrate into soils and rocks if the slope gradient is gentle; rainfall is unlikely to infiltrate effectively if the slope gradient is steep. The relationship between the slope and the dip of strata, together with the occurrence of fracture networks, is the main factor influencing the recharge rate. A gentle slope gradient with the strata dipping away is good for recharge if the slope angle is less than the dip angle (Figure 6.11), but an escarpment with the strata dipping in the opposite direction hampers recharge, which is illustrated by the snow cover on the slope in Boland area. Snow stays at a moderate slope, but no snow accumulate on steep slopes (Figure 6.12). A slope surface with strata forming the surface is the worst-case scenario of recharge if there are not well open fracture networks for infiltrating. The Ladismith is a typical example as shown in Figure 6.13.

Figure 6.11 Moderate slope near the Theewaterskloof Dam

Figure 6.12 Slope and snow in Boland (Cape Nature Reserve？)

Figure 6.13 Layer slope in Ladismith

6.4.2 Form of slope

Estimating the impact of the concavity, convexity, regularity or warp of a slope on recharge is a very delicate procedure. These factors are often neglected so that such divergent results are come up. Slope length will increase rainfall directly infiltrating in convex slope. The outcrops of the TMG usually have a convex slope; an example is in Citrusdal (Figure 6.14). The presence of concave slopes in a landscape indicates that there must be trapping, siltation and colluvial deposits in the valley. A concave ground surface or slope surface can often hold a certain amount of water after rainfall. For instance, it can hold water in hollows such as on the top of the Table Mountain (Figure 6.15). It is advantageous for infiltration if micro fractures occur under hollows and free water vapour occurs simultaneously.

Figure 6.14 Convex slopes in Citrusdal

Figure 6.15 Held water (brown) in hollows on the top of Table Mountain

6.4.3 Slope gradient

As the gradient increases, the kinetic energy of rainfall remains constant, but transport accelerates toward the foot as the kinetic energy of the runoff increases and outweighs the kinetic energy of the rainfall. This occurs when the slope (S) exceeds 15% (Roose, 1996). Roose (1996) also mention that runoff does not necessarily increase with slope. In general, there are mesa on the top of mountain and long cuesta with steep transection valley in the outcrop of the TMG area. A gentle watershed occurs in most of the outcrop area of the TMG in the western and eastern section (refer to Figure 4.3), for instance, Witteberg Mountain (Figure 6.16). In the syntax area, precipitous cliffs and narrow valley are domination; the slope gradients of the banks of valley are greater than 30° in most cases, but gentle slope on the foot of valley (Figure 6.17). There are wide slope on the gentle side where the slope is coincide with strata dip and narrow slope on the steep side where the slope is opposite to the strata dip in the cuesta. A typical example is the Langeberg Range (Figure 6.18). More complex slope gradient occurs in some areas, such as the Swartberg Pass (Figure 6.19). In the hydrogeological unit 3 and 6, there is a broad and gentle land surface with an approximately horizontal dip of strata. Based on the slope character, three grades of the slope gradients are classified, namely 10-20°, 20-30° and >30°. More effective recharge occurs in the slope of less than 30° in the outcrops of the TMG area.

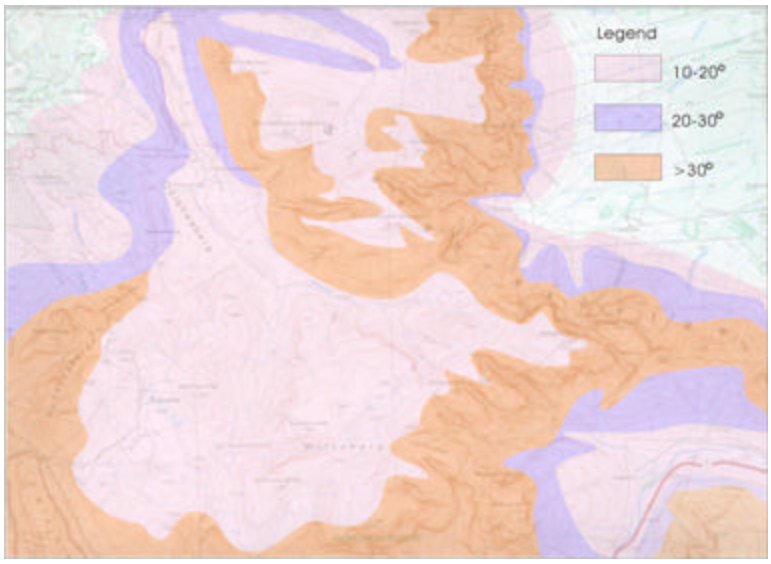

Figure 6.16 Slope gradient in the Witteberg Mountain

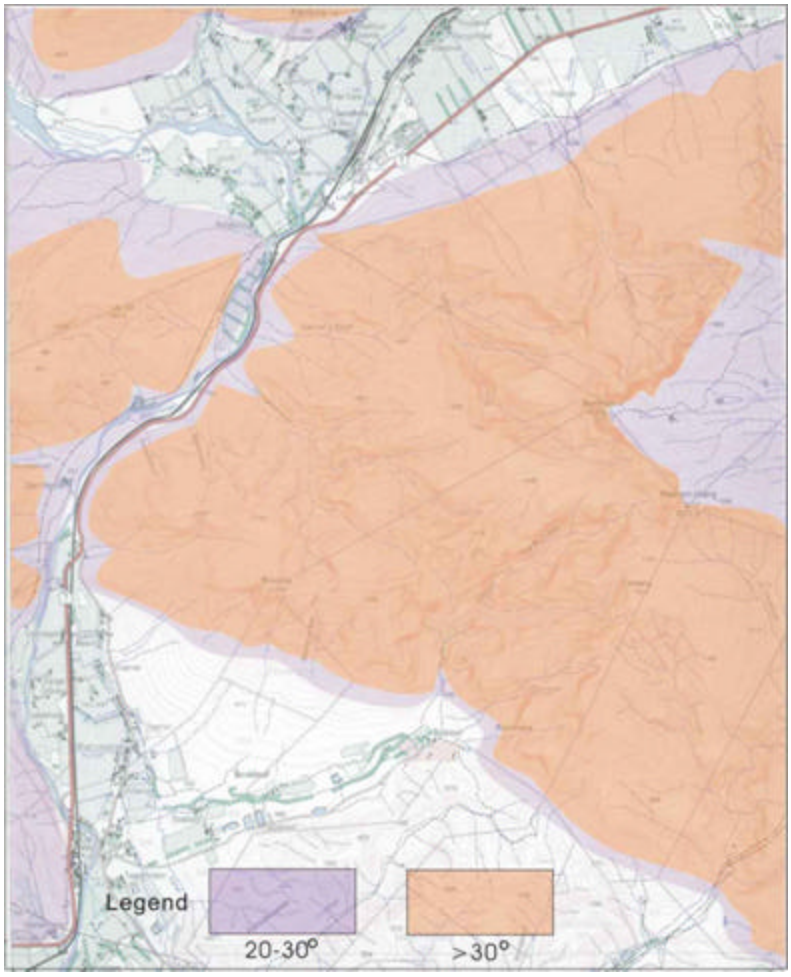

Figure 6.17 Slope gradient in the Hex River Mountain

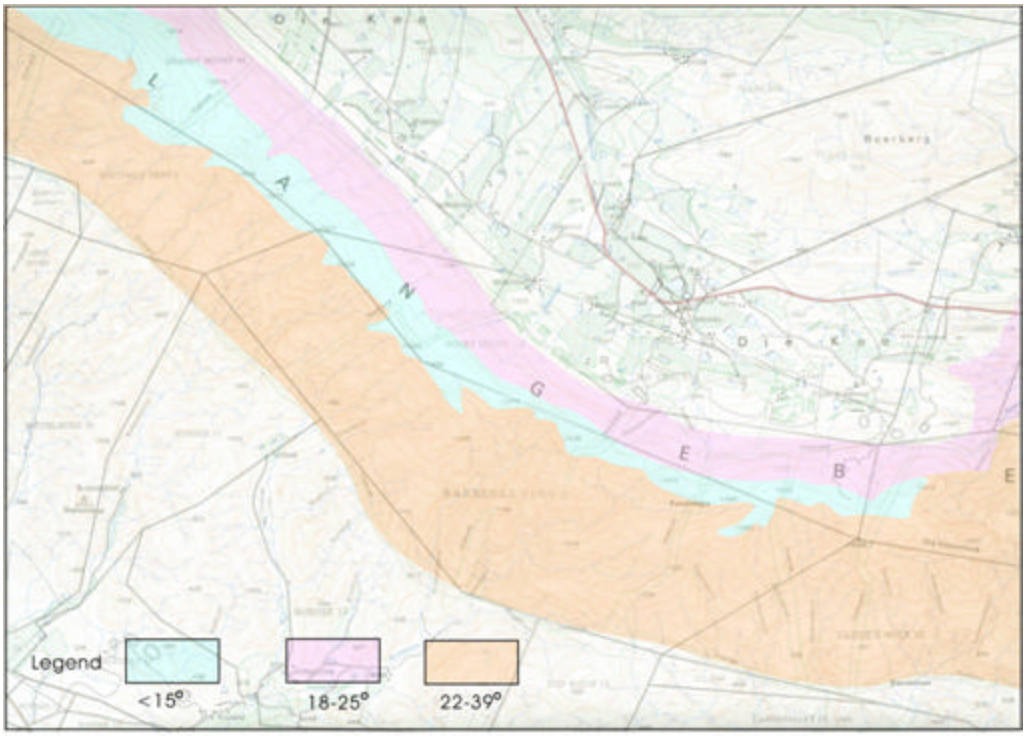

Figure 6.18 Slope gradient in the Langeberg Mountain

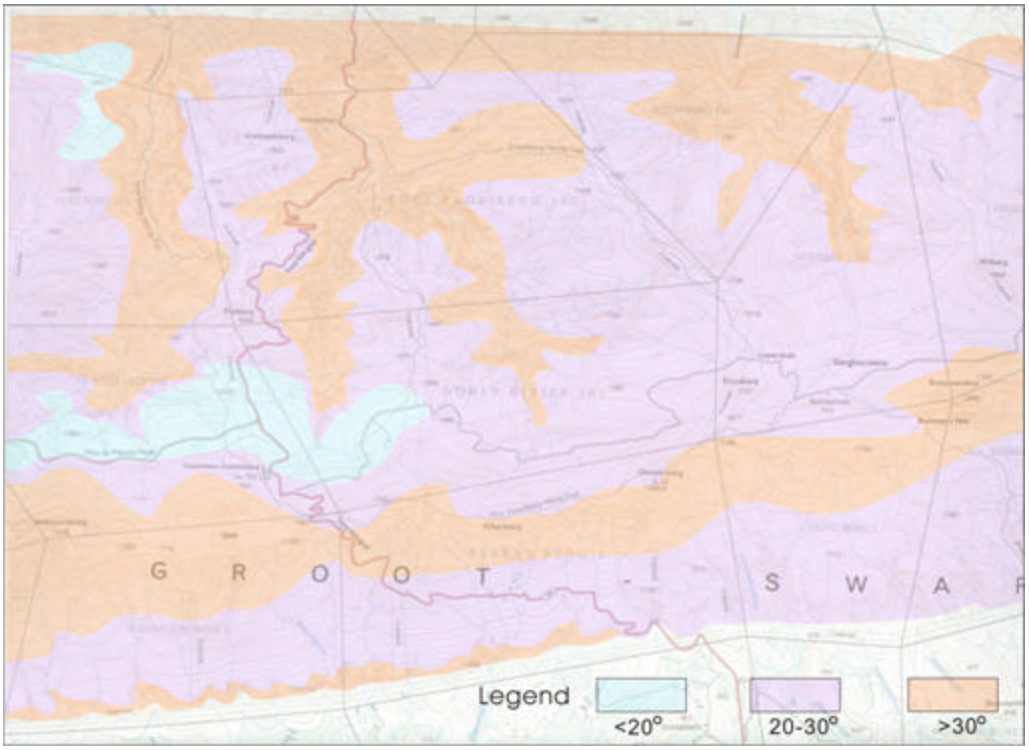

Figure6.19 Slope gradient in the Swartberg Mountain

6.5 IMPACT OF VEGETATION ON RECHARGE

6.5.1 Vegetation type

Impact of vegetation on recharge can be observed in many ways, such as interception and transpiration. The vegetation can consume water from deep soils and fractures. Three types of vegetation are dominant in the recharge area of the TMG aquiger, namely indigenous Mountain Fynbos, exotic plants and sparse or no vegetation. The most common of which is the Fynbos, an example of which can be seen in Figure 6.20. The sparse vegetation can often be seen in the outcrop of the Skurweberg Formation, an example of which can be witnessed in the Michell's pass area (Figure 6.21). Exotics, such as *Pinus* and *Eucalyptus* species are planted at the foot of the mountains or gentle slopes (Figure 6.22 and Figure 6.23). Due to natural spreading some areas later become invaded. For the outcrops of the TMG, there is a high vegetation cover rate on the gentle slopes and sparse vegetation on the steep slopes because of the soil thickness.

Figure 6.20 Mountain Fynbos in the Mont Rochelle Nature Reserve

Figure 6.21 Sparse vegetation in the Michell's Pass

Figure 6.22 Exotic-*Pinus* in Grabouw

Figure 6.23 Exotic–*Eucalyptus* in the Sir Lowry's Pass

6.5.2 Impact of exotic plants on recharge

The first robust estimate of the impacts of plantations at a national scale, was based on the forestry impact curves and catchment mean annual runoff (MAR) calculated by HRU (1981). Plantations were estimated to be using an additional 1 284× 10^6 m^3 of water in 1980, which is approximately 7.9% of the usable portion of total water resources (DWA, 1986). Given a total plantation area of 1.13 × 10^6 ha (DWA, 1986), an average reduction in annual runoff from afforested land of 113.6 mm (Scott et al., 1998).

The estimated impact of invading exotics on the water resources of South Africa, at approximately 6.7% of the total surface runoff, is substantial. Even at a conservative rate of new invasion of 5% per year, the size of the invaded area could double in 15 years, potentially doubling the water use (Versfeld et al., 1998). There is clear evidence that exotic species will increase in extent and density if given time and sufficient area to invade to use an even greater proportion of the available water in catchment areas (Le Maitre et al., 2000).

About 10 million ha (8.28%) of South Africa area have been invaded to some degree by a wide range of exotic species. If the invaded area is 'condensed' to adjust to 100% of the cover, then the equivalent of approximate 1.7 million ha (1.39%) has been fully invaded. The invaded area in the TMG area is presented in Table 6.1.

Table 6.1 Areas invaded by exotic plants in the different primary catchments

(After Le Maitre et al., 2000)

Primary catchment	Drainage system	Area (ha)	Total area invaded area		Condensed invaded area	
			(ha)	%	(ha)	%
E	Olifants (W Cape)	4 906	528 972	10.78	37 623	0.77
G	Agulhas coast	2 524	1 597 036	63.26	384 636	15.24
H	Breede, SW Cape	1 551	741 408	47.78	84 398	5.44
J	Gouritz	4 513	711 436	15.76	59 399	1.32
K	S Cape coast	716 816	132 030	18.42	52 993	7.39
L	Gamtoos	3 473	277 428	7.99	34 289	0.99
M	Port Elizabeth region	261 156	70 376	26.95	11 358	4.35
N	Sundays	2 122	25 191	1.19	3 964	0.19

The top 10 invading species or groups of species in South Africa ranked by condensed invaded area are listed in Table 6.2. Habitat - indicates the main habitats invaded by the species, which are: landscape (l), riparian (r) and alluvial plants (r(a)). The condensed area is the total area adjusted to bring the cover to the equivalent of 100%. Density is the estimated mean cover over the total invaded area.

Table 6.2 Top 10 invading species or groups of species in South Africa ranked by condensed invaded area (After Le Maitre et al., 2000)

Species	Habitat	Condensed	Total invaded	Density
Acacia Cyclops	l	339 153	1 855 792	18.28
Prosopis spp.	R (a)	173 149	1 809 229	9.57
Acacia mearnsii	r, l	131 341	2 477 278	5.30
Acacia saligna	l, r	108 004	1 852 155	5.83
Solanum	r, l	89 374	1 760 978	5.08
Pinus spp.	l	76 994	2 953 529	2.61
Opuntia spp.	l	75 356	1 816 714	4.15
Melia azedarach	r l	72 625	3 039 002	2.39
Lantana camara	r	69 211	2 235 395	3.10
Hakea spp.	l	64 089	723 449	8.86

The impact of invading exotic plants on mean annual runoff is 5.58 % and 15.82% of MAP for water use in the Eastern and Western Cape Provinces, respectively. The impact of water use by invading exotic plants on the mean annual runoff (MAR) in primary catchment areas of the TMG is present in Table 6.3. The highest impact appears on the Agulhas coast in the hydrogeological unit 11.

Table 6.3 Impact of water use by invading exotic plants on MAR in primary catchment areas of the TMG (After Le Maitre et al., 2000)

Primary Catchment	Drainage system	MAR invaded ($\times 10^6$ m^3)	Condensed water use area (ha)	Incremental use ($\times 10^6$ m^3)	Water use MAP (mm)	Reduction Equivalents (mm)
E	Olifants Sout, Doring	1 008.35	37 623	35.52	3.52	94
G	Agulhas coast	2 056.75	384 636	646.50	31.43	168
H	Breede, Riversdale	2 088.35	84 398	181.63	8.70	215
J	Gouritz	670.63	59 399	74.79	11.15	126
K	S Cape coast	1 297.30	52 993	134.46	10.36	254
L	Gamtoos	494.71	34 289	96.53	19.51	282
M	PE Coast Swartkops,	150.04	11 358	40.18	26.78	354
N	Sundays	279.89	3 964	8.34	2.98	210

The ranks of the invading species are present in Table 6.4. As a group the *acacias,* with seven species in the top 25 - notably *A. mearnsii, A. cyclops and A. dealbata* - are the prime water users, accounting for 55% of the total water used. They are followed by the *Pinus, Eucalyptus, Prosopis* species and *Melia azedarach*. The top ten account for 81% of all water used by invading exotics. The impact of the latter species (11-25 in Table 6.4) on surface runoff is limited because of its coastal distribution pattern, except where communities depend on groundwater supplies, as in the case of the town of Atlantis in the Western Cape (Le Maitre et al., 2000).

The effects on stream flow by *E. grandis* were assumed to be representative of all eucalypt species planted in plantations at present. An analysis of some measurements of transpiration by poplars suggested that their annual water use was similar to pines (Scott and Le Maitre, 1993). Nevertheless, because all hardwoods (e.g. poplars and oaks) were grouped with eucalypts in the National Forestry Coverage Map (Thompson, 1995), the flow-reduction curves for Eucalypts were used for all hardwoods except Wattles. The inclusion of Poplars and other species under Eucalypts is unlikely to have a significant impact on the estimates because the areas planted with these species only amount to about 0.6% of the total afforested area (DWAF, 1996). The impact of Eucalyptus and Pines on flow is illustrated in Figure 6.24. An adult tree would use more water and reduce flow more.

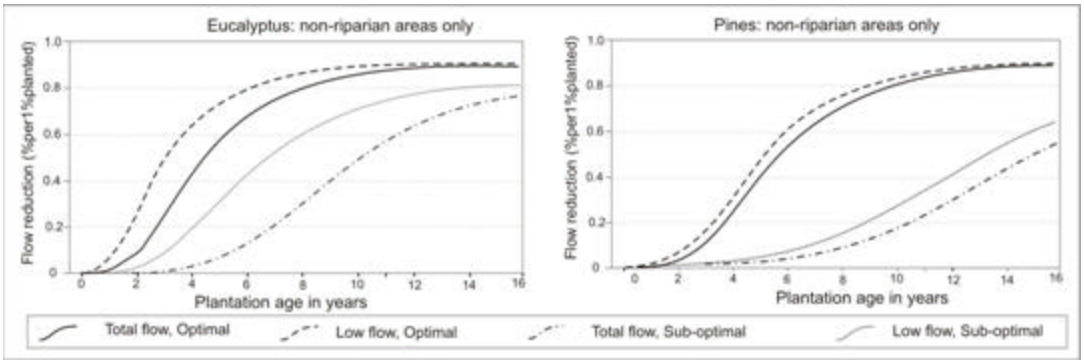

Figure 6.24 Flow reduction curves for Eucalyptus and Pines (Scott et al., 1998)

Several studies concentrated on the impact of the exotic species on runoff, but the impact of the exotic species on recharge has not yet been discussed. Although the invading exotic plants consume large amounts of water in the whole TMG area, the

cover rate and density of the exotic plants in the outcrop of the TMG is still small. From the water balance point of view, the exotic plants consume more water than indigenous plants and this can reduce the recharge rate as well. Further studies of the impact of exotic species on recharge are necessary.

Table 6.4 Rank of the mean annual water use of invading species in South Africa

(After Le Maitre et al., 2000)

No.	**Species**	Water Use (millions of m^3)	Cumulative percentage of the total water use
1	*Acacia mearnsii*	576.58	17.46
2	*Acacia Cyclops*	487.63	32.22
3	*Acacia dealbata*	248.32	39.74
4	*Acacia* mixed spp.	242.63	47.08
5	*Pinus* spp.	231.53	54.09
6	*Eucalyptus* spp.	213.98	60.57
7	*Prosopis* spp.	191.94	66.38
8	*Acacia saligna*	171.13	71.56
9	*Melia azedarach*	164.91	76.56
10	*Solanum*	139.97	80.79
11	*Lantana camara*	97.14	83.73
12	*Chromolaena*	68.26	85.80
13	*Hakea* spp.	66.30	87.81
14	*Populus* spp.	53.83	89.44
15	*Jacaranda*	48.40	90.90
16	*Sesbania punicea*	42.57	92.19
17	*Rubus* spp.	41.33	93.44
18	*Acacia longifolia*	38.73	94.62
19	*Psidium guajava*	37.31	95.75
20	*Caesalpinia*	33.82	96.77
21	*Salix* spp.	33.21	97.78
22	*Acacia melanoxylon*	32.20	98.75
23	*Acacia decurrens*	9.83	99.05
24	*Quercus* spp.	7.24	99.27
25	Other spp.	17.27	100.00

6.6 RECHARGE PROCESSES RELATED TO TOPOGRAPHY

Recharge processes are related to topography, structure and texture of soils and rock fractures and rainfall patterns in the TMG area. The rainfall intensity is one of the important controlling factors. An example of the effective infiltration depth is shown in Figure 6. 25. The infiltration depth varies from 20 to 40cm near Brandvelei in June 6, 2004 after about 30mm of rainfall. Infiltration is reduced due to the surface sealing effect resulting enhanced rainfall intensities and rain splash. The infiltration depth is slightly deep along the roots of plants and macro pores. The soil moisture is also one of the factors, which influence the infiltration depth.

Figure 6. 25 Infiltration depths near Brandvelei in June 6, 2004

Based on geomorphology and hydrogeology, six models of the recharge processes in the TMG area are conceptualised, namely (1) recharge processes in soil zones, (2) recharge processes in horizontal strata zones, (3) recharge processes in upright strata zones, (4) recharge processes in incline strata zones including three different cases.

6.6.1 Recharge processes in soil zones

The recharge process with soil cover is depicted in Figure 6.26. This model contains:

1) The unsaturated zone, which is composed of soil and rock zones. The infiltration processes in the unsaturated zone are much more complex. Four zones can be characterised: the leach zone, the illuvial zone, the root zone and a no impact zone. Moisture in the eluviation and root zones is lost by direct evaporation or transpiration of plants.
2) Rainfall, which contributes to both runoff and infiltration. During a rainfall event the rate of precipitation can exceed the infiltration capacity of soils, in which case excess water will pond on the soil surface. It is the ponded water that is available for overland flow to surface streams.

3) The concentration of runoff that varies from place to place, depending upon the surface environments. Its concentration C_1 is greater than C_r.
4) The concentration of infiltration water noted as C_1, which is greater than C_r. When the infiltration water emerges as interflow, its chloride concentration is termed C_{11} with $C_{11} = C_1$.
5) The concentration in the illuvial zone C_2, with $C_2 > C_1$. When the infiltration water emerges as interflow, its chloride concentration is termed C_{21} with $C_{21} = C_2$. There is a maximum concentration (C_{21}) in the scenario.
6) The concentration of chloride from the illuvial zone is C_{22} with $C_{22} = C_2$. When the infiltration water emerges as interflow, its chloride concentration is termed as C_{22}.
7) The infiltration water recharges groundwater with concentration C_{22}.
8) The chloride concentration of interflow (C_{in}) should satisfy

$$C_{in} \times V_{in} = C_{11} \times V_{11} + C_{21} \times V_{21} + C_{22} \times V_{22}$$
$$V_{in} = V_{11} + V_{21} + V_{22}$$

The concentration of surface water should satisfy:

$$C_s \times V_s = C_{in} \times V_{in} + C_{01} \times V_e$$
$$V_s = V_{in} + V_e$$

The mixture concentration of groundwater should satisfy

$$C_g \times V_g = C_{g0} \times V_{g0} + C_{22} \times V_{22}$$

C_{g0} is the chloride concentration of old storage water in aquifer. The subscript of volume (V) is corresponding to the components of concentration.
9) The infiltration water, which temporarily stayed in the unsaturated zone, would have a constant concentration. This water may be flushed into the water table by sequential infiltration events.
10) In any given topography, only one or two types of interflows can prevail.
11) The concentration C_{21} is similar to C_{22} in most scenarios because it originates from the same zone.

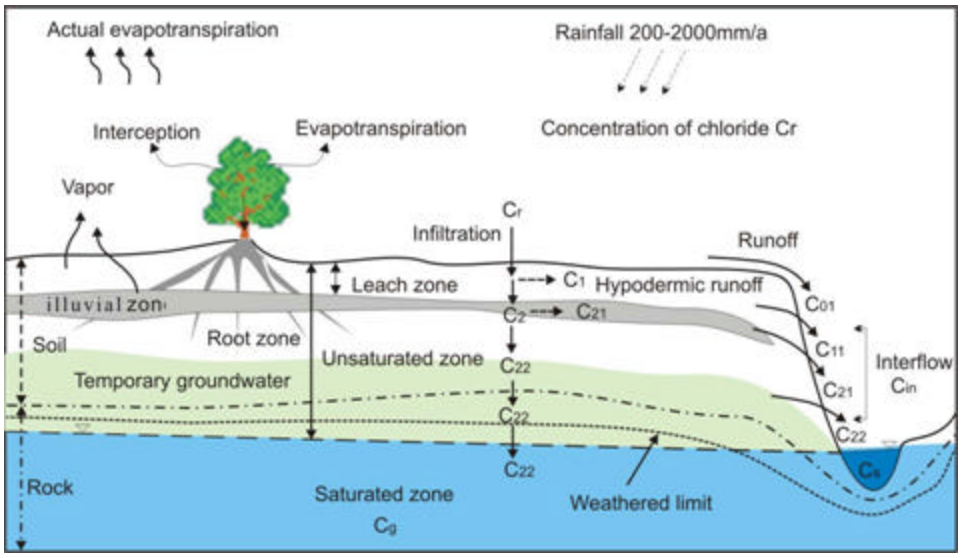

C_r - chloride concentration of rainfall

C_s - chloride concentration of surface water

C_g - chloride concentration of groundwater

C_{in} - chloride concentration of interflow

C_{01}- chloride concentration of runoff (sheet flow)

C_1 and C_{11}- chloride concentration of hypodermic runoff (Hypodermic runoff is one of the runoff within the loosen materials near the land surface, such as worm pipe etc..)

C_2 -illuvial (salt deposit) zone

C_{21}- interflow from illuvial zone

C_{22} -chloride concentration of infiltrating water

Figure 6.26 Sketch of recharge processes: case 1 with soil cover

The model depicted in Figure 6.26 would occur mostly in valleys in the TMG areas. For example, the Vermaaks valley belongs to the model as shown in Figure 6.27. The seepage zone with growing grass is the start point of the Vermaaks valley.

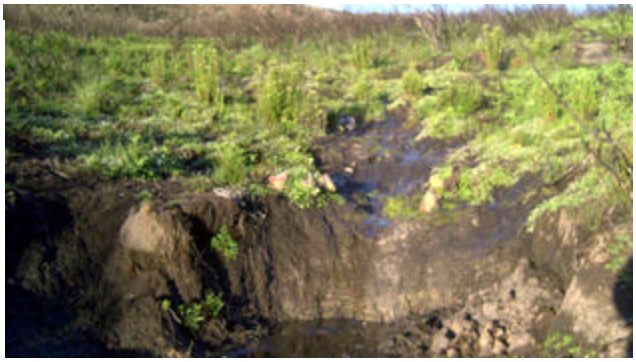

Figure 6.27 Interflow originated from soils zone in the Vermaaks valley

6.6.2 Recharge processes in horizontal strata zones

Figure 6.28 depicts the recharge process in horizontal strata zones (mesa). In this model, the following assumptions are made:

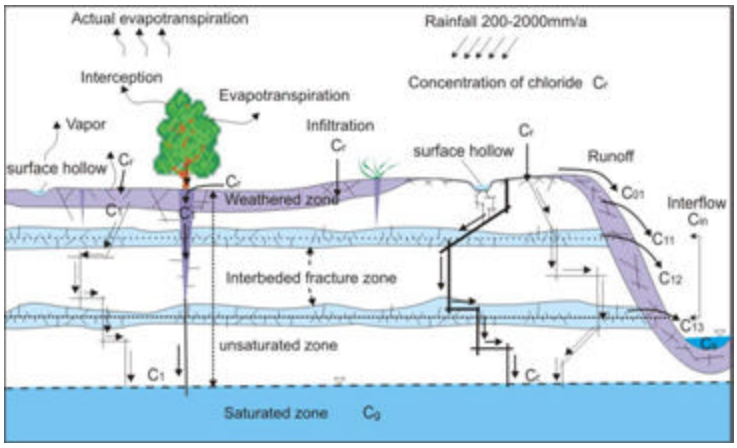

C_r - *chloride concentration of rainfall*

C_s - *chloride concentration of surface water*

C_g - *chloride concentration of groundwater*

C_e - *chloride concentration of sheet flow*

C_{in} - *chloride concentration of interflow*

C_{01} - *chloride concentration of runoff (sheet flow)*

C_1 *and* C_{11} - *chloride concentration of water from weathered zone*

C_{12} *and* C_{13} - *chloride concentration of water from preferential bedding fractures*

Figure 6.28 Recharge processes: case 2 with horizontal strata

1) The strata are almost horizontal. The weathered zone only occurs in a certain area.
2) The plants thrive along fractures or weathered zones.
3) Hollows occur on ground or rock surface. Evaporation is considerable if water is held in hollows.
4) There is a preferential fracture zone between strata layers and many preferential fractures in a rock mass.
5) Evaporation occurs near the surface and evapotranspiration occurs along the fracture through plants.

6) The chloride concentration of preferential flow stays stable; it is similar to that of rainfall.
7) The concentration of runoff is C_{01} with $C_{01}>C_r$.
8) Concentration of interflow is the max value of the output of the weathered zone.
9) The concentration of infiltration water in fractures with plants is C_1 with $C_1>C_r$, but the recharge volume can be smaller than that through preferential fractures.
10) When the infiltration water seeps as interflow through the weathered zone or preferential fracture zone, the chloride concentrations denote as C_{11}, C_{12} ad C_{13}. The concentrations are almost similar in most scenarios.
11) The concentration of groundwater is a mixture of rainfall, interflow and regional flow. They satisfy

$$C_g \times V_g = C_{g0} \times V_{g0} + C_1 \times V_1 + C_r \times V_r$$

C_{g0} is the chloride concentration of old storage water in aquifer. The subscript of volume (V) is corresponding to the components of concentration.

Typical physical model expressed in the conceptual model (Figure 6.28) can be found near the Maclear's Beacon on the Table Mountain (Figure 6.29).

Figure 6.29 Preferential fractures with plants near the Maclear's Beacon on Table Mountain

6.6.3 Recharge processes in upright strata

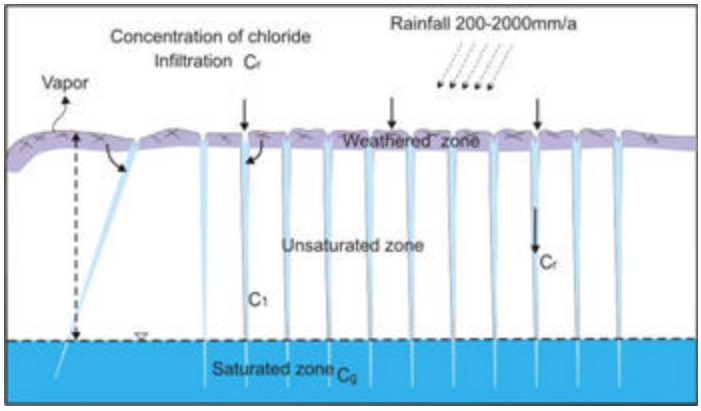

C_r - chloride concentration of rainfall

C_g - chloride concentration of groundwater

C_1 - chloride concentration of water leakage from weathered zone

Figure 6.30 Recharge processes: case 3 with upright strata

Figure 6.30 shows the model of the recharge process in almost upright strata. In this model, the assumptions are the following:

1) The strata are almost upright. Weathered zone only occurs in a certain area. There is a weathered zone with potential high hydraulic conductivity.
2) There is preferential fracture zone between strata layers and many vertical preferential fractures in the rock mass.
3) Evaporation occurs on the surface of a weathered zone. Salinity can accumulate in weathered zones by evaporation.
4) The chloride concentration of preferential flow remains stable; it is similar to rainfall. The chloride concentration of infiltration water in the weathered zone is C_1 with $C_1 > C_r$. The concentration of groundwater is a mixture of those of rainfall, interflow and old aquifer storage. They satisfy

$$C_g \times V_g = C_{g0} \times V_{g0} + C_1 \times V_1 + C_r \times V_r$$

C_{g0} is the chloride concentration of old storage water in aquifer. The subscript of volume (V) is corresponding to the components of concentration.

The typical topography expressed in the conceptual model (Figure 6.30) occurs in the core of anticline, such as Old English fort in Montagu and Uniondale Poort- Upright strata with open fractures shown in Figure 6.31 and Figure 6.32.

Figure 6.31 Upright strata with open fractures in Montagu

Figure 6.32 Upright strata with open fractures in the Uniondale Poort

6.6.4 Recharge processes in incline strata zones

In this scenario, three recharge processes related to dip and slope in cuesta or inclined topography areas are considered, there are as follows:

- the angle of dip is less than the angle of slope (case 4, Figure 6.33 A),
- the angle of dip exceeds the angle of slope (case 5, Figure 6.33 B) and
- the angle of dip is opposite to the slope (case 6, Figure 6.33 C)

From the above models, some common feathers can be drawn as follows:

1) The strata are monocline, and the dip angle is less or greater than the slope angle.
2) The weathered zone only occurs in a certain area. Stress relief fractures are located in relief. There is a preferential fracture zone between strata layers and many vertical preferential fractures in a rock mass.
3) Infiltration water may recharge the aquifer in the opposite catchment area through preferential fracture networks.
4) Part of the rainfall intercepted by plants infiltrates into soil along trunks of plants. Evaporation occurs on the surface. Evapotranspiration occurs along the fractures with plants.

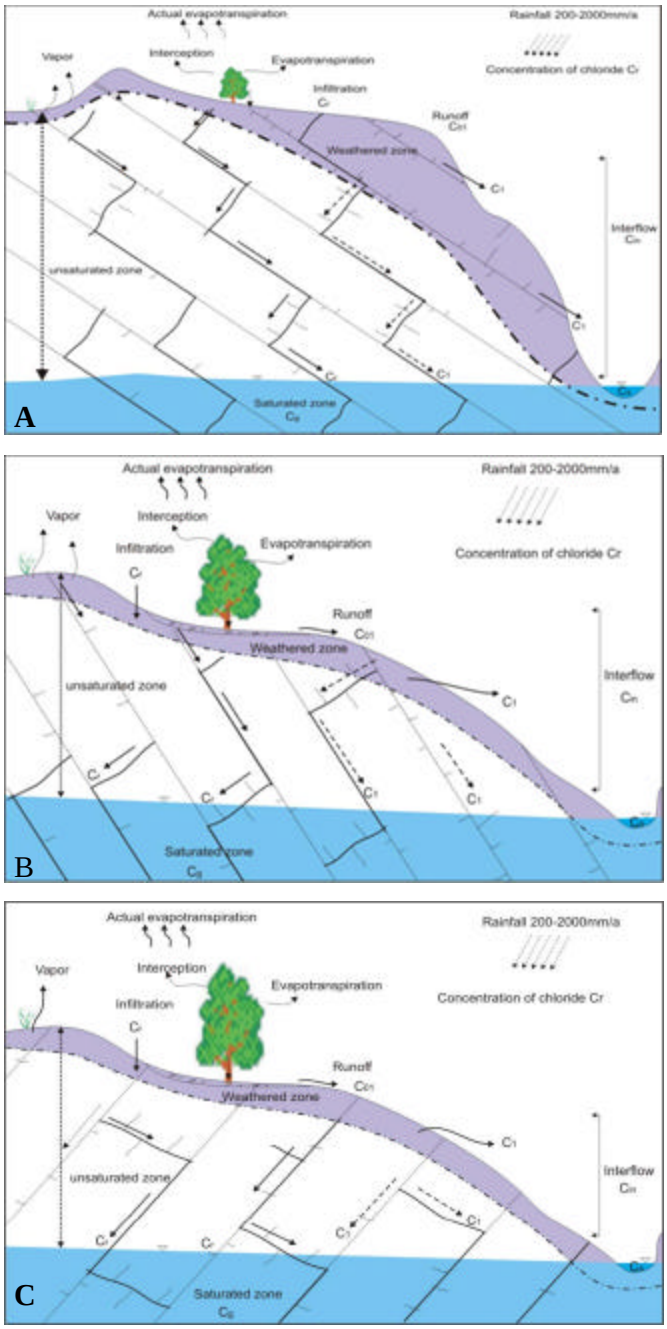

C_r - chloride concentration of rainfall, C_s - chloride concentration of surface water, C_g - chloride concentration of groundwater, C_e- chloride concentration of sheet flow,C_{in} - chloride concentration of interflow, C_{01}- chloride concentration of runoff (sheet flow), C_1 - chloride concentration of water from weathered zone.

A: case 4 with strata dip smaller than slope angle

B: case 5 with strata dip bigger than slope angle

C: case 6 with strata dip opposite to the slope

Figure 6.33 Recharge processes in the incline area

5) The chloride concentrations of the preferential flow are almost similar to that of rainfall. The chloride concentration of water in the weathered zone is C_1 with $C_1 > C_r$. The concentration of groundwater is a mixture of rainfall, interflow and old storage water. They satisfy:

$$C_g \times V_g = C_{g0} \times V_{g0} + C_1 \times V_1 + C_r \times V_r$$

C_{g0} is the chloride concentration of old storage water in aquifer. The subscript of volume (V) is corresponding to the components of concentration.

6) Interflow occurs in the weathered and preferential fracture zones above the elevation of local stream or river. The chloride concentrations of interflow are almost same in most scenarios. Interflow occurs more easily in case 4 than in the other two cases because bedding fractures are cut by valley.

The typical scenarios of these cases occur in a limb of a fold. Typical examples of case 4 and case 5 are shown in Figure 6.34 and Figure 6.35. The case 6 can be referred to Figure 6.2.

Figure 6.34 Dip angle less than the slope angle in the Bain's Kloof

Figure 6.35 Dip angle bigger than the slope angle in the Piketberg Pass

6.7 SUMMARY

Recharge processes in horizontal zones, incline and upright zones are discussed. The factors of recharge processes include topography, characteristics of fracture, texture and thickness of soil and vegetation etc. Infiltration rate is related to characteristics of

ground surface; the percolation rate to the aquifer is not only constrained by the infiltration rate but also by fracture characteristics at depth. In most cases, the percolation rate is much smaller than infiltration rate. Interflow occurs in the weathered and preferential fracture zones above the elevation of the local stream or river due to the limitation of percolation rate.

In the TMG area, the fracturing of quartzitic sandstone into breccia and a cataclastic rock can increase both the porosity and permeability of the rock mass considerably. However, recementation of the breccia by secondary silica, deposited from silicic solutions and complexes in water circulating through the fractures since the time of its formation can further reduce porosity and permeability. The presence of both vertical and horizontal fractures is of importance for infiltration water movement. Most of the recharge occurs along the vertical fractures, while the actual groundwater flow is controlled by both vertical and horizontal fractures. The structural fractures in shallow rock layers together with fissures by weathering near the surface are the most important factors for rainfall infiltration and groundwater recharge in the outcrop of the TMG area.

The six models of recharge processes, namely soil zones, horizontal strata zones, upright strata zones and three incline strata zones, are identified and discussed. In the most of the TMG area, the mentioned models can be combined with each other thus forming a more complex model of recharge processes. Three types of vegetation, namely the Mountain Fynbos shrub, sparse or no vegetation and exotic plants, are dominant in the recharge area of the TMG aquifer. The most common vegetation is the Fynbos shrub. The exotic plants consume more water than indigenous plants and they can also reduce more recharge. Several studies focusing on the impact of the exotic species on runoff suggest that study of the impact of exotic plants on recharge is necessary in the future.

Chapter 7
Spatial and Temporal Rainfall Variability and Trends in the Kammanassie Area

7.1 INTRODUCTION

The type of rainfall is often used to formulate management strategies of the limited water resources. The Kammanassie area is located in the eastern section of the Klein Karoo, which is known as a semi-arid region. The annual average precipitation of arid and semi-arid is 50-200mm and 200-500mm, respectively (Lloyd, 1986). There is not a distinctive bimodal seasonal cycle and a general positive rainfall trend since 1925, but a general negative trend in short period appears from 1971 to 2001 (Cleaver et al., 2003). The low precipitation and large spatial and temporal variation lead to more complexity of recharge estimation in the study area.

This chapter aims to determine spatial distribution, temporal variability and tendency of rainfall in the Kammanassie area in order to facilitate the evaluation of the recharge in response to change of rainfall.

7.2 PRECIPITATION

The standard 15 homogeneous rainfall districts over the TMG area defined by the South African Weather Service (SAWS) is shown in Figure 7.1. The Kammanassie area belonged to the temperate-maritime type is located in district 10 and 11. The Outeniqua Mountains form a barrier between the Klein Karoo and a relatively narrow coastal plain to the south. The northern boundary of the Klein Karoo is formed by the Great Swartberg, which separates the region from the rest of the country. The Kammanassie Mountain lies between the two mountains (Figure 7.2). This topography limits the spatial distribution of the rainfall; thereby it results in more complicated spatial distribution of recharge.

The average monthly rainfall data captured from the WR90 for 111 rainfall stations over the Kammanassie and surrounding region from 1920 to 1989 has been used in a

spatial distribution analysis. The dot marked in the Figure 7.2, namely Parshall, V-notch, Wildebeesvlakte and Purification Works East rainfall stations, were used to analyse rainfall pattern in the Kammanassie mountainous area in 1994-2003. Approximately 400 to 600mm of the Mean Annual Precipitation (MAP) are observed from the contour map made by Kriging's method in the Kammanassie area (Figure 7.3). The rainfall in the northern area of the Kammanassie Mountain is lower than that in the southern area. The rainfall is more than 800 $mm \cdot a^{-1}$ in the Outeniqua Mountains, which is an obvious rainfall boundary.

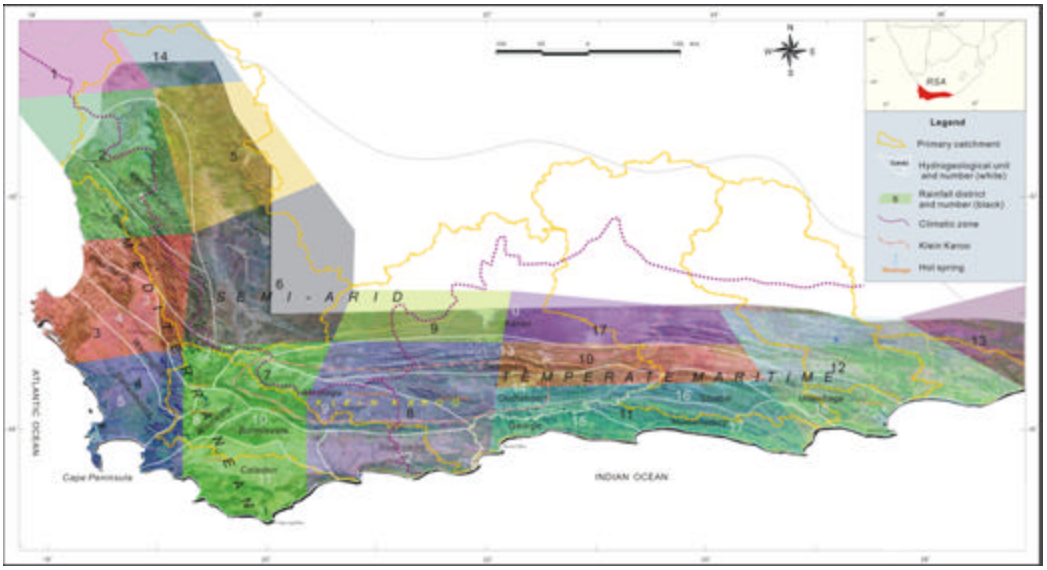

Figure 7.1 Homogeneous rainfall districts over the TMG area

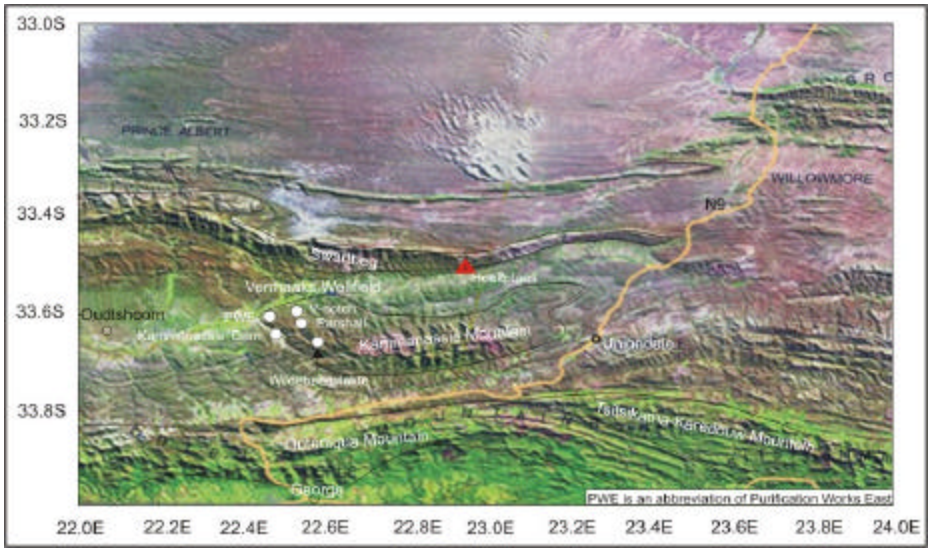

Figure 7.2: Selected area for rainfall analysis

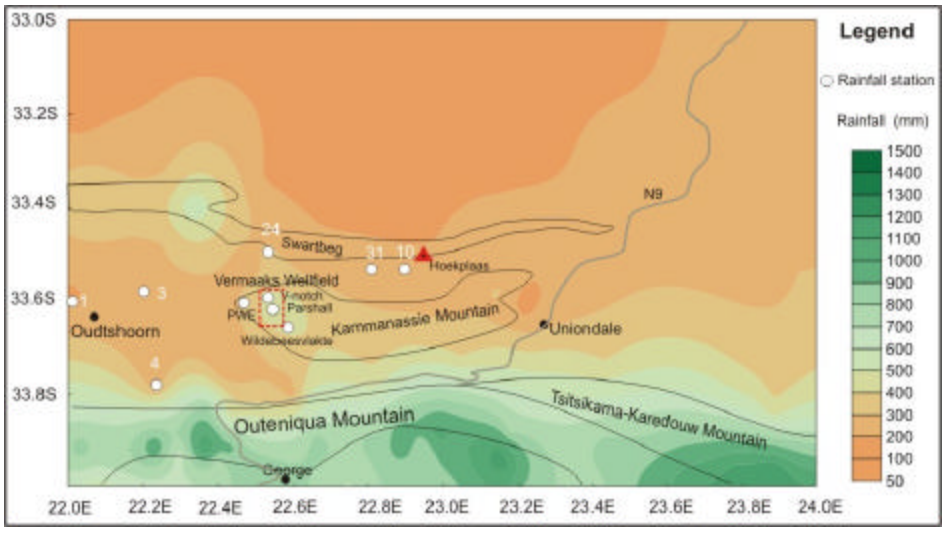

Figure 7.3 Contour of the mean annual precipitation in the Kammanassie area

For discussion the impact of seasonal rainfall on recharge, the monthly average rainfall over a period of 76 years (1921-1996) is shown in Figure 7.4 (Cleaver et al., 2003), in which the fresh grey is 1921-1996 for district 10, the grey is 1971-2000 for rainfall stations 1, 3, 4, 10, 24 and 31 (see to Figure 7.3); the black is 1926-1966 for Oudtshoorn. The relative effective recharge may mainly occur in March, April and November because its higher average monthly rainfall. This may result in limited recharge, but rainfall including high rainfall events in the other months can contribute to the recharge as well.

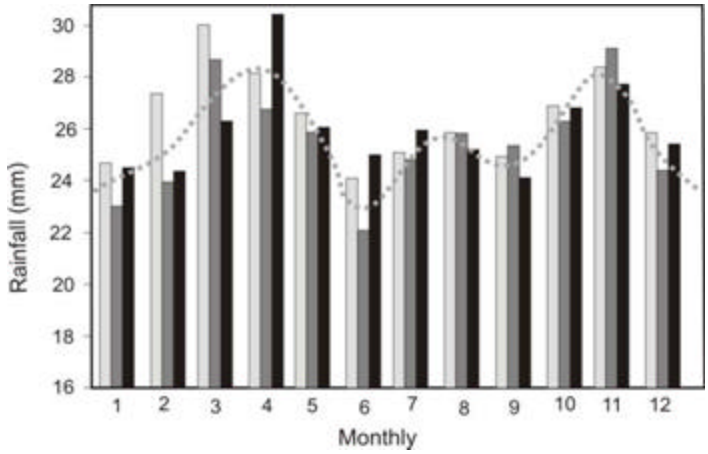

French grey -district 10; Grey-stations 1, 3, 4, 10, 24 in Figure 7; Black-Oudtshoorn

Figure 7.4 Monthly average rainfall calculated for district 10 from 1925 to 1996

(After Cleaver et al., 2003)

7.3 VARIATION OF RAINFALL

Rainfall variation with time scales is another important factor for recharge. The rainfall records (1925-2000) of Hoekplaas rainfall station for the Klein Karoo, the records (1925-2000) in the Kammanassie Dam for the southern Kammanassie Mountaion area, and the records (1994-2003) in Wildebeevlakte, Parshall, V-notch and Purification Works East rainfall stations especially for the Kammanassie Mountain area, are selected to address the long-term and short-term issues (see to Figure 7.2).

7.3.1 Long-term tendency

Hoekplaas rainfall station is located at 33° 33' 03"S and 22° 58' 30" E (owned by Mr. I Barnard, unofficial site, location indicated by a triangle in Figure 7.1). Linear regression indicates that the record contains a gradual positive trend with a slope of +0.55 in monthly rainfall time series since 1925 (Figure 7.5), but the one-tailed probability (9.72E-22) from the F-Test that indicates the variances in time and the MAP is no significance. The high rainfall values were measured in 1981, 1985 and 1996. The CRD has increased since 1966 (98.5mm), and increased considerably after 1992. The frequency of an extreme rainfall event has increased as well after 1978.

To avoid the impact of extreme rainfall events on the positive trend, the new regression in which extreme values greater than 400mm·a^{-1} are replaced with average values of 232.1mm in 1981, 1985 and 1996 are shown in Figure 7.6. The positive trend with a slope of 0.0672 still appears. This would illustrate that the positive trend is not influenced by the extremely high rainfall events after the 1980's. Of course, the one-tailed probability (3.46E-14) from the F-Test is no significance as well. For the short period of recent 30/31 years (1971-200), a general negative trend appears (Cleaver et al., 2003).

For the Kammanassie Dam rainfall station, a gradual positive trend with a slope of +0.6156 in the monthly rainfall series occurred since 1925 (Figure 7.7). The coefficient of correlation and the one-tailed probability of F-Test between time (1925-2002) and MAP are 0.14 and 5.41E-29, respectively. Thus, there is not significant

correlation. The high rainfall values measured in 1980/1981, 1992/1993 and 1996/1997 indicate an increase in the magnitude of rainfall totals implying an increase in the magnitude of extreme rainfall events. The CRD seems to have the period of 43 years from 1948/1949 to 1990/1991. The new increasing period began in 1990/1991 although an extremely low rainfall event occurred in 1997/1998.

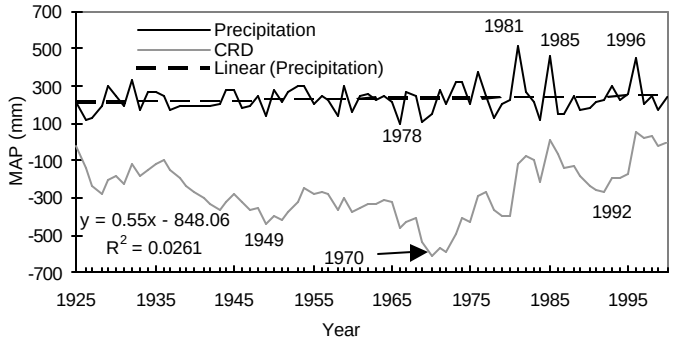

Figure 7.5: Rainfall and CRD patterns of the period 1925-2000 in the Hoekplaas

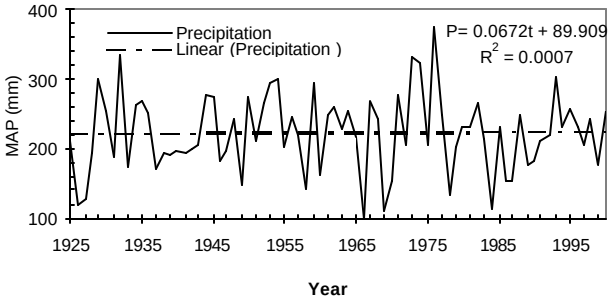

Figure 7.6 Trend of rainfall in the Hoekplaas rainfall station (Precipitations in 1981, 1985 and 1996 are replaced with mean of great average value of 232.1mm.)

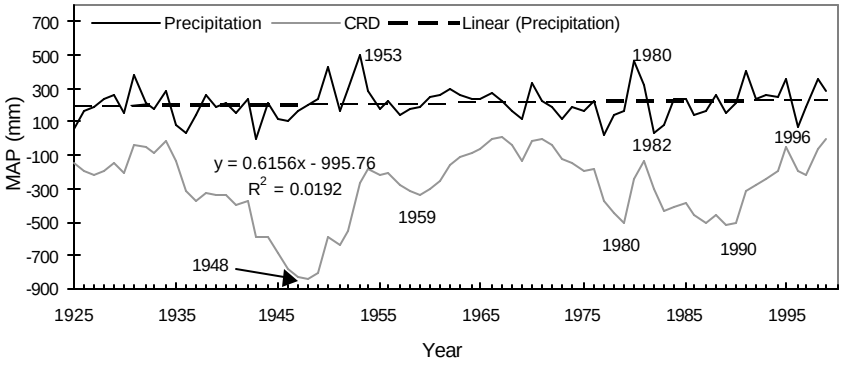

Figure 7.7 Rainfall trend in the Kammanassie Dam rainfall station (1925-2001)

7.3.2 Seasonal variation

Recharge may be significantly influenced by seasonal variation of rainfall. Some seasons may have more recharge; the others may be less. Four seasons have been distinguished (Cleaver et al., 2003) in the Klein Karoo, namely December-January-February (DJF), March-April-May (? ? ?), June-July-August (JJA) and September-October-November (SON).

A large ranges with low mean monthly rainfall are listed in Table 7.1. The lowest precipitation with mean values from 11.9 to 12.9mm·a^{-1} occurs in the DJF season. The highest one is from 19.1 to 21.5 mm per month in MAM season. A high standard deviation value was found in the each month. Perhaps this would be major issue in recharge estimation. The effective recharge may be contributed by extreme rainfall event due to highest monthly rainfall from 74 to 140mm (Figure 7.8).

Table 7.1 Seasonal rainfall patterns at the Kammanassie Dam rainfall station (1925-2001)

Statistic analysis	SON			DJF			MAM			JJG		
	SEP	OCT	NOV	DEC	JAN	FEB	MAR	APR	MAY	JUN	JUL	AUG
Size	75	75	74	74	74	74	74	74	74	75	75	75
Min (mm)	0	0	0	0	0	0	0	0	0	0	0	0
Max (mm)	104	77	137	82	114	94	83	140	114	86	74	118
Mean (mm)	17.8	19.2	20.3	12.2	11.9	12.9	21.5	21.1	19.1	16.4	19.1	20.3
Stand. deviation	20.4	19.1	27.1	17.0	20.2	17.9	19.8	26.0	21.0	17.0	17.6	23.6
Coef. of variation	114.9	99.4	133.3	139.0	170.6	138.7	92.3	122.9	110.0	103.6	91.9	116.4

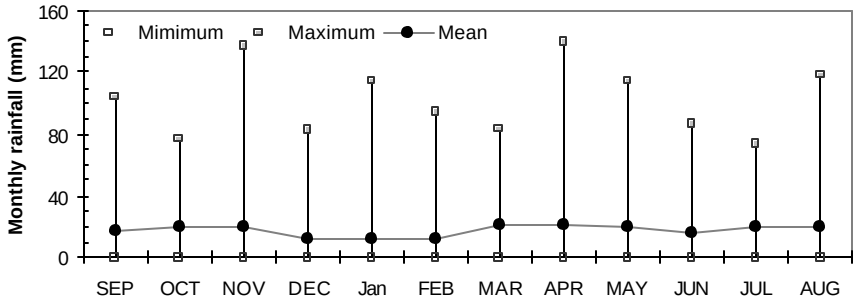

Figure 7.8 Ranges of monthly rainfall in the Kammanassie Dam rainfall station

7.3.2.1 Monthly trend

Figure 7. 9 to Figure 7.12 express the monthly tendency in the different seasons. There are positive trends in January, April, June, October, November and December. The other months have negative trends. The F-Test shows relative significant tendencies in January, March, May, August, September and October although the coefficient of relation is small (Table 7.2). In general, excluding influence of extreme rainfall event, more effective recharge may occur in the positive trend month; but less recharge in the negative trend one in recent years.

Table 7.2 Seasonal tendencies in the Kammanassie Dam rainfall station

Month	Tendency	Correl.	F-Test	Month	Tendency	Correl.	F-Test
Jan.	y = 0.0951x - 174.98	0.10	0.52	Jul.	y = -0.0046x + 28.223	-0.01	0.07
Feb.	y = -0.0711x + 152.59	-0.09	0.10	Aug.	y = -0.0361x + 91.218	-0.03	0.49
Mar.	y = -0.0797x + 177.97	-0.09	0.43	Sep.	y = -0.0234x + 63.748	-0.02	0.58
Apr.	y = 0.272x - 512.87	0.23	0.13	Oct.	y = 0.0634x - 105.18	0.07	0.25
May	y = -0.0568x + 130.64	-0.06	0.76	Nov.	y = 0.1442x - 262.78	0.11	0.06
Jun.	y = 0.0892x - 158.75	0.11	0.04	Dec.	y = 0.1058x - 195.53	0.13	0.04

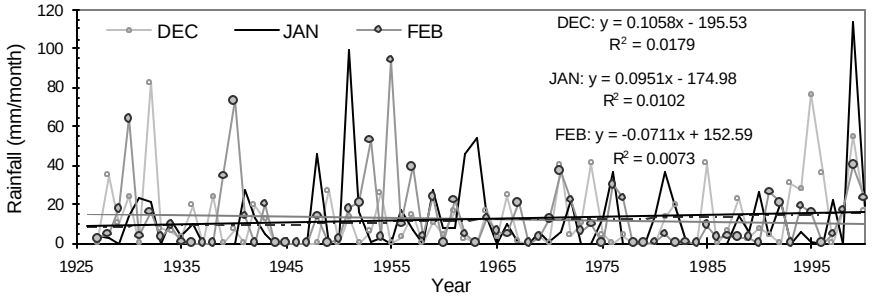

Figure 79 Rainfall tendency in the DJF season

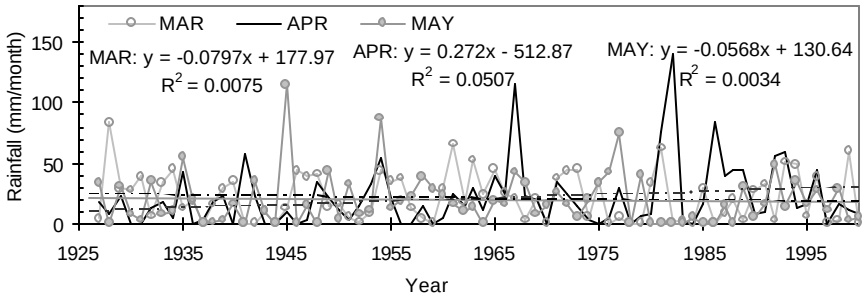

Figure 7.10 Rainfall tendency in the MAM season

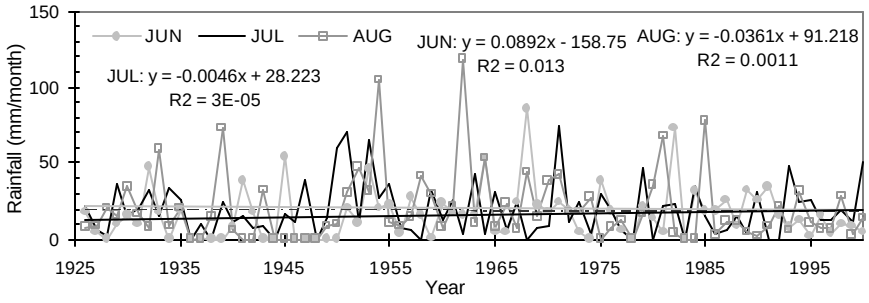

Figure 7.11 Rainfall tendency in the JJA season

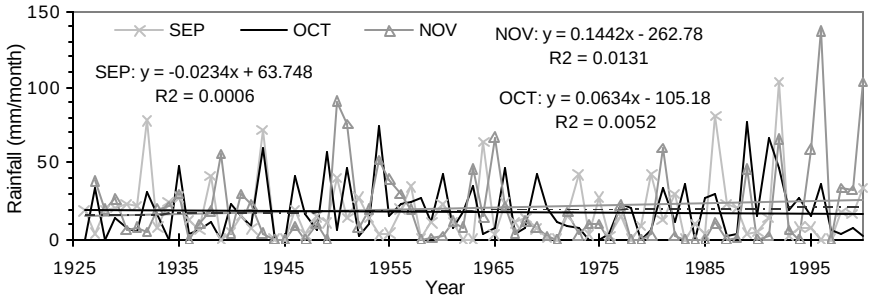

Figure 7.12 Rainfall tendency in the SON season

7.3.2.2 Monthly variation

The rainfall in the same month has its own variation in long-term. This would lead to more complex recharge process. For any month, the increased monthly rainfall in a time series would potentially increase recharge in the period. The period with increasing or decreasing rainfall is identified through the pattern of the CRD. The increasing CRD indicates relative more rainfall than monthly average rainfall. The decreasing CRD pattern implies less rainfall than monthly average rainfall. The records in the Kammanassie Dam rainfall station are used to perform the CRD analysis. The monthly CRD (1925- 2000) in the different seasons is shown in Figure 7.13 to Figure 7.16. The following observations were made:

- In December, the decrease in the CRD was sustained from 1933 to 1992.
- In January, the first continuous decreasing CRD period was in 1933 to 1958; the second period started in 1964 and ended in 1998 after a short period of increase.

- In February, the lowest CRD was in 1938, 1951 and 1998; the longest sustaining period of unusually scarce rainfall was for 1959 to 1997.
- The period of more rainfall started in 1992 with increasing CRD in the DJF season.
- A similar tendency occurred in March and May. The period of increase for CRD was from 1944 to 1979 and from 1992 to 2001. The period of decrease in the CRD was for 1979 to 1991. Relatively more rainfall occurred from 1944 to 1979 and 1992 to 2001 but unusually scarce rainfall occurred from 1979 to 1991 in March and May.
- The longest period of decrease in the CRD occurred from 1925 to 1980 in April. The CRD increased a little and reduced again from 1964 to 1980. The period of increasing CRD occurred after April 1980. An anomalous scarce rainfall period lasted for 65 years in April. More rainfall has been occurring since 1980 in the MAM season.
- A period of increase in the CRD started in the 1990's in the MAM season.
- The period of increase in the CRD was from 1951 to 1992 in June, and from 1949 to 1972 in July. The period of decrease in the CRD occurred after 1972 in July. Relatively more rainfall was recorded in 1951 to 1992 in June and unusually scarce rainfall occurred after 1972 in July. A period of decreasing CRD started since 1992 in the JJA season.
- For September, the decreasing period of the decreasing CRD patterns had been occurring since 1943. For November, the period of decreasing CRD pattern was from 1966 to 1994. An unusually scarce rainfall occurred in these years, and relatively more rainfall occurred in November after 1994, but up to now the scarce rainfall period occurs in September.
- The points of the lowest CRD patterns occurred in 1942 and 1988 in October. In the 1925 to 2001 period, two scarce rainfall periods and two high rainfall seasons occurred in October.

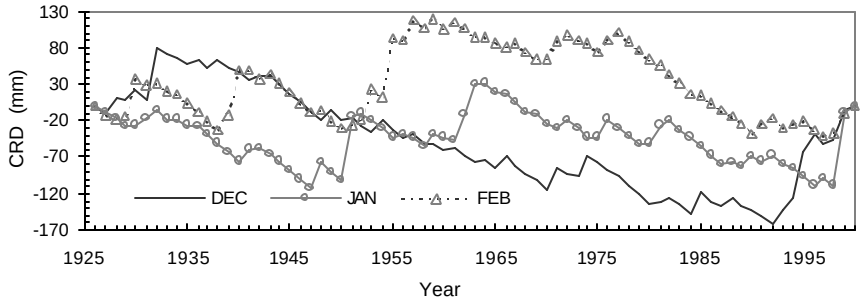

Figure 7.13 CRD patterns in the DJF season

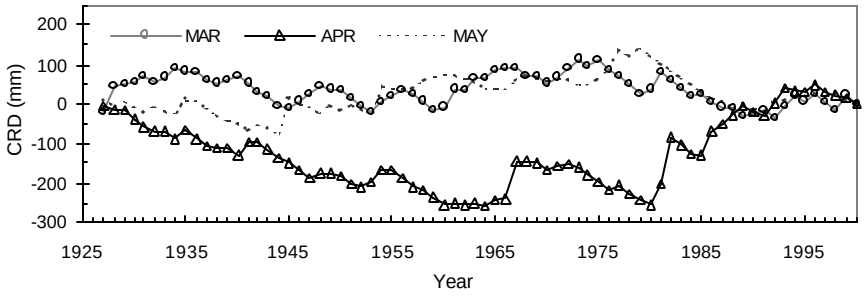

Figure 7.14 CRD patterns in the MAM season

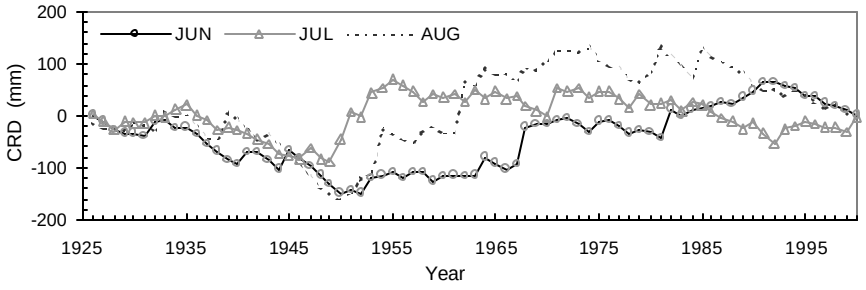

Figure 7.15 CRD patterns in the JJA season

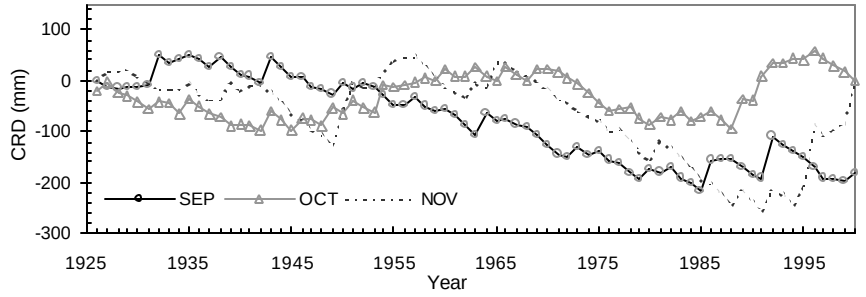

Figure 7.16 CRD patterns in the SON season

7.3.3 Extreme rainfall event

The extreme rainfall event may play a major role in the recharge in the study area. There is a smaller average value as well as the amplitude of rainfall event in the Kammanassie area than those in the Hoekplaas rainfall station (Table 7.3). For the Hoekplaas rainfall station, the average value is 232.1mm·a^{-1}; the minimum mean of the rainfall is less than the average value, which is 181.3mm·a^{-1}; the maximum mean of the rainfall is higher than the total average values, which is 295.5mm·a^{-1}. The anomaly events with 16 extremely low rainfall events and 12 extremely high rainfall events are identified (Table 7.5 and Table 7.6) using the critical values (Table 7.4).

Table 7.3 Statistical results of precipitation in the Kammanassie area (mm·a^{-1})

Rainfall station	Hoekplaas (I. Barnard)			Kammanassie Dam		
Item	Total	Below total average	Above total average	Total	Below total average	Above total average
Years	75/76	42	34	75	38	37
Minimum	98.5	98.5	240.8	0.0	0.0	214.0
Maximum	517.3	231.3	517.3	498.0	208.0	498.0
Mean	232.1	181.3	295.5	209.3	138.8	283.9
Geomean	225.5	176.4	300.3	191.0	115.4	275.6
Standard dev.	75.3	35.2	65.8	97.1	54.2	72.6

Table 7.4 Critical value of anomaly

Site	Extremely high rainfall events (mm·a^{-1})		Extremely low rainfall events (mm·a^{-1})	
	Average + Standard deviation	Average above total average	Average - Standard deviation	Average below average
Hoekplaas	307.3	295.5	156.8	181.3
Kammanassie Dam	306.3	283.4	112.4	138.8

Table 7.5 Extremely low rainfall events in the Hoekplaas rainfall station

Year	1926	1927	1933[1)]	1937[1)]	1949	1958	1960[1)]	1966	1969	1970	1978	1984	1986	1987	1989[1)]	1999
P(mm)	116.8	128.0	172.8	171.0	145.5	143.3	161.0	98.5	110.3	151.5	132.5	114.5	152.0	154.8	174.8	176.8

[1)] The events are identified by critical value of 181.3mm·a^{-1}.

Table 7.6 Extremely high rainfall events in the Hoekplaas rainfall station

Year	1929[2)]	1932[2)]	1953[2)]	1954[2)]	1959[2)]	1973	1974	1976	1981	1985	1993[2)]	1996
P(mm)	302.3	334.0	293.3	300.0	294.0	330.5	322.0	375.5	517.3	454.3	303.8	452.5

[2)] The events are identified by critical value of 295.5mm·a^{-1}.

A major variation in the precipitation occurs in the two rainfall stations although they were in the same "homogeneous" rainfall districts. For the Kammanassie Dam rainfall station, there were 8 extremely low and 8 high rainfall events (Table 7.7). The year with extremely high rainfall events may produce more recharge, but the extremely low rainfall year results in less recharge at annual scale. Of couse, the indivadually high rainfall event must not be ignored.

Table 7.7 Extreme rainfall events in the Kammanssie Dam rainfall station

Low events	Critical value 112.38 $mm \cdot a^{-1}$	Year	1925/ 1926	1935/ 1936	1936/ 1937	1943/ 1944	1977/ 1978	1982/ 1983	1984/ 1985	1997/ 1998
		P (mm)	67	85	36	0	21	41	82	68
High events	Critical value 306.28 $mm \cdot a^{-1}$	Year	1950/ 1951	1953/ 1954	1970/ 1971	1980/ 1981	1981/1 982	1992/ 1993	1996/ 1997	1999/ 2000
		P (mm)	430	498	331	470	325	411	355	361

7.4 RAINFALL IN MOUNTAINOUS AREAS

The rainfall pattern in the mountainous area is the most important issuse for the recharge, because almost entire recharge areas of the TMG aquifer distribute in the mountainous areas. Four rainfall stations, namely Parshall, V-notch, Wildebeesvlakte and Purification Works East, are used to perform the CRD analysis in finding the patterns, which impact on the recharge. There are similar rainfall patterns, difference in magnitude from September of 1993 to March of 2003 (Figure 7.17). The highest rainfall occurs in the Wildebeesvlakte rainfall station, and the lowest one in the Purification Works East rainfall station.

The observations from the CRD pattern (Figure 7.18) are as follows:

1) There are similar patterns of the CRD but different magnitude in the four rainfall stations. The sequence of the CRD patterns from maximum to minimum is the Wildebeeslvakte, Parshall, V-notch and Purification works East rainfall stations.
2) The wave patterns occurred in September of 1993 to September of 1996.
3) The positive trend pattern occurred in from September of 1996 to June of 1997. Negative patterns occurred from July of 1997 to May of 2002.

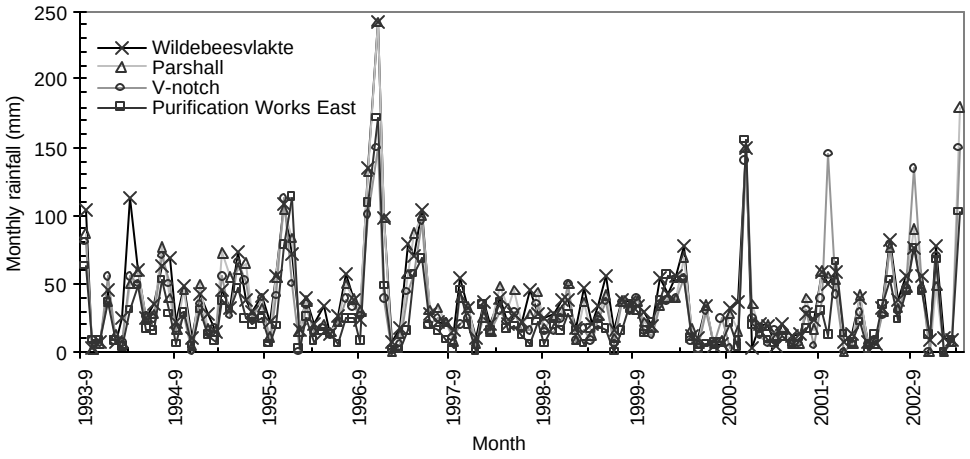

Figure 7.17 Rainfall patterns in the Kammanassie mountainous area

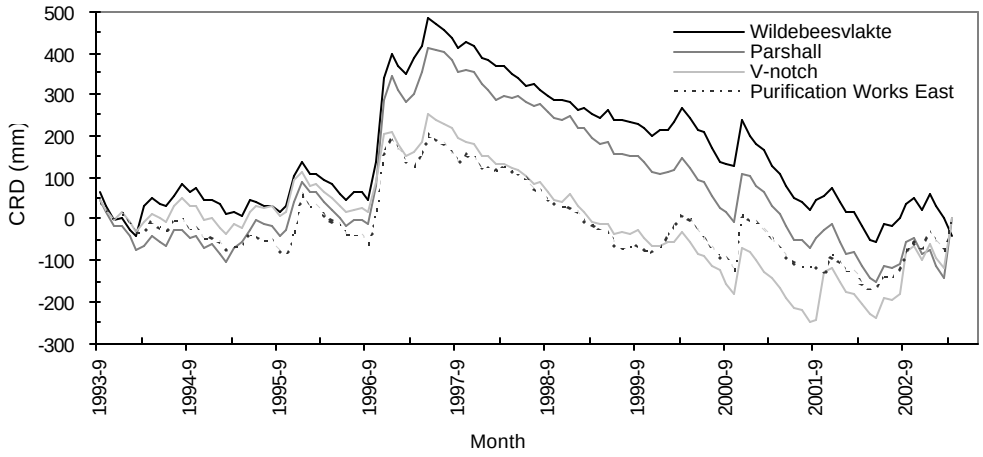

Figure7. 18 CRD patterns in the Kammanassie mountainous area

High correlation coefficients occur between the four rainfall stations, but the F-Test probabilities are low except between the Parshall and Wildebeevlakte rainfall stations (Table 7.8). The significant correlation may occur between the Parshall and Wildebeevlakte rainfall stations because of the highest probability of 55.8%. From this point of view, the selection of the rainfall station should be worked out carefully if rainfall records are used to estimate recharge. For the Parshall and Wildebeevlakte rainfall stations, a same distribution of rainfall frequency occurred in 1994-2003 (Figure 7.19); the frequencies of rainfall events were 20.7% and 26.1% for rainfall higher than 50mm per month, and 50.5% and 52.3% for higher than 30mm per month, respectively.

Table 7.8 Cross correlation analysis and F-Test

Rainfall station	Parshall VS Wildebeesvlakte	Parshal L VS V-notch	Parshal L VS Purification Works East	Wildebeesvlakte VS Purification Works East	Wildebeesvlakte VS V-notch	V-notch VS Purification Works East
Coe.correl.	0.98	0.75	0.86	0.81	0.68	0.92
F-Test probability	5.58E-01	8.06E-03	7.32E-09	1.66E-07	3.84E-02	1.20E-03

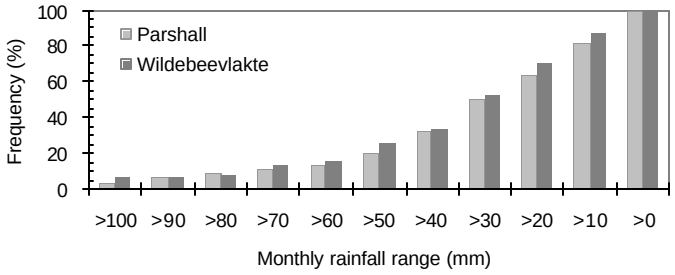

Figure 7.19 Rainfall event frequencies of the Parshall and Wildebeevlakte rainfall stations from April 1994 to March 2003

7.5 RAINFALL RELATED TO TEMPERATURE

Recharge may be affected by temperature through evaportranspirstion. The similar patterns of monthly minimum and maximum temperatures occur in the Kammanassie mountainous area (Figure 7.20 and Figure 7.21). The highest temperature occurs in February, and the lowest one occurs in June. The relationship between rainfall and temperature is illustrated in Figure 7.22. A lower difference in the temperature but higher rainfall occur in March, April and November, thus the recharge indicate by comparsion may also be higher. Although the lowest temperature and difference in temperature occur in June and July, the recharge may be low because of low rainfall.

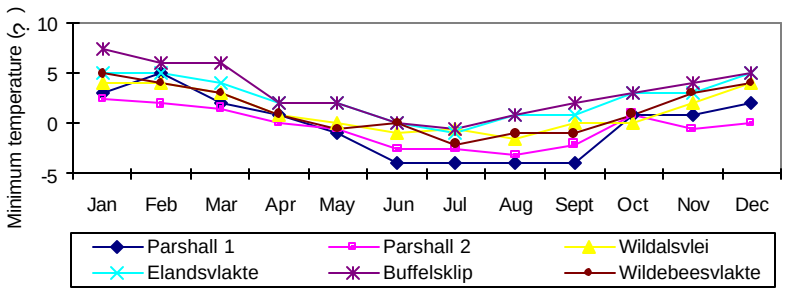

Figure 720 Minimum temperatures in the Kammanassie mountainous area

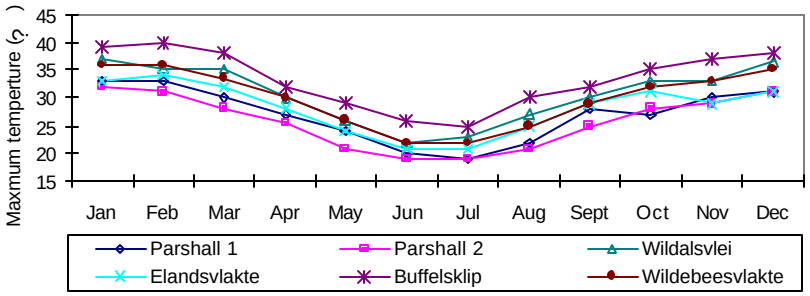

Figure 7.21 Maximum temperatures in the Kammanassie mountainous area

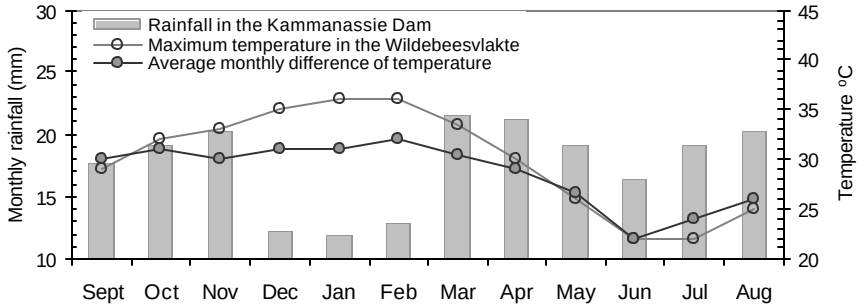

Figure 7.22 Relationship between rainfall and temperature

7.6 SUMMARY

Based on the discussion above, the following observations are generalised:

- A gradual positive trend of rainfall occurred in the Hoekplaas rainfall station in 1925-2002, but the trend is no significance. The anomalous events with 16 extremely low rainfall events and 12 extremely high rainfall events are identified by different critical values.
- A gradual positive trend with low one-tailed probability occurred in the Kammanassie Dam rainfall station since1925. There was a positive tendency in January, April, June, October, November and December, and a negative tendency in the other months in the Kammanassie Dam rainfall station. Negative CRD patterns occurred in the mountainous area from July 1997 to May 2002.

- The similar patterns of CRD are observed in the Kammanassie Mountainous area. Negative patterns of CRD occurred from July of 1997 to May of 2002. A significant correlation occurred between Parshall and Wildbeesvlakte rainfall stations.
- Positive trend of rainfall does not mean positive recharge trend. Neither does the seasonal trend. The variation of monthly rainfall results in more complicated water level response.

Chapter 8

Hydrogeology in the Kammanassie Area

8.1 INTRODUCTION

Understanding of the characteristics of the fractured rock of the TMG in the Kammanassie area would assist the analysis of recharge process and recharge estimation. The storativity (porosity) and the connectivity of the TMG aquifer rocks are major factors response of controlling the recharge. The secondary porosity of the Kouga and Peninsula quartzites is estimated to be the order of 0.1 to 1%; while the secondary porosity of the Vermaaks Keystone Block is order of 5%, even as high as 7% along the faults based on geological conjecture (Hälbich and Greef, 1995, Kotze, 2002). The width of open joints in the Kouga and Peninsula Formations is estimated to range between 1mm and 10 mm per metre (0.1% to 1.0 % of porosity) and the storativity of the Peninsula Aquifer are from 1‰ to 2.2‰ (Kotze, 2002). From west to east of the Kammanassie Anticline, four different structural domains (see to Figure 8.14, Chevallier, 1999) related to different types of fracturing prevailing show a different fracture pattern, which could imply different recharge processes.

Groundwater regime in the Vermaaks River area is conditioned by both precipitations and wellfield developments. The water level has declined as 27.54m-50.60m below the initial water level because of an annual abstraction of 137,000 to 281,000 m^3. A number of cold springs used to occur along the lower western slopes of the Kammanassie Range but have dried up since the early 1970's. These still occasionally run very weakly after rainfall events according to Mr Haasbroek of Overberg water. Three small separate hot springs emanated in the valley floor below the Bokkraal Wellfield until the early 1970's (Smart, 2000).

This chapter aims to comprehend the conceptual hydrogeological model of the study area including the identification of the recharge area, the feed mechanism of the springs in the Kammanassie area and storativity of the fractured rock aquifer, in order to aid analysing the relationship between the water level fluctuation and rainfall and estimating recharge.

8.2 PHYSIOGRAPHY

Western Kammanassie area including Vermaaks River catchment of 21.6km^2 and Marnewicks catchment of 25.3km^2 within the southern part of the Quaternary catchment (code: J33E) in the Klein Karoo region, is between a latitude of 33°34' and 33°38' south and a longitude of 22°30' and 22°42' east (Figure 8.1). The Vermaaks River Wellfield consists of four production boreholes (VR6, VR7, VR8 and VR11) at depths range from 177 to 251.3 m in the upper Vermaaks catchment of 10.85 km^2 within the Peninsula Formation window of 40.6km^2 is separated by Cedarberg Formation.

One of the climatic features of the area is the very large diurnal and seasonal fluctuation in temperature. Daily average minimum and maximum temperatures for summer and winter vary between 15 to 42 °C and -3 to 18.5 °C, respectively. The annual precipitation range is between 299mm and 714mm in the Parshall rainfall station from 1994 to 2002. Average annual evaporation varies between 1760mm·a^{-1} and 2050 mm·a^{-1}. The study area comprises a narrow valley with an elevation of approximate 500m to 1340 m above mean sea level (a.m.s.l.) surrounded by the Kammanassie Mountains, which have a maximum altitude of 1950 a.m.s.l. on the south side. The main drainage in this region is westward, where the perennial Olifants River drains the area to the north of the Kammanassie Mountain Range. The Vermaaks River and Marnewicks River, which have a relatively short tributary are ephemeral in the steep upper reaches, with more sustained flow in the lower reaches, and drain northward into the Olifants River.

The slope gradients are measured at less than 10°, 10-20°, 20-30° and greater than 30° (Figure 8.1). The slope gradient less than 10° distributes along the ridge of the mountain. The 10-20° slopes extensively spread in the Kammanassie area. The slopes with gradient 20-30° stretch along the lower Range. The slopes with gradient greater than 30° extend along the banks of the Vermaaks and Manewicks valleys. From the slope length point of view, most areas are good for rainfall infiltrating except the banks of the steep valley.

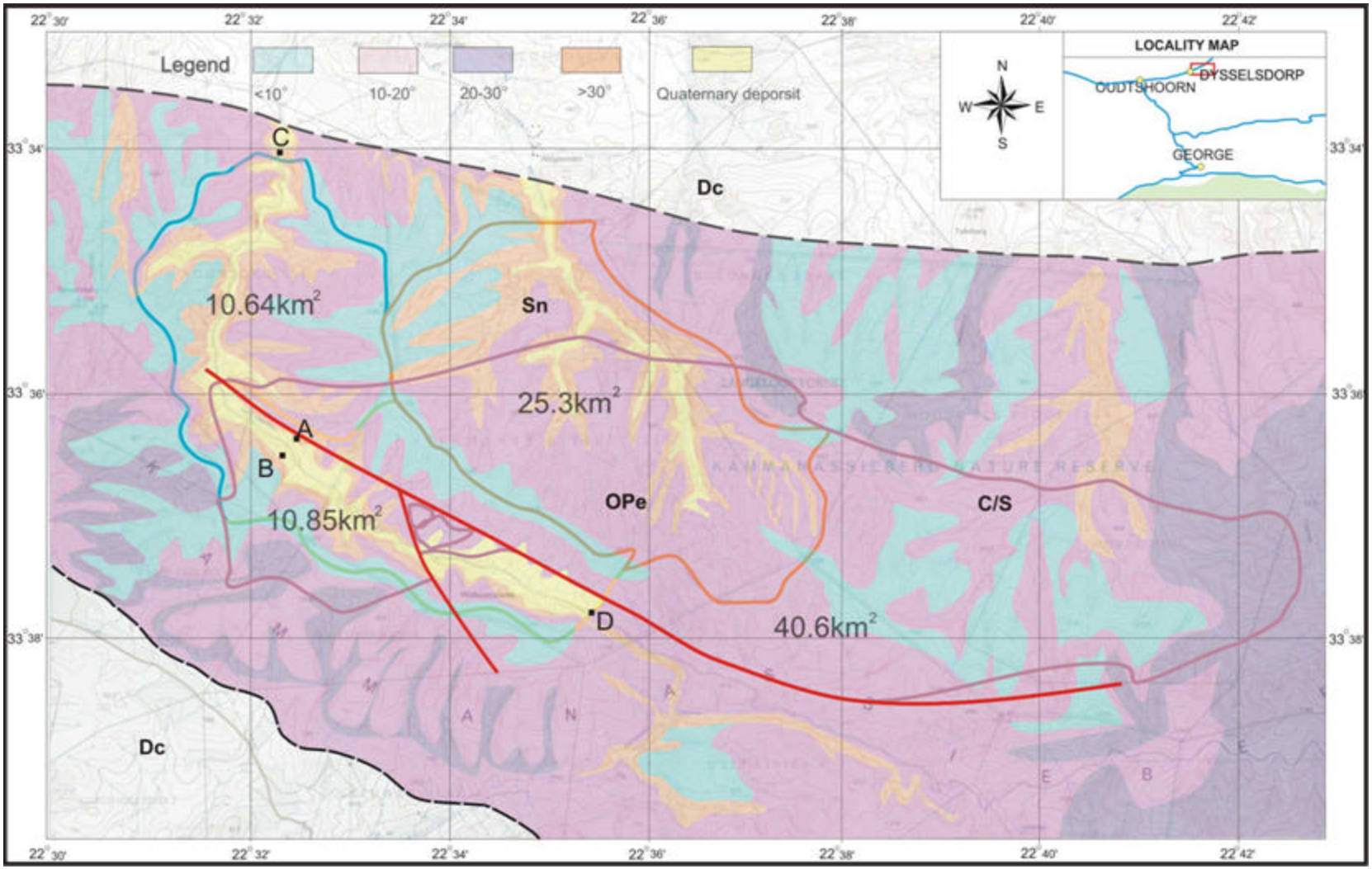

Figure 8.1 Physiography in the Western Kammanassie area

8.3 HYDROGEOLOGY

8.3.1 Aquifer

The TMG aquifer includes Peninsula and Nardouw aquifers, which are separated by Cedarberg aquitard (Figure 8.2). The aquifers strike EW; coincide with the axial plane trace of the Kammanassie mega anticline. The outcrops of the TMG form the main recharge area of the TMG aquifer.

The Peninsula Aquifer distributes along the mountain crests and comprises two thirds of the total thickness of the TMG (1 800m to 2 150 m, Kotze, 2002). The recharge areas of the Peninsula Aquifer are the outcrop of the Peninsula Formation, which are composed of a uniform succession of medium to coarse grained, thickly bedded, grey sandstones, characterised by cross bedding (Figure 8.3). The recharge areas are approximately 40.6km^2.

The Nardouw Aquifer distributes around Peninsula Aquifer, which outcrops in the centre of the Kammanassie mega anticline. The rocks of the Nardouw Subgroup are, in general, more brownish on weathered surfaces and thin intercalations of shale are more plentiful than in the Peninsula Formation (Figure 8.4). They become more feldspathic towards the top. Due to this higher shale content they are less competent than the Peninsula Formation and deformation tends to be more ductile, giving rise to the spectacular fold geometries. Much more complicated characteristics of the aquifer and inhomogeneous recharge occur in the Nardouw Aquifer system. The thickness of the Nardouw Aquifer cannot be estimated due to the folded formation.

The Cedarberg Formation comprises a 50m to 120 m thick shale layer (Kotze, 2002). It is a clear marker horizon because it weathers deeply to a smooth outcrop, which contrasts with the grey crags of the sandstones above and below (Figure 8.5). The shale is greenish and extremely fine grained where fresh. It forms a clear aquitard between the Peninsula and Nardouw aquifers.

Alluvial and slope deposits, consisting of sand, gravel and other unconsolidated materials, are distributed at the foot of the mountain and along the valley floor. The

thickness of these deposits is up to 15m (Kotze, 2002). The TMG aquifer is likely to receive infiltration from both open fracture networks of the outcrop rocks and the loose deposits.

A simple hydrogeological section depicting the aquifer system is illustrated in Figure 8.6. The Kammanassie Mountain is an eroded remnant of resistant TMG quartz arenites, also referred to as the Kammanassie mega-anticline, which were reconstructed (Hälbich and Greef, 1995). In the Nardouw subgroup, that is the Kouga, Baviaanskloof and most of the lower part of the Bokkeveld Group (Gydo Formation), the folds are overturned. Due to the repetition of small-scale folding, the outcrop length of the Kouga Formation is particularly long (Woodford et al., 1998). The Vermaaks fault cut the mega anticline along NW-SE strike (see to Figure 8.2). The Vermaaks fault comprises two parts: the centre zone is cemented breccias (silicification), where is impermeable; the zones beside the centre zone may have high permeability due to branch fault. High mountainous area forms the recharge area and the hydrodynamic head. The contact of the Cedarberg shale and Peninsula Formation is the natural discharge zone at valley floor. The regional flow seems to flow deeply. The faults linking to the Peninsula and Nardouw aquifers may be leakage zone.

8.3.2 Wellfields

There are 9 production boreholes (Appendix II), 27 monitoring boreholes (Appendix III) and 19 boreholes with no detailed data in the study area. Their location is shown in Figure 8.7. Boreholes VR6, VR7, VR8 and VR11 are the only boreholes drilled in the Peninsula Formation. The production boreholes, namely DP10, DP12 and DP29 in Varkieskloof Wellfield, DP28, DP15 and DP25 in Bokkraal Wellfield and VG3 in Voorzorg, were drilled in the Nardouw Subgroup. From the information of boreholes, the features of water strike, which is the unexpected strike with relevant high hydraulic conductivity in the TMG aquifer are as follow: two or three water strikes with a thickness of 1.5-15m were found along the 250m depths of the boreholes. The first water strike is usually drilled below 100m depths that are from 107m to 228m. The total thickness of the entire water strike is from 7m to 23 m. There is a difference in position between two strikes at different borehole site. The space varies from 15m to 62m.

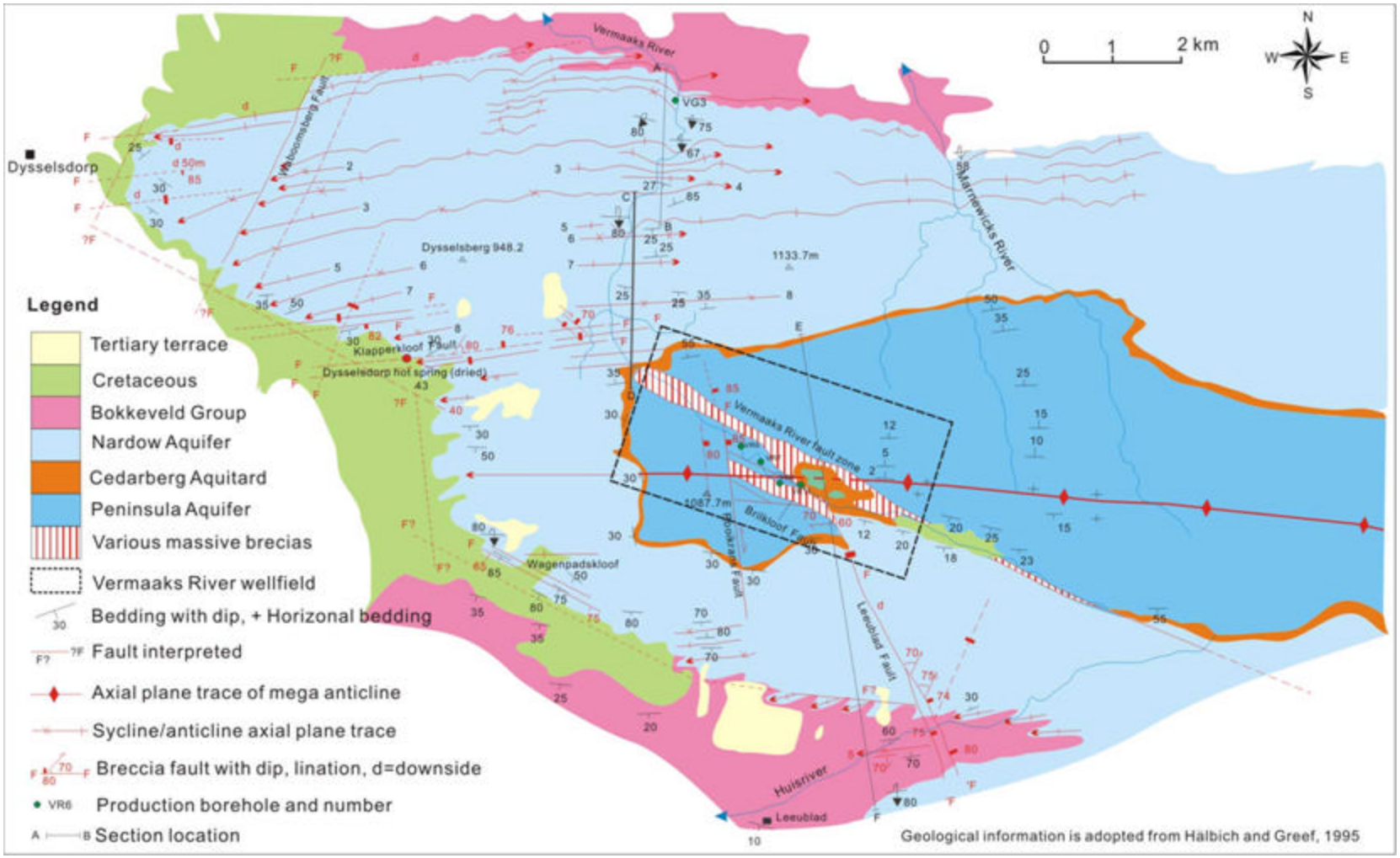

Figure 8.2 Hydrogeological map in the Kammanassie area

Figure 83 Peninsula sandstone in the Vermaaks River valley

Figure 8.4 Nardouw Subgroup in the Vermaaks River valley

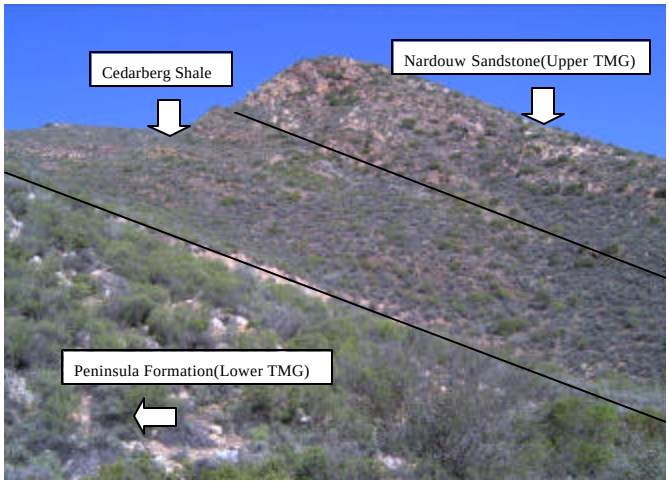

Figure 8.5 Cedarberg shale near the G40171 borehole

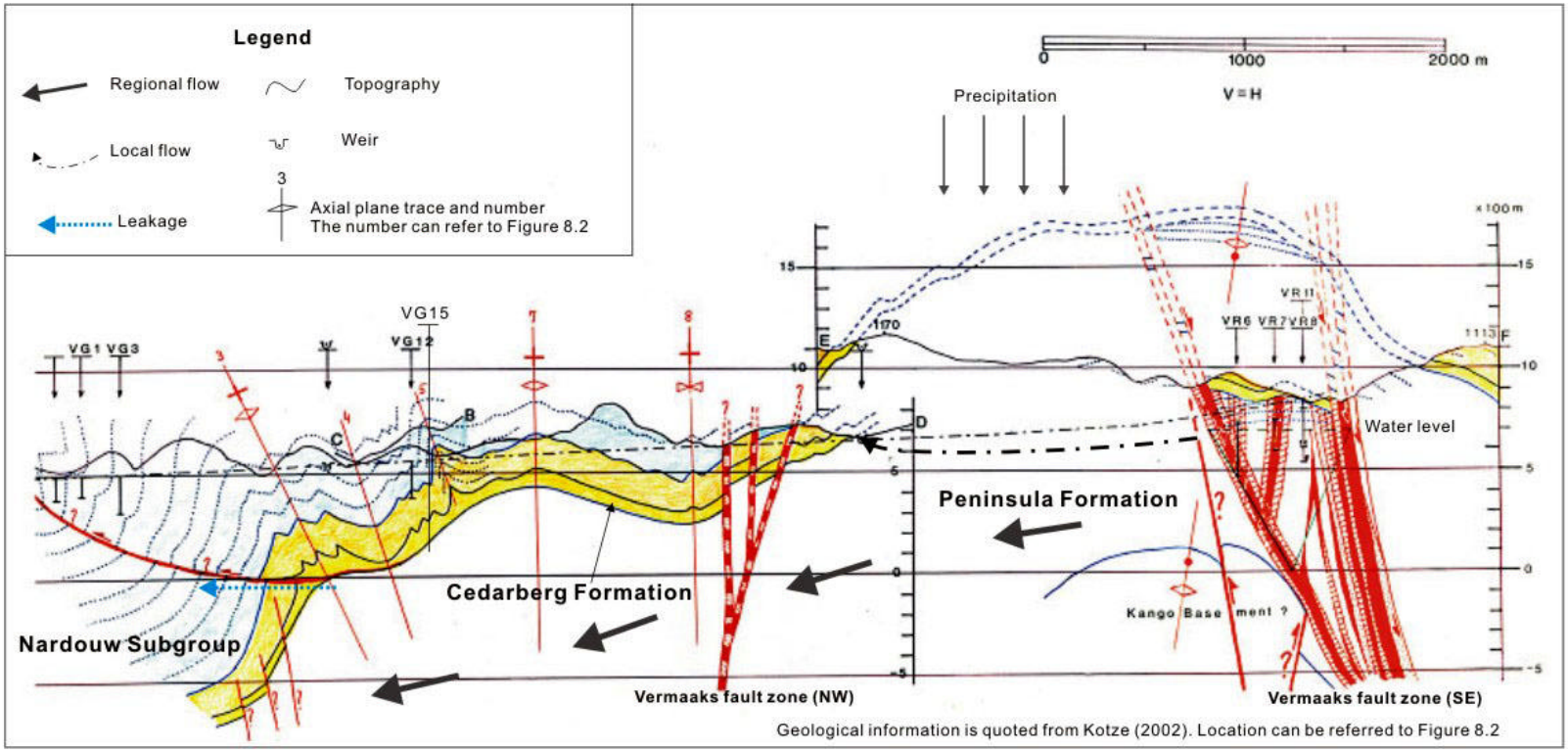

Figure 8.6 Hydrogeological section of the Kammanassie mega-anticline

8.3.3 Monitoring networks

The unsuccessful production boreholes of the KKRWSS, are currently used as monitoring boreholes (Appendix III). The boreholes, namely DG, are drilled near the Droëkloof production borehole DG110. VR5 and WN101 are situated in the Nardouw Aquifer (Baviaanskloof Formation, just south of the Marnewicks v-notch). VG12 is an important monitoring borehole, midway between the VG3 and the Cedarberg shale layer in the Vermaaks River Valley. DP27 is situated near the Varkieskloof production boreholes, and DP13, 14 and 20 near the Bokkraal production boreholes (Figure 8.7).

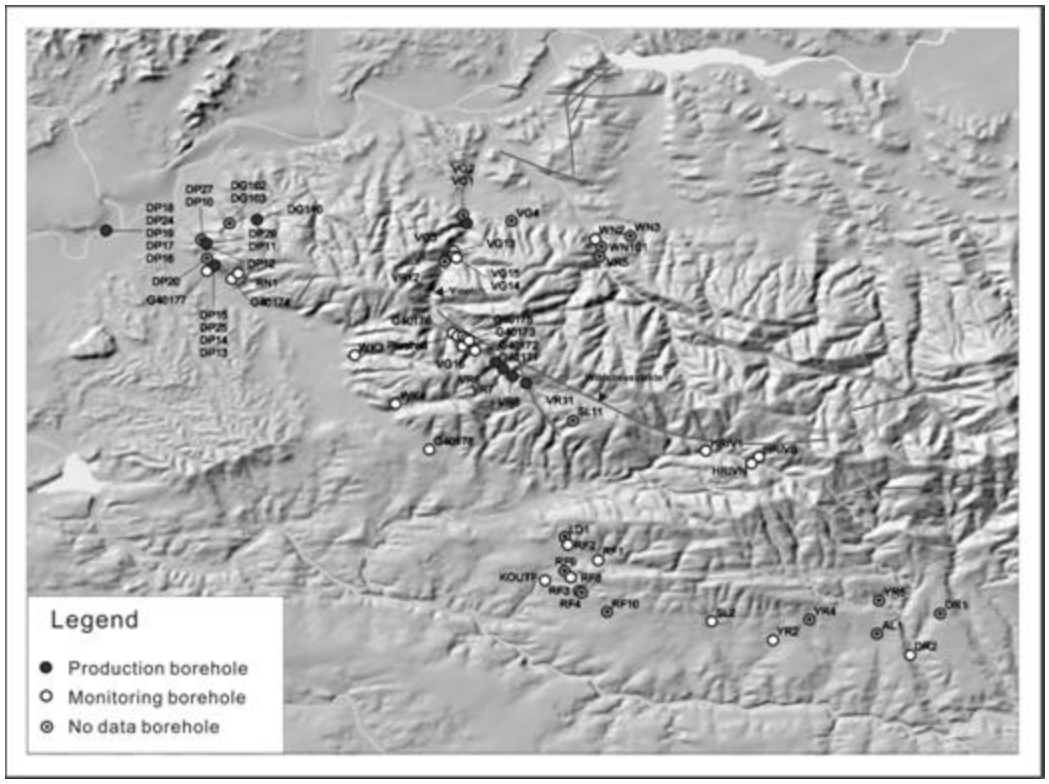

Figure 8.7 Borehole site in the Kammanassie area

The monitoring boreholes (Appendix IV) have their individual purpose and specific monitoring requirements. G40171, G40172 and G40173 are shallow boreholes drilled on the farm Voorzorg 124, upstream of the Cedarberg shale layer to monitor the inter-relationships between alluvial and TMG groundwater. G40174 was drilled on the farm Rietfontein 142 to monitor the water level responses to abstraction from private

abstraction borehole RN1. G40175 was drilled to a depth of 126 m on the farm Voorzorg 124, it subsequently collapsed and was grouted. It was replaced by the nearby G40175A, next to the abandoned G40175. The purpose of this borehole was to investigate the effectiveness of the C/S layer as an aquitard. G40176 was drilled on the farm Voorzorg downstream of the Cedarberg shale layer. G40177 was drilled south of the Bokkraal Wellfield to monitor water level responses to abstraction from the above-mentioned Wellfield. G40178 was drilled on the southern flanks of the Kammanassie Mountain to monitor long-term water level fluctuations arising from private and commercial abstraction from the Vermaaks River Wellfield. The use of these boreholes seems not to be effective to monitor the water level fluctuation in responding to the abstraction in the Kammanassie area at different scale.

8.3.4 Water level fluctuation in the Vermaaks River Wellfield

The groundwater levels of the production boreholes have been declining since 1984 in the Vermaaks catchment (Figure 8.8). Only the water level of VG16 responds to that of the production borehole. The other monitoring bore holes have their own fluctuation. There are about 26 private boreholes with a total annual abstraction of $1.85\times10^{6}m^{3}\cdot a^{-1}$ in the Kammanassie Mountain area (Kotze, 2002). This makes more complex and uncertain in the water level fluctuation in response to the rainfall.

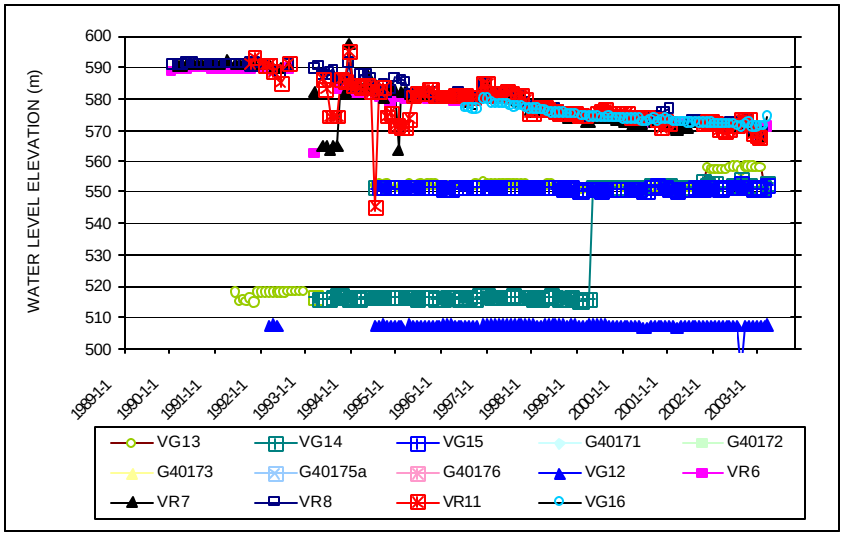

Figure 8.8 Water level fluctuation in the Vermaaks area

8.4 CONCEPTUAL HYDROGEOLOGICAL MODEL

A weir for spring monitoring was built on the Vermaaks River (Figure 8.9). The perennial pond suggests beds of relatively low permeability at the bottom. There are no perennial springs in the catchment except the spring in the monitoring station. The relationship between weathered zones and fractured rock aquifer is illustrated in Figure 8.10 and Figure 8.11. The shallow zone is extensively weathered with fractures partly filled in by clayey materials. Groundwater outflow from this zone is in the form of gravitational springs and seepage zones. The pond is maintained in part of by overflow from the Peninsula Aquifer and a local shallow groundwater or weathered zone. The artesian borehole G40175A, which is drilled through the Cedarberg shale, may confirm this. Due to the abstraction from the Vermaaks River Wellfiled, the spring (code: 051) dried up, and the water level dropped lower than first water strike (Figure 8.11).

Figure 8.9 Monitoring station in the Vermaaks catchment

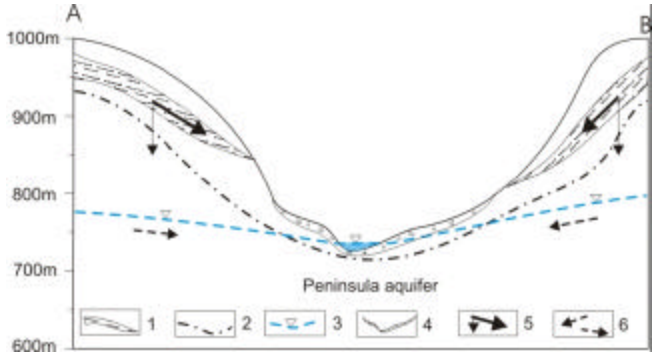

Box 1: weathered zone with high hydraulic connectivity;
Box 2: weathering limit; Box 3: water level; Box 4: new deposit;
Box 5: infiltrating direction; Box 6: flow direction

Figure 8.10 Hydrogeological section along transect A-B

(See Figure 8.1 for location)

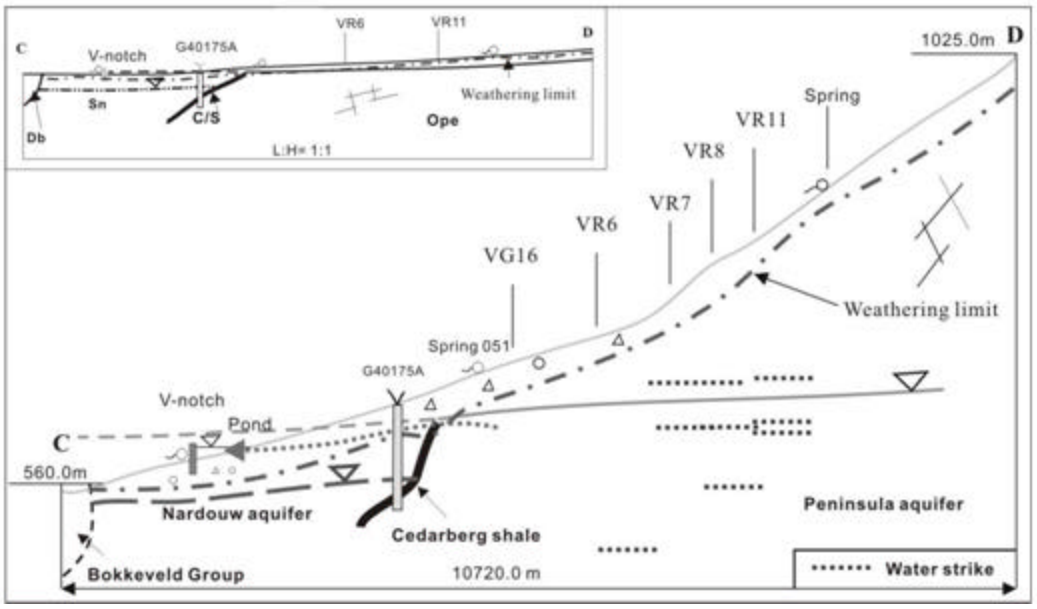

Figure 8.11 Hydrogeological section along the Vermaaks River

8.5 DISCUSSION OF FRACTURE SYSTEM AND RECHARGE

8.5.1 Fracture feature and connectivity

The E-W and N-S fracture systems have different characteristics, in terms of fracture geometries, fracture length and connection. Schematic presentations of the detailed geometry of (a) E-W and (b) N-S trending fracture systems are shown in Figures 8.12. The fracture density seems to be high, especially along the major fault.

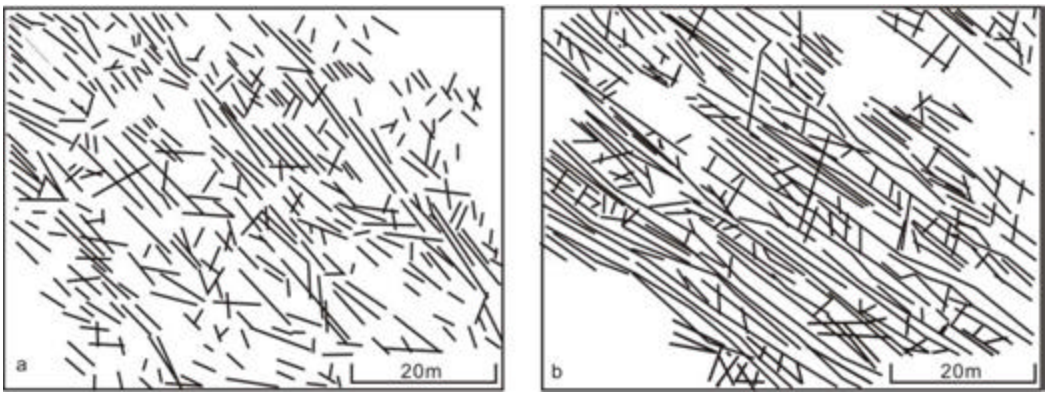

Figure 8.12 Fracture geometries in the Kammanassie area (After Kotze, 2002)

The E-W trending fault system has an anatomizing pattern with an acute angle in-between the three main fractures or joint orientations. Major faults are marked by a concentration of anatomizing fractures or joints (Figure 8.12a, Kotze, 2002). The N-S system comprises three sets of intersecting fractures and master joints with NNW-SSE, NNE-SSW and N-S orientations. Each set of joints has systematic and non-systematic joints perpendicular to each other (Figure 8.12b, Kotze, 2002). The systematic joints dominate and are often long fractures (>1 km), which are easily identified with remote sensing image. The three sets of systematic joints do not seem to correlate with major faults in the study area, and regional fracture density has an irregular distribution (Kotze, 2002). NNW-SSE trending fractures compose of the major fracture orientation for recharge in the Kammanassie area. Although the fractures possess orientation but the fracture density is high on the land surface, the recharge possesses diffuse pattern on the land surface in general, but preferential recharge occurs at depth because the fracture density would be decreased.

The NNW fractures and lineaments are very well developed in the TMG and are likely to be permeable to groundwater movement. The fractures trending NNE-SSW and fractures reactivated in E-W, WNW, N-S orientations are the preferred orientations for groundwater recharge and flow (Kotze, 2002), such as Rooikrans and Leeublad Faults. Higher recharge may occur along these faults.

A 200 m wide and 9 km long fracture zone occurs along the Vermaaks River valley, to smaller fault lines with sharply defined planes with up to 20 m wide breccia zones (see Figure 8.2). These include the ESE trending Brilkloof, SSE-trending Leeublad and Rooikrans and three E-W-trending Klapperskloof Faults. The ENE and NNE – trending fractures are lying with an angle between 40° and 90° to the direction of maximum compression, tectonic reactivation will be difficult in this orientation (Chevallier et al., 1999). Breccia, consists of rounded and rotated fragments in a fine-grained ground mass. A homogeneous mass of a very fine grained cataclasite, which is partly recemented and extremely hard (Figure 8.13). Thus the permeability of these faults should be very low.

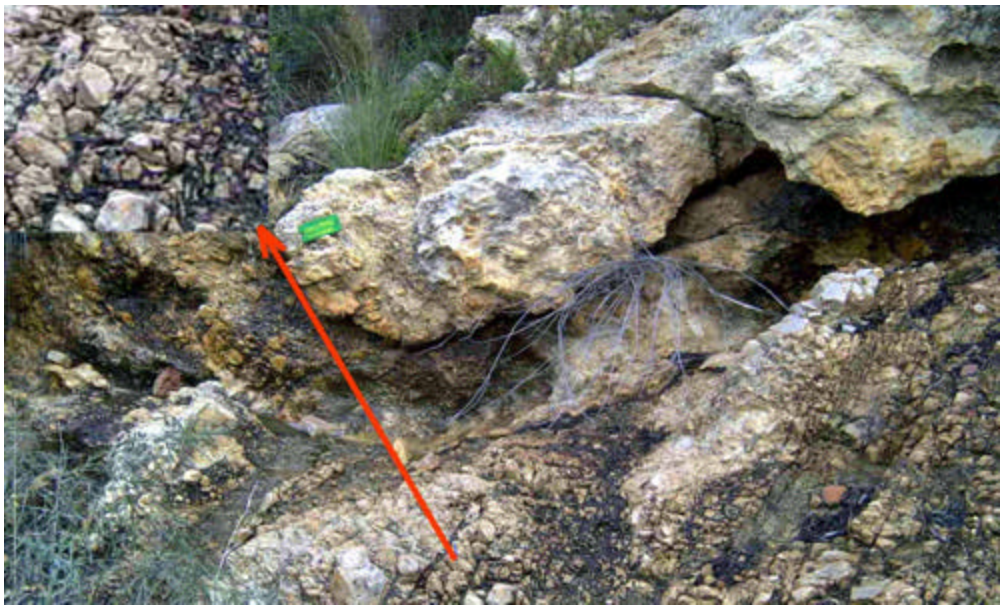

Figure 8.13 Breccia in fault zone in the Vermaaks valley

The patterns of the four different structural domains (Figure 8.14, Kotze, 2002) from west to east in the Kammanassie Mega Anticline are included:

- Domain A: WNW and NNE fracture systems intersect each other. Space NE: 650m-2300m; NW: 650m-1300m, EW: 300m-2700m.
- Domain B: The NNW overprint is very strong and dominant. Fracture networks connect each other by NNE with a broad fracture space with1000m-3000m.
- Domain C: NW, NE and E-W fracture systems connect each other in central joints. Fracture space is from 400m to 2000m.
- Domain D: NW, NE and E-W fracture systems connect each other by E-NE or near E-W conduit fracture. Fracture space is 500m-3000m.

The recharge pattern should be different in the for domain zones. Notice that the area of the block is more than 200km^2, which means the connectivity is only a surface phenomenon and more detail should be considered together with stress orientation.

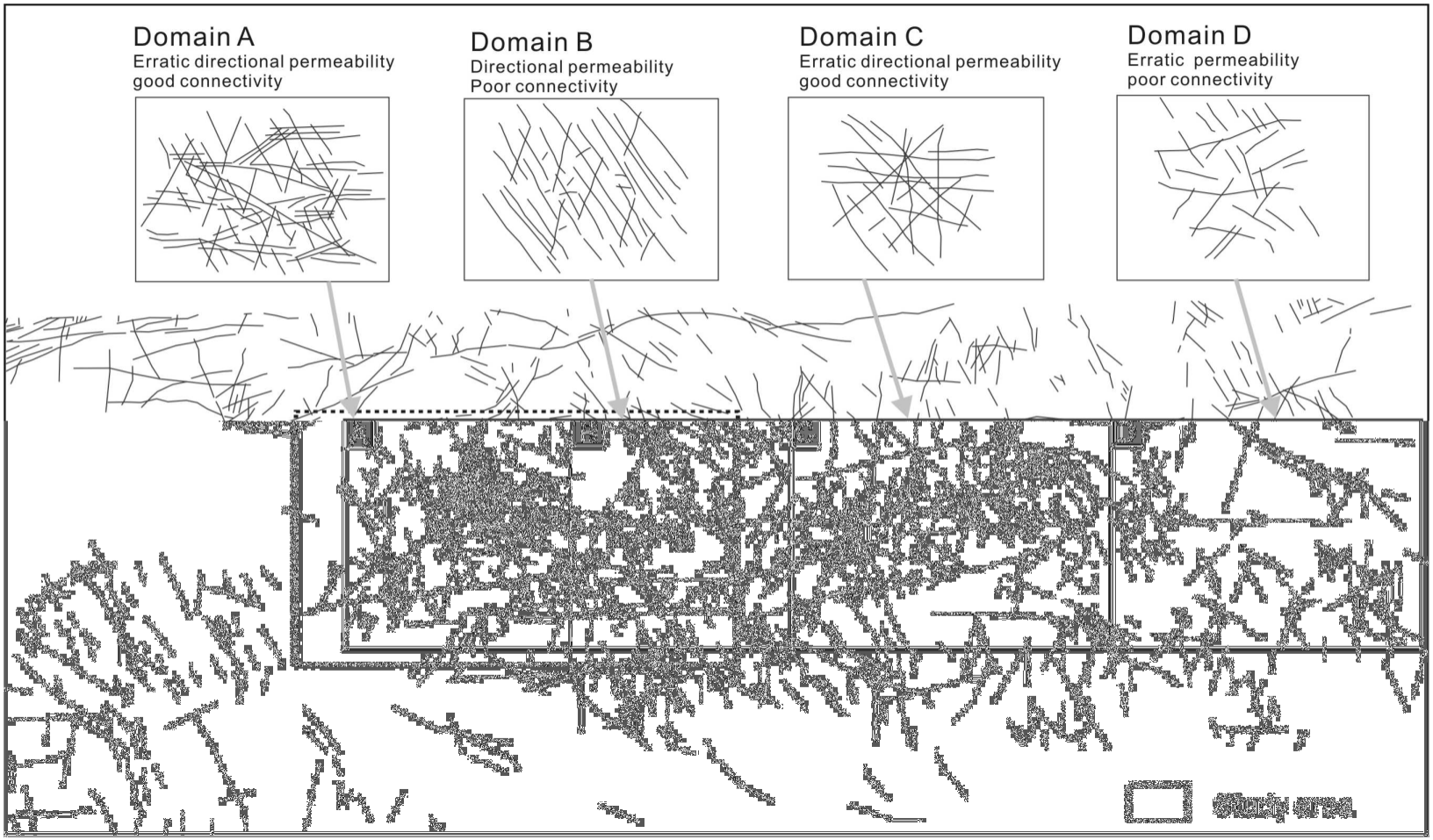

Figure 8.14 Lineaments of satellite image in the Kammanassie area (After Kotze, 2002)

8.5.2 Porosity and storativity

Porosity or storativity of an aquifer is a major factor in many methods for recharge estimation. There are large irregular spatial differences of the porosity and storativity in an aquifer. The accuracy and variation of the porosity or storativity is extremely related to the estimation methods. This would affect the accuracy of the recharge estimation.

The rock of the Peninsula Aquifer is a pure quartz arenite with a very low primary porosity due to the cementation of individual sand grains and later recrystallisation. However, increased rock induration led to a higher potential for brittle fracturing during latter deformation, as well as higher fracture frequencies and thus forming secondary porosity. The Nardouw Subgroup contains more silty and shaley interbeds and is associated with high feldspar content. Shale layers have a great impact on the fracturing and folding style of Nardouw Aquifers, which gives rise to large variations in the storativity.

For bedding, joint fractures and massive fault block in the Vermaaks area, the secondary porosity was estimated up to 5% by Kotze (2002), even in fault zone as high as 7% (Hälbich et al., 1995). However, it is observed these figures seem to be overestimated. For discussion purposes, the fracture state of 5% porosity of rock mass is theoretically equal to one fracture of 1000mm×1000mm×50mm or one pipe of 252.3mm diameter in $1m^3$ rock mass (Figure 8.15).

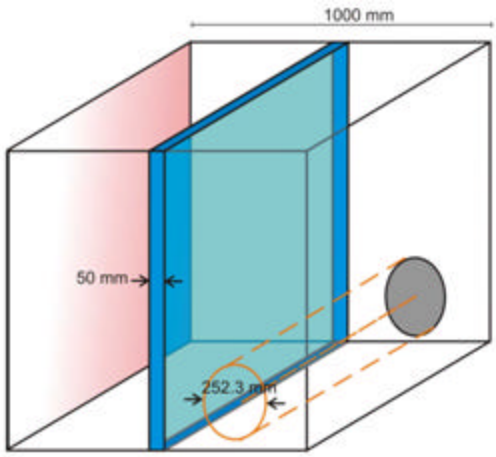

Figure 8.15 Fracture model with porosity of 5% in 1 m^3 rock mass

The theoretical results based on the fracture model are listed in Table 8.1. The width of a single fissure in a $1m^3$ rock mass with 0.1%, 1% and 5% porosity and 1, 2, 3, 6 and 9 fractures are from 1-0.111, 10-1.11 and 50-5.556mm under a parallel condition, respectively; the width of a fracture should be wider under cross condition. These theoretical results demonstrate that 1%-5% porosity could not easily occur in the TMG aquifer, especially at depth.

Table 8.1 Theoretic aperture of fracture in $1m^3$ cubic rock mass with gross section of $1m^2$

Condition / Items of fracture		Pipe Diameter (mm)	Parallel (mm)					Cross (mm)			
								1×1	1×1×1	2×2×2	3×3×3
Porosity %	Volume of facture m^3	1	1	2	3	6	9	2	3	6	9
0.1	0.001	3.568	1.00	0.50	0.333	0.167	0.111	0.500	0.333	0.167	0.111
1	0.01	11.284	10.00	5.00	3.333	1.667	1.111	5.013	3.345	1.672	1.115
5	0.05	252.313	50.00	25.00	16.667	8.333	5.556	25.321	16.954	8.477	5.651

The ranges of transmissivity (T) and storativity (S) in the Vermaaks River Wellfield are listed in Table 8.2. These also illustrate low storativity does not match the supposed high porosity. The accredited storativity value should be from 0.1‰ to 1‰ based on above discussion.

Table 8.2 Ranges of transmissivity and storativity in the Vermaaks River Wellfield (After Kotze, 2002)

Conditions	$\mathbf{T}_{min}(m^2 \cdot d^{-1})$	$\mathbf{T}_{max}(m^2 \cdot d^{-1})$	$\mathbf{T}_{aver.}(m^2 \cdot d^{-1})$	$\mathbf{S}_{min}$	$\mathbf{S}_{max}$	$\mathbf{S}_{aver.}$
Extreme	7	424	103.9	1.0E-3	2.2E-3	1.35E-3
Condition A	5	144	61.25	1.0E-3	2.2E-3	1.08E-3
Condition B	29	424	191.72	1.0E-3	2.2E-3	1.08E-3
Condition C	17	276	178.92	1.0E-3	2.2E-3	1.08E-3
Condition D	7	161	90.86	1.0E-3	2.2E-3	1.08E-3
Condition E	7	161	90.86	1.0E-3	2.2E-3	1.96E-3

8.5.3 Geological origin of the hot springs

The hot spring at Calitzdorp is located at the intersection between faults in the TMG and the basal shale layer of the Gydo Formation (Bokkeveld Group), occuring where the ENE-WSW trending faults connect with the NE trending faults near the base of

the Bokkeveld Group (Figure 8.16). The site of the hot spring should be the regional discharge area. Figure 8.17 shows the site of the Dysselsdorp hot spring (dried), which is also located at the intersection between faults in the TMG and Bokkeveld Group. Three small separate hot springs emanated within an area of approximately 100m^2 in the valley floor below the Bokkraal Wellfield until the early 1970's. The water temperature is indicative of deep circulating groundwater, which is up welling along a geological fault/fracture (Smart, 2000). Andreoli et al (1996) showed the positions of epicenters of a post Karoo rock age in South Africa. The positions of epicentres seem to correspond well with the localities of the hot springs. The Dysselsdorp hot spring dried and this could not only be associated with the earthquake, but also with a large abstraction near the site and climatic changes (Earthquake: A, Tulbagh in 1969, Magnitude: 6.5. B, Oudtshoorn: Date: 28 October 2001, Latitude: -33.542N, Longitude: 22.228E, Magnitude: 3.6, Depth: 5.0 km).

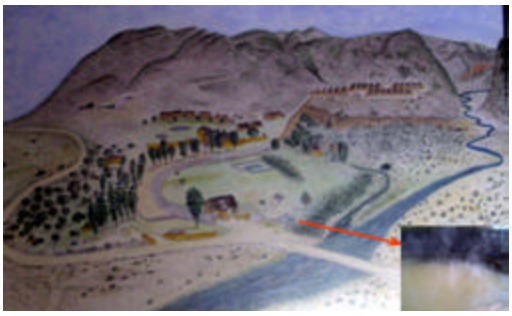

Figure 8.16 Calitzdorp hot spring
(The painting from Calitzdorp Spa)

Figure 8.17 The site of dried Dysselsdorp hot spring

A model for relation between interflow, local flow and regional flow is conceptualised (Figure 8.18). The interflow occurs in the mountainous areas with elevation of 220 to 1950m. The local flow may occur 220-1700m, but regional flow can flow at depth related to the distribution of the TMG aquifer. The regional discharge area supposed is located at Calitzdorp Spa based on the following reasons:

- For regional TMG aquifer with about 500km^2 recharge areas distributed in the Kammanassie area must have regional discharge zones or points.
- Two hot spring discharge points were found near the Kammanassie area, one is the dried Dysselsdorp hot spring used to occur on the elevation of 500m at the western foot of the Kammanassie Mountain, this would still illustrate the

region flow direction is from east to west in the Kammanassie area because the regional flow direction cannot be changed largely in short time. The other one is Calitzdorp hot spring located on the elevation of 220m in the western border of the Oudtshoorh Basin.

- The north and northeast boundaries are Cango Fault and Baviaanskloof Fault, which are supposed as the hydrogeological boundaries. There are no hot spring discharge zone or points along the faults.
- From stratigraphy point of view, the Cango Group is the bottom strata of southern boundary in the Outeniqua Mountain. No discharge zones or points of hot spring are found.
- From topography point of view, the highest peak (1950 a.m.s.l) is located at Kammanassie Mountain. The main drainage (Olifants River) in this region is westward, the Calitzdorp hot spring discharge at elevation of 220m located on the left bank of the Olifants River. This point is almost the lowest point of the basin.

It is important to note that the Calitzdorp hot spring can be fed not only by the recharge from the Kammanassie area, but also by the southern mountainous area.

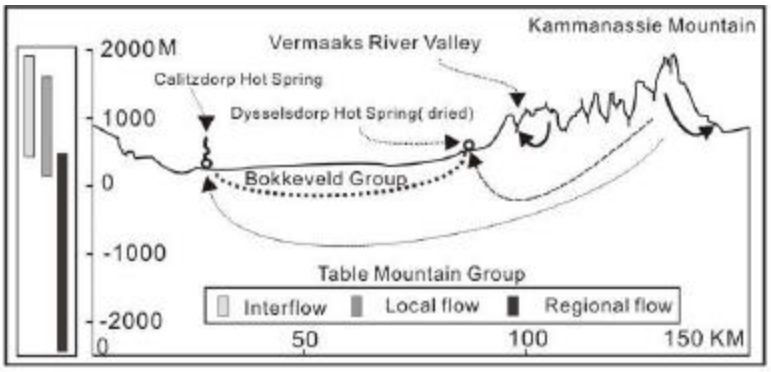

Figure 8.18 Relation between interflow, local flow and regional flow

8.5.4 Recharge area

For the Vermaaks River Wellfield, analysis of satellite imagery and hydrogeological settings suggests that recharge probably takes place within the outcrops of the Peninsula Formation window of 40.6 km^2. The Cedarberg shale and the breccias fault

form the recharge boundary of the Vermaaks River Wellfield. High density of fracture intersections and frequencies appear to facilitate recharge to the deep Peninsula aquifer system.

8.6 SUMMARY

The following points are concluded based on the above discussion:

- The watershed of the Vermaaks catchment is a natural recharge boundary at natural state, but the Cedarberg Formation and the fault along the breccias are actually hydrodynamic boundary as well as recharge boundary under pumping condition.
- The spring in the V-notch is mainly fed by leakages of shallow aquifer and partially by overflows of the local or regional aquifer.
- Effective recharge mainly occurs if the slope gradient is less than 30°. The interflow appears in steep even upright topography area. The soil deposited on the bottom of the valley should affect the recharge to the fractured rock aquifer. The different recharge processes occur in the mountainous area and valley. The preferential recharge is domination in the fractured rocks.
- The recharge possesses diffuse pattern on the land surface with high fracture density, but preferential recharge occurs at depth.
- The secondary porosity of bedding, joint fractures and massive fault block with 1%- 7% in the Vermaaks area is regarded to be too high based on geological conjecture. The accredited storativity value is from 0.1‰ to 1‰.

Chapter 9

Hydrogeochemical Characteristics in the Kammanassie Area

9.1 INTRODUCTION

This chapter aims to work out hydrogeochemical characteristics of the TMG aquifer in order to distinguish the difference between hot springs, springs, borehole water, interflow water and surface water. Based on isotopic information, groundwater circulation, residence time and recharge elevation are addressed. The main purpose is to assist in finding the components of the mixing model and providing the proof of the recharge processes through the use of hydrochemical data.

Hydrogeochemical data have potential to reduce uncertainties and evaluate site-specific long-term hydrogeological conditions and groundwater flow (Plummer et al., 1990). There may be a significant bias, both in time and sampling dimensions, between the data sets, which they represent (Pitkänen et al., 1999). Some conservative tracers like chloride and stable isotopes, which may originate from several sources, are often used as tracers for determining the water provenance (Epstein and Mayeda, 1953; Kennedy et al., 1986; Maule et al., 1994; Mayo and Loucks, 1995; Liu et al., 1995; Simpkins, 1995; Wood, 1999), for delineating the mixing of surface and groundwater (Fritz et al., 1976). Isotopes and chlorofluorocarbons (CFC) have been used as tracers for interpreting the groundwater dating and recharge estimation (Mazor, 1991; Cook and Solomon, 1997).

9.2 OUTLINE OF HYDROGEOCHEMICAL CHARACTERISTICS

As the start of KKRWSS in 1984, the chemical samples were discontinuously obtained. The earlier samples were collected from National Groundwater Data Base (NGBD) of South Africa in 1992 and 1994. Concentrations of some constituents are given in monthly report of the Overberg Board Water Management since 1994. The data used in this study include new measurements of rain water, and in addition to water samples, soils were sampled from rainfall gauges, boreholes and deposits in the

Vermaaks valley, specifically collected for the TMG recharge project (2002-2004) and existing groundwater and surface water data from the NGDB and Kotze (2001). The sampling included in all, more than 40 sets of samples was collected at groundwater sites (boreholes and springs) across the area. Borehole depths ranges from 23m to 150m, with median of 75m, water level range from 10m to 151m below land surface, with a median water level of 92.4m. The sampling sites in the study area are shown in Figure 9.1. The existing data from Kotze (2002) and NGDB (from the Department of Water Affairs and Forestry (DWAF), Bellville), include pH, TDS, EC, anions (F^-, Cl^-, HCO_3^-, SO_4^{2-}, PO_4^{3-}, NO_3^-), cations (Na^+, K^+, Ca^{2+}, Mg^{2+}), nitrogen components, Fe, Mn, Sr, Ba, SiO_2 and isotopes of O-18, H-2, C-14, C-13.

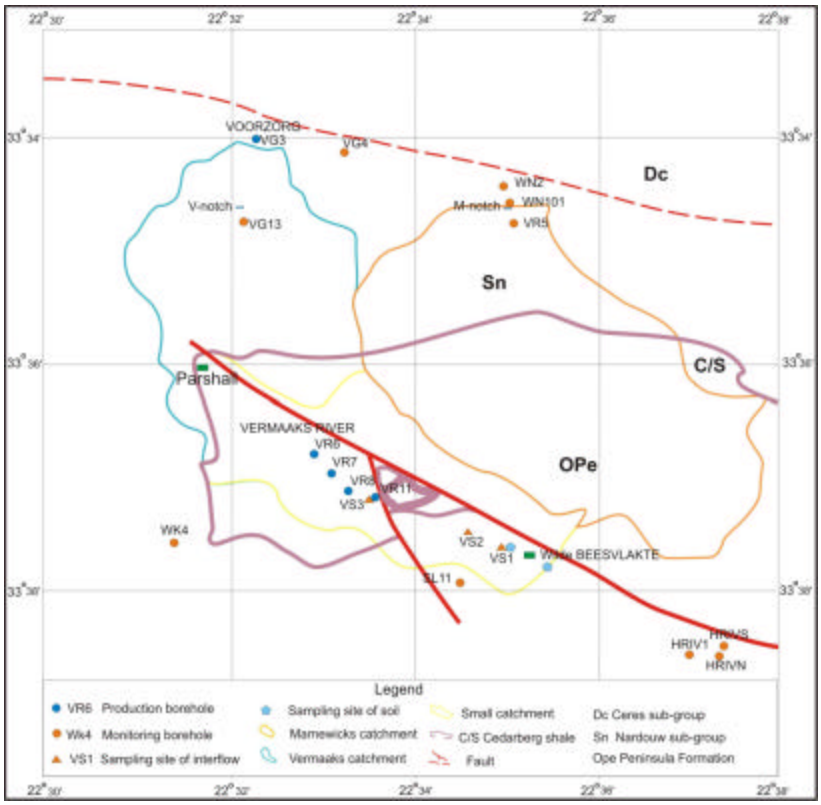

Figure 9.1 Sampling sites in the Kammanassie area

The results of the analysis of water quality in the Vermaaks area are presented in Appendix V. The main hydrogeochemical characteristics is summarised as follows:

- The ranges of average TDS in production boreholes of the Peninsula and Nardouw aquifers are 40-60.4 and 86.8mg·ℓ^{-1}, respectively. The TDS in

monitoring boreholes varies from 52 to 71.4mg·ℓ^{-1} when pH<7 and from 96 to 110mg·ℓ^{-1} when pH>7.

- The TDS values of spring water in the V-notch, rainfall and interflow (VS1, VS2, VS3) are 79, 136.5 and 144-266.8mg·ℓ^{-1}, respectively. Na^+ and Cl^- are predominant; their concentration ranges are 11.90-56.56mg·ℓ^{-1} and 16.9-83.7mg·ℓ^{-1}, respectively.
- The concentration ranges of HCO_3^-, SO_4^{2-} and NO_3^- are 6.0-152.2mg·ℓ^{-1}, 0.01-12.3 and 0.01-2.07mg·ℓ^{-1}, respectively.
- The concentrations of K^+, Mg^{2+} and Ca^{2+} range 0.8-6.51 mg·ℓ^{-1}, 1.6-13.46 mg·ℓ^{-1} and 1.6-20.88 mg·ℓ^{-1}, respectively.
- Water samples with pH>7 are very few with the maximum being 7.43.
- Water quality in the V-notch is similar to that in production boreholes.

The following points are observed through the Piper diagram shown in Figure 9.2 and Figure 9.3:

- Chloride is the major anion and Na^+ is the major cation in the TMG aquifers. Water quality is of the Cl-Na type.
- The plots of Piper are concentrated in certain areas close to the Calitzdorp hot spring and the G40175 artesian borehole. The plot of DP18 (alluvial aquifer) is located between boreholes in the TMG and the hot spring. There is a slight difference between VR7 and VR6, VR8, and VR11. The SL2, Koutf, DP25 and DP28 can be grouped together.
- The hot springs are clustered together (Figure 9.3). The Montagu and Caledon hot springs can be distinguished from the other hot springs. Both of them are end members of the group. The Caledon hot spring is closer to the seawater side and the Montagu hot spring is nearer to the rainfall side.
- Interflow samples (VS1, VS2 and VS3) are divided into two groups. The one group with chloride meq % greater than 80% seeps from unconsolidated deposit, the other issues from weathered zones.

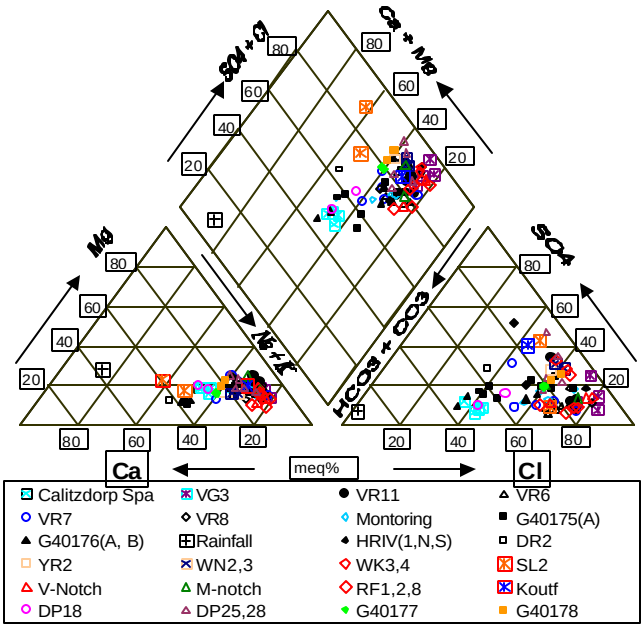

Figure 9.2 Piper diagram of groundwater in the Karmmanassie area

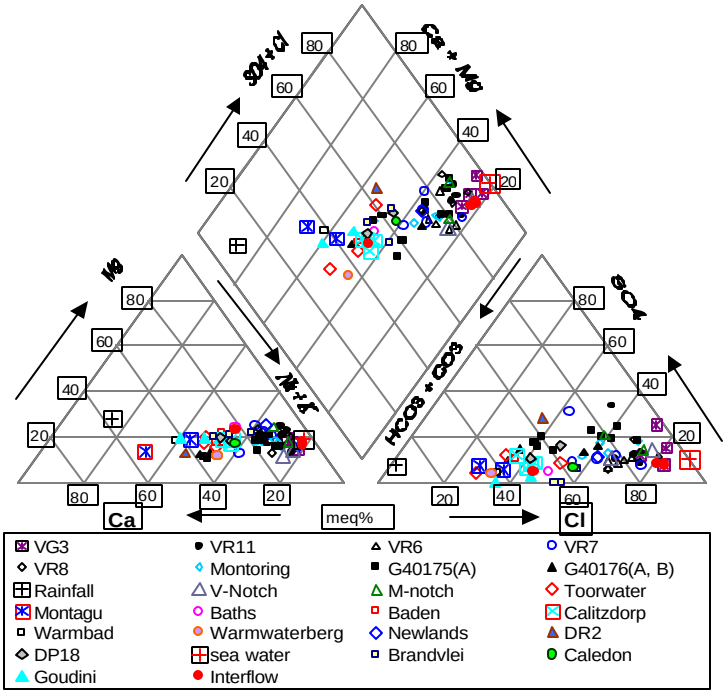

Figure 9.3 Piper diagram of the hot springs

9.3 CHEMICAL CHARACTERISTICS OF CHLORIDE AND SODIUM

The chloride and sodium are very important ions in the study area. The chloride concentration was discussed in detail because it was used as a tracer in the recharge estimation.

9.3.1 Chloride

Some chemical characteristics of the chloride in the Vermaaks area is presented in Table 9.1 and shown in Figure 9.4 and Figure 9.5. The observation are obtained as follows:

1) From concentration point of view, the sequence is $Cl^- > Na^+ > Mg^{2+} \cong Ca^{2+}$.
2) The chloride concentration in the boreholes is only half of that of the interflow.
3) The ranges of chloride concentrations in VR6, VR7, VR8, VR11 and VG3 are 19.0- 60.0, 18.0- 46.0, 17.0-56.0, 18.0-50.0 and 20-86 $mg \cdot \ell^{-1}$, respectively; their average values are 34.97, 33.26, 30.78, 34.41 and 56.48 $mg \cdot \ell^{-1}$, respectively.
4) The average value of chloride in production boreholes of VR6, VR7, VR8 and VR11 is 32.51$mg \cdot \ell^{-1}$. The concentration in the Nardouw aquifer is near two times that of the Peninsula Aquifer.
5) The chloride concentrations are less than 50$mg \cdot \ell^{-1}$ in most boreholes, but the concentrations in SL2, G40178 and G40177 are much higher than that of others in the Nardouw aquifer (Figure 9.5).

Table 9.1 Statistical results of chloride in the Vermaaks area

Statistical result	VR6	VR7	VR8	VR11	VG3	VR6, VR7, VR8 and VR11
Count	88	92	81	65	86	326
Min	19	18	17	18	20	17
Median	34	32.5	30	30	56	32
Max	60	46	56	50	86	60
Average	34.97	33.26	30.78	31.41	56.48	32.5
Geomean	33.96	32.27	29.90	30.62	53.38	-
Harmean	33.27	31.60	29.21	29.87	50.73	31.03
Standard deviation	7.09	6.38	6.95	7.20	13.62	7.03
Confidence	1.24	1.09	1.27	1.47	2.42	0.64

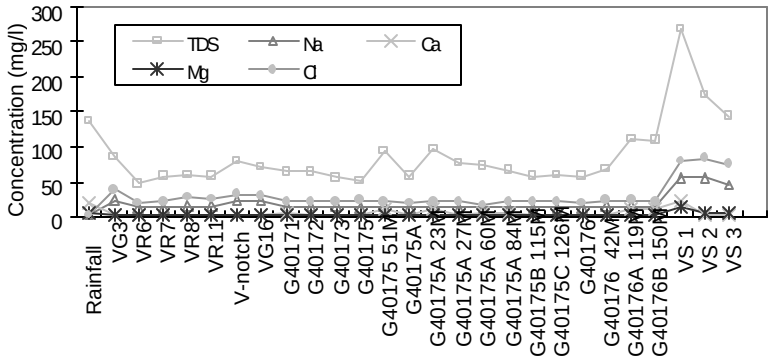

Figure 9.4 Fingerprint of the major ions in the Vermaaks area

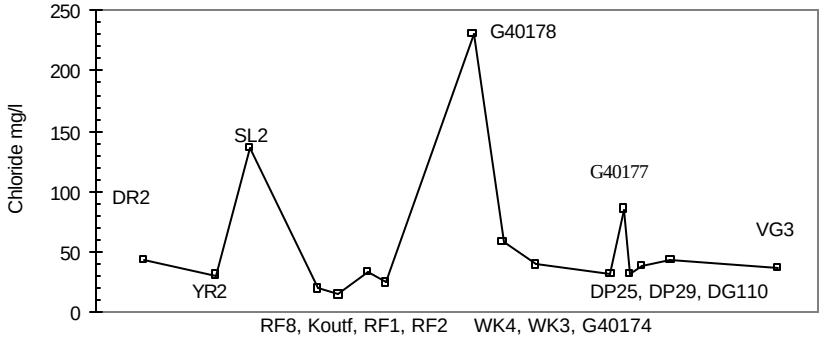

Figure 9.5 Distributions of chloride in the Nardouw Subgroup

9.3.2 Sodium

The sodium concentrations are smaller than chloride concentration (Figure 9.6). Considerable differences in range of ion ratios in groundwater, rainwater and soils are listed in Table 9.2. The ?Na/?Cl ratios of groundwater are close to 1, but the ratios in soil are very low due to ion exchange. Large range of the ratios of other ions occur in the Vermaaks area, such as (?Na-?Cl)/?SO_4, (?Cl-?Na)/?Mg. Most of the SAR values in groundwater are less than 1.5. The SAR values greater than 1.5 occur in VG3, VG16 and interflow. Large ranges in SAR and ?Mg/?Ca, but small variation in ?Na/?Cl can be seen in Figure 9.7.

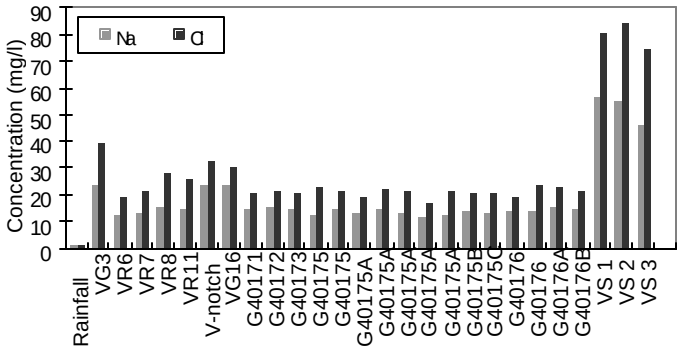

Figure 9.6 Column diagrams of chloride and Sodium

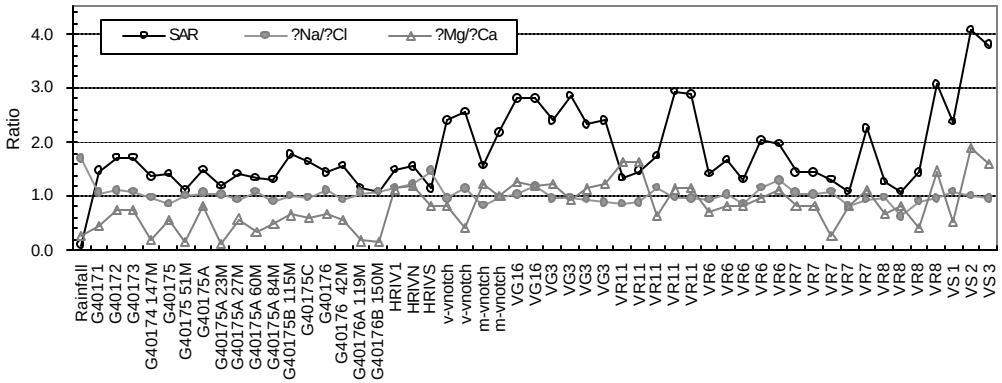

Figure 9.7 Diagram of ion ratios in the Vermaaks area

Table 9.2 Ratio of ions in the Vermaaks area

Item	Groundwater					Rain water	Soil
	SAR[1)]	$\frac{gNa}{gCl}$	$\frac{gNa-gCl}{gSO_4}$	$\frac{gCl-gNa}{gMg}$	$\frac{gMg}{gCa}$	$\frac{gNa}{gCl}$	$\frac{gNa}{gCl}$
Min	0.097	0.631	-2.751	-1.958	0.136	0.071	0.006
Median	1.560	0.996	-0.033	0.033	0.825	0.271	0.016
Max	5.334	1.702	4.643	2.784	1.896	1.703	0.018
Average	1.905	1.011	-0.019	0.059	0.808	0.271	0.014

1) $SAR=Na/[(Ca+Mg)/2]^{0.5}$

9.4 TRACE ELEMENTS

Most of the trace element data including Al, Sr, Sr, Ba, Fe and Mn were adapted from NGDB and Kotze (2001). These elements are characterized by low concentration. The

elements of B, Be V Cr Ni, Cu Zn, Mo, Pb, Ti, Hg, Co etc., are analysed and the concentrations are very low or out of the range of the detection.

9.4.1 Al and Si

The most of Si concentrations are less than 5mg·ℓ^{-1} as can be seen in Figure 9.8. The Al concentration is very low (out of limit of detection). It seems to indicate the low degree of weathering in the rocks of TMG aquifer. The higher concentrations of Si in G40177, G40178 and SL2 show normal solubility range of minerals of quartz, opal and chalcedony.

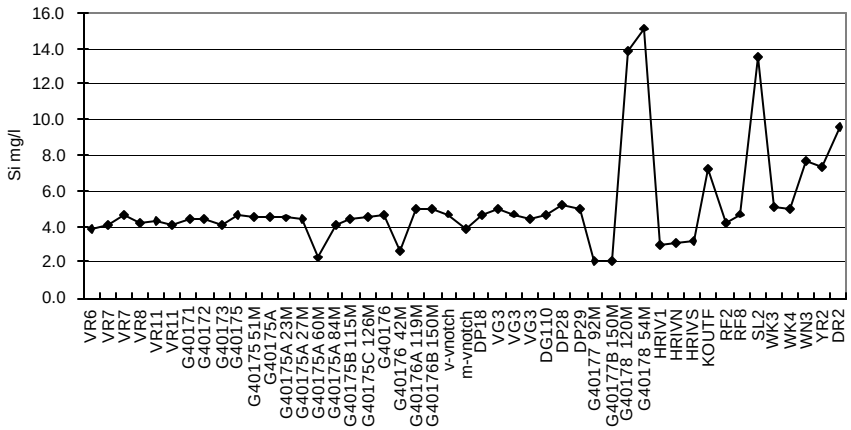

Figure 9.8 Si concentrations of groundwater in the Kammassie area

9.4.2 Sr and Ba

The Sr concentrations in the Nardouw, Peninsula and alluvial aquifers, are less than 0.011mg·ℓ^{-1}, 0.011-0.058mg·ℓ^{-1} and higher than 0.406mg·ℓ^{-1}, respectively. Similarly, the Ba concentrations are less than 0.002mg·ℓ^{-1}, 0.002-0.03mg·ℓ^{-1} and higher than 0.03mg·ℓ^{-1}, respectively. Perhaps the concentrations of Sr and Ba are associated with the presence of shale or evaporation.

9.4.3 Fe and Mn

The concentrations of Fe and Mn in the Nardouw Aquifer are usually higher than those in the Peninsula Aquifer. In the Peninsula Aquifer, the concentration of Fe in

production boreholes is less than 0.005mg·ℓ^{-1}, while the concentrations in monitoring boreholes are from 0.003 to 0.306mg·ℓ^{-1}. The concentration features of Fe and Mn (Table 9.3) based on monthly report of the Overberg Board Water Management are as follows:

1) The concentration pattern of Fe in the Nardouw Aquifer is similar to that of the Peninsula Aquifer in range, median and average. But Fe concentrations in the alluvial aquifer are 5 times greater than those in the TMG aquifer.
2) The average concentrations of Mn in the Peninsula and Nardow aquifers are 0.074- 0.133mg·ℓ^{-1} and 0.428mg·ℓ^{-1}, respectively; but their standard deviation values are 0.077- 0.041mg·ℓ^{-1} and 0.925mg·ℓ^{-1}, respectively.
3) Mn in the alluvial aquifer is similar in magnitude to that in the Nardouw Aquifer, but the range is smaller than that in the Nardouw Aquifer.
4) There is a large coefficient of variation of Fe and Mn concentrations due to lithology or weathering, thus they cannot be used as tracer.

Table 93 Statistical results of the Fe and Mn in the production boreholes

Trace element	Statistic	VR6	VR7	VR8	VR11	VG3	DP18
	Size	82	89	77	62	83	26
Fe	Min	<0.001	<0.001	<0.001	<0.001	<0.001	0.03
	Median	0.025	0.040	0.020	0.030	0.040	0.300
	Max	0.500	1.020	0.800	2.070	1.240	1.200
	Average	0.094	0.074	0.045	0.111	0.085	0.445
	Standard deviation	0.156	0.149	0.106	0.277	0.197	0.334
	Confidence	0.028	0.026	0.020	0.058	0.036	0.108
	Coefficient of variation	165.96	201.35	235.56	249.55	231.76	75.06
Mn	Min	<0.001	<0.001	<0.001	<0.001	<0.001	0.1
	Median	0.08	0.10	0.10	0.10	0.20	0.35
	Max	0.50	0.30	1.00	1.00	6.00	0.70
	Average	0.074	0.081	0.097	0.133	0.428	0.389
	Standard deviation	0.105	0.077	0.140	0.195	0.925	0.239
	Confidence	0.019	0.014	0.026	0.041	0.168	0.077
	Coefficient of variation	141.89	95.06	144.33	146.62	216.12	61.44

9.4.4 Correlations between chloride and EC and TDS

Significant differences of chloride and sodium occur between groundwater and rain water (Table 9.4). This illustrates the components have been changed due to reaction

or additional constituents added in recharge processes. Relationships seem to occur between the chloride concentration, EC and TDS (Figure 9.9 and Figure 9.10), but the F-Test probabilities are 3.55×10^{-10} and 3.65×10^{-53}, respectively. For purpose of quick estimation of water quality, the correlation equations between chloride and EC and TDS are constructed as follows:

$$TDS=7.0306EC-35.503 \qquad R^2=0.9911 \qquad (9.1)$$

$$Cl=1.9238EC-1.3914 \qquad R^2=0.966 \qquad (9.2)$$

Table 9.4 Statistical results of chemical data in the Kammanassie area (mg·ℓ^{-1})

Item	Groundwater												Rain water	
	pH	TDS	EC	Na	K	Mg	Ca	F	Cl	NO_3	SO_4	PO_4	Na	Cl
Min	3.7	12	2.8	2	0.2	0.6	0.4	0.05	4	0	1.9	0.001	0.38	1.74
Max	8.4	1310	182.0	381	22.5	63.0	87.0	1.73	367	11.75	199.0	0.203	1.88	14.5
Median	6.6	89	17.8	20	1.4	2.9	3.5	0.13	32	0.10	12.2	0.011	7.19	28.9
Mean	6.5	187.2	31.9	38.7	3.9	6.2	10.8	0.20	60	0.30	24.5	0.000	1.88	14.5
Standev.	0.8	259.4	37.6	58.7	5.1	9.5	16.8	0.20	74	1.30	35.2	0.000	1.75	5.76
Confidence	0.1	43.8	6.3	9.9	0.9	1.6	2.8	0.00	12.4	0.20	6.0	0.000	0.03	0.4

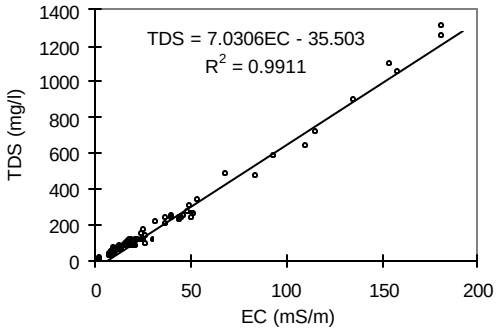

Figure 9.9 EC versus TDS

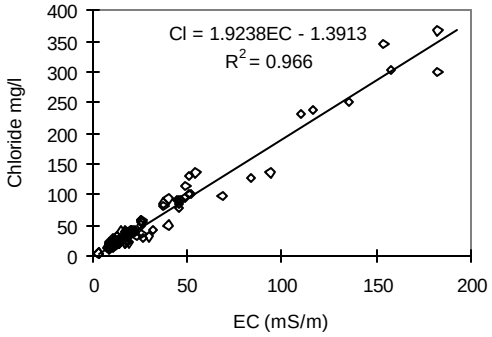

Figure 9.10 EC versus chloride

9.5 ISOTOPES

9.5.1 Deuterium and oxygen-18

Isotopic characteristics can be used to discriminate water origins. Values of ^{2}H or ^{18}O are more negative if the source of the water vapour at the origin of the precipitation is further away (distance effect). If a large part of the water vapour is precipitated from the cloud (reservoir effect) or if the temperature is lower. It can be ascribed to impoverishment in heavy isotopes during successive precipitations, due to depletion of the water vapour from the cloud or to a higher value of the equilibrium fractionation coefficients for oxygen 18 and deuterium with lower temperature. Deuterium excess is the independent term of the equation $D=8^{18}O+d$ corresponding to what is referred to as the Meteoric Water Line (Vandenschrick et al, 2002). If evaporation rates are high, because of high temperature and low relative humidity in the atmosphere during the formation of the water vapour, there is a strong kinetic isotopic effect, and *d* becomes higher (Jouzel and Merlivat, 1984). Deuterium excess is usually considered as a more or less conservative property in the part of the atmospheric water cycle beginning with water vapour formation by evaporation to rainfall just below cloud level (Ciais and Jouzel, 1994). Deuterium excess in rainfall of Mediterranean origin generally has a relatively high value. This is due to a strong kinetic isotopic effect during evaporation in the summer above the Mediterranean Sea because of the low relative humidity of the atmosphere. Conversely, Atlantic precipitation has deuterium excess around +10‰. If the rain results from a mixing between water vapours of Mediterranean and Atlantic origins, it will be represented, in a D- ^{18}O diagram, on a straight line called a mixing line. This line will connect a pole of Atlantic points characterised by *d*-values around +10‰, to a Mediterranean pole with higher *d*-values (Vandenschrick et al., 2002).

The Kammanassie MWL ($D=7.4^{18}O+9.1$, $R^2=0.75$) d-value is 9.1. Slopes close to 8 are displayed for the Kammanassie area (Figure 9.9), indicating a common origin for all events or at least similar kinetic conditions at the water vapour source (relative air humidity and temperature). By contrast, the slope less than 8 for South Africa MWL (IAEA, 1981) could be the signature of evaporation during precipitation travel from

the cloud to the ground surface. This evaporation would be responsible for enrichment in heavy isotopes of the residual liquid water and for a decrease in deuterium excess.

Interpretation of the isotopic signature of the different water types in the Kammanassie area is facilitated by a discussion of the regional precipitation. Stable isotopes data are adopted from NGDB and Kotze (2001) as listed in Appendix ? . A comparison of the environmental isotope data for various surveys showed more depleted $\delta^{18}O$ signatures for July 1997 than those for the same borehole during the survey of January 1996. These differences are postulated to be the result of the effect of the rainfall amount. The ranges ^{18}O and ^{2}H are shown in Figure 9.11. The observations are as follows:

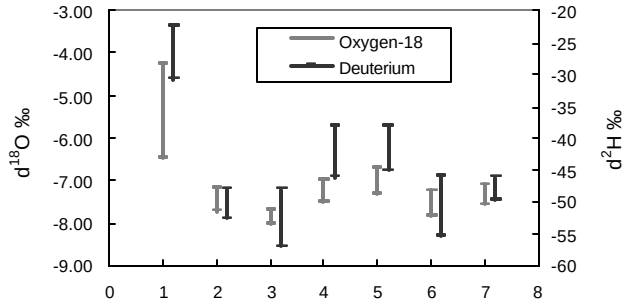

1rainfall, 2 production boreholes of Peninsula Aquifer, 3 production boreholes of Nardouw Aquifer, 4 monitoring boreholes of Peninsula Aquifer, 5 monitoring boreholes of Nardouw aquifer, 6 V-notch and M-notch, 7 hot springs near Karmmanassie area

Figure 9.11 Ranges of the ^{18}O and ^{2}H in the Kammanassie area

- The isotope pattern in production boreholes is different from that of monitoring boreholes. ^{2}H in production boreholes is more affected by evaporation or altitude than those in monitoring boreholes. It illustrates that different sources or infiltration paths occur.
- Isotopes of the notches in the Vermaaks and Manewicks are clearly concentrated on evaporation.
- Isotope patterns of hot springs differentiate from those of boreholes. The water in the borehole recharges from low elevation areas (more negative value), but the hot springs recharge from high elevation areas or low elevation during a

colder period. This would imply the flow paths are different. The flow of the boreholes is local, while the hot spring flow is regional.

The $\delta^{18}O$ and $\delta^{2}H$ relationships for groundwater and rainfall in the Kammanassie area are presented in Figure 9.12. The following can be observed:

a) Three groups are identified, which are A: rainfall, B: alluvial aquifer and C: fractured rock aquifer.
b) For group A, the isotopic pattern is similar to that of the rainfall. It illustrates that direct infiltration occurs before evaporation.
c) For group C, four subgroups are identified, namely monitoring boreholes (C1) and the hot springs (C2). C3 are the boreholes in the Baviaaanskloof Aquifer. C4 is VG3 in the Skurweberg Aquifer and the notch water. VG3 is clearly related to water in the V-notch (Figure 9.13). It is worth noting that VG3 is located in the lower part of the Vermaaks notch. Part of the notch water may recharge the Nardouw Aquifer again.
d) All points of the boreholes in the diagram clearly show an enrichment of heavy isotopes with respect to the South Africa MWL (IAEA, 1981), but only VR7, VR8, VR, VG3, V-notch, M-notch, the Toorwater and Calitzdorp hot springs possess the characteristics with respect to the Global MWL (Dansgaard, 1964). All rainfall points show an enrichment of heavy isotopes with the Cape MWL (Diamond, 1997). This is due to the amount effect and the heavy rainfall event, whereby a greater amount of precipitation will give a more negative $\delta^{18}O$ signature. The Kammanassie MWL is suggested as equation (9.3). The slope (7.4) less than 8 in the Kammanassie is in fact a mixing line, joining a pole of Mediterranean water vapour to a pole of Atlantic water vapour.

$$D=7.4^{18}O+9.1 \qquad R^2=0.75 \qquad (9.3)$$

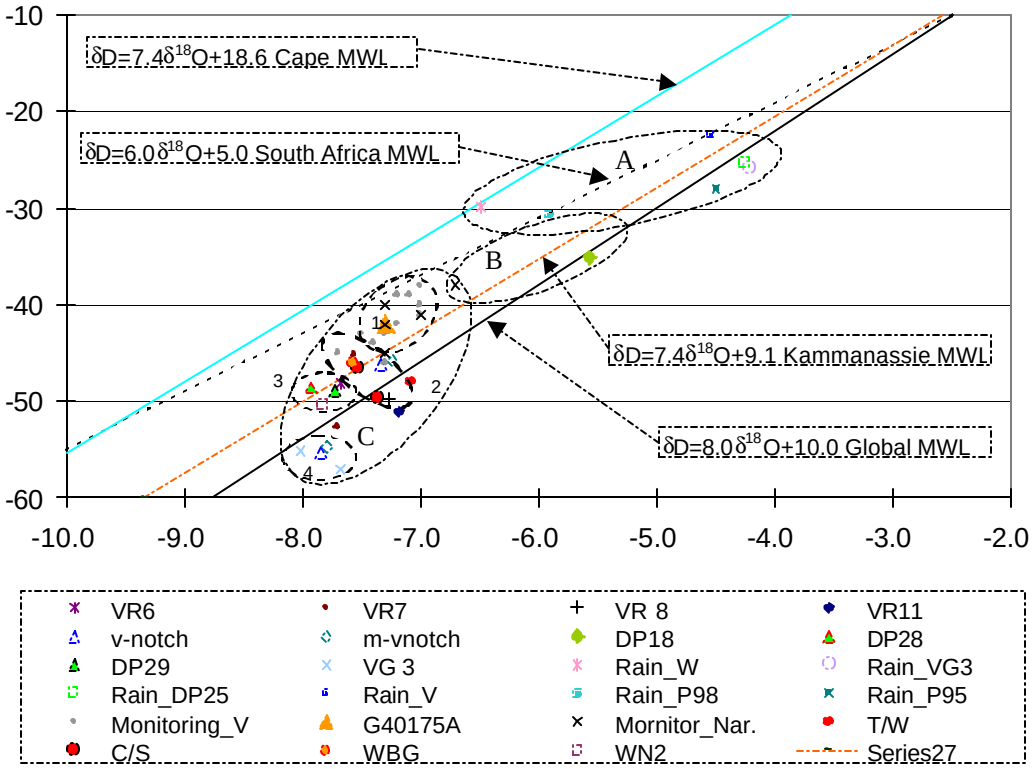

Figure 9.12 d ^{18}O and d ^{2}H diagram in the Kammanassie area

Rainfall and mountain seepage (interflow) samples become progressively lighter (more negative) with increasing altitude (lower temperature). This is particularly true for the lighter signatures of rain samples taken at the Wildebeesvlakte and Parshall rain gauges as opposed to the rain samples collected at lower altitudes (Kotze, 2002). The $\delta^{18}O$ versus altitude diagram seems to identify the sources of water and the precipitation altitude as shown in Figure 9.14. This regional isotopic gradient is approximate 0.44%. It is higher than the average universal gradient (0.3%). The equation of the gradient used is

$$d^{18}O = -2.1 - 0.0044Alt. \qquad R^2=0.7191 \qquad (9.4)$$

The ranges of recharge altitude of the borehole water are according to the equation (9.4) shown in Figure 9.15. The range of altitude of mountainous area is from 900-1500m except DP18. It seems to correspond to the mean altitude of the recharge area.

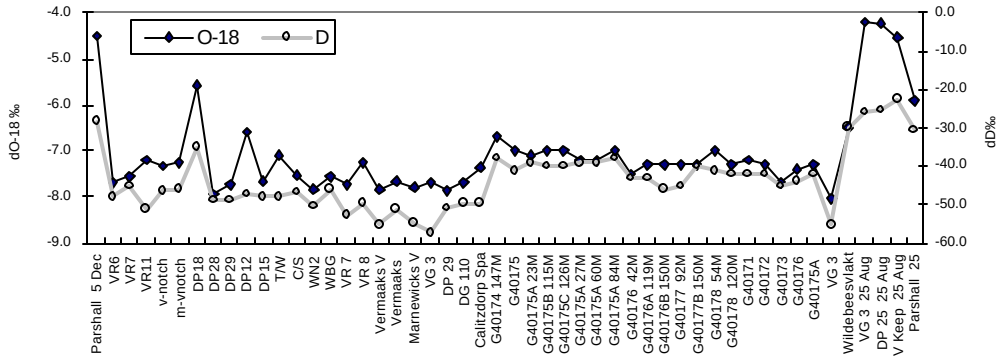

Figure 9.13 Fingerprint of isotopes in the study area from 1995 to 1998

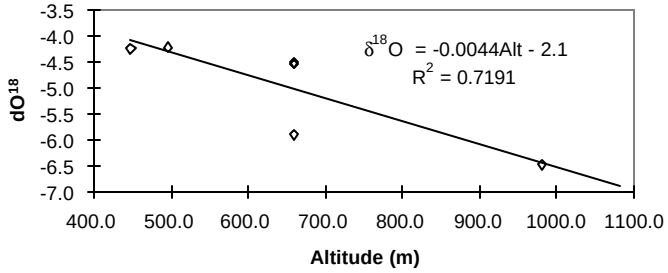

Figure 9.14 Altitude effect of the isotope

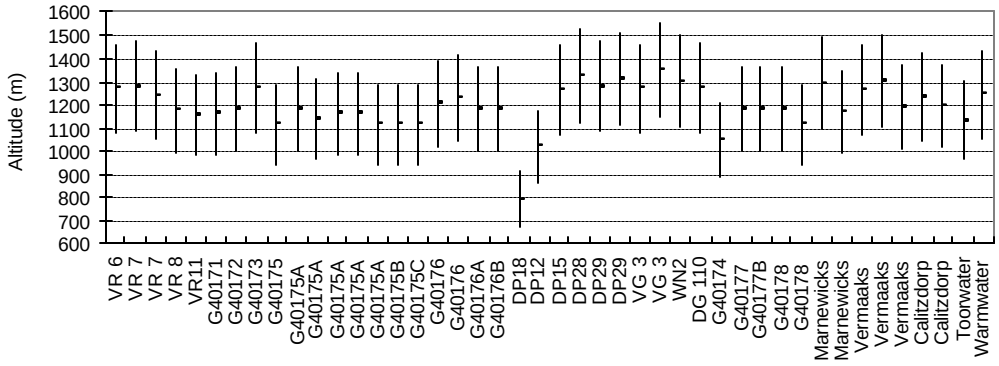

Figure 9.15 Recharge altitude of groundwater

Isotopes of ^{18}O are used as indicators of the groundwater component of stream flow during periods of storm runoff and the relation is obtained as (Fritz et al. 1976):

$$Q_g = Q_w \left(\frac{d\ ^{18}O_w - d\ ^{18}O_g}{d\ ^{18}O_g - d\ ^{18}O_{Run}} \right) \tag{9.5}$$

where $d^{18}O$ denotes the ^{18}O content in per mille relative to the SMOW standard and the subscripts *w*, *g*, and *Run* indicate stream water, shallow groundwater, and runoff water derived from the rainfall ($Q_w = Q_g + Q_{Run}$). This relation provides for separation of the rain-derived component from the component of the streamflow represented by water that was in storage in the groundwater zone prior to the rainfall event. From the mass-balance point of view, the spring flow (Q_s) recorded at the V-notch consists of the upstream groundwater (Q_g) of Peninsula Formation and the perched water flow (Q_p) in weathered zone as seen in Figure 8.11, i.e.

$$Q_s = Q_g + Q_p$$

where the term Q_p is apparently influenced by rainfall infiltration. The equation (9.5) changes to

$$\frac{Q_g}{Qs} = \left(\frac{d\ ^{18}O_w - d\ ^{18}O_g}{d\ ^{18}O_g - d\ ^{18}O_p} \right) \qquad (9.6)$$

where, average $d^{18}O$ of rain, spring, production borehole and monitoring borehole are –4.86‰, –7.45‰, $d^{18}O$ –7.33‰ and –7.25‰, respectively (original isotope data can be referred as presented in Appendix VI). About 8.37% and 4.86% of spring flow comes from shallow aquifer same as monitoring borehole and Peninsula Aquifer as production borehole, respectively. It confirms the conceptual model shown in Fig 8.12.

9.5.2 Tritium

Tritium is the heavy isotope of hydrogen. Tritium atoms are unstable and disintegrate radioactively, forming stable ^3He atoms. The half-life of the tritium is 12.3 yeas. The concentration of tritium in water is expressed by the ratio of tritium (T) atoms to hydrogen (H) atoms:

A ratio of $T/H=10^{-18}$ is defined as 1 Tritium unit (1TU)

Tritium concentrations in groundwater may be used as indicators of groundwater age based on a comparison with historical records of elevated tritium levels in

precipitation (maximum 3000TU in the northern hemisphere), attributed to atmospheric thermonuclear testing between the 1950s and the late 1996 (Schlosser et al., 1988; Busenberg and Plummer, 1993; Dindane et al., 2003). The tritium level in young groundwater is about the same level as in precipitation, but ^{3}H is significantly diluted by water content of the unsaturated zone. Since the mid-eighties the tritium values in rain water are 10 TU in the northern hemisphere (Mook, 2001). The semi-quantitative dating is possible and very informative (Mazor, 1991):

- Water with zero (in practice<0.5TU) has a pre-1952 age.
- Water with significant tritium concentrations (in practice >10TU) is of a post-1952 age.
- Water with little, but measurable, tritium (between 0.5 and 10TU) seems to be a mixture of pre-1952 and post-1952 water.

The variation of the tritium contents (Appendix VI) seems to show two types of water: (i) deep circulation old water including all fractured rock aquifers that is not influenced by the modern recharge (lower than 1.0 TU). (ii) Mixing water near the surface including alluvial aquifers, which have modern water contributions (3.2TU).

The resident time of groundwater samples in summer season seems to have a short to long sequence as follows (Figure 9.16): DP18 (3.2TU) to the notch in the Vermaaks and Manewicks River (1.6TU) to VG3 (1.3TU) to VR7 (1.0TU) to VR6, VR8, DP28 (0.4TU) to VR11, DP12, WN2 (0.3TU) to DP29, DG110 (0.1TU). For winter samples, the tritium (0.5TU) in the notch of the Vermaaks and Manewicks Rivers corresponds to VR6 and VR7. It seems to demonstrate that the water in the V-notch is partially fed both by local flow and by rainfall in summer season, but totally fed by groundwater in winter season. The sequence seems to illustrate the circulation is deeper or slower in VR6, VR8 and VR11 than that in VR7 and VG3, or preferential recharge paths occur in VR7 and VG3.

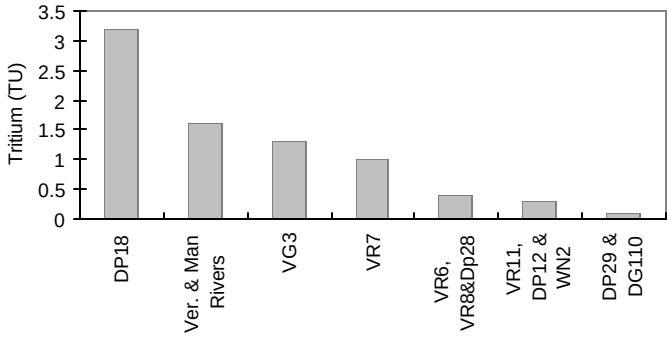

Figure 9.16 Fingerprint of tritium

9.5.3 Carbon-13 and carbon-14

Stable carbon isotopes ^{13}C of water samples were analysed to aid in determining the flow paths of water entering the boreholes and to distinguish between source waters. Based on piston flow model, new water should have a more negative ^{13}C signature relative to the 'old' water in the system, since new water is heavily influenced by contact with soil zone CO_2. The ^{13}C in water of boreholes and hot springs varies from -18.8 to -21.3‰ PDB and -14.5 to –17.3‰ PDB, respectively. These seem to indicate more modern water components in boreholes than those in the hot springs. For ^{13}C in the alluvial waters is as heavy as, or heavier than, ^{13}C measured in the hot spring and in the TMG aquifer. This borehole water, in theory, should represent 'old' water.

The pattern of distribution of ^{13}C and ^{14}C tends to be opposite to each other except for sample DP18 (Figure 9.17). The ^{14}C values for the boreholes in the Peninsula Aquifer are from 74.6 to 83pmc. Boreholes in the Nardouw Aquifer give a value of 41.2-62.3pmc, which is much lower than those in the Peninsula Aquifer. The carbon isotopes in the Calitzdorp, Toorwater and Warmwaterberg hot springs are completely different from those of boreholes. The lower ^{14}C and higher ^{13}C to demonstrate that hot spring water is much older than that in boreholes. The results further suggest that the groundwater flow of boreholes in the Peninsula Aquifer is faster than that in the Nardouw Aquifer and the hot springs.

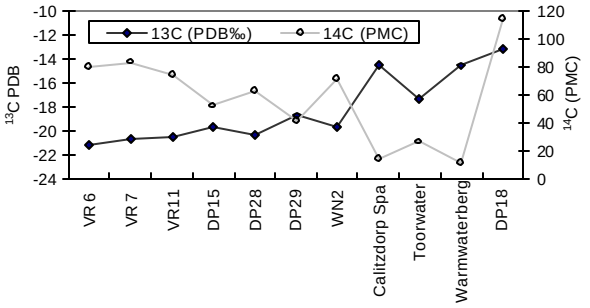

Figure 9.17 Diagram of carbon isotopes in the study area

The law of radioactive decay describes the rate at which the activity of ^{14}C and all other radioactive substances decreases with time. This is expressed as (quoted from Freeze and Cherry, 1979):

$$A = A_0 2^{-t/T} \tag{9.7}$$

where A_0 is the radioactivity level at some initial time, A is the level of radioactivity after time t, and T is the half-life of the isotope. Use of ^{14}C for dating of groundwater was first proposed by Munnich (1957). A formula to calculate how old a sample is by carbon-14 and tritium dating is rearranged as:

$$t = [\ \ln (A_f/A_o) / (-0.693)\ ] \times T \tag{9.8}$$

where ln is the natural logarithm, A_f/A_o is the percent of carbon-14 in the sample compared to the amount in DP18 (alluvial aquifer), and T is the half-life of carbon-14 (5,730 years) and tritium (12.3 years).

Difference tracers may also give different ages where mixing of very young and very old groundwater (Cook and Solomon, 1997). In comparison to DP18, the relevant resident time from carbon-14 and tritium shows large differences (Table 9.5). The hot spring water would be old water and piston flow feeding. The water in code of DP boreholes would have components of old water. The water in VG3 is probably young. For the borehole water, the resident time of ^{14}C is from 2628.6 to 8968.7 years; but the resident time of tritium is from 12.3 to 61.5 years. For springs in the notches, the tritium ages are 10.2 –36.9 years. For the hot springs, the ^{14}C ages are from 12364.2 to

19348.5 years. It is important to note that the resident time estimated here would be higher than actual ages because A_0 of carbon-14 must be larger than that in DP18. The measured $^3H/^3He$ age will reflect the resident time of the younger water component, because the $^3H/^3He$ ratio is unaffected by dilution with old (greater than 50years) water (Kamensky et al., 1991). CFC ages of 30-45 years (Weaver et al., 1999) may also reflect the younger water component. Therefore the abstraction may be the mixture of the old water (old storage) and new recharge water. Similarly, the spring water may have more younger water component. High ^{14}C seems to be the indication of the recharge, while low ^{14}C may attribute to the low source of the ^{14}C, otherwise, the recharge process does not obey the piston model or mixing and the dilution process occur in the fractured rock aquifer system. The relations between temperature, tritium, CFC age and ^{14}C can be seen in Figure 9.18. The VR6, VR7 and VR8 in Peninsula Aquifer seem to be a group, but VG3, DP15, DP25 and DP28 in the Nardouw Aquifer are another group.

Table 9.5 Dating results from carbon-14 and tritium

Site	DATE	^{14}C (pmc)	T (TU)	Resident time in comparison to DP18 (years)			
				^{14}C		^3H	
				Minimum	Maximum	Minimum	Maximum
DP18	1996-1-31	114.2	3.2	0.0		0.0	
VR6	1996-1-31	79.4	0.4	3005.2		36.9	
VR7	1997 7-1	80.6±2.5	1.0±0.2	2628.6	3141.7	17.4	24.6
VR7	1996-1-31	83	0	2638.5		12.3	
VR8	1997-7-1	79.3±2.5	0.4±0.1	2758.9	3280.5	32.9	42.0
VR11	1996-1-31	74.6	0.3	3520.8		42.0	
DP12	1996-1-31		0.3			42.0	
DP15	1996-1-31	52		6504.8			
DP28	1996-1-31	62.3	0.4	5010.6		36.9	
DP29	1996-1-31	41.2	0.1	8429.7		61.5	
DP29	1997-7-1	40.6±2.0	0.0±0.2	8153.4	8968.7	49.2	
VG3	1997-7-1	78.1±2.5	1.3±0.2	2881.1	3410.7	13.4	19.0
VG3	1998-6-1	65.7±2.3		4286.7	4865.8		
WN2	1996-1-31	72	0.3	3814.1		42.0	
DG 110	1997-7-1	41.0±2.0	0.0±0.2	8076.2	8883.5	49.2	
Marnewicks Notch	1997-7-1		1.6+0.2			10.2	14.7
Marnewicks Notch	1996-1-31		0.5			32.9	
Vermaaks (Partial)	1997-7-1		0.5±0.1			29.7	36.9
Vermaaks Notch	1997-7-1		1.6±0.2			10.2	14.7
Vermaaks Notch	1996-1-31		0.5			32.9	
Calitzdorp hot spring	1996-1-31	13		17967.2			
Toorwater hot spring	1996-1-31	25.6		12364.2			
Warmwaterberg hot spring	1996-1-31	11		19348.5			

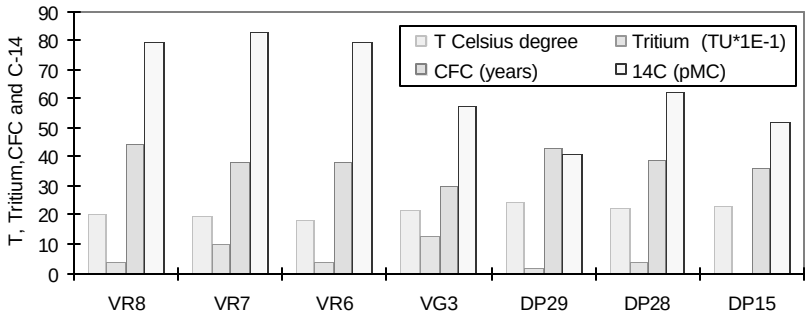

Figure 9.18 Diagram of temperature, tritium, CFC and carbon-14

According to piston model, flow velocity of the water for production boreholes are estimated based on the distance between the borehole and the watershed and the maximum eastern lithological boundary (Table 9.6). Large ranges of flow velocity and recharge rate occur in the Nardouw Aquifer because the recharge can occur in the whole outcrops of the Nardouw Subgroups. If the recharge area is close to the borehole, the recharge should be less than these values. From the watershed point of view, the recharge rate in the Peninsula Formation is larger than that in the Nardouw Subgroup; but the water resident time of VR11 is older than those of other boreholes of the Peninsula Aquifer, although VR11 is closer to the watershed than the other boreholes. Perhaps the flow paths are different in the fracture nets.

Table 9.6 Flow velocity and recharge based on resident time of ^{14}C

Borehole	^{14}C Ages (years)	Distance (m)		Flow velocity ($m \cdot a^{-1}$)		Recharge, if S=1‰ ($mm \cdot a^{-1}$)	
		To watershed	To eastern boundary of Nardouw/Peninsula	Min	Max	Min	Max
WN2	3,814.1	6,100	44,900	1.60	11.77	1.60	11.77
VG3	4,865.8	8,150	46,950	1.67	9.65	1.67	9.65
DG110	8,883.5	12,000	50,800	1.35	5.72	1.35	5.72
DP29	8,429.7	14,750	53,550	1.75	6.35	1.75	14.04
VR6	3,005.2	7,500	15,500	2.50	5.16	2.50	5.16
VR7	2,628.6	7,250	15,250	2.76	5.80	2.76	5.80
VR7	2,638.5	7,250	15,000	2.75	5.68	2.75	5.68
VR8	2,758.9	7,000	14,750	2.54	5.35	2.54	5.35
VR11	3,520.8	6,750	14,500	1.92	4.12	1.92	4.12

9.6 SURFACE WATER QUALITY

The chemical data of the surface water in the study area are discontinuously recorded monthly in the NGDB. The chemical features of surface water, including Stompdrift

Kammanassie, Calitzdorp, Gamkapoort and Koos Rauben Dams in the surrounding area are illustrated in Table 9.7. The concentrations of constituent, especially major ions Cl^- and Na^+ in the dams are higher than those in the boreholes except for the Koos Raubenheimer Dam (refer to Appendix V). Values of pH are usually greater than 7.0. Low chloride concentrations near the Kammanassie Dam were accompanied with extremely high rainfall events from 1985 to 2003 (Figure 9.19). The chloride concentration appeared to be increasing until a new extremely high rainfall event occurred in 1996 to 2001. Perhaps the high chloride concentrations are attributed to high evaportranspiration. The chloride concentrations of the dam water input in period of flood are lower than that stored in the dam result in the dilution of chloride concentrations; but the chloride concentrations are still higher than those of the boreholes in the Kammanassie area.

Table 9.7 Chemical characteristics of surface water in the surrounding areas of the Kammanassie in 1992-1998 (mg·ℓ^{-1})

Station	EC mS·m^{-1}	TDS	pH	Na	K	Mg	Ca	F	Cl	NO_3 as N	SO_4	P	Si	NH_4^+ as N	Alk
Stompdrift Dam	96.02	604.39	8.3	112.8	6.0	21.9	44.0	0.4	164.8	0.3	82.5	0.0	1.7	0.1	139.4
Kammanassie Dam	43.12	264.51	7.8	50.8	7.1	10.3	15.3	0.2	80.2	0.3	25.6	0.1	2.3	0.6	63.5
Calitzdorp Dam	26.16	192.05	8.0	16.4	6.2	7.9	22.9	1.0	15.4	0.1	16.9	1.1	2.2	0.1	99.1
Gamkapoort Dam	62.79	422.09	8.2	65.5	7.3	12.5	38.7	0.3	78.8	0.5	55.9	0.1	4.0	0.1	131.5
Koos Rauben. Dam	7.20	49.18	7.3	6.1	0.5	1.9	4.1	0.2	8.5	0.1	5.8	0.0	1.9	0.0	17.9

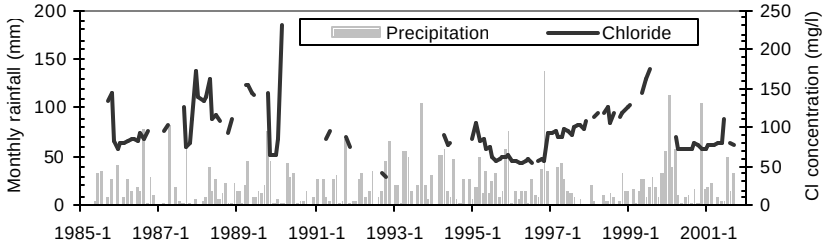

Figure 9.19 Chloride concentration versus rainfall in the Kammanassie Dam

9.7 SUMMARY

From the Piper plot, the groundwater with low TDS in the TMG aquifer was classified as Cl-Na type water, as all other ions were present at very low concentrations. The ranges of average TDS in the production boreholes of the Peninsula are lower than in

Nardouw aquifers. The concentrations of constituents especially Cl and Na^+ in surface water are higher than those in groundwater.

Large ranges occurred in SAR and ?Mg/?Ca. Most of the SAR values are less than 1.5. In both the Peninsula and Nardouw aquifers, ?Na/?Cl values trend to 1, which indicates the state of lixiviation. Although many data of trace elements or other constituents are available, the incomplete data sets limit their utilisation. The Fe and Mn cannot be used as tracers because they have large variation in time and spatial and many reactions lead to components input and output.

The isotopic signatures in the production boreholes were different from those in the monitoring boreholes. All rainfall oxygen and deuterium isotopes show an enrichment of heavy isotopes with the Cape MWL. The elevation of groundwater recharge for the production boreholes are the mountainous area of 900 to 1500m based on the altitude effect of the isotope.

Tritium concentrations demonstrate that preferential recharge paths occurred in the Vermaaks River Wellfield. The variation of the tritium in the aquifer shows two types of deep circulation old water and recent mixing water. The ^{3}H cannot be used to estimate recharge rate in the TMG fractured rock aquifer due to both insufficient data and its own limitation. The ^{13}C values indicate that recent water component in the boreholes is more than that of the hot springs. The resident time of ^{14}C gives rough rages of recharge estimates due to both its initial level and the uncertain infiltration sites.

Chapter 10

Recharge Estimation in the Kammanassie Area

10.1 INTRODUCTION

In the last 10 years, several recharge studies of the TMG aquifer using CMB, SVF, CRD and EARTH methods and hydrograph separation technique were carried out in the Kammanassie area. The recharge rates estimated using these methods are very different for the Kammanassie area. The estimated recharge rate was as high as 17% of mean annual precipitation (Bredenkamp, 1995). The recommended abstractions were adjusted many times in an attempt to stop the continued declining of groundwater level in the Vermaaks River field since 1984. In order to estimate realistic recharge rates of the TMG aquifers in the Kammanassie area, conceptual recharge models need to be developed. Several new methods were used to cross validate the results of the other methods.

This chapter aims to quantify the recharge rate using hydrogeochemical, water level, spring flux and rainfall data.

10.2 RECHARGE ESTIMATION WITH MIXING MODEL OF CMB

From a water balance point of view, groundwater abstraction from an aquifer can be considered a mixture of recent recharge and old storage. A mixing model of CMB is developed to differentiate ratio between the recent recharge and the old storage. The recharge rates are converted through the recharge volume over recharge areas and the annual average precipitation of the study area.

A conceptual model for the abstraction from recharge and aquifer storage is shown in Figure 10.1 (Wu and Xu, 2004). The following information is illustrated:

- Direct recharge, which is recharge through preferential fracture networks without additional chloride input. The chloride concentration of the water thus remains the same as that of the rainfall infiltration though the fracture.

- Indirect recharge through the unsaturated zone dissolves additional chloride. From the intermix, the chloride concentration of the recharge water will increase during the infiltration process.
- Interflow, which flows along the shallow weathered zone and discharges to local drainage systems in a short time. The chloride concentration of the indirect recharge is similar to that of the interflow.
- Local flow (old aquifer storage) discharges into wells.

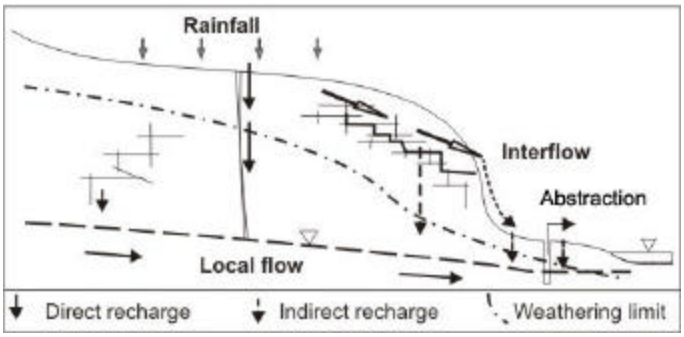

Figure 10.1 Conceptual mixing model

10.2.1 Mixing model

A proposed two-component mixing model assumes that the abstraction consists of old aquifer storage and recent recharge. In the three-component mixing model, the rainfall water component is further divided into direct and indirect recharge components. The three-component mass balance equations were obtained by sequentially expanding the two-component mass balance equations.

10.2.1.1 Two-component mixing model

Based on the conceptual model in Figure 10.1, the two-component chloride mass balance are written as

$$Q_p = Q_r + Q_s \tag{10.1}$$

$$Q_p C_p = Q_r C_r + Q_s C_s \tag{10.2}$$

where Q_p is the volumes of abstraction from production boreholes, Q_r is volumes of recharge, Q_s is volumes of aquifer storage and the chloride concentrations of the abstraction water, recharge water and aquifer storage water represented by C_p, C_r and C_s, respectively.

For direct recharge, an amount of recharge water with low chloride concentration would dilute that of storage. In this case, the equation for the recharge can be derived from equation (10.1) and equation (10.2) as follows

$$Q_r = Q_p \frac{C_p - C_s}{C_r - C_s} \qquad \text{when } C_p < C_s \qquad (10.3)$$

For indirect recharge, an amount of recharge water with high chloride concentration would increase that of storage. In this case, the equation for the recharge can be derived from equation (10.1) and equation (10.2) as follows

$$Q_V = Q_p \frac{C_p - C_s}{C_V - C_s} \qquad \text{when } C_p > C_s \qquad (10.4)$$

where Q_v is the volumes of indirect recharge and C_v is the chloride concentration of indirect recharge.

10.2.1.2 Three-component mixing model

The limitation of the two-component model is that direct and indirect recharge cannot be considered together at a time; one of them must be ignored. Sequel to this and the need of further recharge estimation, the three-component mass balance equations based on the abstraction of the production boreholes can be written as

$$Q_p = Q_r + Q_v + Q_s \qquad (10.5)$$

$$Q_p \times C_p = Q_r \times C_r + Q_v \times C_v + Q_s \times C_s \qquad (10.6)$$

where Q and C represent abstraction (L^3T^{-1}) and concentration of chloride (ML^{-3}) in direct recharge (r), indirect recharge (v) and aquifer storage (s), respectively. If equation (10.5) and equation (10.6) is divided by Q_p, the following equations are obtained:

$$1 = Q_r^{'} + Q_v^{'} + Q_s^{'} \tag{10.7}$$

$$C_p = Q_r^{'} C_r + Q_v^{'} C_v + Q_s^{'} C_s \tag{10.8}$$

where $Q_r^{'} = Q_r / Q_p$, $Q_v^{'} = Q_v / Q_p$ *and* $Q_f^{'} = Q_v / Q_p$ are the relative contributions to the abstraction in the Vermaaks River Wellfield at any given time from the direct and indirect recharge and aquifer storage, respectively. Rearranging equation (10.7) and equation (10.8), the following equations are derived:

$$Q'_V = \frac{Q'_r (C_s - C_r) + (C_p - C_s)}{C_v - C_s} \tag{10.9}$$

$$Q_s^{'} = 1 - (Q_r^{'} + Q_v^{'}) \tag{10.10}$$

The solution of the set of the above equations can refer to the solution of implicit functions (Geary et al, 1963). For achieving the approach to the solution of the set of the equation (10.9) and equation (10.10), one of the ways is the utilization of the rainfall component ($Q_r^{'}$) defined by equation (10.3) or equation (10.4). From equation (10.9) and equation (10.10), the relative contributions of each water component to the production borehole in the Vermaaks River Wellfield at any instant could be determined, although errors occur in the solutions.

The three-component mixing model over a given time interval i (month) was constructed as follows

$$\sum_{i=1}^{n} C_i Q_i = \sum_{i=1}^{n} [C_{si} Q_{si} + C_{ri} Q_{ri} + C_{vi} Q_{vi}] \qquad i = 1, 2, 3 \cdots n \tag{10.11}$$

$$\sum_{i=1}^{n} Q_i = \sum_{i=1}^{n} [Q_{si} + Q_{ri} + Q_{vi}] \qquad i = 1,2,3 \cdots n \qquad (10.12)$$

where, C_i is monthly chloride concentration in pumping borehole, C_{si}, C_{ri} and C_{vi} are concentrations of chloride in aquifer storage, rainfall and unsaturated zone, respectively. Q_i is monthly abstraction. Q_{si}, Q_{ri} and Q_{vi} are flux from aquifer storage, direct and indirect recharge, respectively.

10.2.2 Chloride concentration of recharge components

Based on the above models, the chloride concentrations of the abstraction are the result of the mixing of the different components including storage, direct and indirect recharge. Therefore, the chloride concentration of the different components should initially be identified.

10.2.2.1 Chloride concentration of the old storage

From a hydrogeochemical evolution point of view, the initial concentration of the storage water in an aquifer can be represented by the background chloride concentration. The background concentration may change due to effects of recharge water on the concentration. Therefore, it is very important to determine the background chloride concentration and its evolution in an aquifer. To identify the background value and the evolution, a statistical analysis method is used:

A classical time series of chloride concentration may be written as

$$C = C_{tr}(t) \cdot C_{cy}(t) \cdot C_{se}(t) \cdot C_{ir}(t) \qquad (10.13)$$

where C is the chloride concentration, and $C_{tr}(t)$, $C_{cy}(t)$, $C_{se}(t)$ and $C_{ir}(t)$ are the trend, cyclical, seasonal and irregular, respectively; t is the time.

The trend describes the net influence of long-term factors whose effects on the chloride concentration tend to change gradually. Generally, these factors include

changes in size as well as geological and hydrogeochemical evolution. This value would represent the chloride background value. The cyclical component describes the net influence of global and regional climatic change on annual rainfall distribution. It illustrates the relationship between the changes of the concentration of chloride with a change of rainfall. The seasonal component describes effects that occur regularly over a period of a year, quarter, month, day or rainfall event. The irregular component describes residual changes that remain after the other components have been taken into account. Irregular changes reflect effects of unique and nonrecurring factors, such as sampling and analyses.

The relationship between the mean annual precipitation and chloride concentration seems to be negative in the Peninsula Aquifer (VR6, VR7, VR8 and VR11) but positive in the Nardouw Aquifer (VG3) as illustrated in Figure 10.2. The results show that rainfall can produce more direct recharge in the Peninsula Aquifer; otherwise it creates more indirect recharge in the Nardouw Aquifer. The chloride concentrations related to the abstractions in the Vermaaks River Wellfield from 1994 to 2003 are used to perform modelling (Figure 4). It is important to note that the data are only available up to March 2003.

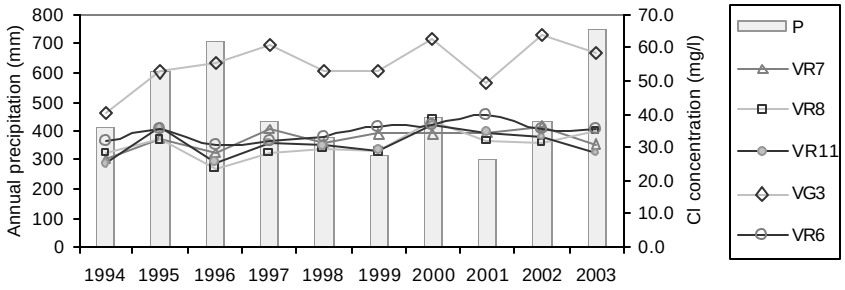

Figure 10.2 Chloride concentrations versus precipitation in the Vermaaks area

To evaluate the hydrogeochemical evolution trend of the TMG aquifer in the Vermaaks area, a time series analysis was performed. The data of chloride concentration were adopted from a monthly report of the Overberg Board Water Management. The chloride concentration evolution trend from 1994 to 2003 in the Vermaaks River Wellfield is demonstrated by regression analysis although the correlation coefficient is low (Figure 10.4). The initial background values of chloride

varied from 25.1- 28.9 mg·ℓ^{-1} and 48.7 mg·ℓ^{-1} for the Peninsula and Nardouw quifers, respectively (Table 10.1). The background values of chloride concentration from 1994 to 2003 are listed in Table 10.2, which forms the basis of calculation for the mixing model.

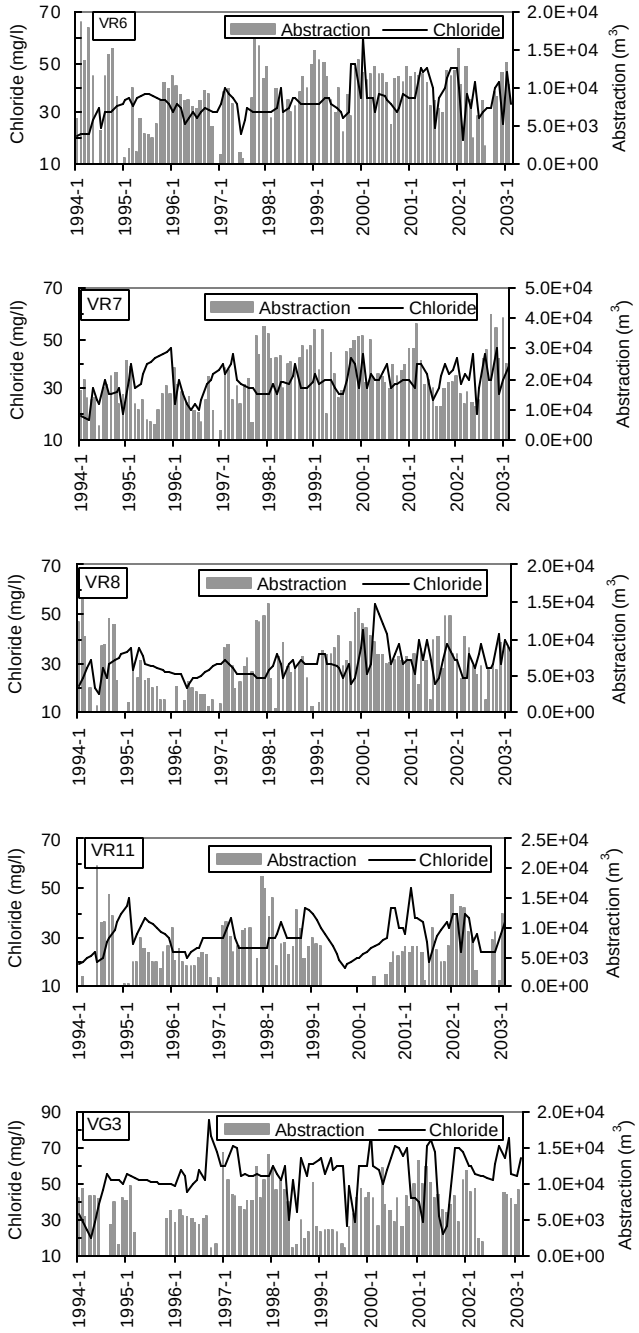

Figure 10.3 Chloride concentrations responding to the abstraction in the Vermaaks River Wellfield

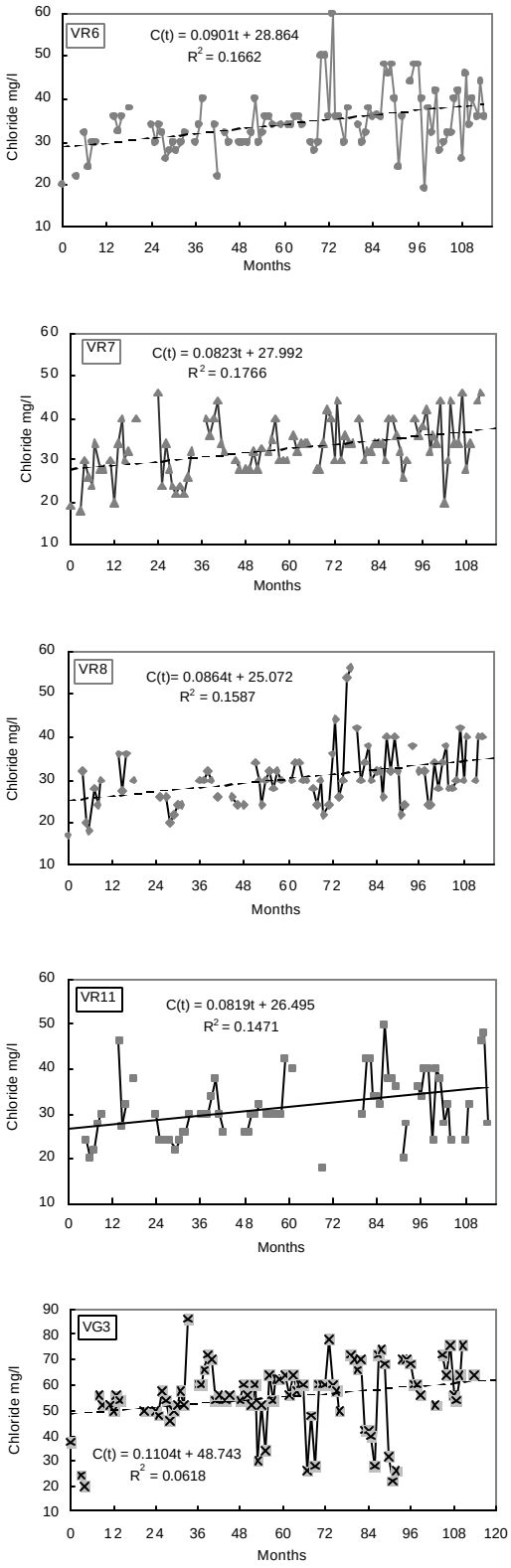

Figure 10.4 Chemograph of boreholes from 1994 to 2003 in the Vermaaks River Wellfield

Table 10.1 Background values of the chloride concentration

Aquifer	Borehole	Regression equation	Coefficient of correlation	Initial background concentration (mg·ℓ^{-1})
Peninsula	VR6	C(t) = 0.0901t + 28.86	R^2 = 0.1662	28.9
	VR7	C(t) = 0.0823t + 27.99	R^2 = 0.1766	28.0
	VR8	C(t) = 0.0864t + 25.07	R^2 = 0.1587	25.1
	VR11	C(t) = 0.0819t + 26.50	R^2 = 0.1471	26.5
Nardouw	VG3	C(t) = 0.1104t + 48.74	R^2 = 0.0618	48.7

Table 10.2 Basis of background values of the chloride concentration (mg·ℓ^{-1})

Borehole	VR6	VR7	VR8	VR11	VG3
1994	28.9	28.0	28.2	24.8	48.7
1995	29.0	28.1	32.4	35.9	48.8
1996	29.0	28.2	23.7	25.4	49.0
1997	29.1	28.2	28.3	31.1	49.1
1998	29.2	28.3	29.3	30.6	49.2
1999	29.3	28.4	28.6	29.0	49.3
2000	29.4	28.5	38.2	37.0	49.4
2001	29.5	28.6	31.8	34.7	49.5
2002	29.9	28.7	31.2	33.3	49.6
2003	29.7	28.7	35.0	28.0	49.7

10.2.2 .2 Chloride concentration of the other components

The chloride concentration of direct recharge is obtained from the rainfall stations in Wildebeesvlakte as well as three new monitoring rainfall stations in the Purification Works at Dysselsdorp. The chloride concentrations of the direct recharge range from 1.33mg·ℓ^{-1} to 1.74mg·ℓ^{-1}. The concentrations of indirect recharge (interflow) were measured as 74.1-83.7 mg·ℓ^{-1} are captured after a rainfall event on May 13, 2003.

10.2.3 Scenarios for modelling

In order to identify the relative contributions of different components to the abstraction, five scenarios are considered. The relative contributions of different components in scenario 1 are computed based on the results of the analysis. The

scenarios 2 to 5 are designed according to the distribution pattern of the chloride concentration and possibility of the extreme event to evaluate the changes of the contributions of the different components with the variation of the chloride concentration input.

Scenario 1 (S1): Based on the information of the results of the analysis: chloride concentration of rainfall (C_r): 1.74 mg·ℓ^{-1}, chloride concentration of indirect recharge (C_v): 74.1 mg·ℓ^{-1} and chloride background concentration of storage water in aquifer (C_s *(t)*).

Scenario 2 (S2): C_r-1.74mg·ℓ^{-1}, C_v -74.1mg·ℓ^{-1} and initial background concentration in considering time series (C_{s0}).

Scenario 3 (S3): C_r: 1.0mg·ℓ^{-1}, C_v: 60.00mg·ℓ^{-1} and chloride background concentration.

Scenario 4 (S4): C_r: 10.0mg·ℓ^{-1}, C_v: 60.00mg·ℓ^{-1} and chloride background concentration.

Scenario 5 (S5): C_r: 1.00mg·ℓ^{-1}, C_v: 85.00mg·ℓ^{-1} and chloride background concentration.

10.2.4 Results

10.2.4.1 Recharge volume from two-component model

The proportions of components based on the two-component model are presented in Appendix VII (a, b). The following patterns are recognised:

- In the ratio of recharge to the abstractions in VR6, VR7, VR8 and VR11 are 0.009 - 0.685, 0.0002 - 0.388, 0.002 - 0.586, 0.010 - 0.488, respectively.
- The ranges of direct recharge ratio to the abstraction in VR6, VR7, VR8 and VR11 vary 0.038 - 0.380, 0.006 - 0.381, 0.002 - 0.346, 0.010 - 0.354, respectively.
- The ranges of indirect recharge ratio to the abstraction in VR6, VR7, VR8 and VR11 range 0.009 - 0.685, 0.0002 - 0.388, 0.007 - 0.586, 0.018 - 0.488, respectively.

- The direct and indirect recharge ratios to the abstraction in VG3 vary from 0.020 to 0.612 and from 0.024 to 1.473, respectively. A ratio value larger than 1.0 indicates that recharge exceeds abstraction.

The frequency of recharge events from 1994 to 2003 is listed in Table 10.3. The frequency of the direct and indirect recharge events in Peninsula and Nardouw aquifers was 14.3% - 26.4% and 73.6% - 85.7%, respectively.

The results of recharge volumes of the scenarios are presented in Appendix VIII. The following observations were addressed:

- The volumes of direct recharge in VR6, VR7, VR8 and VR11 and VG3 from 1994 to 2003 were up to 4874 $m^3 \cdot a^{-1}$, 11220.0 $m^3 \cdot a^{-1}$, 10963.3 $m^3 \cdot a^{-1}$, 3840.5 $m^3 \cdot a^{-1}$and 19345.2 $m^3 \cdot a^{-1}$, respectively.
- The volumes of indirect recharge were constantly larger than that from direct recharge in different scenarios.
- Direct recharge events are often associated with continuous high rainfall events, such as in September, October and November of 2001; the direct recharge occurred over a long period although annual precipitation was small.
- The largest recharge volume of 255413.5m^3 associated with abstraction occurred in VR7; the smallest recharge volume of 65088.3 m^3 is VR11.

Table 10.3 Frequency of the recharge based on direct and indirect recharge (1994 to 2003)

Aquifer	Peninsula								Nardouw	
	VR6		VR7		VR8		VR11		VG3	
Frequency	Direct	Indirect	Direct	Indirect	Direct	Indirect	Direct	Indirect	Direct	Indirect
Count	12	72	21	69	18	64	19	53	17	70
%	14.3	85.7	23.3	76.7	22.0	78.0	26.4	73.6	19.5	80.5

The relationship between recharge and precipitation are shown in Figure 10.5. The recharge volumes seemed to increase from 1996 to 2002. It may imply that the impact of the flood in 1996 lasted for 6 years or the recharge in the flood period continued to reach the production borehole.

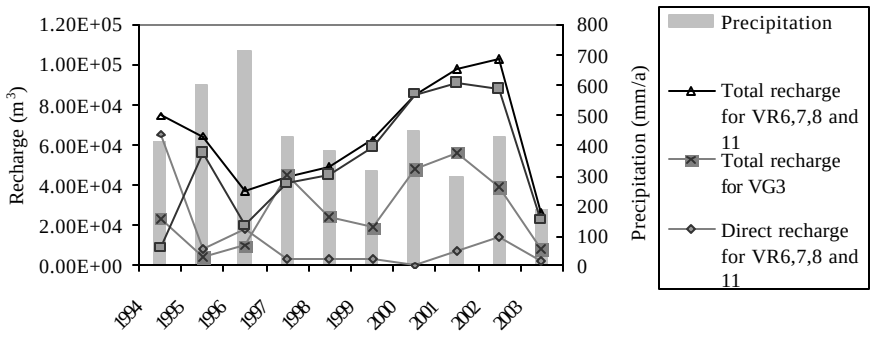

Figure 10.5 Recharge volumes versus precipitation

10.2.4.2 Recharge volume from three-component model

Based on chloride concentrations, volumes of the direct and indirect recharge and aquifer storage water were portioned (presented in Appendix IX). The results of scenario 2 are not included in following because the background chloride value is same as initial background. The following observations were made:

1) The proportions of total recharge volume ($Q_r' + Q_v'$) of VR6, VR7, VR8 and VR11 in scenario 1 were 0.066 - 0.262, 0.073 - 0.204, 0.058 - 0.278 and 0.067 - 0.259, respectively.
2) The minimum and maximum recharge proportions of the boreholes occurred in different years. These demonstrate that there was a different recharge path or recharge area for the boreholes.
3) The minimum proportions related to the maximum precipitation occurred in 1996, but the maximum proportions were related to minimum precipitation for VR6 in 2001.
4) The direct recharge was always small. The proportions of the direct recharge were smaller than those of the indirect recharge except in 1994.
5) The results in different scenarios designed were very close to those of the actual scenario.

The variation of total recharge proportions ($Q_r' + Q_v'$) with time is shown in Figure 10.6. The high recharge proportions occurred during rainfall events with high initial chloride concentrations and indirect recharge with low concentrations, such as

scenario 3. The lowest recharge proportions occurred in the lowest chloride concentration of direct recharge and in the highest chloride concentration of indirect recharge (scenario 4). The highest recharge volume occurs in the scenario 4, and lowest one is scenario 5 (Figure 10.7and Appendix X). The different patterns of the proportions and volumes demonstrate that different recharge processes occur in the region. In other words, the fracture networks may not be hydraulically connected in the Vermaaks River Wellfield.

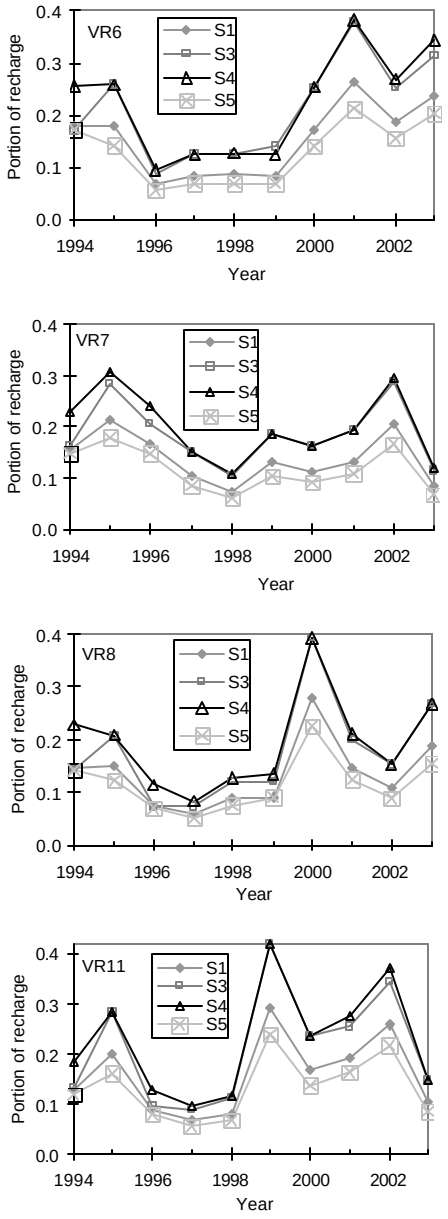

Figure 10.6 Total recharge ratios of the different scenarios in the Vermaaks River Wellfield

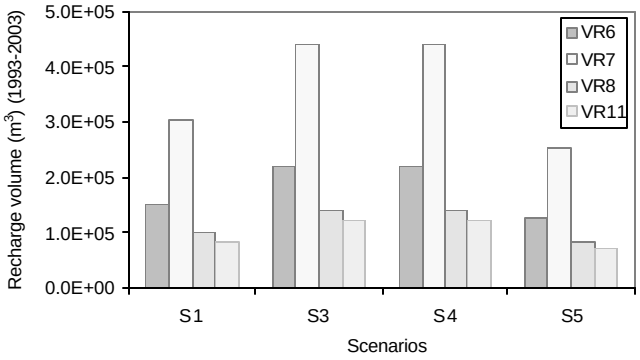

Figure 10.7 Recharge volumes of the different scenarios

10.2.5 Recharge volume to recharge rate

To convert a recharge volume to a recharge rate, the recharge area must be known. In other words, recharge rates are recharge-area dependent. Variations of the recharge areas related to the pumping time result in a number of recharge rates although the recharge volume is unique. In this study, the recharge rates are calculated based on the recharge areas identified from the geological setting and hydrogeological boundary.

For the four scenarios in the two-component model, both the upper catchment and the outcrop window of the Peninsula Formation (see Figure 8.1) are considered over two separate periods. The recharge rates based on the two-component model are listed in Appendix XI. The salient features of the estimated recharge rate are summarized as follows:

1) The recharge rate, on an annual and cumulative annual basis, ranging between 1.54% to 2.09% and 1.41% to 2.04% respectively of the rainfall is obtained based on the upper catchment area, and 0.41% to 0.60% and 0.38% to 0.55% respectively of the rainfall is calculated based on the Peninsula Window area.
2) The recharge rate is affected by the concentration of rainfall input. The higher the chloride concentration of rainfall, the higher the recharge rate.
3) The indirect recharge rates seem to be associated with chloride deposition and dissolution in the unsaturated zone.

4) The recharge rates become smaller if chloride concentrations of old storage water increase.
5) The annual average recharge rates are slight higher than those obtained from the cumulative recharge method.

For scenario 1, the recharge rates against the catchment area in VR6, VR7, VR8 and VR11 were 0.332%, 0.666%, 0.216% and 0.187% of the precipitation, respectively (presented in Appendix XII (a)). The highest recharge rate was obtained from VR 7 but the smallest recharge rate occurred in VR11. From the recharge rate point of view, the infiltration condition in the recharge area of VR7 seems to be the most favourable.

The results of the recharge rates based on the three-component mixing model are presented in Appendix XII (b). The observations are as following:

- The largest recharge rate was related to the catchment area, and the lowest one was related to the area of equivalence of *Theis's* effective radius (see Xu et al. 2002). The rates against the catchment and the equivalence area of *Theis's* effective radius were 1.182%-2.027% and 0.006%-0.011% of the precipitation, respectively. The recharge rates would increase significantly if the size of recharge area became smaller, for example, in the form of the elongated belt zone.
- The recharge rates from the two methods corresponded with each other in the same scenario. Recharge rates from the three-component model were constantly smaller than that of the two-component model. These would be attributed to the critical values of the two-component model representing the minimum recharge scenario.
- The differences of recharge rates between the different scenarios with different initial chloride concentration input appear to be small.

10.2.6 Influence factor of recharge rate

For recharge rates based on the mixing model, the influence factors include the chloride concentration, the time lag and the recharge area. If the time lag were ignored, it would decrease the accuracy of the estimated recharge rate. The uncertainty of the recharge area would lead to unreliable recharge estimates.

The chloride concentration was collected from the monthly report of the Overberg Board Water Management. Some missing data were estimated by an interpolation method. The relationship between the chemograph of chloride and rainfall in the Peninsula Aquifer is shown in Figure 10.8. The figure indicates that the chloride concentrations of the boreholes varying with the variation of rainfall. Chloride concentration seemed to rise after 3-9 month lag accompanying a high rainfall event. The longest time lag appeared about 39-40 months after the flood in November of 1996. The high chloride concentration after a high rainfall event may be a sign of indirect recharge from rainfall. About 23 higher chloride concentrations seemed to be related to rainfall with precipitation more than 50mm per month at the Parshall rainfall station, which mainly contributed to the groundwater recharge.

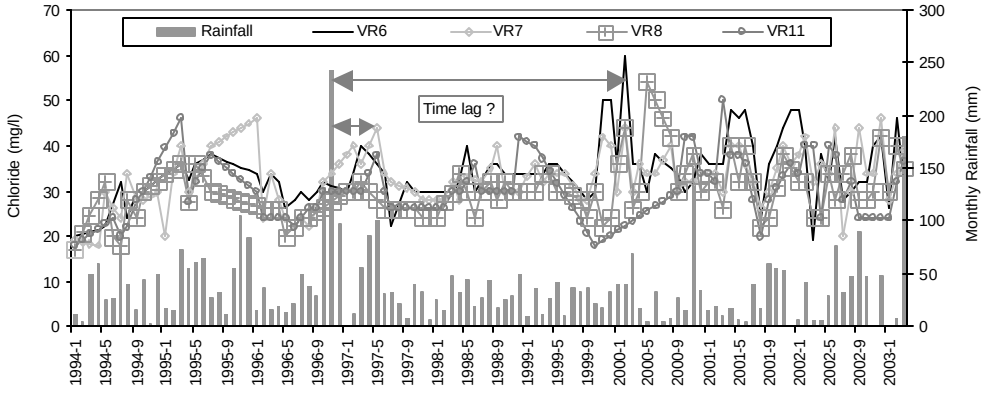

Figure 10.8 Chloride concentrations versus rainfall in the Peninsula Aquifer

The relationship between the chemograph of chloride in the Nardouw Aquifer and the rainfall at the Parshall rainfall station is shown in Figure 10.9. Chloride concentration rises accompany a high rainfall event with no time lag. The low chloride concentration with a time lag of 20-34 months seems to be associated with a high

rainfall event. These should be attributed to the direct recharge via fracture networks originating in mountainous areas.

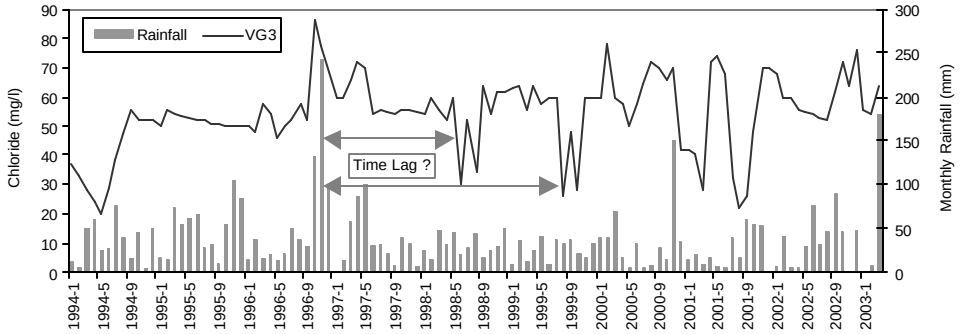

Figure 10.9 Chloride concentrations versus rainfall in the Nardouw Aquifer

However, the time lag observed in the Figure 10. 8 and Figure 10.9 cannot be accepted without scientific explanation, hence auto-regression and cross-correlation for time lag have to be done. An auto-regression and F-Test was performed to confirm the time lag (Figure10.10). The quickest response to the rainfall is approximately 1-4 months, the longest one is about 54moths (Table 10.4). From continuously higher one-tailed probability, the chloride concentration has complex response to the rainfall; the later short response may affect the long one. There are similar response patterns in the Peninsula Aquifer, but large different from the Nardouw Aquifer

Table 10.4 Time lag and its probability

Peninsular Aquifer													Nardouw Aquifer			
Borehole	VR6			VR7			VR8		VR11				VG3			
Time lag (month)	1	20	37	2	11	25	2	33	2	4	15	32	2	5	34	54
Probability	0.84	0.97	0.56	0.85	0.61	0.45	0.9	0.98	0.94	0.77	0.79	0.98	0.96	0.94	0.75	0.87

Although the auto-regression can work out the time lag, the cross-correlation is not significant (Figure 10.11). Therefore, it is difficult to construct the one-to-one relation between the rainfall and the chloride concentration under the conditions, perhaps the time series is not long enough. For the effects of time lag on recharge estimation, the cumulative rainfall from 1994 to 2003 is considered instead of monthly rainfall at present.

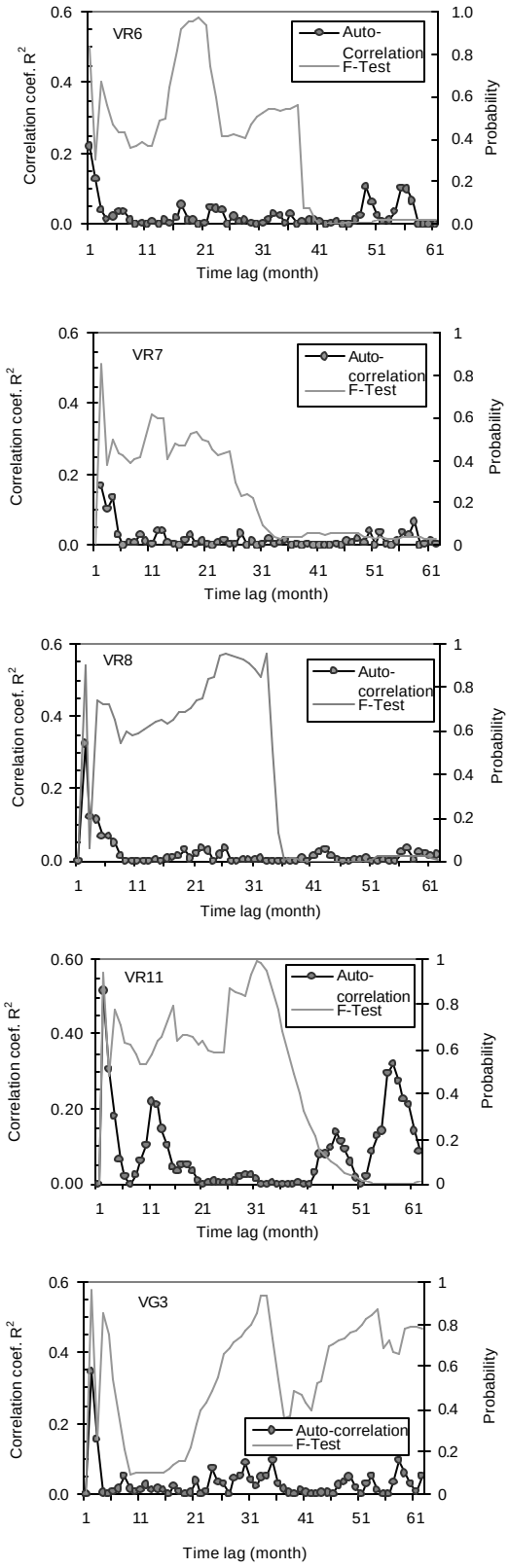

Figure 10.10 Auto-regression and F-Test of chloride concentration in the Vermaaks River Wellfield

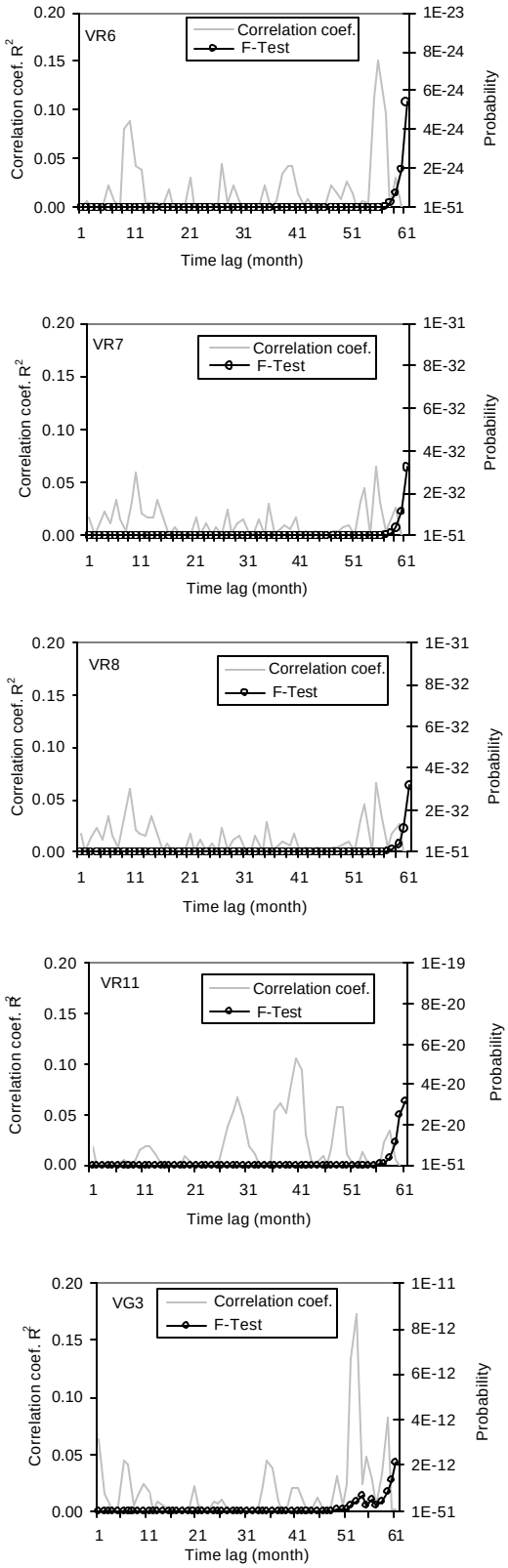

Figure 10.11 Cross-correlation and F-Test of chloride concentration in the Vermaaks River Wellfield

10.3 RECHARGE ESTIMATION WITH WATER LEVEL FLUCTUATION

The type of the groundwater regime, including climatic rainfall-infiltration, evapotranspiration, abstraction, runoff, hydraulic, irrigation, frozen and leakage types, can be used to analyse the cause of a particular groundwater level fluctuation (Fang et al., 1996, refer to Appendix XIII), but some of them, such as the climatic rainfall-infiltration type, can be used to estimate recharge because of clear relationship between rainfall and groundwater fluctuation. Thus, identification of the type of groundwater regime is important for recharge estimation by groundwater fluctuation.

10.3.1 Model of cumulative water level departure

To keep the dimension of Cumulative Water level Departure (CWD) consistent with the Cumulative Rainfall Departure (CRD) in process of data analysis, the CWD is defined as follows:

A time series of water level fluctuation [L]: $X_1, X_2, \ldots X_n$

The average value [L]: $\overline{X} = \frac{\sum_{i=1}^{n} X_i}{n}$

The departure [L]: $D_i = X_i - \overline{X}$

The cumulative water level departure [L]: CWD= $\sum_{i=1}^{n} D_i$

The following information can be seen in Figure 10.12:

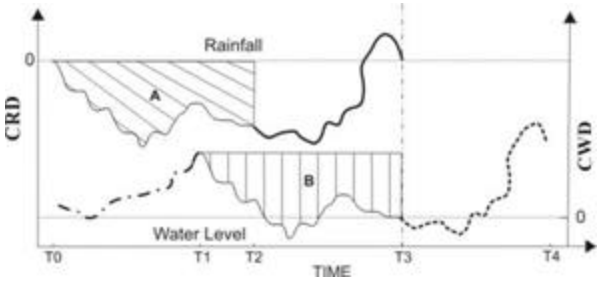

Figure10.12 Model of CRD-CWD method

- The statistical period is from T0 to T3.
- There is a resemblance between A (CRD) and B (CWD). The period of A is from T0 to T2 and B is from T1 to T3. Lag time is assumedas T1-T0.

- The dash curve extrapolated from T3 to T4 period might be related to the black bold solid line from T2 to T3 period.

A simple water balance equation based on the water level response is written as

$$CWD \times S \times B + Q = rCRD \times A \tag{10.14}$$

where CWD is the cumulative water-level departure [L]; CRD is the cumulative rainfall departure [L]; S is the aquifer storativity; A is the catchment area [L^2]; B is the groundwater catchment area [L^2]; r is the recharge rate. Q is the abstraction [L^3] is defined as:

$$Q = \Delta h \times S \times A_R, with \;\; A_R = p \;\; R^2$$

Δh is the average drawdown related effective radius; R is the effective radius, R=f(t), t is pumping time.

Let $CWD \times S \times B + Q = y \quad and \quad CRD \times A = x$, then

the equation (10.14) changes as

$$y = rx \tag{10.15}$$

This is similar to the linear equation $y=kx+c_0$ with c_0=0. Therefore, r is the slope of the CWD~CRD. Equation (10.15) is rewritten as

$$r = \frac{CWD \times S \times B + Q}{CRD \times A} \tag{10.16}$$

Suppose A=B and Q=0 in a monitoring borehole , thus

$$r = \frac{CWD \times S}{CRD} \tag{10.17}$$

The resemblance can be determined by correlation analysis. If the plotting series is long enough, the maximum and minimum points in CWD and CRD curves could be found. We call these points as peak points (similar to the maximum amplitude of a sine wave). If the minimum error and maximum correlation coefficient between block A and block B are found in a certain period, the resemblance is identified. Another method is to use the CRD and CWD to perform a correlation, trend regression analysis and F-Test with time lag.

10.3.2 CRD and CWD patterns in the Kammanassie area

In the Varkieskloof area, the CRD curve patterns of the Purification Works East (PWE) rainfall station do not match with their CWD curve patterns in DP12, DP15 and DP27, but they match well in DP18 (Figure 10.13 and Figure 10.14). The matched patterns of the CRD and CWD in DP18 seem to have the quickest response between rainfall and the water level. It may be due to the fact that the borehole is located in the alluvial deposits near the banks of the Olifants River.

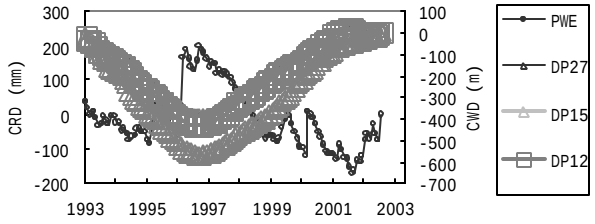

Figure 10.13 CWD patterns of boreholes versus CRD of the PWE rainfall station in the Varkieskloof area

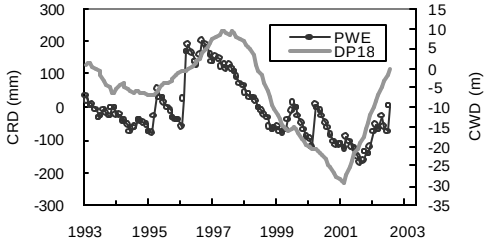

Figure 10.14 CWD patterns of borehole DP18 versus CRD of the PWE rainfall station

The records of four rainfall stations were used for CRD analysis in the Kammanassie area from September 1993 to March 2003 (Figure 10. 15). In the Voorzorg area, the CWD of VG 1 and the CRD of the Parshall rainfall station shows a matching pattern The CWD of VG 14 and VG15 shows a very good match with the CRD in the Parshall rainfall station as well. The clear peaks of these CWD patterns occur due to the high rainfall season of September to November 1996, although a different time lag exists. Borehole WN3 in the Marnewicks valley shows no match pattern between CWD and CRD, but the peak of the CWD seems to have similar peak to the boreholes in the Voorzorg area. These phenomena would imply that high rainfall events are very important to recharge.

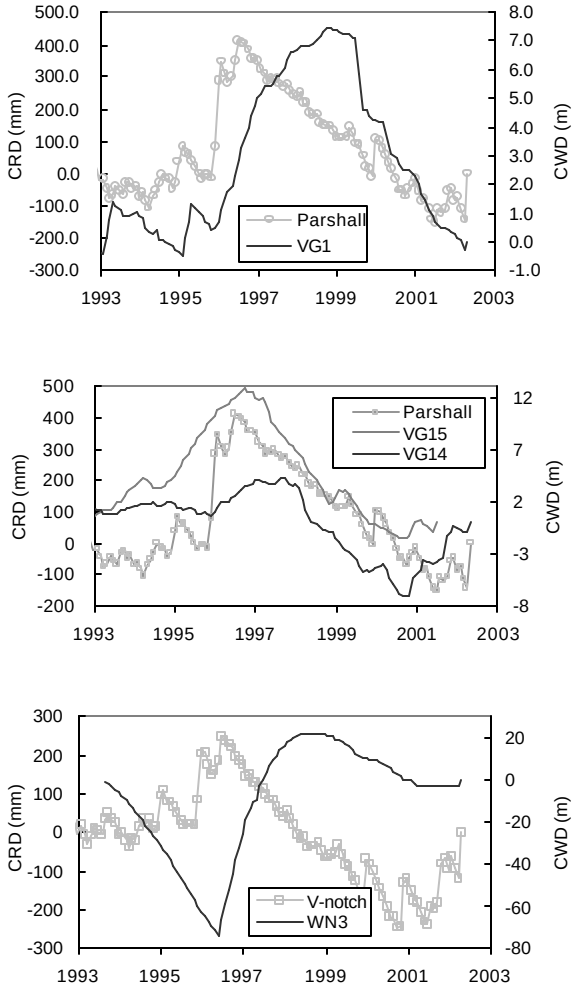

Figure 10.15 CWD patterns of boreholes versus CRD in the Kammanassie area

10.3 .3 CRD and CWD patterns in the Vermaaks River Wellfield

The groundwater level of the production boreholes has been declining in the Vermaaks River Wellfield from 1994 to 2003 as can be seen in Figure 10.16. The water level recovered a little after a few heavy rainfall events, such as in October 1996, December 2000 and May 2002. This is attributed to not only more recharge but also a reduction in abstraction (see to Figure 10.4).

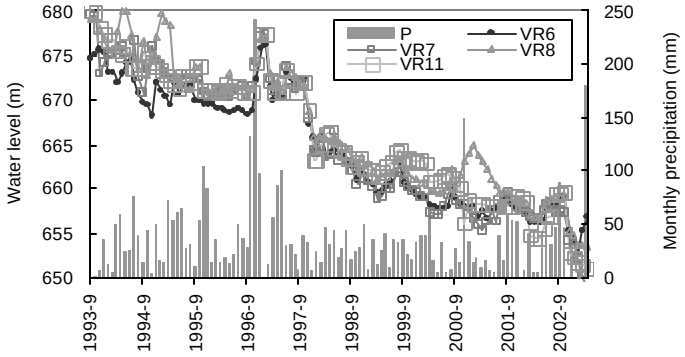

Figure 10.16 Groundwater levels in the Vermaaks River Wellfield

A similar CWD patterns occurred in VR6, VR7 and VR11 although there was a large difference in abstraction (Figure 10.17). A positive trend occurred in VR6, VR7 and VR11from September 1994 until May 1998 and a negative trend from May 1998 onwards. There were some correlation between CRD and CWD in VR6, VR7 and VR11. A positive trend occurred in VR8 from September 1994 to January 2001 and a negative trend from January 1998 onwards. The peak point on the CWD matched the peak point on the CRD have a 49 month lag for monitoring boreholes of G40171 and G40173 (Figure 10.18).

The variances in CRD of the Wildbeesvlakte rainfall station versus the CWD of the VR6, VR7 and VR8 are not significantly different based on an F-test for the one-tailed probability test (Figure 10.19). The coefficient of correlation (R^2) has the maximum value while the lag time is 52 months. However, the one-tailed probability of the CRD of the Wildbeesvlakte rainfall station versus the CWD of the VR6, VR7 and VR8 are 0.121, 0.020 and 0.0177, respectively. Therefore, there are significant correlation between CRD of the Wildbeesvlakte rainfall station versus the CWD of

the VR6, VR7 and VR8. It is important to note that the size of the time series, which is used to perform time lag analysis reduce from 157 to 106 with increase in time lag. It would increase the coefficient of correlation (R^2). That is why there is a higher coefficient of correlation (R^2) with 0.76 after a 45 months lag time (see to Figure 10.8). Although there are no time lag between the CRD and the CWD in VR6 and VR7, cross-correlation analysis can determine the time lag between the curves. The lag time is not clear between P-WL and P-P_{av}-WL-Wl_{av} pattern (Figure 10.20 and Figure 10.21). These types of curves cannot be used in lag time analysis in the Vermaaks River Wellfield. It is important to note that the best match of the CRD and the CWD should be selected for recharge estimation.

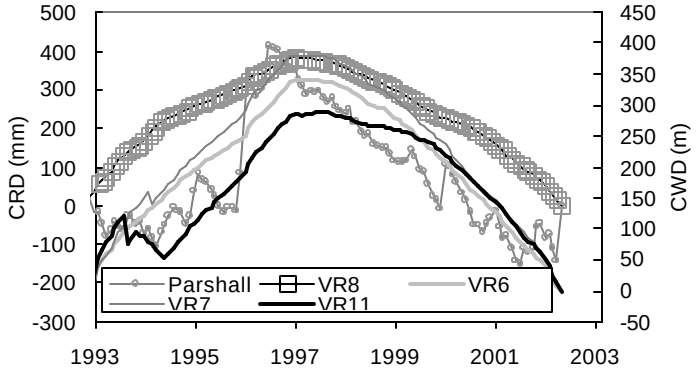

Figure 10.17 CWD patterns of production boreholes versus CRD of the Parshall rainfall station

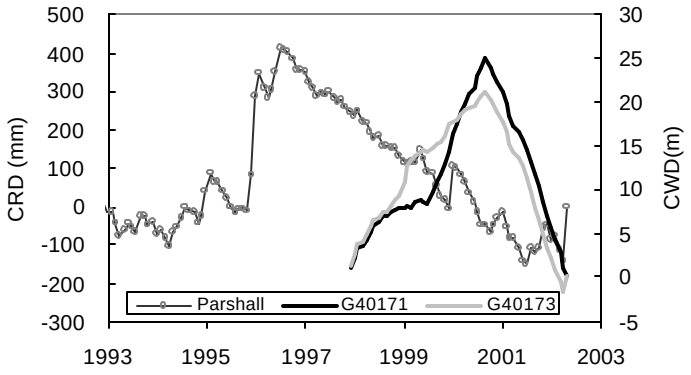

Figure 10.18 CWD patterns of G40171 and G40173 versus CRD of the Parshall rainfall station

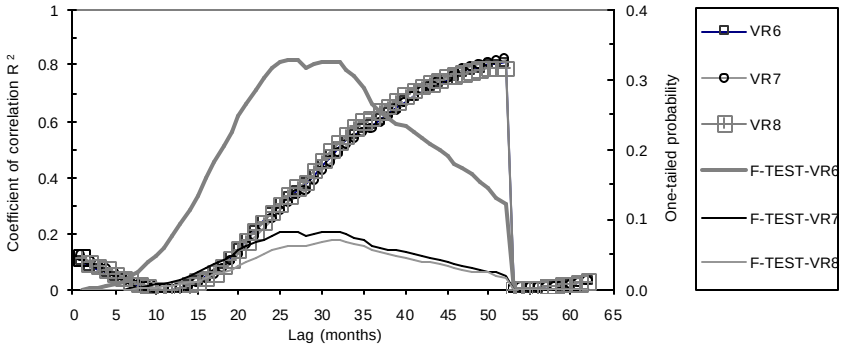

Figure 10.19 Time lag and F-Test of CWD and CRD in the Vermaaks River Wellfield

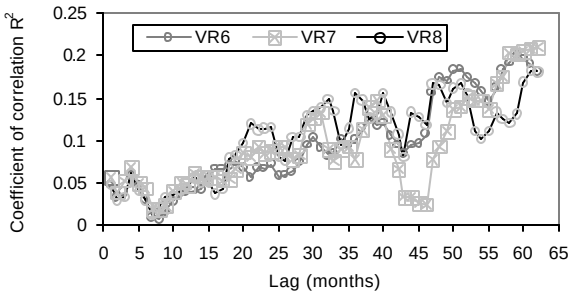

Figure 10.20 Time lag analysis using WL versus P of the Wildebeesvlakte in the Vermaaks River Wellfield

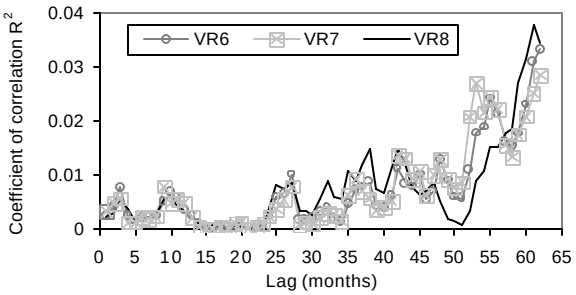

Figure 10.21 Time lag analysis using WL-WL_{av} versus P-P_{av} of the Wildebeesvlakte in the Vermaaks River Wellfield

For confirming the cyclical period of rainfall, the auto-regression of the rainfall time series in the Wildebeesvlate was performed (Figure 10.22). The cyclical pattern is not clear due to length of the time series. In other words, the time series is not long enough to illustrate the effect of the long-term effect of the rainfall on the water levels.

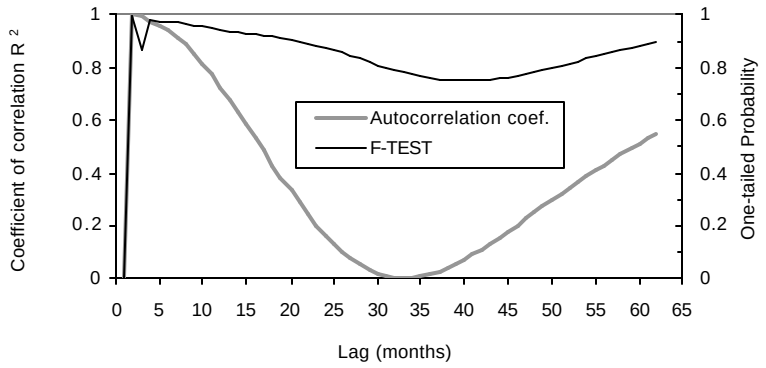

Figure 10.22 Auto-regression lag analysis and F-Test in the Wildebeesvlakte rainfall station

10.3.4 Recharge estimation with CRD and CWD

Figure 10.23 is an example of the regression analysis for recharge estimation. The recharge rates vary from 0.24% to 24.34% of the precipitation in VG15 using the CWD-CRD regression analysis based on different storativity (Table 10.5). This suggests that the accuracy of estimates is dependent on the storativity of the aquifer. Another example of the correlation coefficients of the resemblances between the CRD of different rainfall station and the CWD of G40171 are listed in Table 10.6. The observations are as follows:

1) The coefficients of correlation and regression constant are positive values.
2) The recharge rates are positively related to storativity (s): a high recharge rates are associated with high storativity.
3) High recharge rates values range from 27.4% to 75.64% of the precipitation if storativity is 1%. These values are obviously overestimated.
4) Each CRD-CWD match could be used to estimate recharge rate due to relevant high coefficient of correlation. This suggests that one match with the highest coefficient of correlation should be adopted preferentially. In this study, the best one is CRD of the V-notch versus CWD of G40171.

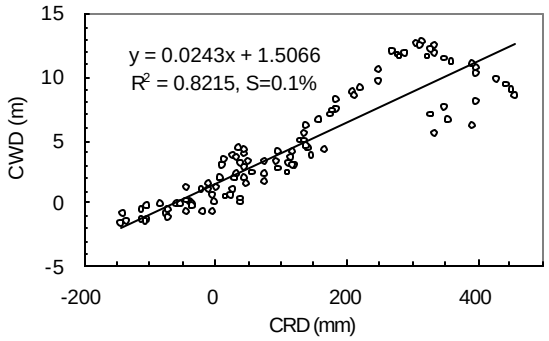

Figure 10.23 Regression of CWD - CRD of VG15

Table 10.5 Regression analysis results of VG15 using CRD of the Parshall rainfall station

S (‰)	Regression equation	RE (%)	C (mm)	RE (mm)
0.1	CWD = 0.0024CRD + 0.1507	0.24	0.15	1.07
0.5	CWD = 0.0122CRD + 0.7533	1.22	0.75	5.46
1	CWD = 0.0243CRD + 1.5066	2.43	1.51	10.88
5	CWD = 0.1217CRD + 7.5328	12.17	7.53	54.48
10	CWD = 0.2434CRD + 15.066	24.34	15.07	108.96

Table 10.6 Results of regression analysis of G40171

Coefficient of correlation	S (‰)	Regression equation	RE (%)	C (mm)	RE_{av} (mm)
V-notch 0.83	0.1	CWD = 0.0076CRD + 0.51	0.76	0.51	2.88
	0.5	CWD = 0.0378CRD + 2.55	3.78	2.55	14.31
	1	CWD = 0.0756CRD + 5.1	7.56	5.10	28.62
	5	CWD = 0.3781CRD + 25.49	37.81	25.49	143.15
	10	CWD = 0.7562CRD + 50.98	75.62	50.98	286.31
Purification Works East 0.76	0.1	CWD = 0.0061CRD + 0.901	0.61	0.90	1.94
	0.5	CWD = 0.0305CRD + 4.50	3.05	4.50	9.69
	1	CWD = 0.061CRD + 9.01	6.1	9.01	19.37
	5	CWD = 0.3048CRD + 45.03	30.48	45.03	9.68
	10	CWD = 0.6095CRD + 90.06	60.95	90.06	193.56
Wildebeesvlake 0.70	0.1	CWD = 0.003CRD + 0.53	0.304	0.53	1.45
	0.5	CWD = 0.0152CRD + 2.66	1.52	2.66	7.27
	1	CWD = 0.0304CRD + 5.32	3.04	5.32	14.54
	5	CWD = 0.1518CRD + 26.61	15.18	26.61	72.58
	10	CWD = 0.3035CRD + 53.21	30.35	53.21	145.11
Parshall 0.67	0.1	CWD = 0.0027CRD + 0.762	0.27	0.76	1.21
	0.5	CWD = 0.0137CRD + 3.81	1.37	3.81	6.13
	1	CWD = 0.0274CRD + 7.62	2.74	7.62	12.27
	5	CWD = 0.137CRD + 38.11	13.7	38.11	61.33
	10	CWD = 0.274CRD + 76.22	27.40	76.22	122.66

The recharge estimates of borehole VR6 using the CWD-CRD regression analysis are listed in Table 10.7. The recharge rate varies from 5.98% to 299.12% based on storativity from 0.1‰ to 5‰. The results could not be used in practice although the correlation coefficient is 0.86 (R^2=0.74) because abstractions are ignored. It also illustrates that the CRD-CWD method is unsuited for estimating the recharge under conditions where the storativity is unreliable, even though the correlation coefficient is very high. The CRD-CWD method can not work adequately under most pumping conditions because the effective radius could not be calculated precisely, that is, more errors would be introduced due to uncertain factors, especially under unsteady state and discontinuous pumping conditions.

Table 10.7 Regression analysis results of VR6 using CRD in the Parshall rainfall station

S (‰)	Regression equation	RE (%)	C (mm)	RE (mm)
0.1	CWD = 0.0598CRD + 10.685	5.98	10.69	22.64
0.5	CWD = 0.2991CRD + 53.424	29.91	53.42	113.24
1	CWD = 0.5982CRD + 106.85	59.82	106.85	226.49
5	CWD = 2.9912CRD + 534.24	299.12	534.24	1132.50

10.3.5 Comparison of the results with RIB

The water level series is simulated using a computer program named RIB (Xu and Beekman, 2003). The average pumping rate is 820m^3/d for the production boreholes. Simulated water levels are compared with observed levels in Figure 10.24, where dh (crd) refers to water levels calculated by CRD method (Bredenkamp et al., 1995), while dh (rib) represent water levels calculated using Equation (3.18). For storativity of 1‰ and recharge area of 11km^2, the average recharge rates modeled for VR6, VR7, VR8 and VR11 are 2.25%, 2.55%, 2.14% and 2.17% of the rainfall, respectively, although there are disparities in curve match. These results are consistent with the results by CRD-CWD as previously indicated

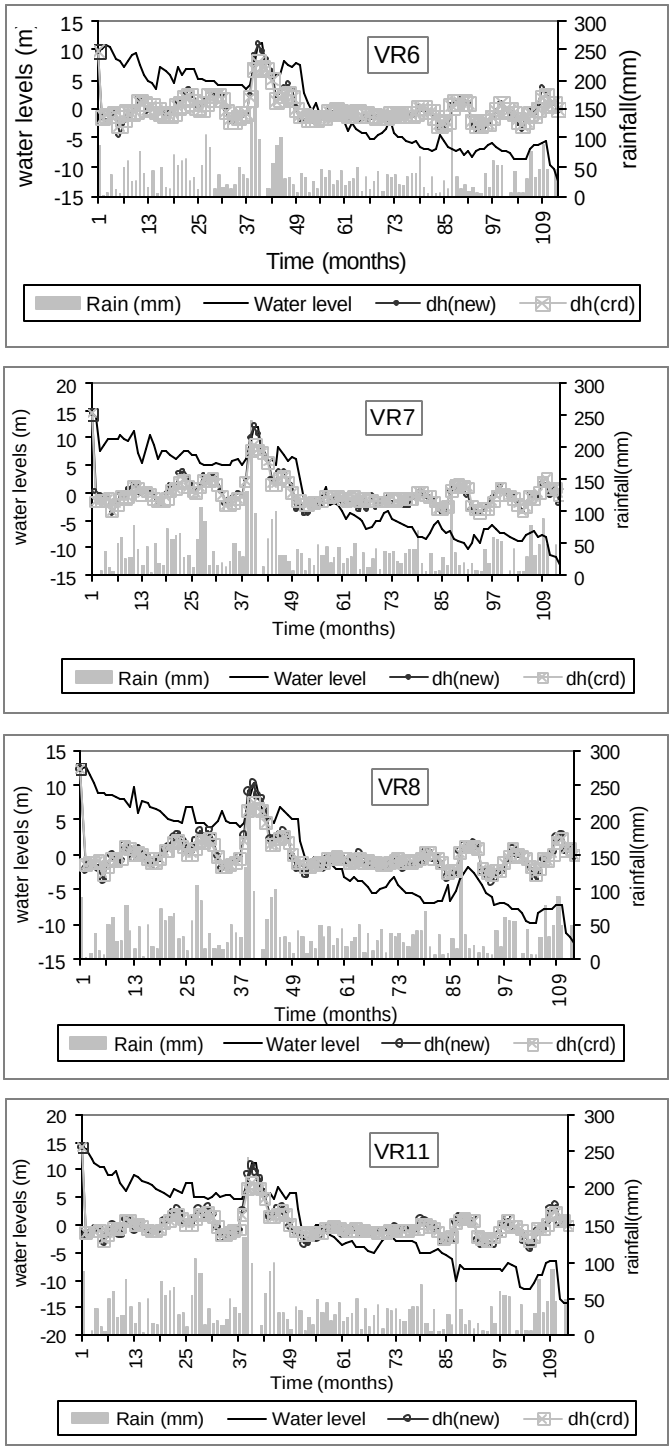

Figure 10.24 Results of RIB analysis in the Vermaaks River Wellfield

10.3.6 Impact of preceding rainfall on recharge

Impact of preceding rainfall (X_a, a is the time of the maximum water level) on recharge is calculated as follows (Sheng et al. 1985):

$$x_{a,t}=K(x_{a,t-1}+x_{t-1})$$
$$x_{a,t-1}=K(x_{a,t-2}+x_{t-2})$$
……
$$X_{a,t}=K x_{t-1}+K^2 x_{t-2}+K^3 x_{t-3}+\ldots+K^n x_{t-n}+K^n x_{a,t-n} \quad (10.18)$$

If time is long enough before the study period

$$K^n x_{a,t-n}=0$$

where $x_{a,t}$ is rainfall influenced by preceding period during the study period [L, mm].

$x_{a,t-1}$ is rainfall influenced by preceding period during former period before the study period [L, mm].

x_{t-1} is rainfall of preceding period [L, mm].

K is ratio of degression (0.8~0.9, average 0.85).

n is the interval of two rainfall events [T, days].

The impact of preceding rainfall on recharge rate can be computed as follows:

1) x_a is calculated, which influence water level increasing obviously

$$x_{a,t}=K x_{t-1}+K^2 x_{t-2}+K^3 x_{t-3}+\ldots+K^n x_{t-n}+K^n x_{a,t-n}$$

2) x_{s1} (the first time of the flux increasing in the study period) is calculated by

$$x_{s1}=x_a+x_1 \quad (10.23)$$

3) Second time ……. repeat step 1, 2

4) Calculate recharge rate *RE*

$$RE=s\times\frac{\sum\Delta H}{\sum x}100\% \quad (10.24)$$

where ? ? H is cumulative water level increased (mm) and ? x is cumulative rainfall (mm), which influences water level in time series.

Eight periods with increased water level responding to rainfall event were observed from 1998 to 2001 in G40171. The recharge rates are calculated with a storativity value of 1‰ as presented in Appendix XIV(a). The maximum recharge rate, related to 69mm of preceding rainfall from May to August 2001, is 10.87% of the precipitation. The minimum recharge rate is 0.69% of the precipitation, which is associated with 41mm of preceding rainfall from July to September 2000. The average recharge rate is 5.38 % of the precipitation or 48.67 mm from November 1998 to December 2001. This equals to 3.88% of precipitation of 1256mm in the period. The recharge rate is 24.34mm if s=0.5‰, which is 1.94 % of the total precipitation in the period. The results coincide with those estimated from the CWD-CRD method.

10.3.7 Discussion

The constant of regression (C_0) value will always be a positive value because the aquifer has certain storage before the water level fluctuation disappears. The C_0 value could be related to ranges of water level under a no recharge condition, and then the C_0 value is the basic water level change. For instance, there is a 5.1m basic water change in G40171 under conditions of C_0=5.1mm and s=1‰ if no recharge occurs. If the water level range is 4.05m (C_0) this means 4.05mm recharge under condition of s=1‰ in G40171.

Storativity is a very sensitive parameter in estimating recharge with CWD-CRD method. Based on the storativity range of 1‰-2.2 ‰ (the storativity data were adopted Kotze, 2002), the recharge would be 7.56%-16.63 % and 2.43%-5.35 % of the rainfall in G40171 and VG15, respectively. The large interval of the recharge occurs because of the uncertainty of the storativity.

In order to confirm the storativity, different water level fluctuation and storativity are assumed to simulate the recharge area of the hot springs. If the area simulated is close to the natural recharge area, the storativity is assumed to be reliable. The recharge

areas simulated are listed in Table 10.8 and Table 10.9. The simulated recharge area with 24,600 km^2 and 24,156.5 km^2 are close to the area of 24,650km^2 based on the geological boundaries if the storativity is 0.1‰-0.5 ‰. It confirms that the storativity of the TMG should be from 0.1‰ to 1‰. Based on the above discussion, the recharge rate of 0.24%-7.56% of the rainfall seems to be accredited in G40171 under storativity of 0.1‰-1‰.

Table 10.8 Recharge area simulation based on the storativity and flow rates of hot springs: 1.0m water level fluctuation.

Storativity (‰)			0.1	0.5	1	5	10
Specific recharge ($m^3 \cdot yr^{-1} \cdot km^{-2}$)			100	500	1000	5000	10000
Hot Spring	$l \cdot s^{-1}$	$m^3 \cdot yr^{-1}$	Recharge area from 1.0 m change of water level (km^2)				
The Baths (Citrusdal)	29	914,544	9,145.4	1,829.1	914.5	182.9	91.5
Goudini	11	346,896	3,469	693.8	346.9	69.4	34.7
Brandvlei	127	4,005,072	40050.7	8,010.1	4,005.1	801	400.5
Caledon	9	283,824	2,838.2	567.6	283.8	56.8	28.4
Avalon(Montagu)	38	1,198,368	11,983.7	2,396.7	1,198.4	239.7	119.8
Baden	37	1,166,832	11,668.3	2,333.7	1,166.8	233.4	116.7
Warmwaterberg	37	1,166,832	11,668.3	2,333.7	1,166.8	233.4	116.7
Calitzdorp	8	252,288	2,522.9	504.6	252.3	50.5	25.2
Tooverwater	11	346,896	3,469	693.8	346.9	69.4	34.7
Studtis	31	977,616	9,776.2	1,955.2	977.6	195.5	97.8
Uitenhage	45	1,419,120	14,191.2	2,838.2	1,419.1	283.8	141.9
Total	383	12,078,288	120,782.9	2,4156.5	1,2078.2	2,415.8	1,207.9

Table 10.9 Recharge area simulation based on the storativity and flow rates of hot springs: 3.0m water level fluctuation.

Storativity (‰)			0.1	0.5	1	5	10
Special recharge ($m^3 \cdot yr^{-1} \cdot km^{-2}$)			300	1,500	3,000	1,5000	30,000
Hot Spring	$l \cdot s^{-1}$	$m^3 \cdot yr^{-1}$	Recharge area from 3.0 m change of water level (km^2)				
The Baths (Citrusdal)	29	914,544	3,048.5	609.7	304.8	61	30.5
Goudini	11	346,896	1,156.3	231.3	115.6	23.1	11.6
Brandvlei	127	4,005,072	13,350.2	2670	1335	267	133.5
Caledon	9	283,824	946.1	189.2	94.6	18.9	9.5
Avalon (Montagu)	38	1,198,368	3,994.6	798.9	399.5	79.9	39.9
Baden	37	1,166,832	3,889.4	777.9	388.9	77.8	38.9
Warmwaterberg	37	1,166,832	3,889.4	777.9	388.9	77.8	38.9
Calitzdorp	8	252,288	841	168.2	84.1	16.8	8.4
Tooverwater	11	346,896	1,156.3	231.3	115.6	23.1	11.6
Studtis	31	977,616	3,258.7	651.7	325.9	65.2	32.6
Uitenhage	45	1,419,120	4,730.4	946.1	473	94.6	47.3
Total	383	12,078,288	2.46E+04	1.00E+01	2.04E-03	8.31E-08	1.69E-12

10.4 RECHARGE ESTIMATION WITH SPRING FLUX FLUCTUATION

Spring flow fluctuation is a direct indicator of groundwater recharge. Two perennial ponds occur at the geological contact zone between the Peninsula and Cedarburg Formations in the Vermaaks and Marnewicks valleys. The springs are maintained in part of by overflow from the Peninsula Aquifer and a local shallow groundwater (see to Figure 8.13). Flows have been recorded since 1994 at the V-notch rainfall station, the monthly average fluxes, in litres, are available (Kotze, 2002). A good spring flux curve seems to respond to rainfall (Figure 10.25). Large flow appeared after a time lag of a few months since the rainfall. The curve based on rainfall-spring is therefore used to estimate recharge by regression.

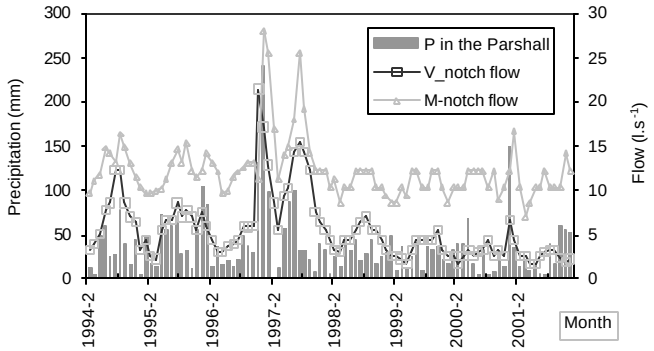

Figure 10.25 Hydrographs of the Vermaaks and Marnewicks Rivers

10.4.1 Theory

According to the hydrogeological model (Figure 8.13), the spring flux is fraction of the total rainfall, assuming the recharge area is equal to the catchment area, a simple water balance over a given time interval i can be formulated as follows:

$$\sum_{i=1}^{n} Q_{si} = r\sum_{i=1}^{n} Q_{Rfi} + c \qquad (i = 1,2,3...n) \quad with$$

$$Q_{si} = q_i \times A \times t_i \qquad (10.25)$$

where Q_{si} is spring flux, Q_{Rfi} is rainfall, A is the recharge area; q_i is the special flow of the spring and t_i is the time. c is a constant of regression.

10.4.2 Regression

10.4.2.1 Vermaaks catchment

A statistical analysis was carried out to examine relationships between cumulative flow (CF) and rainfall (CR), cumulative flow departure (CFD) and rainfall departure (CRD). The results are given in Table 10. 10. A stay correlation coefficient 0.9963 between CF of the V-notch and CR of the Parshall rainfall station exists. The one-tailed probabilities from the F-Test between CF in the Vermaaks and Marnewicks and CR in the Parshall are 0.190 and 0.183, respectively. The best correlation coefficient of 0.9966 between CF and rainfall exists in the preceding month. This suggests that rainfall from both the current and preceding months is important to estimate recharge. Therefore, the CF and CR are used to perform the regression analysis for recharge estimation.

The results of recharge rate by regression analysis with V-notch spring data and rainfall in different rainfall stations from 1994 to 2001 are listed in Table 10. 11. An example of a regression, based on flow in the V-notch and rainfall in the Parshall against the catchment area, is shown in Figure 10.26. The recharge of 3.7% of the precipitation is adopted because it has the highest correlation coefficient between the CR of the Parshall rainfall station and the CF. Considering about 11.32 % of the spring water is derived from the local aquifer (8.37% from the shallow aquifer as monitoring borehole and 4.86% from Peninsula Aquifer as production borehole , see Chapter 8), the actual recharge rate should be 3.21% of the precipitation.

Table 10.10 Statistical results between different components

Pair of Factors		CF Versus CR[1)]	CF Versus CR	CFD Versus CRD	Flow Versus Rainfall	CRD Versus CTF	CR Versus CRD	Rainfall Versus CRD
Vermaaks	r	0.9966	0.9963	0.9032	0.5756	0.4038	0.3770	0.1154
	F-Test	1.61E-11	1.90E-1	2.3E-8	1.1E-4	2.3E-8	1.1E-5	8.4E-6
Marnewicks	r	0.9962	0.9959	0.7302	0.1454	0.2984	0.3770	0.1154
	F-Test	1.21E-11	1.83E-1	3.1E-8	2.9E-4	3.1E-8	5.93E-5	1.6E-5

1) $CR = \sum_{i=1}^{n} (0.2P_i + 0.8P_{i-1}) \qquad i = 1,2 \cdots n \; month$

Table 10.11 Recharge estimated with V-notch spring related to different rainfall stations from 1994 to 2001 by the CF method against recharge area of 10.85 km ^{2}

Station	% of Precipitation	C	R^2
Parshall	3.7	3.11	0.9926
Wildebeesvlate	3.54	1.74	0.991
V-notch	4.77	1.23	0.9874
Voorzorg	4.88	4.31	0.9842
Dorekloof	5.59	1.6	0.9882

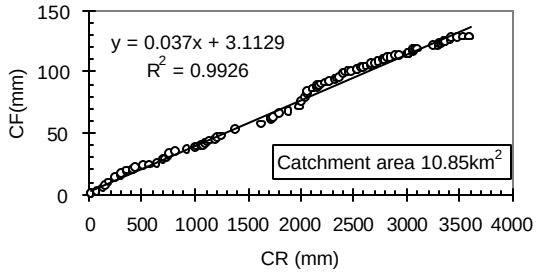

Figure 10.26 Regression based on flow in the V-notch and rainfall in the Parshall against the catchment area

10.4.2.2 Marnewicks catchment

The same method of regression analysis is used in the analysis of the Marnewicks Spring. The recharge rates ranges from 3.65% to 5.76 % of the precipitation from different rainfall stations for the 1994 to 2001 using the CF method against the area of Marnewicks catchment (Table 10. 12). A recharge rate of 3.65 % of the precipitation is related to the maximum correlation coefficient between CR in the Wildbeesvalakte rainfall station and CF in the Marnewicks flow gauge (Figure 10.27).

Table 10.12 Recharge rates related to different rainfall station from 1994 to 2001 against the Marnewicks catchment area

Station	% of precipitation	C	R^2
Parshall	3.82	-2.8	0.9954
Wildebeesvlakte	3.65	-4.3	0.9961
V-notch	4.93	-4.83	0.9926
Voorzorg	5.05	-1.85	0.9947
Dorekloof	5.76	-7.58	0.9989

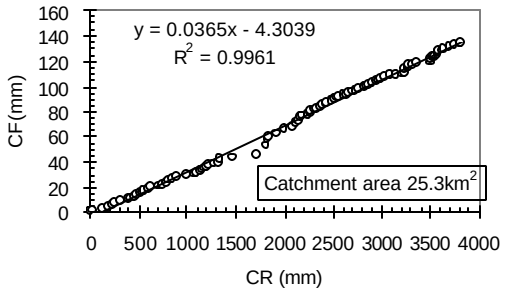

Figure 10.27 Regression based on flow in the M-notch and rainfall in the Wildebeesvlakte against the catchment area

10.4.3 Discussion

10.4.3.1 Impact of flood on recharge

The recharge rate before the flood is slightly higher than after the flood in all rainfall stations (Table 10. 13). If the floods are removed, the recharge rate ranges from 3.93% to 4.03%, based on different rainfall station data from 1994 to 2001 (Table 10.14).

Table 10.13 Recharge rate against recharge area of 10.85 km ^{2} from 1994 to 2001

Station	Before flood			After flood		
	% of P	C	R^2	% of P	C	R^2
Parshall	3.55	3.37	0.9873	3.36	10.87	0.9622
Wildebeesvlakte	3.53	0.8	0.9919	3.31	11.24	0.9575
V-notch	4.27	2.53	0.9906	4.07	12.25	0.9489
Voorzorg	5.38	-0.33	0.9923	3.87	11.34	0.956
Dorekloof	4.74	1.72	0.988	5.05	14.43	0.9484

Table 10.14 Regression results with runoff removed from 1994 to 2001

Catchment	Station	% of the P	C	R^2	Flood removed (mm)
Vermaaks	Parshall	4.03	5.56	0.991	250.9
Marnewicks	Wildebeesvlakte	3.97	-4.51	0.995	270.2
Total	Wildebeesvlakte	3.93	-2.68	0.994	270.2

10.4.3.2 Recharge area

As equation (10.25) has shown, the recharge area is a principal factor in regression analysis when special flow is converted to a volume. The recharge related to the

recharge area of the Vermaaks and Marnewicks catchments are shown in Figure 10.28. It illustrates the recharge rate is recharge-area dependent. This is the limitation of the method. The recharge rate range from 4.01% to 3.29 % based on a ±10% difference between the natural catchment and recharge area. This means there is a recharge rate increase of 0.09% of the precipitation if the recharge area is reduced by 10%, and recharge rate decrease of 0.33% of the precipitation if the area increases 10%. The recharge rate is underestimated because the impact of abstraction is ignored.

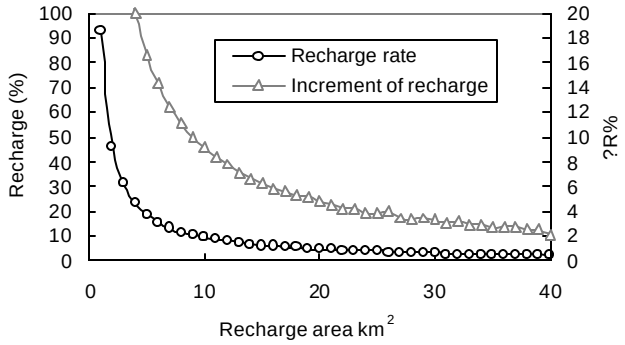

Figure 10.28 Relationship between recharge rates and recharge area

Due to the hydrogeological contact of the Marnewicks and Vermaaks catchments, the recharge rate with 3.2% of the precipitation is computed against two catchment areas as shown in Figure 10.29 (13.23% of the aquifer leakage was taken out). This result is only slightly different from the result of the separate catchment. The result removes the impact of the watershed of groundwater catchment between the two catchments.

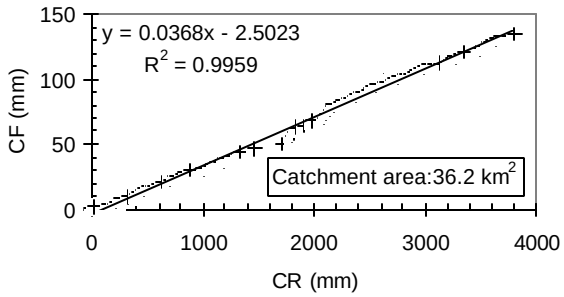

Figure 10.29 Regression based on total flow in the two catchments and rainfall in the Wildebeesvlakte rainfall station

10.4.3.3 Regression constant

The slope of the regression equation or the recharge rate is given in Table 10.11 to Table10.13. The basis of base flow is the constant in the regression equation. A positive constant *c* occurs in the Vermaaks catchment. The influence of abstraction leads to the dewatering of the aquifer in the upper Vermaaks catchment. Spring flow is not only fed by recharge, but also by aquifer storage. There is a very small or no aquifer storage contribution to the spring in the Marnewicks catchment because a negative *c* value occurs.

10.4.3.4 Impact of preceding rainfall on spring flux

Impact of preceding rainfall on spring flux can be computed as shown in section 10.3.7. The recharge rate is calculated as follows

$$RE = \frac{\sum \Delta H}{\sum x} 100\% \qquad (10.26)$$

where ? ? H is cumulative increment of flux and ? x is cumulative rainfall which influences recharge in time series.

Three periods with an increasing spring flux were observed from 1994 to 2003. The recharge rates are calculated using the Parshall rainfall data over an upper catchment area of 10.85km^2 as presented in Appendix XIV(b). The maximum recharge rate is 5.21% of the precipitation, which is associated with a preceding rainfall of 257mm from February to June 1997. The minimum recharge rate is 1.73% of precipitation, which is related to preceding rainfall of 97mm from April to July 1998. The recharge rate is linked to the rainfall of the study period, such as period 3; the 1.38% and 1.92% of the precipitation are related to 42mm and 37mm, respectively. The recharge rate is 2.42% of the precipitation of 867mm from February 1997 to March 1999. The recharge rate is 0.81% of the precipitation of 2,593mm from January 1994 to March 1999 if two or more years lag. This may be attributed to ignore of the recharge contribution to the spring flow.

10.5 NUMERIC SIMULATION

Assuming the abstraction of the Vermaaks River Wellfield from 1993 to 2002 is equal to the recharge rate for the same period, it gives crude recharge estimates in percentage of precipitation as 11.09% and 2.96% over the areas of the upper Vermaaks catchment (10.85km^2) and Peninsula Formation Window (40.6km^2), respectively. As water level in the wellfield experienced a continued decline over the period, the above-estimated recharge rate would be larger than realistic recharge rate. In other words, the recharge rate must be smaller than the crude estimates.

For confirming the water budget, two 3D models were constructed as shown in Figure 10.30. The aquifer thickness is 750m deduced from Figure 8.7. In the model, the Cedarberg shale is supposed to act as an inactive boundary because the abstraction from the Vermaaks River Wellfield can come from the entire Peninsula Formation closed by Cedarberg Formation. The boundary of the Peninsula Formation and Nardouw Subgroup is another inactive boundary in the south. The parameters of the models are listed in Table 10.15. The initial transmissivity can be referred to in Table 8.5. The horizontal transmissivity assigned to each layer is based on weight factors of borehole penetration and water strike of 0.1 and 0.9, respectively. The ratio of horizontal transmissivity to vertical transmissivity (T_h/T_v) is 10. The time step is 10 seconds in the transient model. The period modeled is from 1993 to 2002.

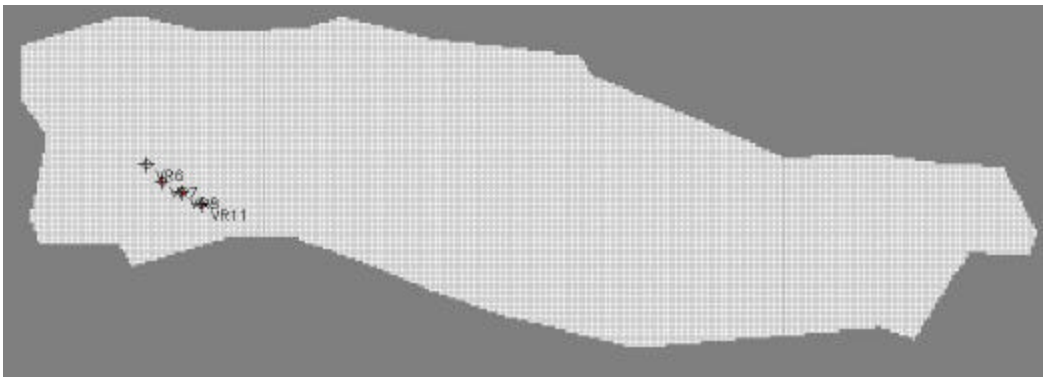

Figure 10.30 Model grids of the Peninsula Formation Windows

Flows are calculated for each zone in each layer and each time step. The unit of the flows is [$m^3 \cdot s^{-1}$]. Flows are considered IN, if they are entering a zone. Flows between

subregions are given in a Flow Matrix. HORIZ. EXCHANGE gives the flow rate horizontally across the boundary of a zone. EXCHANGE (UPPER) gives the flow rate coming from (IN) or going to (OUT) to the upper adjacent layer. EXCHANGE (LOWER) gives the flow rate coming from (IN) or going to (OUT) to the lower adjacent layer. The percent discrepancy is calculated by 100 · (IN - OUT) / (IN + OUT) / 2 (Chiang and Kinzelbach, 2001).

Table 10.15 Parameters of the models

Model	Layer	Thickness (m)	T ($m^2 \cdot s^{-1}$)	n_e	Pumping ($m^3 \cdot s^{-1}$)			
A	1	50	6.55E-5 (Fold limb) 6.42E-4(Fold axis)	0.5~2‰	VR6	VR7	VR8	VR11
	2	50	6.55E-5 (Fold limb) 6.42E-4(Fold axis)	1-2‰	-	3.64E-3	8.44E-4	7.08E-4
	3	50	6.55E-5 (Fold limb) 5E-4(Fold axis)	1-2‰	-	3.64E-3	8.44E-4	1.42E-3
	4	50	6.55E-5 (Fold limb) 6.42E-4(Fold axis)	1.5-2‰	-	-	8.44E-4	-
	5	50	6.55E-5 (Fold limb) 6.42E-4(Fold axis)	1-1.5‰	3.50E-3	-	-	-
	6	50	6.55E-05	1‰	-	-	-	-
	7	50	6.55E-05	1‰	-	-	-	-
	8	50	6.55E-05	1‰	-	-	-	-
	9	50	6.55E-05	1‰	-	-	-	-
	10	50	6.55E-05	1‰	-	-	-	-
	11	50	6.55E-05	1‰	-	-	-	-
	12	50	6.55E-05	1‰	-	-	-	-
	13	50	6.55E-05	1‰	-	-	-	-
	14	50	2.65E-05	1‰	-	-	-	-
	15	50	2.65E-05	1‰	-	-	-	-
B	1	250	6.55E-5 (Fold limb) 6.42E-4(Fold axis)	0.5~2‰	3.50E-3	7.28E-3	2.53E-3	2.128E-3

The water budget at steady state using PMWIN is listed in Table 10.16. Calibration is performed using a recharge rate of 0.316% ($4.23\times10^{-11} m \cdot s^{-1}$) from a three-component mixing model in the transient model and the results are listed in Table 10.17. The observations are obtained as follows:

- For the model A, negative water balance occurs if recharge is $1.22\times10^{-10} m \cdot s^{-1}$ and $2.44\times10^{-10} m \cdot s^{-1}$. The discrepancy is −65.54% and −1.5%, respectively. Positive budget occurs if the recharge rate is $2.5\times10^{-10} m \cdot s^{-1}$ in the model A. It means that the recharge rate cannot be higher than 1.96% of rainfall because the water level had been declining since 1993.

- For the model B, the same scenario of the water budget occurs. A positive budget occurs if the recharge rate is 2.427×10^{-10} m·s^{-1} in the model B.
- The simulated water level is higher than those measured if the recharge rate is 4.23×10^{-11} m·s^{-1}. The errors of VR 6, VR7, VR8 and VR11 between water levels from the transient flow model and measurement are 1.8, 2.41, 1.18 and 3.50m, respectively.

Table 10.16 Water budget of the steady s tate model flow

Recharge rate (%)		Recharge (m·s^{-1})	Discrepancy of the Peninsula Formation Window budget (%)
Model A	0.96	1.22×10^{-10}	-65.54
	1.91	2.44×10^{-10}	-1.50
	1.96	2.5×10^{-10}	0.91
Model B	0.96	1.22×10^{-10}	-63.89
	1.88	2.40×10^{-10}	-0.3
	1.90	2.427×10^{-10}	0.75
	1.91	2.44×10^{-10}	1.32

Table 10.17 Water level running 10 years with recharge of 4.23×10^{-11} m·s^{-1} at transient state for model A

Boreholes	VR6	VR7	VR8	VR11
Measured water level in Dec. 2002 (m)	654.40	653.87	654.82	652.27
Simulation water level in Dec. 2002(m)	656.20	656.28	656.00	655.77
Error (m)	1.80	2.41	1.18	3.50

10.6 INTEGRATED RECHARGE RATE IN THE KAMMANASSIE AREA

It is well known that different results are produced from different methods. Each result can present the degree that is close to the realistic recharge rate based on the understanding of the recharge mechanisms and hydrogeological settings. The recharge can be divided into manageable and unmanageable. The recharge rate estimated from the production borehole is a reflection of manageable recharge. The others may represent the total recharge. The research objective of this section is to develop a new method for integrating such estimates in the TMG area. The uncertainties of factors related to the methods are analysed, and the reliability of the conversion would be improved by analysing raw and empirical data. The determination of weighting factors is considered as the largest uncertainties for the model in the study area. A

method will be developed to calculate the weighting factors based on the role of the factors in recharge estimation processes. Four patterns of recharge rate can be estimated, namely a: highly discrete and bias, b: highly discrete and lowly bias, c: lowly discrete and bias, d: lowly discrete and highly bias (Figure 10.31). The pattern c would be our ultimate objective, which should be the representation of the actual recharge rate.

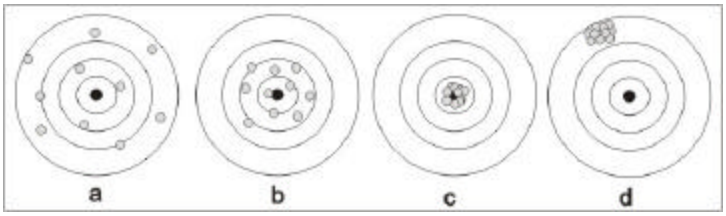

a: highly discrete and bias b: highly discrete and lowly bias

c: lowly discrete and bias d: lowly discrete and highly bias

Figure 10.31 Four patterns of recharge estimates

The factors of the methods are listed in Table 10. 18. The factors size of the mixing model, CWD-CRD, regression of CF as well as water balance are 4, 3, 3 and 9, respectively. Generally, the results derived from the complication of effect factors may create more discrepancy because of error propagation.

Table 10.18 Factors of the methods in the study

Method	Factor	Size	Size of domination factor
CMB Mixing Model	C_r, C_v, C_s recharge area A (refer to equation 10.8 and equation10.9)	4	recharge area A
CWD-CRD	CWD, CRD and storativity of the aquifer (refer to equation 10.16)	3	storativity
Regression of CF	CR, CF, recharge area A (refer to equation 10.25)	3	recharge area A
Water Balance	Precipitation (P), maximum (T_{max}), minimum (T_{min}), soil factors (f_s), vegetation cover (f_v), rainfall last time (f_i), CN, R_A and ? (refer to equation 11.3, equation 11.7 and equation 11.8)	9	Precipitation (P), difference of the temperature, soil factors (f_s) and Vegetation cover

For the purpose of better expression of the different results, the integrated recharge rate is computed as follows:

$$R_{\text{int}} = \sum_{i=1}^{n} R_i W_i \tag{10.27}$$

where R_{int} is integrated recharge rate, R_i is the result of the i^{th} method, W_i is the weight of the i^{th} method.

The total factors of methods considered is defined as

$$W = \sum_{i=1}^{n} S_i \text{ , i=1,2,.. n method} \tag{10.28}$$

where S_i is the factor size of the i^{th} method.

The weight of the i^{th} method is defined as

$$M_i = \left[\frac{S_i}{W}\right]^{-1} \tag{10.29}$$

The normalization weight is defined as

$$F_i = \left[\sum_{i=1}^{n} M_i\right]^{-1}, \text{ i=1,2,…n} \tag{10.30}$$

The normalization weight of domination factor can be written as

$$F_{di} = \left[\sum_{i=1}^{n} M_{di}\right]^{-1}, \text{ i=1,2,.. n} \tag{10.31}$$

The integrated weight is written as

$$W_i = \frac{F_i \times F_{di}}{\sum_{i=1}^{n} (F_i \times F_{di})}, \text{ i=1,2,.. n} \tag{10.32}$$

The factor size and integrated recharge rate are listed in Table 10.19. The integrated recharge rates are related to total factors, dominating factors and the integrated weight of the four methods are 1.68%-4.72%, 1.65%-4.52% and 1.63%-4.75% of the precipitation, respectively. The recharge rate with 1.63%-4.75% of the precipitation is preferentially recommended in the Kammanassie area.

Table 10.19 Factor size and integrated recharge estimates

Recharge Method		Total Factors		Dominating Factors		Integrated
		Size	Weight	Size	Weight	Weight
CMB Mixing Model		4	0.243	1	0.308	0.26
CWD-CRD		3	0.324	1	0.308	0.35
Regression of CF		3	0.324	1	0.308	0.35
Water Balance		9	0.108	4	0.077	0.03
Integrated recharge estimates (%)	Minimum	1.68		1.65		1.63
	Maximum	4.72		4.52		4.75

10.7 CONFIDENCE INTERVAL FOR RECHARGE RATE

The complexities of the hydrogeological settings make estimating local or regional recharge difficult. The spatial variation of rainfall and topographic conditions result in complex recharge mechanism. Not all of the components of the mixing model can be measured accurately within a given catchment. Inputs such as precipitation and abstraction are quantifiable; however, the time lag has changed significantly relative to the residence time of the water, and the solutions of three-component model mostly rely on the results from the two-component model, even the mixing model cannot include piston flow, which likely occurs in the preferential fracture system. The recharge area size may not be determined accurately in a fractured rock aquifer. Under these limitations, estimates of recharge from the mixing model are subject to large potential errors.

The sum of the deviations of the X_i values from their mean $\overline{X}$ is zero in a time series. This may lead to incorrect resemblances identified from the CWD-CRD curves. The aquifer area is different from the catchment area, and the storativity of the aquifer is inexactitude as well as high variation. These would produce more discrepancy in the CWD-CRD, the CTF-CTR and the other area-dependent or storativity-dependent methods.

The results of recharge estimation from several methods are summarized in Appendix XV. The range of the recharge estimates is 1.07-28.62 $mm \cdot a^{-1}$ (0.21%-7.56%) with coefficient variation from 46.07% to 68.16% (Table 10.20). The estimates have significant variation. The recharge interval based on equation (2.9) for 95% and 90% confidence is 12.18-14.92 $mm \cdot a^{-1}$ (2.17%-2.93%) and 12.4-14.70 $mm \cdot a^{-1}$ (2.23%-2.87%), respectively.

Table 10.20 Outline of the recharge estimates

Statistical analysis	Annual recharge Rate (%)	Annual Recharge ($mm \cdot a^{-1}$)
Minimum	0.24	1.07
Maximum	7.56	28.62
Mean	2.55	13.55
Median	2.20	14.86
Standard deviation	1.74	6.24
Coefficient variation (%)	68.16	46.07
Confidence interval (95%) Equation (2.9)	2.17-2.93	12.18-14.92
Confidence interval (90%) Equation (2.9)	2.23-2.87	12.4-14.70

To place the heavy reliance either on the assumption or on the sample sizes, the nonparametric procedures (Neter et al., 1988) are conducted. The nonparametric procedures are concerned with the median of a single population. When the population is highly skewed, the population median (h) is located more in the center of the distribution than the population mean and thus may be more meaningful of position; when the population is symmetrical, the population mean and the population median coincide and thus are equally meaningful measures of position (Neter et al., 1988). The inference procedures for the population median has the following two assumptions (Neter et al., 1988):

- The population is continuous.
- The sample is a random one.

The estimated recharge rates satisfy the two assumptions obviously; therefore, a confidence interval for the population median of the recharge rate is performed. A random sample of 80-recharge rate has been selected in ascending order. It is desired to construct a 95% and 90% confidence interval for the population median amount of

recharge rate. Based on Eq. (2.10), the integer numbers of r are 31 and 33 for 95% and 90% confidence interval, respectively.

For 95% confidence interval, the required confidence limits for h are the 31st-smallest (L_{31}) and the 31st-largest (U_{31}) recharge rate in the 80 samples of recharge estimates are: $10.88\,mm \le h \le 16.09\,mm$, or $1.65\% \le h \le 3.30\%$; for 90% confidence interval, the required confidence limits for h are the 33th-smallest (L_{33}) and the 33th-largest (U_{33}) recharge rate in the 80 results of recharge estimates are: $12.27mm \le h \le 15.83mm$, or $1.89\% \le h \le 3.04\%$ (Figure 10.32). Based on the discussion, the annual recharge rate range for 95% and 90% confidence interval is 10.88-16.09mm (1.65%-3.30%) and 12.27-15.83mm (1.89%-3.04%), respectively.

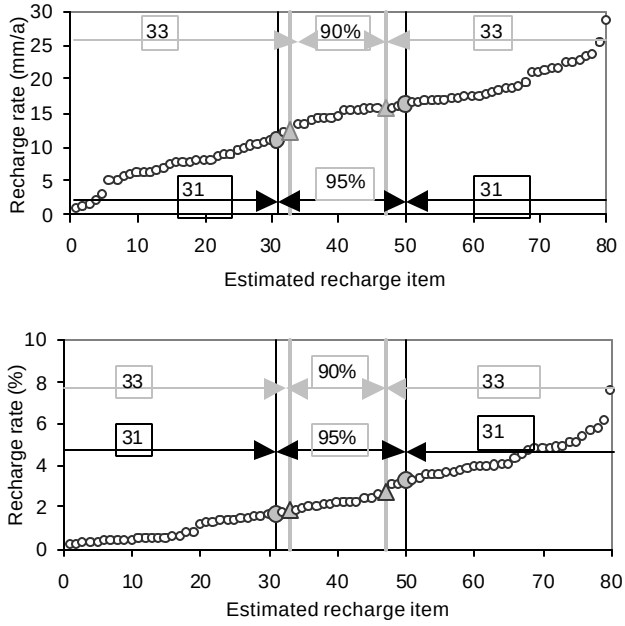

Figure 10.32 A 95% and 90% confidence interval for the population median amount of recharge estimates

10.8 SUMMARY

The accuracy of recharge estimation in the Kammanassie area is largely influenced by the size of the recharge area and the aquifer storativity used in relevant methods in the Kammanassie area. The following points are concluded:

- For a given study area, the recharge rate is recharge-area dependent for the CMB mixing model and regression of CF methods, while the CWD-CRD method is dependent on the storativity of the aquifer. Although only one accurate solution occurs in these methods, the reason deriving the error is the physical parameters, which are not very exact, such as recharge area and storativity.
- The recharge rate ranges between 0.38%-2.04% and 0.007%-4.223% from the two-component and three-component models, respectively.
- The recharge rate increases significantly if the size of recharge area becomes smaller in terms of an elongated belt zone. The recharge rates based on abstraction are actual recharge for production boreholes. The recharge from spring discharge is not included, although spring flow is influenced by abstraction. The spring flow within the study area needs to be further considered at a regional scale.
- The recharge rate varies from 0.24% to 7.56% of the precipitation using a storativity of between 0.1‰ and 1‰ using CWD-CRD method in the G40171, but the average recharge rate from RIB method is 2.28% of rainfall or 94.79mm against storativity of 1‰ from 1994 to 2003. The average recharge rate is 5.38 % of precipitation or 48.67 mm, which equals to 3.88% of total precipitation of 1256mm under storativity of 1‰ in considering impact of preceding rainfall in the G40171 from 1998 to 2001.
- The recharge rate with 3.21% of the precipitation is given by regression of CF-CR method with coefficient of 0.996 in the upper Vermaaks catchment. A recharge rate with 3.65 % of the precipitation is associated with the maximum correlation coefficient between CR of the Wildbeesvalakte and CF of the Marnewicks catchment. The recharge rate with 3.2% of the precipitation is obtained against the entire two catchment areas. The recharge rate before the flood is slightly higher than that after the flood. Floods reduce the recharge rate because of increased runoff. The recharge rate varies from 1.73% to 5.21% of the precipitation considering the influence of the preceding rainfall from three periods with spring flux increasing from 1997 to 1999.
- The integrated recharge rate related to total factors, dominating factors and integrated weight of the methods are 1.68%-4.72%, 1.65%-4.52% and 1.63%-

4.75% of the precipitation, respectively. The integrated recharge rate ranges from 1.63% to 4.75% of the precipitation.

- The annual recharge rate range for 95% and 90% confidence interval is 10.88-16.09mm (1.65%-3.30%) and 12.27-15.83mm (1.89%-3.04%), respectively. These values are preferentially recommended in the Kammanassie area.
- The time lag is considered through cumulative rainfall in CMB mixing model, this would produce an error in the recharge rate. This limitation would be avoided if the time series were longer enough.
- Although the chemograph shows the character of the several of chloride concentrations, the fluctuation and time lag with rainfall were not considered; this is left for future work. The chloride concentration can be affected by the intensity of rainfall, especially direct recharge events are associated with continuous higher intensity rainfall, but the cumulative mass balance remedies the impact of the high intensity of rainfall in the long term. The results should also be influenced by the factors of storativity of the fractured rock aquifer. Groundwater flow in the fractured rock aquifer possessing preferential direction or zone results in complex recharge area. This also produces error of the recharge rate, which is converted from the recharge volume. Under special conditions, in which recharge lags rainfall events over a long time, the two-component mixing model for direct recharge cannot work.

In short, the recharge rate in the Kammanasie area is generally lower than 5%, which is much smaller than that presented in the earlier studies. The estimation of recharge area, storativity and the time lag mainly produced the error. The recharge rate is 2.96% of the precipitation in the Peninsula Formation Window, if the recharge equals the total abstractions in the Vermaaks River Wellfield from 1993 to 2002. The budget of 3-D numeric simulation model confirmed that the recharge rate could not exceed 1.96% of the rainfall at steady state. The results were further corroborated by the 1.65%-3.30% of the annual precipitation for 95% confidence interval.

Chapter 11

Spatial Distribution of Recharge in the TMG Area

11.1 INTRODUCTION

Water balance is often used to estimate hydrologic fluxes in an atmospheric water balance, soil water balance and surface water balance on different scales. Groundwater recharge is only surplus from soil-water budget. It appears negligible in most hydrologic studies because the recharge is a little. Despite numerous uncertainties associated with the simple soil-water budget model, it is still used in many studies from catchment scale to the global water balance and climatic change scenarios (Thornthwaite, 1948; Shiklomanov, 1983; Manabe, 1969; Mather, 1978; Alley, 1984; Willmott et al, 1985; Mintz and Walker, 1993; Mintz and Serafini, 1992). This approach is attractive because of its simplicity, which requires minimal input data: precipitation, potential evapotranspiration and soil-water holding capacity. In its simplest form, the soil-water budget model does not account for situations where the precipitation rate is greater than the infiltration capacity of the soil. A long-term water balance model for a large catchment in semi-arid Western Australia presents the downward process controls on water balance at the annual, monthly and daily scales based on climate, soil and vegetation cover (Jothityangkoon et al., 2001).

11.2 WATER BALANCE APPROACH

11.2.1 Principle

The different terms of the water balance at catchment scale are defined as:

Rainfall = Runoff-Direct + Actual Evapotranspiration ± Change of Field Moisture Capacity of Soils +Groundwater Recharge

Total runoff comprises of direct runoff and base flow. Direct runoff includes surface runoff and interflow follows as:

- Surface runoff: precipitation that cannot be absorbed by the soil because the soil is already saturated with water (saturation excess overland flow); precipitation that exceeds infiltration; the portion of rain, snow melt, irrigation water, or other water that moves across the land surface and enters a wetland, stream, or another body of water (overland flow). Overland flow usually occurs where the soils are very fine textured or heavily compacted (response time about half an hour in a 1 km² basin).
- Interflow that travels laterally or horizontally through the zone of aeration (vadose zone) with high hydraulic connectivity during or immediately after a precipitation event and discharges into a stream or other body of water (response time of several hours in a 1 km² basin, more lag time if the slope is longer. Its hydrogeochemistry with high concentration of chloride appears to have characteristics of lioxiviation.)
- Field Moisture Capacity: The total amount of water remaining in a freely drained soil after the excess has flowed into the underlying unsaturated soil.

Based on the above discussion, the water balance equation is written as

$$R_E(t) = P(t) - E(t) - R(t) \pm \Delta w(t) \qquad (11.1)$$

where $R_E(t)$ is groundwater recharge, $P(t)$ is precipitation, $E(t)$ is actual evapotranspiration, $R(t)$ is direct runoff and $??(t)$ is change in volumetric water content in soils. The term (t) designates that the terms are distributed through time. Monthly records of a site $P(t)$ were obtained from the WR90. $E(t)$ and $R(t)$ were initially estimated based on meteorological and site-specific data by simple methods described in a later section. Assuming $?? (t)$ is negligible between subsequent years, an annual estimate of $R_E(t)$ can be calculated following the flow diagram shown in Figure 11.1.

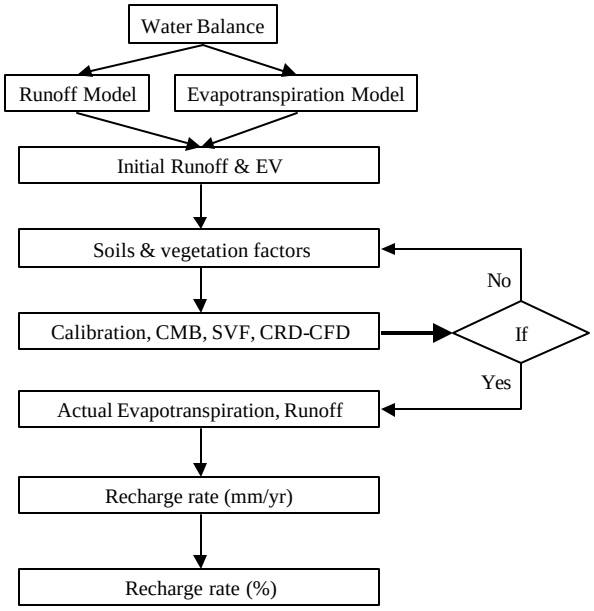

Figure 11.1 A flow diagram of recharge e stimation based on water balance

11.2.2 Model selection

A common approach for approximating $E(t)$ involves initial estimates of evapotranspiration for a reference soil, vegetation and coverage of plants, $E_{tr}(t)$, such as grass or Fynbos. Additive $E_t(t)$ is then calculated by multiplying $E_{tr}(t)$ by a group coefficient, $K_c(t)$, an experimentally defined crop-specific and soil moisture variable whose value varies throughout the round year, such that:

$$E_t(t) = K_c(t)E_{tr}(t) \tag{11.2}$$

The initially estimates $E_{tr}(t)$ as follows (Hargreaves and Samani, 1985):

$$E_{tr}(t) = 0.0023 R_A T_D^{1/2}(T + 17.8) \tag{11.3}$$

where T_D is the difference between average monthly maximum and minimum temperatures (℃), T is average monthly temperature (℃), R_A is extraterrestrial radiation (MJ m^{-2} d^{-1}). R_A is represented as follows (Duffie and Beckman, 1980):

$$R_A = G_{SC} d_r \frac{(w_s)\sin(f)\sin(d) + \cos(f)\sin(d)\sin(w_s)}{p} \tag{11.4}$$

where F is latitude (radians; positive for north, negative for south), and

$$d = 0.4093\sin[2p(284+j)/365]$$

$$d_r = 1+0.033\cos(2pJ/365)$$

$$w_s = \arccos[-\tan(f)\tan(d)]$$

G_{sc} is the solar constant with a value of 118. 1 $MJ\ m^{-2}\ d^{-1}$, and J represents the number of days since January 1 of the current year. Values from equation (11.5) were converted to units of md^{-1} by:

$$E_{tr}(t)[md^{-1}] = \frac{E_{tr}(t)[MJm^{-2}d^{-1}]}{l[MJkg^{-1}]r[kgm^{-3}]} \tag{11.5}$$

where r is the density of water; ? is the latent heat of vaporization, given by (Harrison, 1963):

$$l[MJkg^{-1}] = 2.501 - 2.361\times10^{-3}T[T\ in^{\circ}C] \tag{11.6}$$

The $K_c(t)$ is expressed as

$$K_c(t) = \frac{1}{200}P(f_s + fv\times f_c + f_i)(t) \tag{11.7}$$

where P is the precipitation (mm), f_s is the soil factor, f_v is the vegetation factor, f_c is the coverage of vegetation, f_i is the factor of intensity of the rainfall with $f_i = h_r/T_t$, h_r is the rainfall lasting time, T_t is the monthly total time.

A common method to estimate Q is to apply the runoff equation (USDA-SCS, 1985):

$$Q_r = \frac{(P-0.2S)^2}{P+0.8S};\quad P \geq 0.2S \quad with$$

$$S = \frac{1000}{CN} - 10 \tag{11.8}$$

where CN is the curve number. CN, based on site conditions, ranges from 36 to 99

(USDA-SCS, 1985). Considering the features of the landform of the TMG, the ranges of *CN* are 80 to 98. Measured *P(t)* was used in equation (11.8) to estimate Q_r.

11.2.3 Model calibration

The parameters related to the soil and vegetation are empirical values as shown in the equation (11.7). These values should be calibrated using scientific method. The calibration in the model is conducted as follows:

- The factors of vegetation adopted from Midgley et al. (1994) remain constant in the model.
- The variation of temperatures including maximum and minimum temperature is controlled ±2°C because the long-term (1925-2003) change of the average temperature should not exceed range of 4°C. The range of the temperature is usually controlled within ±0.5°C.
- The intensity rainfall is considered as three classes, which are A: less than 5hrs per month, B: 5 to 10hrs per month and C: exceeds 10 hrs per month.
- The coverage percentage of vegetation is estimated based on field investigation, the distribution of lithology and the feature of topography including slope gradient and land surface forms.
- The soil factors are changeable parameters in the model. The soils factor values are empirical values in initial calculation process; the values are given in referred to the type, thickness and distribution of soil defined by Midgley et al. (1994). The calibrated value for soil factor is based on the trial calculation in the Kammanassie area with the critical value of annual recharge rage of 10.88-16.09mm derived from Chapter 10. The soil factor in other TMG area are given based on the trial calculation in the Kammanassie area but the error range does not exceed 10% under similar condition of lithology and topography.

11.3 DISTRIBUTION OF MEAN ANNUAL PRECIPITATION (MAP) IN THE TMG AREA

For discussion of the distribution of the MAP, entire 478 rainfall stations with codes shown in Figure 11.2 are used to make contour MAP with Kriging method in the TMG area. The raw data of the rainfall stations are adopted WR90 (Midgley et al., 1990). The MAP is higher than 500mm occurs in the hydrogeological unit 4, 5, 6, 15 and 17 as can be seen in Figure 11.2. The precipitation in the most areas of the other hydrogeological units is less than 500 $mm \cdot a^{-1}$. The precipitation with more than 800 $mm \cdot a^{-1}$ distributes in the mountainous areas close to Franschhoek, Knysna and Humansdorp. The precipitation in the northern of the Outeniqua Mountains and Langeberg Ranges is obviously less than that in the southern side due to the mountainous barrier, which are the southern boundaries of Klein Karoo. The precipitation gradually decreases from south close to Indian Ocean (hydrogeological unit 15) to the north in the Karoo (hydrogeological unit 13). In the hydrogeological unit 2, the precipitation in the high elevation area of the Cedarberg Mountain is from 300 to500$mm \cdot a^{-1}$, but rainfall in the lower elevation area is less than 300 $mm \cdot a^{-1}$. The precipitation in the Swartberg Mountain (hydrogeological unit 13) ranges from 100 to 400$mm \cdot a^{-1}$. It is important to note that there is no rainfall station in most of the mountainous area of the TMG.

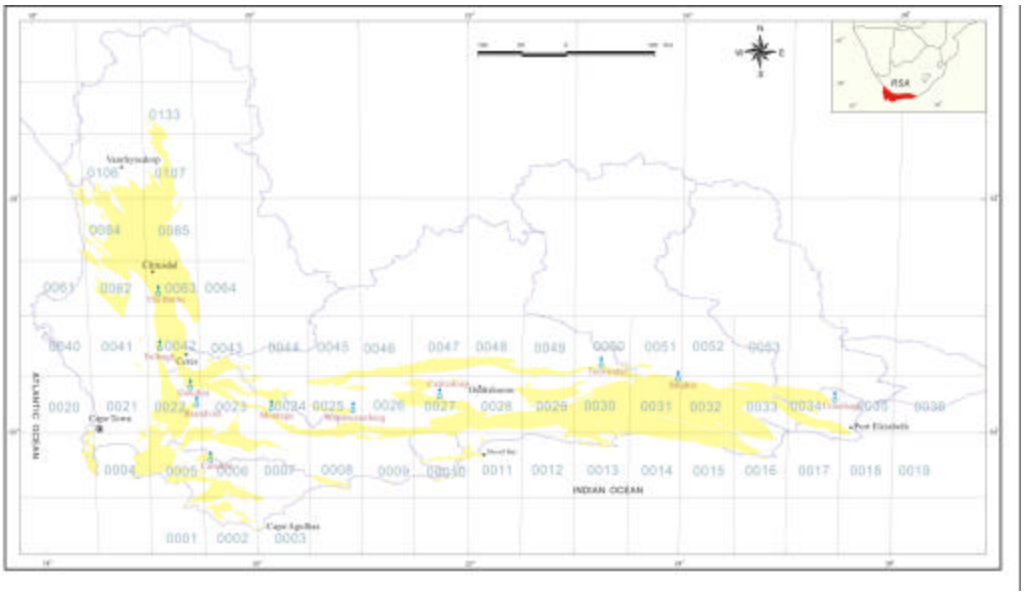

Figure 11.2 Rainfall station codes in the TMG area

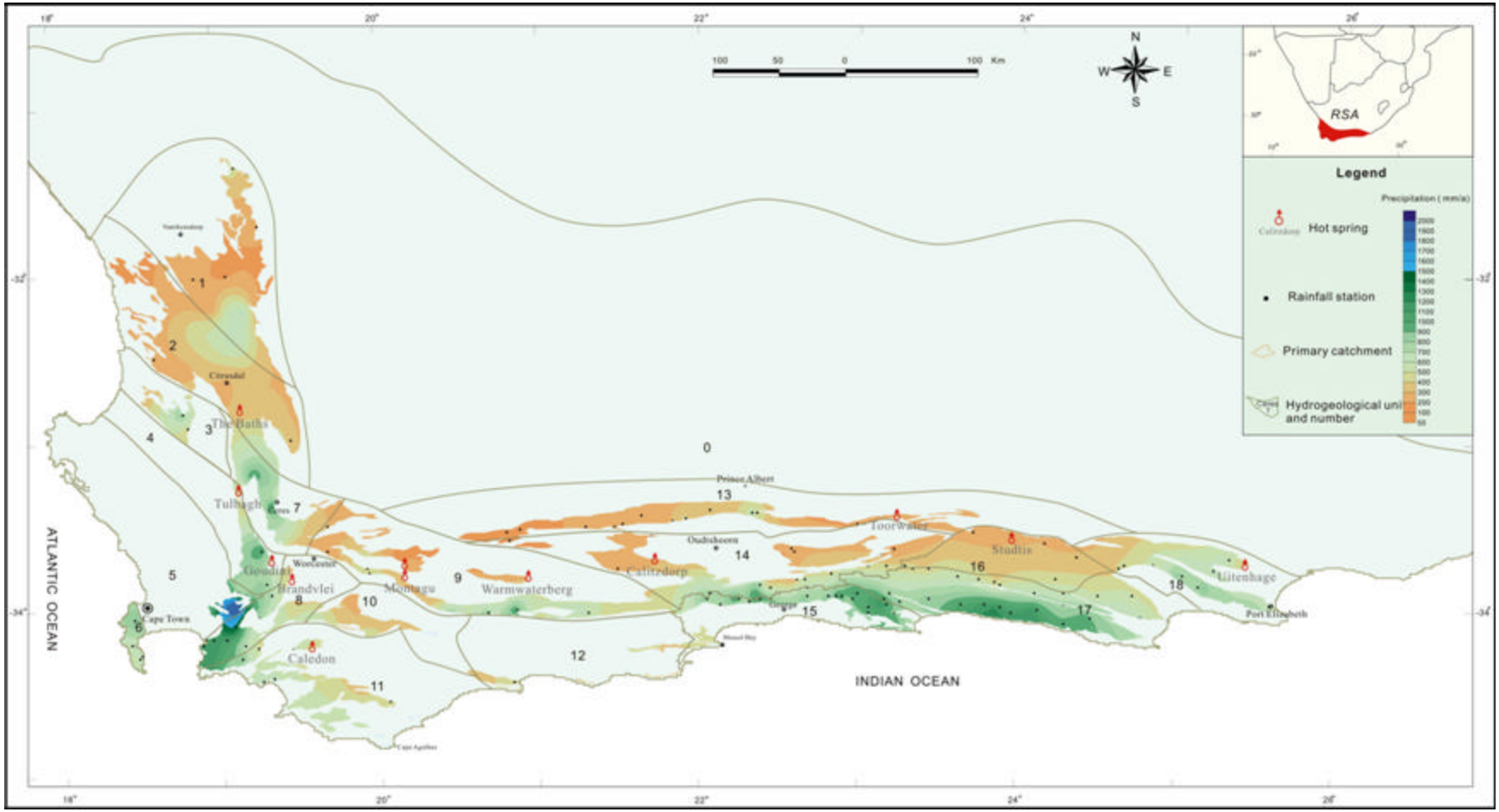

Figure 11.3 Annual average precipitation in the TMG area

11.4 RUNOFF AND ACTUAL EVAPOTRANSPIRATION

The runoff was estimated based on 175 rainfall stations near or on the outcrop of the TMG using equation (11.8). The runoff contour map is made using Kriging's method as shown in Figure 11.4. Runoff is less than 150mm·a^{-1} (yellow) in most areas. A low runoff with lees than 25mm·a^{-1} in light yellow occurs in the hydrogeological unit1, 11, 11, 14 and 16. A large amount of runoff with more than 150-500mm·a^{-1} in green and blue occurs in the hydrogeological unit 5 and 6, but the data are more than 500mm·a^{-1} from WR90 (Midgley et al., 1994). In general, the runoff in quantity is smaller than that of WR90.

The data were selected before they were used in the calculation by comparing the background conditions, such as homogeneous rainfall districts, catchment size and potential evaporation. Soil factors were adopted according to types, texture and thickness of soils in referring to the WR90 database. The empirical parameters of soil factors and coverage percentages of vegetation in the TMG area used in the model were according to the filed investigation as listed in Table 11.1. The factors of vegetation in the outcrop of the TMG are listed in Table 11.2. The temperatures used in initial evapotranspiration model are presented Table11.3.

Table 11.1 Soil factor and coverage percentages of vegetation

Hydrostatigraphic unit No.	Soil factor	Coverage percentage		Hydrostatigraphic unit No.	Soil factor	Coverage percentage
1	0.25-0.30	5-35		10	0.25-0.30	20-40
2	0.25-0.35	10-30		11	0.25-0.30	20-55
3	0.25-0.30	15-65		12	0.03-0.40	30-40
4	0.20-0.25	20-70		13	0.35-0.40	5-45
5	0.20-0.25	25-75		14	0.02-0.35	10-45
6	0.20-0.25	40-60		15	0.25-0.30	15-65
7	0.25-0.30	50-75		16	0.20-0.30	10-35
8	0.20-0.30	25-65		17	0.15-0.25	40-55
9	0.15-0.45	5-50		18	0.25-0.3	20-40

Table 11.2 Factors of vegetation in the outcrop of the TMG (Midgley et al., 1994)

Month	Oct.	Nov.	Dec.	Jan.	Feb.	Mar.	Apr.	May	Jun.	Jul.	Aug.	Sep.
Fynbos factors	0.60	0.60	0.60	0.60	0.55	0.55	0.55	0.45	0.40	0.20	0.35	0.50

Table 11.3 Model of temperature in the TMG area(the temperature data adopted from CNC website)

Month	Greyton		Buffelsklip		Wildalsvlei		Wildebeesvlakte		Elandsvlakte		Paardevlalte1		Paardevlalte2	
Temp. ℃	Max	Min	Max	Min	Max	Min	Max	Min	Max	Min	Max	Min	Max	Min
Jan.	24.5	10	39	7.5	37	4	36	5	33	5	33	3	32	2.5
Feb	26	12.5	40	6	35	4	36	4	34	5	33	5	31	2
Mar.	29	14	38	6	35	3	33.5	3	32	4	30	2	28	1.5
Apr.	30	15	32	2	30	1	30	1	28	2	27	1	25.5	0
May	30	15	29	2	26	0	26	-0.5	24	2	24	-1	21	-0.5
Jun	28	14	26	0	22	-1	22	0	21	0	20	-4	19	-2.5
Jul	25.5	10.5	25	-0.5	23	-0.5	22	-2	21	-1	19	-4	19	-2.5
Aug	22.5	7.5	30	1	27	-1.5	25	-1	25	1	22	-4	21	-3
Sep	20	4.5	32	2	30	0	29	-1	29	1	28	-4	25	-2
Oct.	19.5	4	35	3	33	0	32	1	31	3	27	1	28	1
Nov	20	5.5	37	4	33	2	33	3	29	3	30	1	29	-0.5
Dec.	22	8	38	5	36.5	4	35	4	31	5	31	2	31	0
Ref. Alt. (m)	500-1500		<800		800-1200		800-1500		1000-1300		>1500		>1500	
MAP (mm)	400-500		<350		300-450		400-650		500-800		700-1000		>1000	

The actual annual evapotranspiration is calculated based on the annual average precipitation of 175 rainfall stations as can be seen in Figure11.5. Evapotranspirations with 700-1300mm per year are associated with greater than 900mm of MAP in the hydrogeological unit 5, 8 and 17. There are 700-900 $mm \cdot a^{-1}$ of evapotranspiration in some mountain area of the hydrogeological unit 4, 7, 9, 15 and 18. The actual annual evapotranspiration is less than $500mm \cdot a^{-1}$ in most areas of the areas of the hydrogeological unit 1, 2, 3, 9, 13 and 16. The distribution differentiates clearly from potential evapotranspiration of 1200-2600$mm \cdot a^{-1}$ that is based on an open water surface shown in Figure 11.6. The potential evapotranspiration increases gradually from south to north.

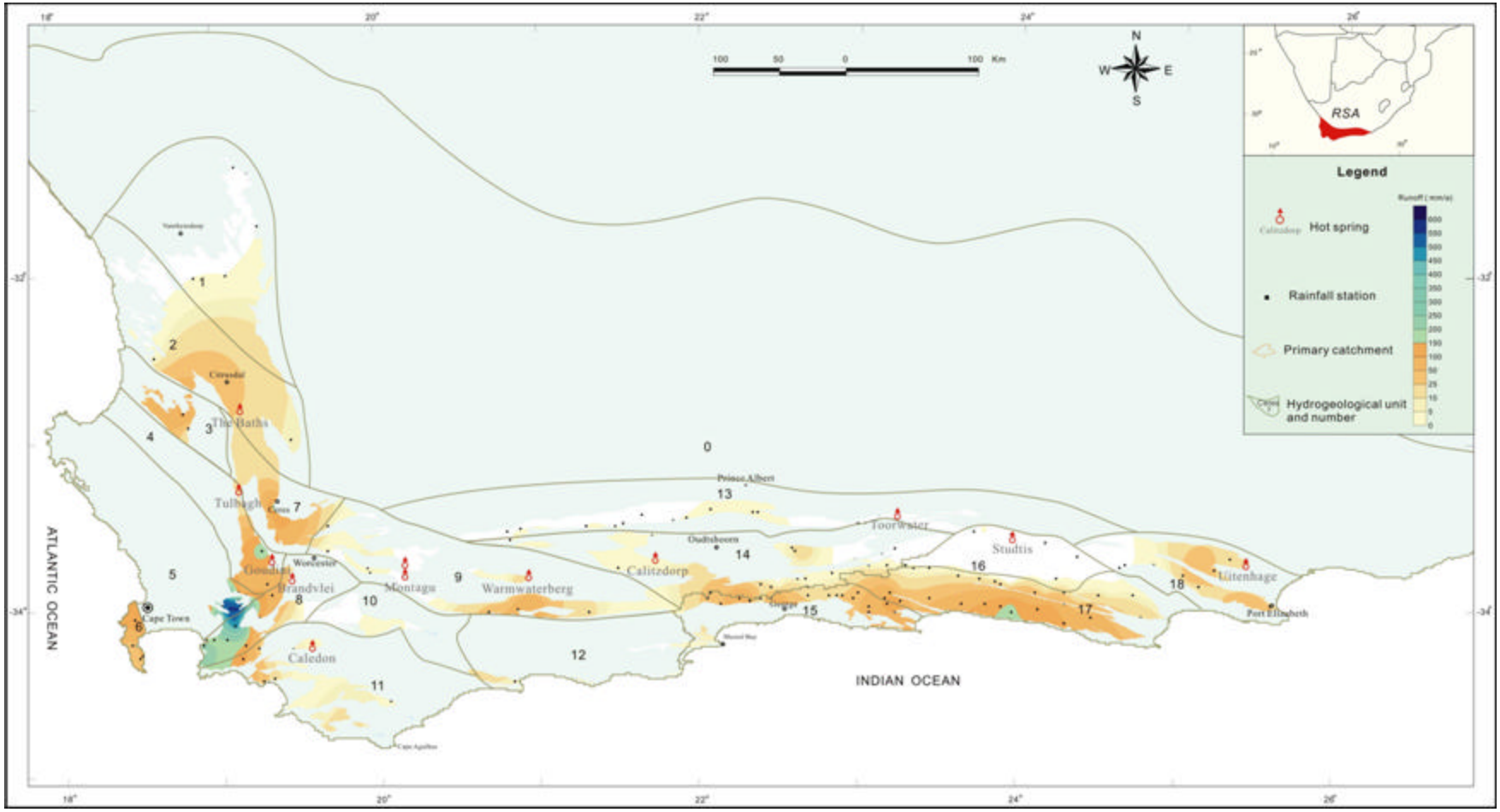

Figure 11.4 Annual average runoff in the TMG area

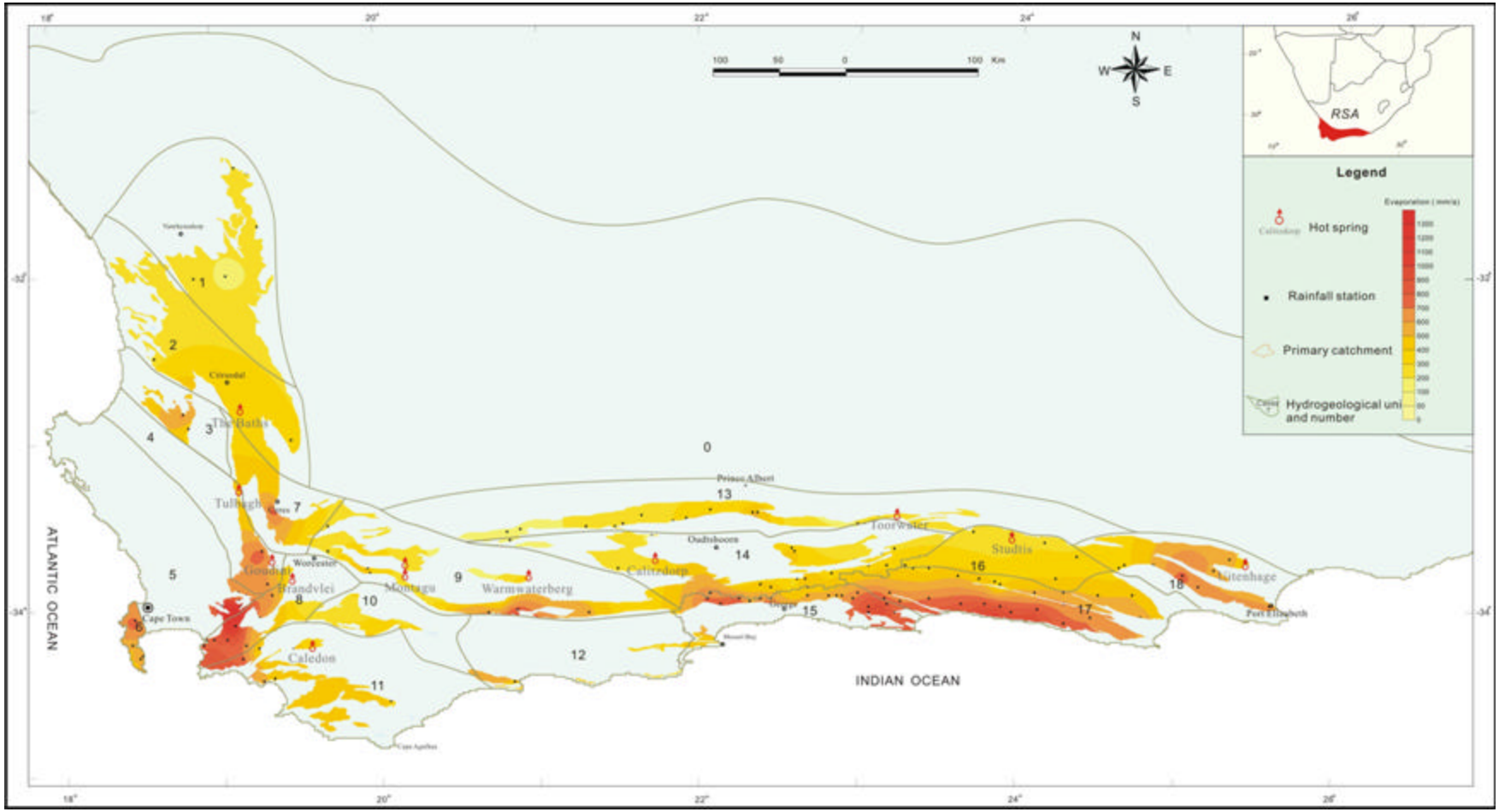

Figure 11.5 Actually annual average evapotranspiration in the TMG area

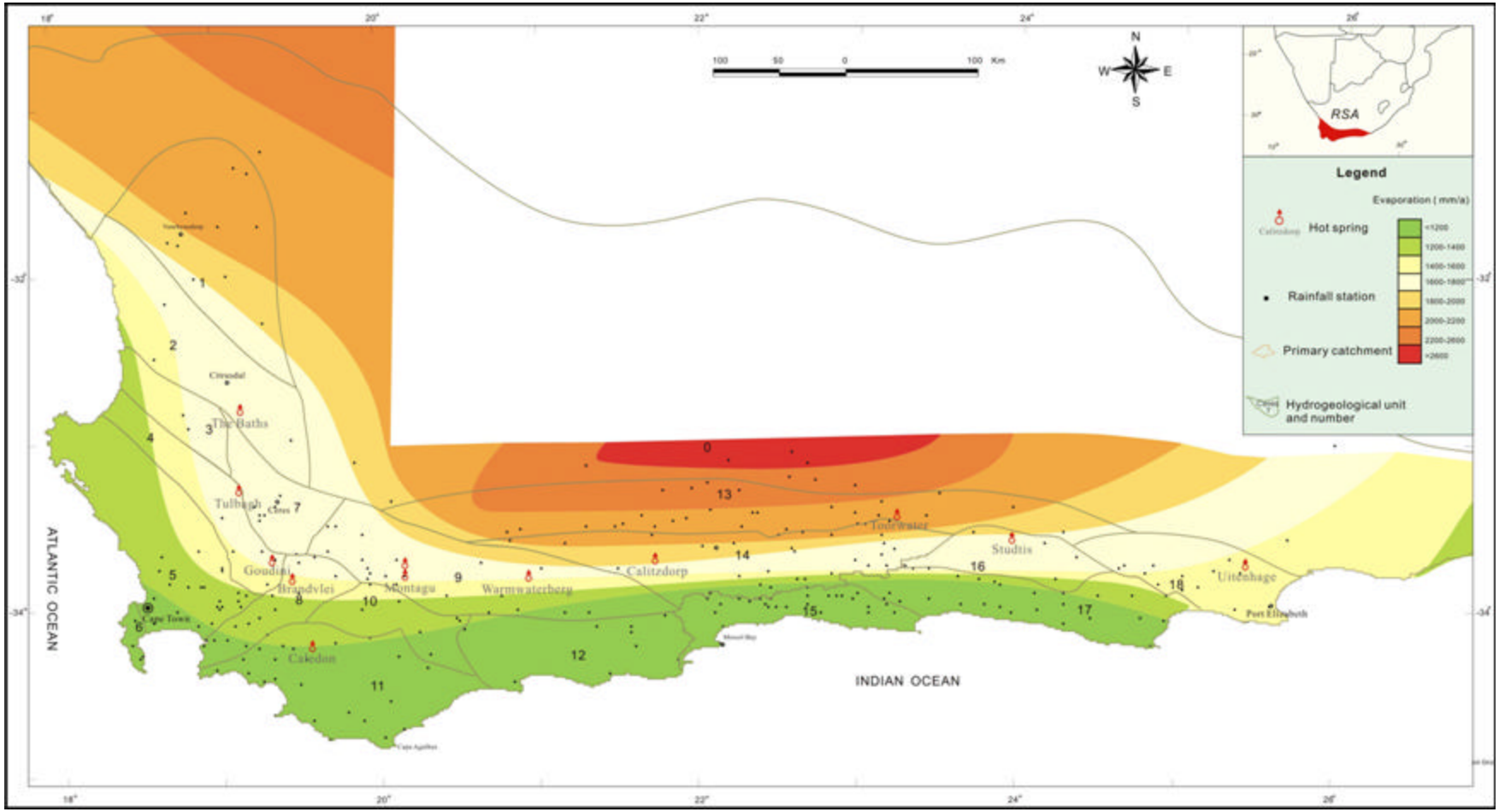

Figure 11.6 Potentially annual average evapotranspiration in the TMG area (After WRC, 1990)

11.5 RECHARGE RATE

11.5.1 Distribution of the recharge rate

The annual average recharge rates given by the water balance method refers to the results from the study in chapter 10 in the modelling process as presented in Appendix XVI. The distribution of recharge rates is illustrated in Figure 11.7. The following observations are made:

1) The average recharge rate is 29.74mm·a^{-1}. The highest recharge rate is 137.4mm·a^{-1} related to 1842.06 mm MAP at rainfall station No. 0022116 in the hydrogeological unit 5; the lowest recharge rate is 0.7mm·a^{-1} related to 163.51mm MAP at rainfall station No. 0048043 in the hydrogeological unit 13.
2) The regions of the recharge rate more than 35mm·a^{-1} occur in the hydrogeological unit 5, 6, 8 and part of the hydrogeological unit 7 and 17. The other areas are less than 35mm·a^{-1}.
3) The recharge rate is from 0.28% of the rainfall at station No. 0107169 in the hydrogeological unit 1 to 12.6% of the rainfall at station No. 0012220 in the hydrogeological unit 15.
4) The recharge rate in the Agter-Witsenberg Mountain is 35.76-97.11mm·a^{-1}.
5) The distribution of the recharge rate in the eastern section from Riversdale to Cape St Francis has a clear boundary consistent with the outline of the mountain, in which a high recharge rate is from 35 to 65mm·a^{-1} in the southern area (green-blue), and less than 35mm·a^{-1} (red-yellow) in the northern area.

The recharge rates are smaller than that from Vegter 1995 as can be seen in Figure 11.8. It is clear that the recharge rates are the same in most areas of the recharge map, which has the same distribution in different climate region and homogeneous rainfall districts.

The outlines of recharge rates in the TMG area are summarised in Table 11.4 and shown in Figure 11. 9. The following observation are summarised:

- The biggest range is from 0.88 to 135.52 mm·a^{-1} in the hydrogeological unit 8, and the smallest range is 0.50 to 1.29mm·a^{-1} in the hydrogeological unit 1.
- The average recharge rate is smaller than 10mm·a^{-1} in the hydrogeological unit 1, 10 and 13.The average recharge rate varies from 10mm·a^{-1} to 25mm·a^{-1} in the hydrogeological unit 2, 9, 14, 16 and 18.
- The average recharge rates are from 25mm·a^{-1} to 50 mm·a^{-1} in the hydrogeological unit 4, 7, 11, 12, 15 and 17.
- The average recharge rate ranges from 50mm·a^{-1} to 85mm·a^{-1} in the hydrogeological unit, 3, 5, 6 and 8.

Table 11.4 Outline of the annual recharge estimates in the TMG area

Hydro-stratigraphic unit No	Annual average precipitation (mm)			Annual average recharge rate (mm)			Annual average recharge rate (%)		
	Minimum	Maximum	Mean	Minimum	Maximum	Mean	Minimum	Maximum	Mean
Unit 1	179.6	238.2	218.6	0.5	1.3	0.8	0.3	0.5	0.4
Unit 2	240.7	369.6	293.1	2.0	24.0	11.9	0.7	6.5	3.7
Unit 3	439.3	830.6	635.0	48.1	96.5	72.3	10.9	11.6	11.3
Unit 4	461.3	1002.7	718.2	11.9	43.4	26.1	2.6	5.1	3.6
Unit 5	558.3	2063.0	1291.7	35.1	137.4	82.4	4.0	8.7	6.4
Unit 6	584.7	922.7	695.1	43.8	67.7	56.4	4.7	11.4	8.5
Unit 7	286.7	1073.3	585.7	14.3	97.1	35.8	2.8	9.0	5.6
Unit 8	237.3	1604.8	854.6	0.9	135.5	75.1	0.4	12.4	8.4
Unit 9	132.4	999.0	442.2	0.9	52.5	13.3	0.4	8.2	2.4
Unit 10	256.6	482.1	331.9	2.2	8.3	5.8	2.0	3.1	2.4
Unit 11	404.5	928.9	525.5	24.7	64.6	41.5	3.2	12.3	8.3
Unit 12	354.8	454.4	417.2	11.4	41.6	27.8	2.5	9.4	6.7
Unit 13	104.9	553.5	277.6	0.7	17.8	4.9	0.4	5.6	1.8
Unit 14	165.7	1049.3	474.9	1.1	43.4	20.1	0.7	8.1	4.0
Unit 15	490.3	1099.3	837.8	3.1	93.0	49.4	2.4	10.4	6.4
Unit 16	256.0	602.3	401.1	9.1	51.3	16.6	1.6	3.8	3.0
Unit 17	415.9	1208.4	781.2	14.1	90.8	38.1	2.7	9.6	4.9
Unit 18	362.1	833.3	544.4	9.2	49.1	22.9	1.8	6.0	4.1

The recharge rate is shown in Figure 11.10. The recharge rates are higher than 11% of the precipitation (in yellow) occurring in the hydrogeological unit 3 and 8, 6-11% of the precipitation (in green) in the hydrogeological unit 3, 6, 8, 11, 12, 15 and 17; 2%-6% of the precipitation in blue in the hydrogeological unit 1,2,4,7,9,10,13,14,16 and 18 and lower than 2% of the precipitation (in reseda) in the other areas. For the management purpose, the recharge rates for the quaternary catchment in the outcrop of the TMG are presented in the Appendix XVII.

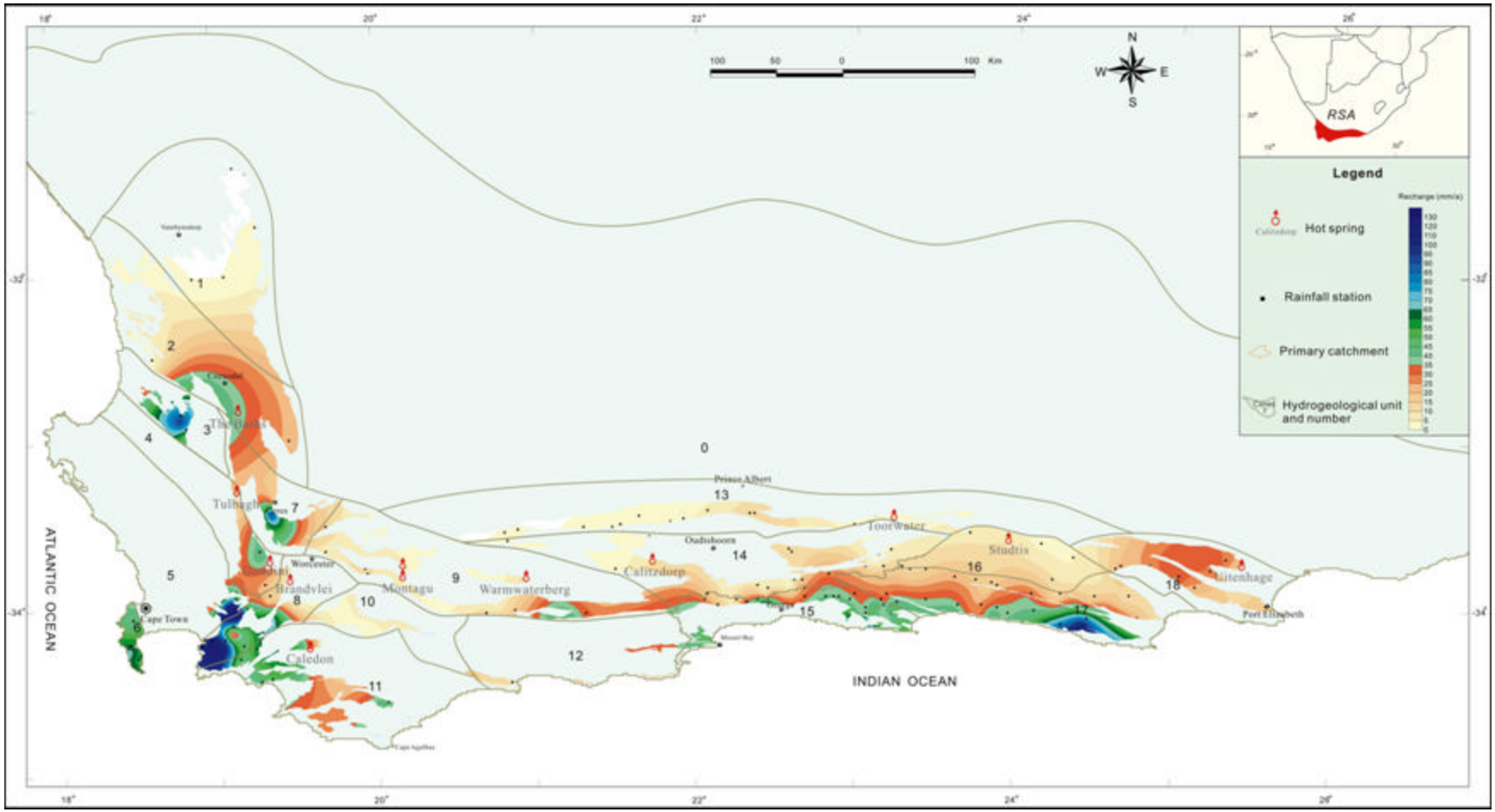

Figure 11.7 Annual average recharge rate in the TMG area

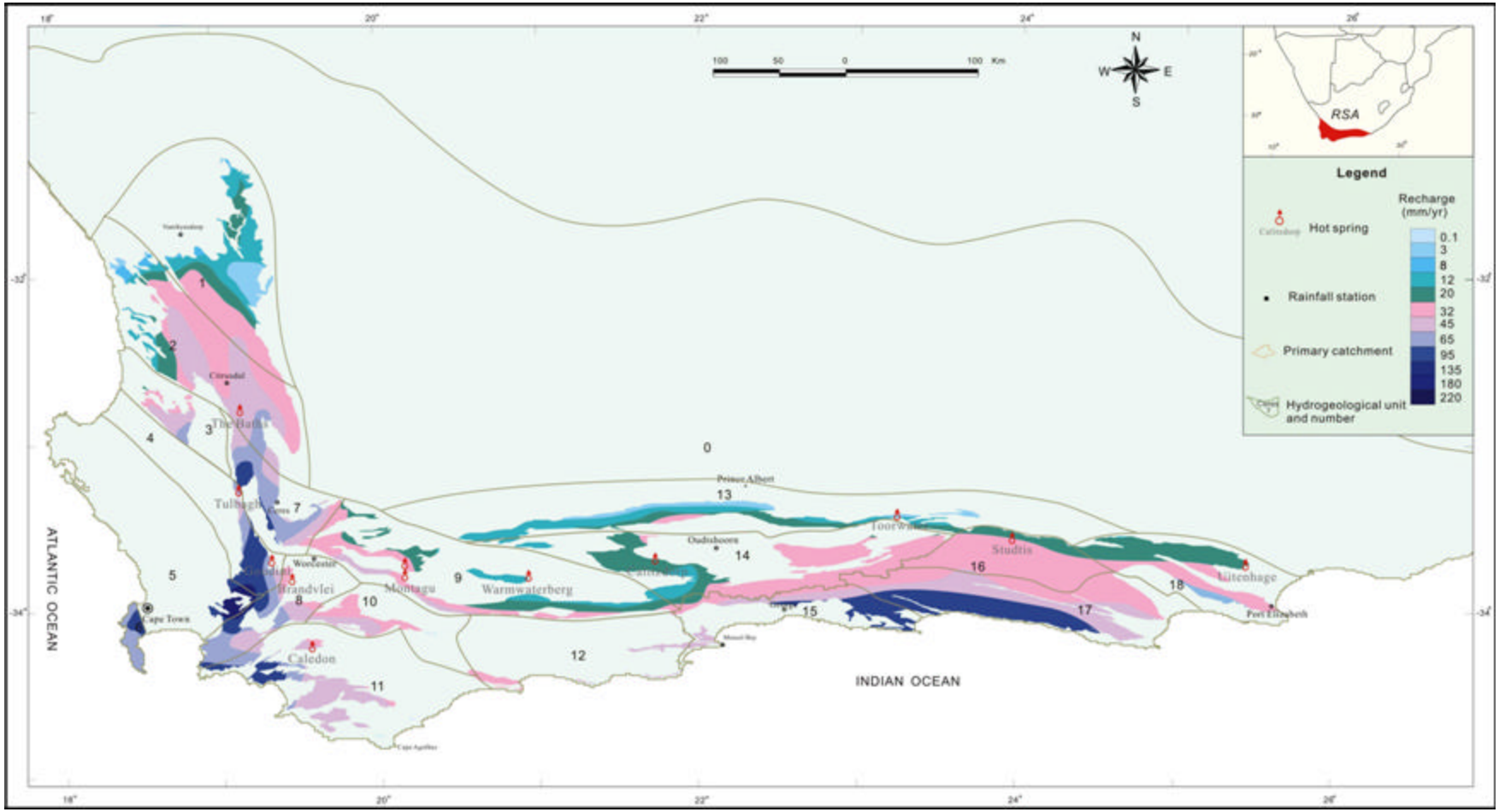

Figure 11.8 Annual average recharge rate in the TMG area (After vegter, 1995)

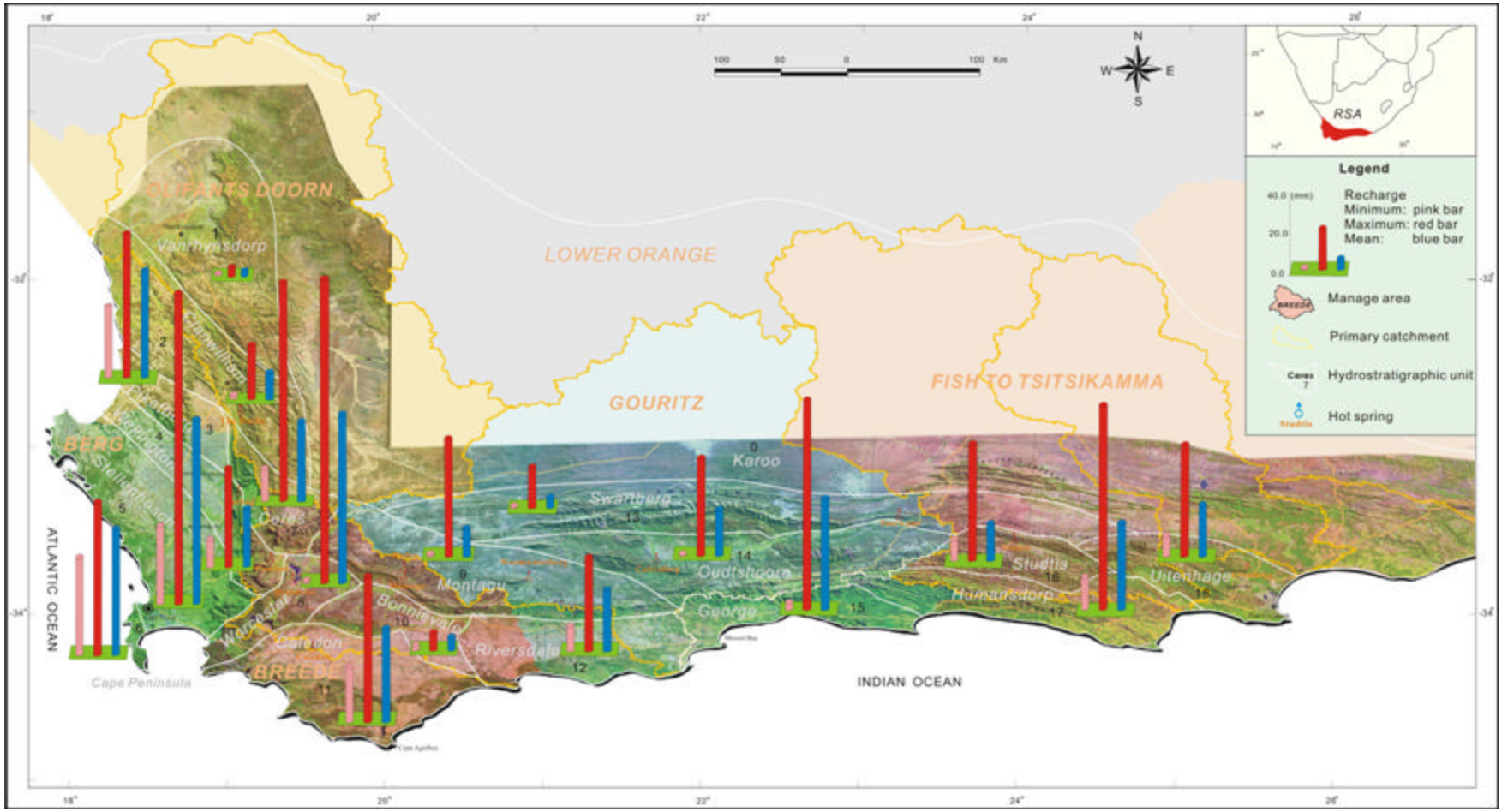

Figure 11.9 Recharge ranges in the hydrogeological units of the TMG

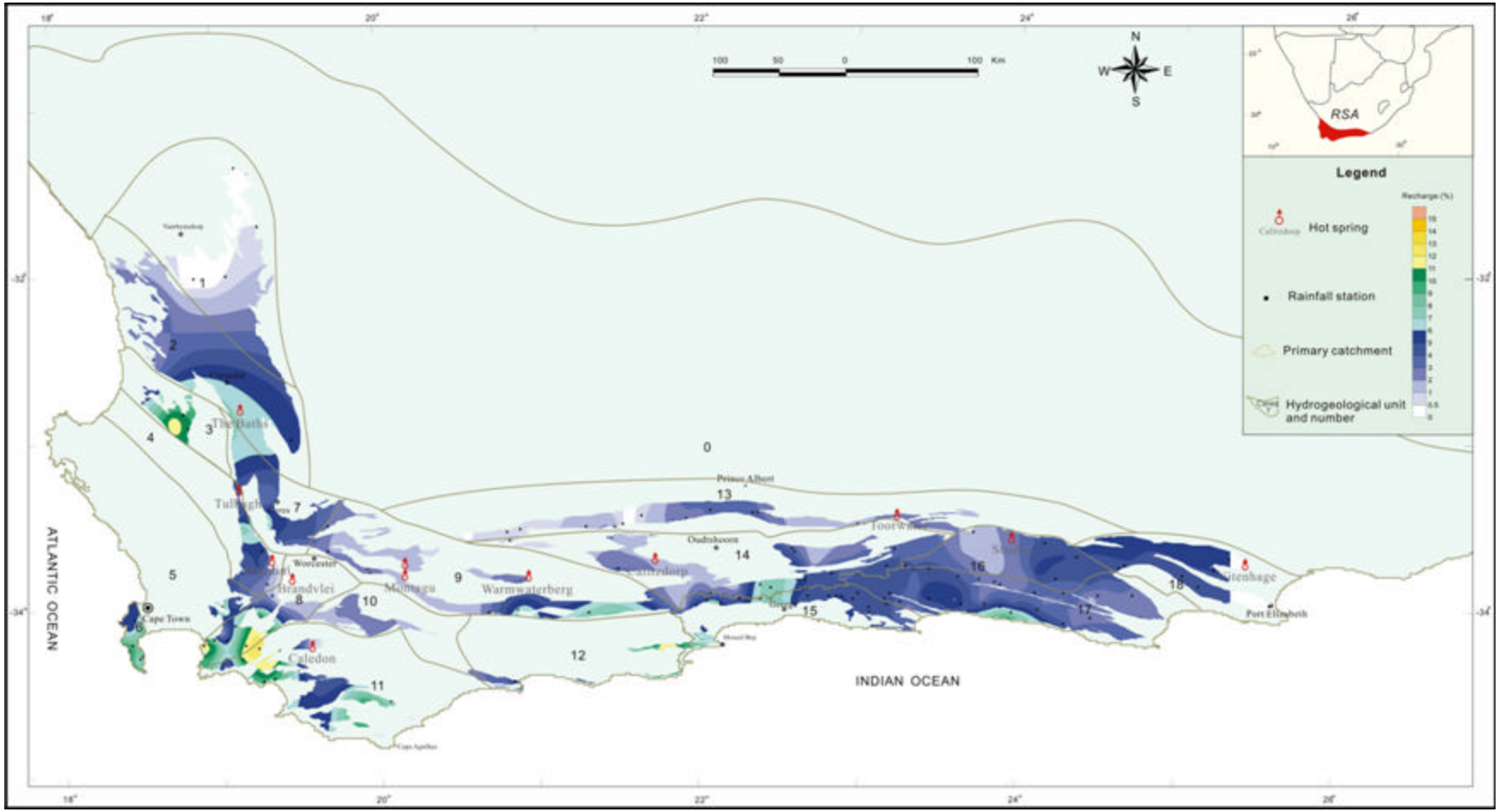

Figure 11.10 Annual recharge percentages in the TMG area

11.5.2 Relationship between the recharge rate and the MAP

For analysing the relationship between the rainfall and the recharge rate, the results of the estimates are grouped into 11 rainfall ranges (Table 11.5). A large range of the recharge rate within the same rainfall interval occurred (Figure 11.11). The observations are as follows:

- The recharge rates from 0.5mm·a^{-1} to 14.5mm·a^{-1} are related to the MAP of 104.9mm-298.5 mm. The recharge rates ranges from 2.66mm·a^{-1} to 32.94mm·a^{-1} in the MAP of 300mm-400 mm.
- A similar range of percentages occurs in the MAP of 400mm-700mm. The recharge rates of 7.19-57.91, 9.23-67.68 and 6.25-60.07mm·a^{-1} are associated with the MAP of 400-500, 500-600 and 600-700 mm, respectively.
- The recharge varies from 19.83mm·a^{-1} to 69.25mm·a^{-1} related to the MAP of 700mm-800mm. ·a^{-1}
- A recharge rate of 35.03-96.52 mm·a^{-1} is related to the MAP of 800-900 mm, but a higher recharge rate of 19.02-115.69mm·a^{-1} is related to the rainfall of 900-1000 mm·a^{-1}.
- A similar recharge rate range if the MAP higher than 1200mm. The recharge rates of 35.00-135.2, 45.69-130.03 and 109.91-137.42mm·a^{-1} are related to the MAP of 1000-1200, 1200-1600 and higher1600mm, respectively.

Table 11.5 Ranges of the recharge estimates related to the precipitation in the TMG area

Range of P (mm)	Recharge rate (mm)			Precipitation (mm)			Station size
	Minimum	Maximum	Mean	Minimum	Maximum	Mean	
<300	0.5	14.25	3.64	104.9	298.5	232	41
300-400	2.66	32.94	14.7	301.7	392.1	355.8	14
400-500	7.19	57.91	24.67	404.1	495.6	444.9	36
500-600	9.23	67.68	31.45	501.5	593.5	542.1	21
600-700	6.25	60.07	36.27	602.3	682.8	640.8	14
700-800	19.83	69.25	37.16	704.2	792.5	752.8	12
800-900	35.03	96.52	55.56	806.8	892.9	844.4	11
900-1000	19.02	115.69	59.77	922.7	999.0	964.1	8
1000-1200	35.00	135.52	65.97	1002.7	1126.3	1085.7	12
1200-1600	45.69	130.03	93.01	1208.4	1604.8	1420.5	5
>1600	109.91	137.42	125.36	1842.1	2063	1975.2	3

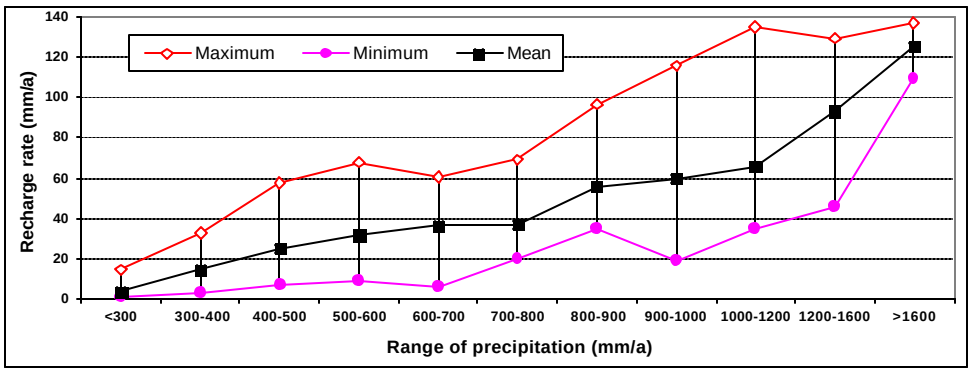

Figure 11.11 Relationship between the recharge range and the MAP range

The recharge rates appear to have non-linear positive relationship with the MAP through the scatter diagram (Figure 11.12). Most high recharge percentages are related to ranges of 300mm to 1100mm rainfall (Figure 11.13). The percentage is low if the MAP is greater than 1100mm, while the low recharge percentages related to rainfall less than 300mm could attribute to high evapotranspiration and low effective infiltration. Actually, the recharge rates are spatially related.

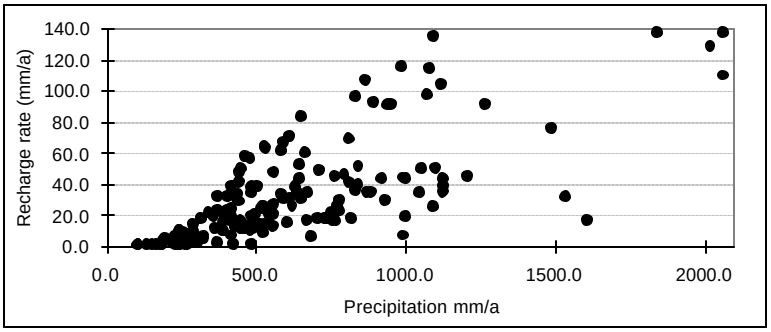

Figure 11.12 Scatter diagram of the recharge rate and the MAP

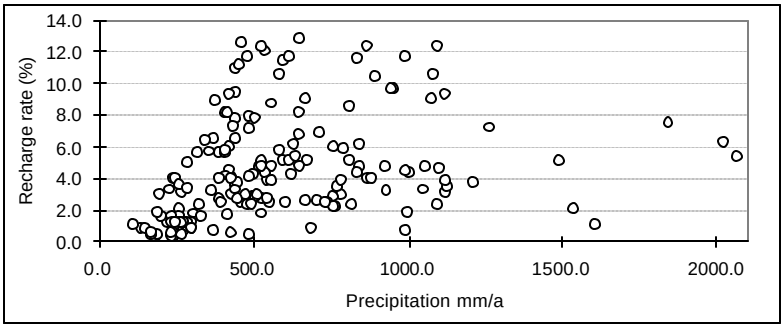

Figure 11.13 Scatter diagram of the recharge percentages and the MAP

11.6 DISCUSSION

11.6.1 Accuracy of the model

Uncertainties and inaccuracies of the model arise from several sources: spatial and temporal variability in processes and parameter values, measurement errors, and the validity of assumptions upon which different methods are based (Healy and Cook, 2002). It is not possible to evaluate the accuracy of $R_E(t)$ estimated with this procedure. However, short-term $R_E(t)$ may be estimated from measured $P(t)$ and simple estimates of $E(t)$ and $R(t)$. Even if the accuracy of $E(t)$ and $R(t)$ is inadequate, they still contain useful information regarding the relative values of individual elements within the distributions. Ideally, recharge estimates should be presented along with statistical confidence levels or as a range of likely values (Healy and Cook, 2002).

The accuracy of recharge estimates based on the water balance approach is controlled by many factors, such as temperature, soils, vegetation and rainfall intensity. In the case of the Kammanassie, the results are calibrated with the critical value of annual recharge range of 10.88-16.09mm (1.65-3.30%) derived from Chapter 10. The recharge rates based on the water balance, the CWD-CRD, the regression of the cumulative spring flux and the mixing model methods are 2.32-3.27%, 0.24-7.56%, 3.29-4.01% and 1.18-2.03% of the precipitation in the Vermaaks area, respectively. These results reflect an identical level in recharge rate, therefore, the recharge rates derived from the evapotranspiration and the runoff model seems to be reliable.

11.6.2 Sensitivity analysis

11.6.2.1 Temperature

The evapotranspiration model is dependent on temperature. The maximum and minimum temperatures are considered (Figure 11.14). Maximum temperatures range from 17°C to 25.5°C in July and from 24°C to 42°C in December, respectively. The high temperatures occur in the Buffelsklip, Wildalsvlei Kammanassie and Montagu-Oudtzshoorn but low temperature in the Uniondale and Cape Town areas in the same season. Minimum temperatures vary from −4°C to 8.8 °C in July and from

2.5 to 18℃ in February, respectively. There are similar low levels of temperature in Buffelsklip, Wildalsvlei Kammanassie, Wildebeesvlakte, Elandsvlakte and Paardevlalte area, but similar high levels of the temperature in the Uniondale Clanwilliam, Langebaanweg, Cape Town, Greyton, Montagu-Oudtzshoorn, Vrolijkheld and George areas in the same season. The temperature pattern in Port Elizabeth is different from the others.

An example of the recharge rate varying with the change of monthly average temperature is shown in Figure 11.15 and Figure 11.16. The recharge rate increases with increasing monthly average maximum temperatures, while reduces with the negative increasing monthly average minimum temperatures. It is the effect of the relative difference in temperature on evapotranspiration. The large difference in temperature leads to more evapotranspiration. Approximate 0.01% of the precipitation should be reduced while the difference in temperature increases by 0.2℃ in the Wildebeesvlakte area.

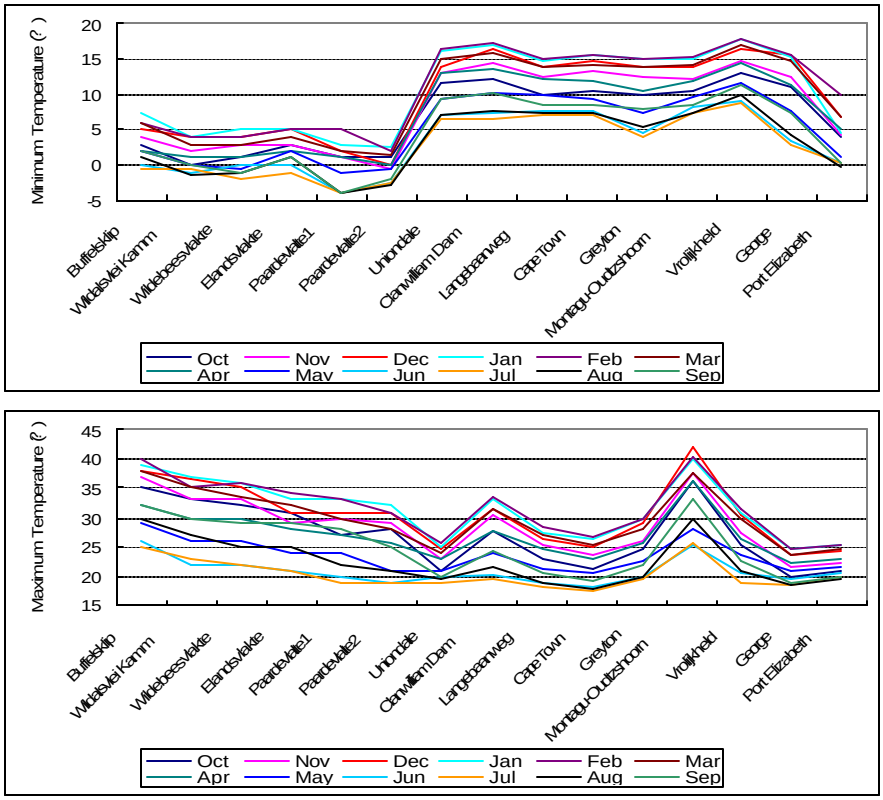

Figure 11.14 Minimum and maximum temperatures in the TMG area(from CNC website)

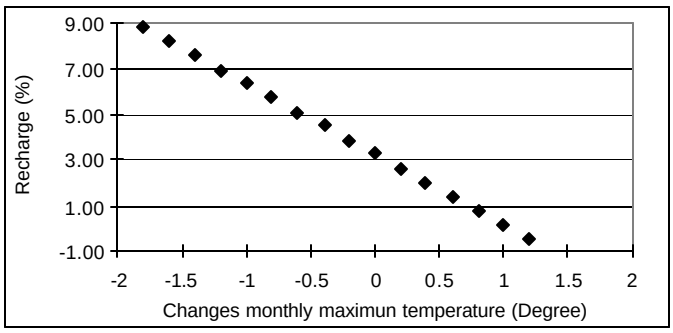

Figure 11.15 Sensitivity of the recharge with changes of monthly maximum temperature in the Wildebeesvlakte

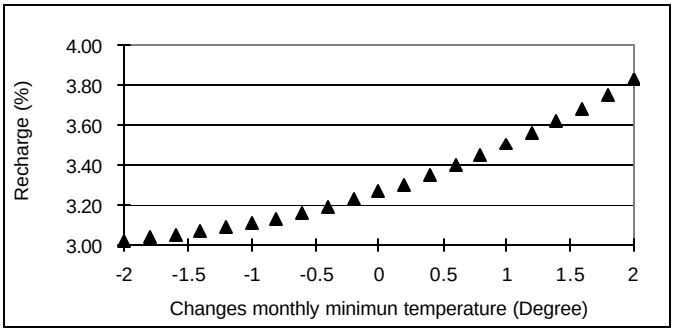

Figure 11.16 Sensitivity of the recharge with changes of monthly minimum temperature in the Wildebeesvlakte

11.6.2.2 Other factors

The recharge rate is negative in relation to factors of soil, vegetation cover and intensity of precipitation. An example is shown in Figure 11.17, Figure 11.18 and Figure 11.19. The degrees of the sensitivity of model related to the factors are listed in Table 11.6. Under similar landscape and hydrogeological settings, the recharge rate reduces about 0.62% if the soil factor increases by 0.01; the recharge reduces by 0.31% when the coverage rate of vegetation increases by 1%; the recharge reduces 0.09% while the rainfall duration increases by 1 hour in a single month.

Table 11.6 Sensitivity of the factors

Factor	T maximum (?)	T min (?)	Soil Factor No dimension	Vegetation Factor No dimension
Delta	0.1	0.1	0.01	0.01
? Re%	0.02	-0.31	-0.62	-0.31

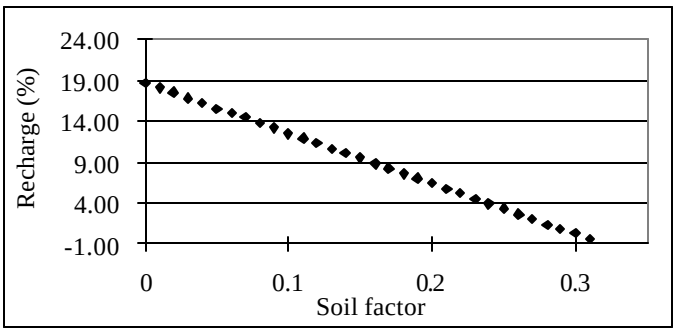

Figure 11.17 Sensitivity of the recharge with changes of soil factor in the Wildebeesvlake

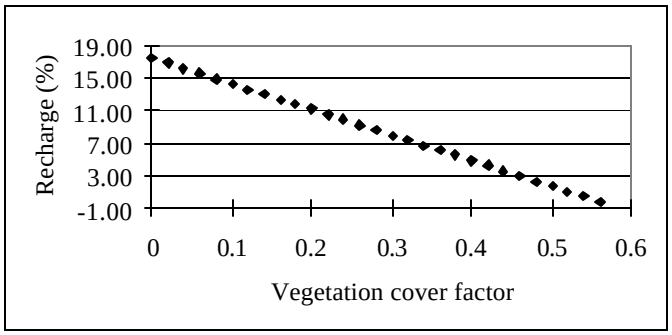

Figure 11.18 Sensitivity of the recharge with changes of vegetation cover factor in the Wildebeesvlakte

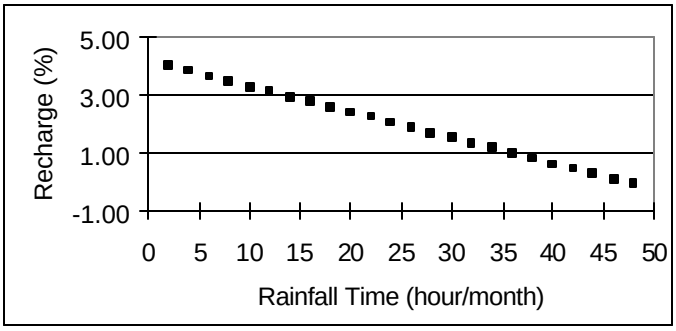

Figure 11.19 Sensitivity of the recharge with changes of rainfall duration in the Wildebeesvlakte

The errors of the model in the Wildebeesvlake are listed in Table 11.7. The extremely high recharge rate is 5.46% of the precipitation, and the extremely low recharge is 1.05% of the precipitation.

Table 11.7 Estimated errors of estimates in the Wildebeesvlakte rainfall station

Condition of recharge	Delta maximum (T ?)	Delta minimum (T ?)	Soil (No dim.)	Vegetation (No dim)	Rainfall time (hrs)	? %	% of the Precipitation	RE (mm)
Extremely low	0.25	-0.25	0.26	0.46	15	-2.21	1.06	5.12
Extremely high	-0.25	0.25	0.24	0.44	5	1.19	5.46	26.41
Model	0	0	0.25	0.45	10	-	3.27	15.80

11.6.3 Snow impact on recharge in the TMG area

11.6.3.1 Spatial distribution of snow

The distribution of snow is associated with topography, season and temperature in the TMG area. Winters in the mountain areas are cold and wet, night temperatures drop sharply and heavy frost and snow may occur. The distribution of snow occurs above 1 000 to1 200m a.m.s.l. of the TMG mountain area in some winter seasons. The distribution of snow in the TMG area is shown on the Landsat 7 Enhanced Thematic Mapper (ETM) images as seen in Figure 11.20 (Wu and Xu, 2005). Different distributions occurred in different seasons or periods, and snow cover remained on the gentle slope sides, eg., the northwest slope of the Hex River Mountain and the northern slope of the Swartberg Mountain. This was also related to wind field and direction. As seen in Figure 11.20A, snow remains slightly longer on the mountain peaks due to snow thickness. On 8 August 2002, a wide distribution of snow occured from the Gydoberg in the north, the Hex River Mountain in the middle to the Du Toitsberg Mountains in the south as can be seen in Figure 11.20B. A small area of snow cover distributes on the peaks of the Kammanassie Mountain and Marloth as shown in Figure 11.20C.

The thickness of snow was up to 600mm in the Langeberg at the Protea Farm and the mountainous peaks near the Franschhoek Pass, as can be seen in Figure 11.21 (Wu and Xu, 2005), and about 300mm of snow occurred on the Villiersdorp Mountain in August 2003 as can be seen Figure 11.22 (Wu and Xu, 2005). The more grass was present, the less snow cover was present. Less snow occurred on the side sheltered from the wind. The interflow from snowmelt could be observed. This means percolation rate was smaller than the snowmelt rate. Based on ETM images and

climatic analysis, the snow-influenced recharge areas in the TMG area are shown in Figure 11.23 (Wu and Xu, 2005). The influenced areas are much wider than the snow cover area. Snow is distributed widely on the mountainous peaks and places of high elevation, but snowmelt can influence the entire catchments or outcrops of the TMG. Therefore, recharge from snowmelt must be considered in these mountainous catchments.

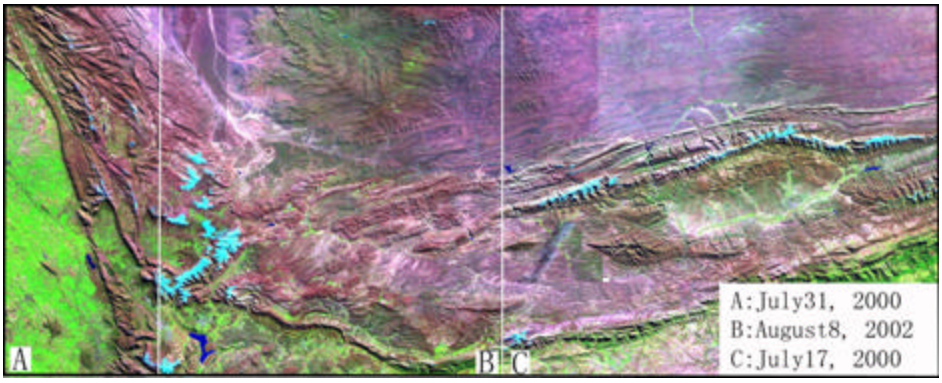

Figure 11.20 ETM images of snow (blue) on the mountain peaks in the TMG

Figure 11.21 Snow on the Langeberg of the Protea Farm (left) and the mountainous peaks near the Franschhoek Pass (right) in 2000

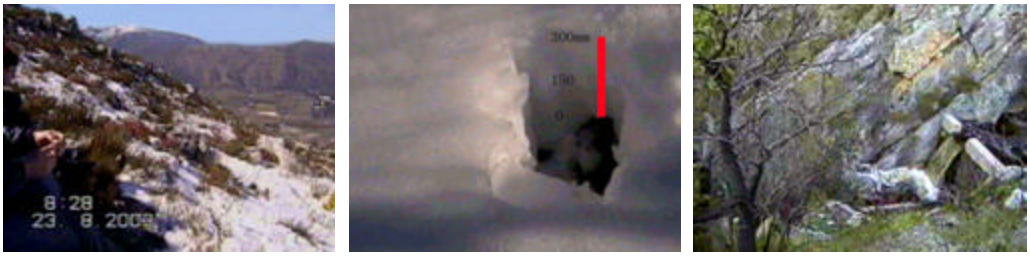

Figure 11.22 Snow and interflow (right) from the snowmelt in the Villiersdorp Mountain

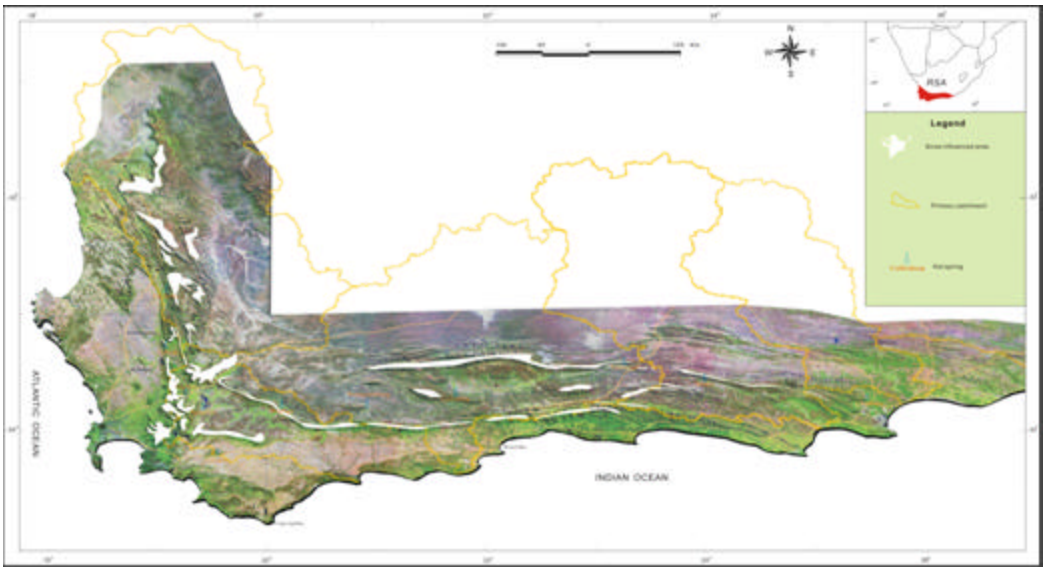

Figure 11.23 Snow influenced area in the TMG area

11.6.3.2 Impact of snowmelt on recharge

Physical processes within the snow pack involve mass and energy balances as well as heat and mass transport. Snowmelt is an energy-driven process. Recharge processes are associated with fractures, soils and vegetation, especially characteristics of fractures at depth. Groundwater recharge from snowmelt is related not only to snowmelt mechanism and to processes but also to recharge processes. Snow water equivalent is used to characterize the snow pack and snowmelt rate. An infiltration experiment is used to compute the percolation rate.

Snowmelt was computed as follows, using a variable degree-day melt factor (?) determined as a function of snow pack density ($?_s$) and vegetation cover (open/forested) (Kuusisto, 1984):

$$g = 0.0104\, r_s - 0.70\,, (1.4 < g < 3.5 \text{ in forested areas } (\text{mmd}^{-1}) \qquad (11.9)$$

$$g = 0.0196\, r_s - 2.39\,, (1.5 < g < 5.5 \text{ in open areas } (\text{mmd}^{-1}) \qquad (11.10)$$

New snowfall density r_{sfall} was assumed to be a function of air temperature (T_{air}),

and was calculated as follows (Hedstrom and Pomeroy, 1998):

$$r_{sfall} = 67.9 + 51.3\exp(T_{air}/2.6) \qquad T_{air} \; ? \; 0℃ \qquad (11.11)$$

$$r_{sfall} = 119.2 + 20.0T_{air} \qquad T_{air} ? \; 0℃ \qquad (11.12)$$

The hourly melt was computed using a standard temperature index approach as follows (Ross et al., 2003):

$$w = \frac{g}{24}(T_{air} - T_{melt}) \qquad (11.13)$$

where w is the hourly melt rate, T_{melt} is the threshold air temperature for snowmelt. There is considerable variability in published values of T_{melt} and a value of less than 0℃ is not physically unrealistic since radiation melt can take place when air temperatures are below freezing (Ross et al., 2003). Kuusisto (1984) obtained T_{melt} values of -1.3℃ and -1.2℃ for open and forested sites in Finland. These values are used for calculating hourly melt rate in the TMG mountainous area.

Based on equation (11.13), the hourly melt rates calculated at air temperatures of 4 and 6℃ are 0.328mm and 0.689mm, respectively. A higher hourly melt rate should occur in cases of higher air temperature. In the TMG mountainous area, the melt time is 6.04 d if the average snow thickness is 100mm, which equals to rainfall of 21.9 mm. Considering infiltrating conditions, more runoff should occur if the snowmelt time is shorter than time of the equivalent rainfall, because recharge is constrained by fracture characteristics while snowmelt rate is not. Note that recharge from snowmelt is very complicated, it is related to snowmelt mechanisms and infiltrating processes. Field studies are necessary in the future.

An infiltration experiment was performed at the Franshhoek Mountain Pass. The source water was overflow of $1.107\ell \cdot s^{-1}$ from a pipe as can be seen in Figure 11.24 (Wu and Xu, 2005). The infiltration area was about $50m^2$, and the specific infiltrating rate is $0.022\ell \cdot s^{-1} \cdot m^{-2}$. The discharge sector is about $385m^2$. The issuing zones are the bedding fractures on the side of the steep slope. A few of more seepage zones were

also observed at lower elevation but with less magnitude. A small temporal weir was used to collect the discharge water in the main discharge area. The discharge rate was measured at 0.956-0.964$\ell \cdot s^{-1}$, which was not total discharge water. The recharge percentage was estimated at 12.9-13.6%. Therefore, most infiltrating water seeps out as interflow. A snowmelt of 0.689mm·h^{-1}, which equals to 1.91×10^{-7} m·s^{-1}·m^{-2}, would still produce much interflow or runoff. Therefore, the recharge rate must be less than that of 1.91×10^{-7} m·s^{-1}·m^{-2}. Suppose 10 % snowmelt is available for recharge in this case, the recharge rate would be 3.59 to7.19% of the 21.9 mm rainfall (derived from 100mm of snow) if snow can remain 1 to 2 d after the snow event. It is worth mentioning that infiltration or recharge cannot occur in whole ground surfaces but only in open fractures or fracture zones (Wu and Xu, 2005).

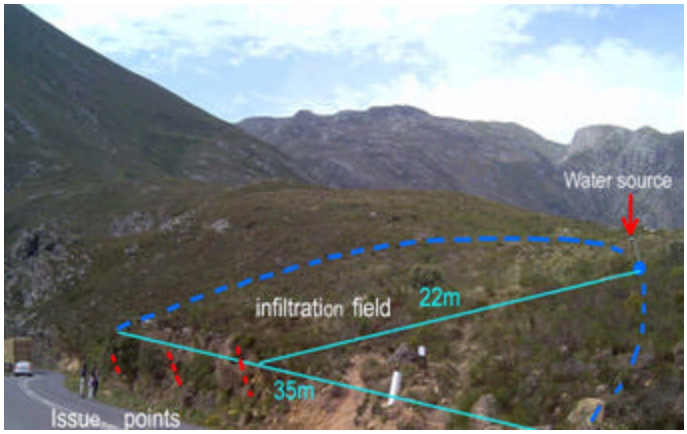

Figure 11.24 Infiltration experiment

11.7 SUMMARY

Recharge rates are related to the spatial distribution of the rainfall. The average recharge rates of the TMG are 29.74mm·a^{-1}. The highest recharge rates are 137.17mm·a^{-1} associated with 1842.06 mm·a^{-1} at 0022116 in the hydrogeological unit 5; the lowest recharge rates are 0.7mm·a^{-1} associated with 163.51mm·a^{-1} at 0048043 in the hydrogeological unit 13. The regions with a recharge rate more than 35mm·a^{-1} occur in the hydrogeological unit 5, 6, 8 and part of the hydrogeological unit 17. The recharge rates in other areas are less than 35mm·a^{-1}. The recharge rate is from 0.28% of the rainfall at rainfall station of No. 0107169 in the hydrogeological unit 1 to 2.86% of the rainfall at station of No. 0017582 in the hydrogeological unit 17. The

recharge rates are smaller tha n that from Vegter 1995.

The recharge rates are a non-linear positive relation to the MAP. Most high recharge percentages are related to rainfall of 300mm·a^{-1} to 1100mm·a^{-1}. The recharge in percentage of rainfall is low if precipitation is greater than 1100mm·a^{-1} or less than 300mm·a^{-1}. The recharge rate is constrained by fracture characteristics but not by infiltrating rate in bulk rainfall or snowmelt rate. The distribution of snow occurs above 1000m-1200m a.m.s.l of the TMG mountain area in some winter seasons. The recharge areas influenced by snowmelt in the TMG are the catchment above 1000 a.m.s.l. The hourly snowmelt rates are estimated at air temperatures 4 and 6°C as 0.328mm and 0.689 mm, respectively. These snowmelt rates are the ceiling of the percolation. A most of snowmelt water emerges in the form of interflow. Recharge rates must be much smaller than snowmelt rates. Further research is needed to compare snowmelt recharge with that of normal rainfall conditions. Discrepancy would be introduced if different temperatures were selected in the model. The recharge rate based on empirical factors in the water balance model should be calibrated with results of other methods before it is used for assessment of groundwater resources in the TMG area.

Chapter 12

Conclusions and Recommendations

The Table Mountain Group (TMG) is a regional fractured rock aquifer system with the potential to become a major source of future bulk water supply to meet both agricultural and urban requirements in the Western and Eastern Cape Provinces in South Africa. The TMG aquifer comprises approximate 4000m thick sequence of sandstone with an outcrop area of 37,000km^2. A wealth of recharge estimation methods for the TMG area is currently available with each method having its own limitations regarding temporal and spatial scale. Confidence in the obtained recharge estimates in the TMG area can be improved by applying multiple methods, which include the CMB, CWD-CRD, SVF and water balance methods.

12.1 CONCEPTUAL HYDROGEOLOGICAL MODEL

Higher fracture frequencies of the TMG during deformation forms secondary porosity. The storativity accredited is from 0.1 to 1‰. According to the occurrence of aquifer, five types of aquifer systems, namely the horizontal terrane aquifer system, incline strata aquifer system, folded strata aquifer system, fractured rock aquifer system and weathered rock (crust) aquifer system, are classified. Based on geological and hydrodynamic characteristics, namely, geomorphology and boundary conditions of groundwater flow, nineteen hydrogeological units in the TMG area are identified, covering the area of 248,000km^2.

The recharge processes are related to topography and fracture networks. Different topography types show different patterns of surface water runoff and infiltration mechanisms. Interflow occurs in the weathering and preferential fracture zones above the elevation of the local basal levels. Infiltration rate is related to characteristics of land surface; and the percolation rate to the aquifer is constrained not only by the infiltration rate but also by fracture characteristics at depths. In most cases, the percolation rate is very small as most of infiltration water seeps out in the form of interflow, especially in mountainous areas. The preferential recharge is domination in the fractured TMG rocks. The recharge possesses diffuse pattern on the land surface

with high fracture density, but preferential recharge occurs at depth. Six models of the recharge processes related to the landform were conceptualised, namely models of soil zones, horizontal strata zones, upright strata zones and three incline strata zones.

The hypothesis that the recharge of the TMG aquifer probably takes place within the outcrops of the TMG was confirmed by analysis of the Landsat 7 ETM images. For local aquifer system, the Cedarberg shale is the recharge boundary obviously. More effective recharge occurs the slope gradient less than 30°. The soil deposited on the bottom of the valley affects recharge water percolating to the fractured rock aquifer at depth. Part of fault zone of some faults cemented by silicate results in complicated recharge processes, in which low or no infiltration occur in cemented zone, but high percolation concentrates in non cemented zones, such as Vermaaks Fault zone.

Groundwater in the Peninsula Aquifer is characterised by its low TDS. The ranges of average TDS in the production boreholes of the Peninsula and Nardouw aquifers in the Kammanassie area are 40-60.4 and 86.8mg·ℓ^{-1}, respectively. According to Piper plots, the groundwater type of the TMG aquifer is classified as Cl-Na type of water, as all other major ions are very low concentrations. The chloride source of TMG aquifer is fallout of precipitation, little additional chloride adds from rocks or formations. Based on the 98 samples distributed in the TMG area, the frequency is 32.7%, 24.5%, 15.3% for concentrations of 10-20mg·ℓ^{-1}, 20-30mg·ℓ^{-1} and 30-40mg·ℓ^{-1}, respectively. The frequency is 8.2% in 50-60mg·ℓ^{-1} and 60-70mg·ℓ^{-1}. The errors between arithmetic and harmonic and geometrical are 38%, and 18%, respectively. Therefore the error would be introduced in the recharge estimation using different mean values.

12.2 RECHARGE RELATED TO RAINFALL PATTERN

Recharge is significantly influenced by seasonal variation of rainfall and extreme rainfall event. A gradual positive trend of rainfall occurred in the Hoekplaas and the Kammanassie rainfall stations in 1925-2002, but the one-tailed probabilities are low. There was a positive tendency in January, April, June, October, November and December, and a negative tendency in the other months in the Kammanassie Dam rainfall station. Negative CRD patterns occurred in the mountainous area from July

1997 to May 2002. Positive trend of rainfall does not mean positive recharge trend. Neither does the seasonal trend. The variation of monthly rainfall results in more complicated water level response.

The same patterns of CRD are observed in the four rainfall stations, namely Parshall, V-notch, Wildebeesvlakte and Purification Works East located on the Kammanassie Mountainous area. Negative patterns of the CRD occur from July of 1997 to May of 2002. A significant correlation occurs in the CRD between the Parshall and Wildbeesvlakte stations. The extremely high rainfall events contribute to the effective recharge. The effective recharge may mainly occur in March, April and November in the Kammanassie mountainous area.

12.3 RECHARGE ESTIMATES IN THE KAMMANASSIE AREA

The recharge rates in the Kammanassie region from 1994 to 2002 using the three-component mixing model of the CMB, CWD-CRD, regression of cumulative spring flux and water balance methods are estimated at 1.182-2.027%, 0.24-7.56%, 3.29-4.01% and 2.32-4.4 % of precipitation (4,217mm), respectively. The influence area of the abstraction and the concentrations of end-member input largely influence the recharge rates with the mixing model of chloride mass balance. Storativity is a very sensitive parameter for recharge estimation in the CWD-CRD method; and the actual recharge area is a very important factor in the spring flux regression method while special flux converts into the volumes. The recharge estimates from each method were integrated in order to qualify the recharge rates using the weights of the different methods to fill the gaps in the different results. The integrated rates indicated 1.63% - 4.75% of the precipitation as recharging the aquifer in the Kammanassie area from 1994 to 2003.

The recharge rate in the Kammanasie area is generally lower than 5%, which is much smaller than that presented in the earlier studies. The estimation of recharge area, storativity and the time lag between rainfall and water level may introduce the errors. The recharge rate is 2.96% of the precipitation against the area of the Peninsula Formation Window, if the recharge equals the total abstractions in the Vermaaks River Wellfield from 1993 to 2002. The budget of 3-D numeric simulation model

confirmed that the recharge rate could not exceed 1.96% of the rainfall at steady state. The results were further corroborated by the 1.65%-3.30% of the annual precipitation for 95% confidence interval.

12.4 SPATIAL DISTRIBUTION OF RECHARGE IN THE TMG AREA

Based on the water budget models, the spatial distribution of the recharge in the TMG outcrop area is presented. The recharge rates from the water budget in the Kammanassie area are calibrated by referring to the results of the CWD, the SVF and the CMB mixing model. Based on the infiltration experiment and the snow distribution from the ETM images and the snow photos, the impact of snowmelt process on groundwater recharge is discussed.

The average recharge rate in the TMG is 29.74mm·a^{-1}, which are generally smaller than the values estimated by Vegter (1995). The highest recharge rate is 137.17mm·a^{-1} related to the MAP of 1842.06 mm·a^{-1} at station No. 0022116 in the hydrogeological unit 5; the lowest recharge rate is 0.7mm·a^{-1} related to the MAP of 163.51mm·a^{-1} at station No. 0048043 in the hydrogeological unit 13. The regions with a recharge rate more than 35mm·a^{-1} occur in the hydrogeological unit 5, 6, 8 and part of the hydrogeological unit 17. The recharge rate in the other areas is less than 35mm·a^{-1}. The recharge percentages are from 0.28% of the MAP at station No. 0107169 in the hydrogeological unit 1 to 12.6% of the MAP at station No. 0012220 in the hydrogeological unit 15.

The recharge rates based on the water balance method have a non-linear positive relationship with the MAP. The recharge rates of 7.19-57.91, 9.23-67.68, 6.25-60.07 19.83-69.25, 35.03-96.52, 19.02-115.69, and 17.45-137.42mm·a^{-1} are associated with MAP of 400-500, 500-600, 600-700 mm, 700-800, 800-900, 900-1,000 and 1000mm upwards, respectively. Most of the high recharge percentages are related to rainfall ranges between 300mm to 1100mm. The low percentages occur in the MAP of greater than 1100mm because more runoff occurs, and the low recharge percentages related to rainfall smaller than 300mm can be attributed to high evapotranspiration and low effective infiltration.

12.5 SUGGESTIONS AND RECOMMENDATIONS

The complexities of the hydrogeological settings make estimating local or regional recharge difficult. The spatial variation of rainfall and topographic conditions result in complex recharge mechanism. Not all of the components of the mixing model can be measured accurately within a given catchment. Inputs such as precipitation and abstraction are quantifiable; however, the time lag has changed significantly related to the residence time of the water, and the solutions of three-component model rely on the results from the two-component model, even the mixing model cannot include piston flow, which likely occurs in the preferential fracture system. The size of recharge area may not be determined accurately in a fractured rock aquifer. Under these limitations, estimates of recharge from the mixing model are subject to large potential errors. In the most important aquifers of the TMG, the common mixing model of CMB is unfit to be applied if recharge processes and areas are not identified.

The validity of assumptions of the methods is the basis of the actual recharge estimates. Errors would be introduced if different parameters were adopted in the empirical model. Uncertainties and inaccuracies arise from spatial and temporal variability of the data. The recharge rate, based on empirical factors in the water balance model, should be crosschecked with other methods before it is used for assessment of groundwater resources in the whole TMG area.

In the Vermaaks River Wellfield, the recharge rates based on the abstraction are actual recharge rates of the Peninsula fractured rock aquifer, which are manageable. Whereas on a local scale, all sorts of discharge should be considered together in recharge estimation with the methods related to discharge. Therefore, the spring flow within the aquifer system should also be considered for total recharge.

Low recharge rates estimated for the TMG area suggests that the caution should be taken when a water supply strategy is formulated for the TMG area. The design of borehole abstraction rates should consider the recharge rates within the relevant recharge areas. In other words, a sustainable abstraction rate in any single borehole should not exceed the natural recharge rate in order to prevent negative environmental impact.

References

Abdulghaffar S. Bazuhair and Warren W. Wood (1996) Chloride mass-balance method for estimating ground water recharge in arid areas: examples from western Saudi Arabia, *J. Hydrol. Volume 186, Issues 1-4, 15 November 1996, Pages 153-159*.

Adams S. (2002) Bulk rainfall samplers and groundwater recharge. Proc. Conf. Tales of a Hidden Treasure, Somerset West, South Africa, 16 Sept. 2002,217-223.

Al-Aswat A.A and Al-Bassam A.M. (1997) *Proposed hydrostratigraphical classification and nomenclature: application to the Palaeozoic in Saudi Arabia. J. Afr. Earth Sci.*, 24 (4) 497-510.

Aller L., Bennet T., Lehr J.H., and Petty R.J. (1987) DRASTIC - A standardised system for evaluating groundwater pollution potential using hydrogeological setting. US EPA Report EPA/600/2-87/035, United States Environmental Protection Agency.

Alley, W.M. (1993) Regional groundwater quality. Van Nostrand Reinhold, New York, USA.

Allison G.B. (1988) A review of some of the physical, chemical and isotopic techniques available for estimating groundwater recharge. In: "Estimation of Natural Groundwater Recharge" (ed.J. Simmers) D. Reidel Publish. Co., Dordrecht/Boston.

Allison G.B., Ston W.J. and Hughes M.W. (1985) Recharge in karst and dune elements of a semi-arid landscape as indicated by natural isotopes and chloride. *J. Hydrol.* 76, 1-26.

Allison GB, Gee GW and Tyler SW (1994) Vadose-zone techniques for estimating groundwater recharge in arid and semiarid regions. *Soil Sci. Soc. Am. J.*, 58, 6-14.

Andreoli M.A.G., van der Vlugt R., Norman N., von Veh M.W. and Andersen N.J.B. (1989) *Interpretative geological map of the pre-Tertiary basement between Gansbaai and Waenhuiskrans - Arniston, S. Cape (1/100 000).* Atomic Energy Corporation of South Africa, Limited

Andreoli MAG, Doucoure M, Van Bever Donker J, Brandt D and Andersen NJB (1996) *Neotectonics of southern Africa - a review.* Africa Geoscience Review, Vol. 3, No.1. pp1-16.

Aston A. and Dunin F. (1977) An empirical model for drainage from soil under rain-fed conditions, Aust. J. Soil Res. 15 (1977) 205–210.

AWRC (1969) The representative basin concept in Australia, Hydrological Series no. 2, Australian Water Resources Council, Canberra, 1969.

Beekman H.E and Sunguro S (2002) Groundwater recharge estimation - Suitability and reliability of three types of rain gauges for monitoring chloride deposition, "Groundwater Division, Western Cape Conference: Tales of a hidden treasure; Somerset West, 16 Sept. 2002", pp 225 –233

Beekman H.E. and Xu Y (2003) Review of groundwater recharge estimation in arid and semi-arid Southern Africa. Xu Y and Beekman HE (Editors, 2003). Groundwater Recharge Estimation in Southern African. IBSN 92-9220-000-3, pp 3-18.

Beekman H.E., Gieske A. and Selaolo E.T. (1996) GRES: Groundwater Recharge Studies in Botswana 1987-1996. Botswana *J. of Earth Sci.*, Vol. Ill, 1-17.

Beekman H.E., Selaolo E.T. and De Vries J.J. (1999) Groundwater recharge and resources assessment in the Botswana Kalahari. GRES II Executive summary and technical reports, pp. 48.

Beekman, H.E., Gieske, A. and Selaolo, E.T., 1996. GRES: Groundwater Recharge Studies in Botswana 1987-1996. Botswana *J. of Earth Sci.*, Vol. III, 1-17.

Beven K. and Germann P. (1982) Macropores and water flow in soils. *Water Resour. Res*. 18, no. 5: 1311-1325.

Black T., Gardiner W. and Thurtell G. (1969) The prediction of evaporation, drainage, and soil water storage for a bare soil, *Soil Sci.Soc.*, Am. Proc. 33 (1969) 655–660.

Booth PWK and Shone RW (1992) Folding and thrusting of the Table Mountain group at Port Elizabeth. Easter Cape. Republic of South Africa. In: De Wit MJ and Ransome IGD (eds) Inversion Tectonics of the Cape Fold Belt, Karoo and Cretaceous Basins of Southern Africa, Balkema, Rotterdam. 207-210.

Boughton W. (1984) A simple model for estimating the water yield of ungauged catchments, Civil Eng. Trans., The Institution of Engineers, Australia CE26 (1984) 83–88.

Boughton W. (1993a) A hydrograph-based model for estimating the water yield of ungauged catchments, in: Proceedings of the Hydrology and Water Resource Symposium, Newcastle, NSW, 1993, pp. 317–324.

Boughton W. (1993b) Direct evaluation of parameters in a rainfall–runoff model, in: Proceedings of the International Congress on Modelling and Simulation, Perth, WA, 1993, pp. 13–18.

Bouma J., Jongerius A., Boersma O., Jager A. and Schoonderbeek D. (1977) The function of different types of macropores during saturated flow through four swelling soil horizons. *Soil Sci. Soc. Am. j.* 41, no. 5: 945-950.

Bredenkamp D.B. and Vogel J.C. (1970) Study of a dolomitic aquifer with carbon-14 and tritium. Isotope Hydrology 1970, Proc. Symp. IAEA, 9-13 March, 1970, 349-371.

Bredenkamp D.B., Schutte J.M. and du Toit G.J. (1974) Recharge of a dolomitic aquifer as determined from tritium profiles. Isotope techniques in groundwater hydrology 1974, Proc. Simp. Vienna 1974 (SM182/5). Hydrology, IAEA, Vienna, pp. 73-94.

Bredenkamp DB (2000) Groundwater monitoring: a critical evaluation of groundwater monitoring in water resources evaluation and management. WRC Report No. 838/1/00.

Bredenkamp DB, Botha LJ, Van Tonder GJ and Van Rensburg HJ (1995) Manual on Quantitative Estimation of Groundwater Recharge Aquifer Storativity. Pretoria: Water Research Commission. TT 73/95.

Broquet CAM (1992) The sedimentary record of the Cape Super group: A review. In: De wit MJ and Ransome IGD (eds). Inversion Tectonics of the Cape Fold Belt. Karoo and Cretaceous Basins of Southern Africa. Balkema, Rotterdam. 159-183.

Busenberg E., Plummer L.N. (1993) Concentration of chlorofluorocarbons and other gases in groundwater at Mirror Lake, New Hampshire. In: Morganwalp, D.W., Aronson, D.A. (Eds.), USGS Toxic Sunstances Hydrology Program Technical Meeting, Colorado Springs, Colorado, Sepember 20-24, pp.151-158.

Carrillo-Rivera J. J., Cardonab A. and Edmundsc W. M. (2002) Use of abstraction regime and knowledge of hydrogeological conditions to control high-fluoride concentration in abstracted groundwater: San Luis Potosí basin, Mexico. *J. Hydrol.* Volume 261, Issues 1-4, 15 April 2002 , Pages 24-47.

Cavé L., Beekman H.E. and Weaver J. (2003) Impact of climate change on groundwater resources. Yongxin Xu and Hans E. Beekman (Editors). Groundwater Recharge Estimation in Southern African. IBSN 92-9220-000-3.

Cavé L., Weaver JMC and Talma AS (2001) The use of geochemistry and isotopes in resource evaluation: A case study from the Agter-Witzenberg Valley. Kevin Pietersen and Roger Parsons (Editors) (2002) A synthesis of the Hydrogeology of the Table Mountain Group-Formation of a Research Strategy, WRC Report NO. TT 158/01, January 2002, (IBSN 1 86845 804 0), Water Research Commission.

Chapman T. (1970) Optimisation of a rainfall–runoff model for an arid zone catchment, IAHS Publication no. 96, 1970, pp. 126–144.

Chapman T.and Malone R. (1999) Comparison of models for estimation of groundwater recharge, using data from a deep weighing lysimeter, in: Proceedings of the International Congress on Modelling and Simulation, Hamilton, New Zealand, 1999, pp. 165–170.

Chapra SC, and Canale RP (1998) Numerical Methods for Engineers with Programming and Software Applications. Third Edition McGraw Hill Companies. 473-474.

Chevallier L. (1999) Regional structural geological interpretation and remote sensing, Little Karoo. WRC Project K8/324.

Chiang W. -H., Kinzelbach W. (2001) 3D-Groundwater Modeling with PMWIN, Springer-Verlag Berlin Heidelberg. ISBN 3-540-67744-5

Chiew F., Stewardson M. and McMahon T. (1993) Comparison of six rainfall–runoff modelling approaches, *J. Hydrol.* 147 (1993) 1–36.

Ciais P. and Jouzel J. (1994) Deuterium and oxygen 18 in precipitation: isotopic model, including mixed cloud processes. *J. Geophy. Research* 99 pp. 16793–16803.

Clark ID and Fritz P (1997) Environmental Isotopes in Hydrogeology, Boca Raton, NY: Lewis Publishers.

Cleaver G, Brown LR, Bredenkamp GJ, Smart MC and Rautenbach CJ de W (2003) Assessment of Environmental Impacts of Groundwater abstraction from Table Mountain Group (TMG) Aquifers on Ecosystems in the Kammanassie Nature Reserve and Environs. WRC Report No. 1115/1/03.ISBNNo: 1-77005-034-5

Cook PG, Hatton TJ, Pidsley D, Herczeg AL, Held A, O'Grady A, Eamus D (1998) Water balance of a tropical woodland ecosytem, northern Australia: a combination of micro-meteorological, soil physical, and groundwater chemical approaches. *J Hydrol* 210:161–177.

Cook PG, Herczeg AL, McEwan KL (2001) Groundwater recharge and stream baseflow, Atherton Tablelands, Queensland. CSIRO Land Water Tech Rep 08/01.

Cook PG, Jolly ID, Leaney FW, Walker GR (1994) Unsaturated zone tritium and chlorine 36 profiles from southern Australia: their use as tracers of soil water movement. *Water Resour Res* 30:1709–1719.

Cook PG, Solomon DK (1995) Transport of atmospheric trace gases to the water table: implications for groundwater dating with chlorofluorocarbons and krypton 85. *Water Resour Res* 31:263–270.

Cook PG, Solomon DK (1997) Recent advances in dating young groundwater: chlorofluorocarbons, 3H/3He and 85Kr. *J Hydrol* 191:245–265.

Cook PG, Walker GR and Jolly ID (1989) Spatial variability of groundwater recharge in a semiarid region. *J. Hydrol.* 111, 195-212.

Council for Geoscience, 1997. Geological Map of the Republic of South Africa and the Kingdoms of Lesotho and Swaziland.

Dansgaard W (1964) *Stable isotopes in precipitation.* Tellus 16: 436-68.

Dawdy D. and O'Donnell T. (1965) Mathematical models of catchment behaviour, Proc. Am. Soc., Civil Eng. 91 (1965) 123–137.

DE Villiers J (1944) A reviews of the Cape Orogeny. Ann. Univ. Stellenbosch 22 (section a) 183-208.

De Vries JJ and Simmers I (2002) Groundwater recharge: an overview of processes and challenges. *Hydroge. J.* 10:5–17.

De Vries JJ (1997) Prediction in hydrogeology: two case histories. Geol Rundschau 86:354–371.

De Vries JJ, Schwan J (2000) Groundwater flow and geological structure of the Algarve, Portugal. Faculty of Earth Sciences, Vrije Universiteit, Amsterdam, 104 pp.

Dettinger M. D. (1989) Reconnaissance estimates of natural recharge to desert basins in Nevada, U.S.A., by using chloride-balance calculations. *J. Hydro l.* 106(1-2): 55-78.

Diamond R. (1997) *Stable isotopes of the thermal springs of the Cape Fold Belt.* Unpubl. MSc thesis, Univ. Cape Town, 81 pp.

Dindane K., Bouchaou L., Hsissou Y. and Krimissa M. (2003) Hydrochemical and isotopic characteristics of groundwater in the Souss Upstream Basin, southwestern Morocco, *J. Afri. Ear. Sci.*, Volume 36, Issue 4, May 2003, Pages 315-327

Du Toit AL (1954) The Geology of South Africa. Oliver and Boyd, Edinburgh. 611pp.

Duffie, J. A., and W. A. Beckman. (1980) *Solar Engineering of Thermal Processes.* New York, N.Y: John Wiley and Sons.

Duvenhage A.W.A, Meyer R. and de Raath C.J (1993) A geoelectrical survey in the Oudtshoorn area to identify potential drilling targets for groundwater. CSIR Division of Earth, Marine and Atmospheric Science and Technology, Report No. EMAP-C-93042.

DWA (1986) Management of the Water Resources of the Republic of South Africa. Department of Water Affairs, Pretoria.

Edmunds WM and Gaye CB (1994) Estimating the spatial variability of groundwater recharge in the Sahel using chloride. *J. Hydrol.* 156, 47-59.

Epstein S. and Mayeda T.K. (1953) Variations of the $^{18}O/^{16}O$ ratio in natural water. Geochimica et Cosmochimica Acta 4 (1953), pp. 213–224.

Eric Roose (1996) Land husbandry - Components and strategy, ISBN 92-5-103451-6

Eriksson E. and Khunakasem V. (1969) Chloride concentration in groundwater, recharge rate and rate of deposition of chloride in the Israel coastal plain, *J. Hydrol.* Vol. 7,178-197.

Eung Seok Lee and Noel C. Krothe (2001) A four-component mixing model for water in a karst terrain in south-central Indiana, USA. Using solute concentration and stable isotopes as tracers. *Chemical Geol.* Volume 179, Issues 1-4, 1 September 2001, Pages 129-143.

Evans J. and Jakeman A. (1998) Development of a simple, catchment-scale, rainfall–evapotranspiration–runoff model, Environ. Modell. Software 13 (1998) 385–393.

Fang P, Wei Z. and Liao Z. (1996) Hydrogeological technology (text book). Beijing: Geological Press. ISBN 7-116-02110-8. p51-52.

Fleming G. (1975) Computer Simulation Techniques in Hydrology, Elsevier, New York.

Fritz P., Cherry J.A. Weyer K.U. and Sklash (1976) Storm runorf analyses using environmental isotopes and major ions. *Interpretation of Environmental Isotope and Hydrochemical Data in Groundwater Hydrology*. Intern. Atomic Energy Agency, Vienna, pp. 111-130.

Fritz R.A. and Cherry J.A (1979) *Groundwater*. Prentice Hall Inc. Englewood Cliffs, New Jersey, p134-35.

Fuller AO and Broquet CAM (1990) Aspects of the Peninsula formation-Table Mountain Group.Abstr. Geocongress '90, Geol. Soc. S. Afr., Cape Town. 169-172.

Gear A., Lowry H.V. and Hayden H.A., 1963. Advanced mathematics for technical students. Part one. p1-2.

Gee GW, Hillel D (1988) Groundwater recharge in arid regions: review and critique of estimation methods. *Hydrol Proc* 2:255–266.

Germann P.F. (1990) Preferential flow and the generation of runoff: 1, Boundary layer *flow* theory. *Water Resour. Res.* 26, no. 12: 3055-3063.

Germann P.P. and Gupte S.M. (1988) Rapid rise of shallow groundwater tables on infiltration-preliminary results and implications on aquifer contamination. In *Proceedings of the FOCUS Conference on Eastern Regional Ground Water Issues,* 325-338. Dublin, Ohio: NWWA.

Gieske A (1992) Dynamics of groundwater recharge: A case study in semi-arid Eastern Botswana. Ph.D Thesis. Vrije Universiteit, Amsterdam.

Gieske ASM, Selaolo ET, McMullen S (1990) Groundwater recharge through the unsaturated zone of southeastern Botswana: a study of chloride and environmental isotopes. IAHS Publ 191:33–44.

Ginn T. R. and Murphy E. M. (1997) A transient flux model for convective infiltration: Forward and inverse solutions for chloride mass balance studies. *Water Resour. Res.* 33(9): 2065-2079.

Gvirtzman H., Ronen D. and Magaritz M. (1986) Anion exclusion during transport through the unsaturated zone. *J. Hydrol.* 87, 267-283.

Haijtema, H.M., 1995. Analytical element modeling of groundwater flow, ISBN 0-12-316550-4, Academic Press, Inc.

Hälbich I.W. and Greef G.J. (1995) *Final report on a structural analysis of the west plunging nose of the Kammanassie Anticline*. Geology Department, University of Stellenbosch, Consulting report to DWAF, Directorate Geohydrology.

Hargreaves G. H., and Samani Z. A. (1985) Reference crop evapotranspiration from temperature. *Applied Eng. inAgric*. 1(2): 96-99.

Harrison L. P. (1963) Fundamental concepts and definitions relating to humidity. In *Humidity and Moisture: Measurement and Control in Science and Industry*. Vol. 3: 105.

Hartnady C.J.H. (1998) A review of the earthquake history and seismotectonic interpretation of the kingdom of Lesotho. IN: Melis and Duplessis consulting Engineers (eds), Review of the current stage of knowledge of the seismotectonic setting of Lesotho and its significance in predicting seismic design parameters for the Katse and Mohale Dams and further phases of the LHWP. *Lesotho Highlands Water Project contract No 1028. Workshop in Maseru, 25 May, 1998.* 37pp.

Hartnady C.J.H. and Hay E.R. (2000) Reconnaissance Investigation into the Development and Utilisation of Table Mountain Group Artesian Groundwater, Using the E10 Catchment as a Pilot Study Area. Final Report to Department of Water Affairs and Forestry by Umvoto Africa/SRK Consulting Joint Venture.

Hartnady C.J.H. and Hay E.R. (2001) Use of structural geology and remote sensing during the hydrogeological exploration of the Olifants and Doring river catchments. Kevin Pietersen and Roger Parsons (Editors) (2002) A synthesis of the Hydrogeology of the Table Mountain Group-Formation of a Research

Strategy, WRC Report NO. TT 158/01, January 2002, (IBSN 1 86845 804 0), Water Research Commission.

Hartnady C.J.H. and Hay E.R. (2002) Deep Artesian Groundwater Exploration in the Greater Oudtshoorn District for Bulk Water Supply (DAGEOS). "Groundwater Divison, western Cape Conference: Tales of a hidden treasure; Somerset West, 16 Sept. 2002. 53-58.

Hattingh J. and Goedhart M.L. (1997) Neotectonic control on drainage evolution in the Algoa basin, southeastern Cape Province. *S. Afr. J. Geol.*, 100, 43- 52.

Healy RW and Cook PG (2002) Using groundwater levels to estimate recharge. *Hydrogeo. J.* 10:91-109.

Hedstrom N.R. and POMEROY J.W. (1998) Measurements and modelling of snow interception in the boreal forest. *Hydrolog. Proc.* **12**: 1611–1625.

Hem J. D. (1985) Study and interpretation of the chemical characteristics of natural water, 3rd Ed. USGS Water Suppl. 2254: 264.

Hess. E.C. and J.H. Parks (1988) Double ring and tension infiltration measurements as a screening tool for con lam man I mobility potential at a hazardous waste site. In *Proceeding of the Second National Outdoor Action Conference on Aquifer Restoration, Ground Water Monitoring and Geophysical Methods.* Vol. 1. 135-152, by National Waler Wetl Association. Dublin. Ohio: NWWA.

Higgins SI, Turpie JK, Costanza R, Cowling RM, Le Maitre DC, Arais C and Midgley GF (1997) An ecological economic simulation model of mountain fynbos ecosystems. Dynamics, valuation and management. *Ecol. Econ*. 22 155-169.

Hill R.S. (1988) Quaternary faulting in the South Eastern Cape Province. *S. Afr. J. Geol*. 91, 399 - 403.

Hornberger G.M., Beven K.J. and Germann P.F. (1990) Inferences about solute transport in macroporous forest soils from time series models. *Ceodcrwa* 46, no. 1/3: 249-262.

HRU (1981) Surface Water Resources of South Africa. Report No's 8/81-13/81, Hydrological Research Unit, University of the Witwatersrand, Johannesburg.

Huggins L. and Monke E. (1967) A mathematical model for simulating the hydrological response of a watershed, Paper H9, in: Proceedings of the 48th Annual Meeting of American Geophysical Union, Washington, DC, 1967.

Jakeman A. and Hornberger G. (1993) How much complexity is warranted in a rainfall–runoff model? *Water Resour. Res.* 29 (1993) 2637–2649.

Johansson P (1987) Methods for estimation of direct natural groundwater recharge in humid climates. Royal Institute of Technology. Dept. of Land Improvement and Drainage. Stockholm.

Johnston C. D. (1987) Distribution of environmental chloride in relation to subsurface hydrology. *J. Hydrol.* 94(1-2): 67-88.

Johnston CD (1987) Preferred water flow and localised recharge in a variable regolith. *J. Hydrol.* 94, 129-142.

Jothityangkoon C, Sivapalan and Farmer D.L. (2001) Process controls of water balance variability in a large semi-arid catchment:downward approach to hydrological model development. *J. Hydrol.* 254(2001)174-198

Jouzel J. and Merlivat L. (1984) Deuterium and oxygen-18 in precipitation: modelling of the isotope effects during snow formation. *J. Geophy. Research* 89, pp. 11749–11757.

Kamensky I.L., Tokarev I.V. and Tolstikhin I.N. (1991) ^{3}H-^{3}He dating: a case for mixing of young and old groundwater. *Geochim. Cosmochim. Acta*, 55: 2895-2899.

Kennedy C., Kendall C., Zellweger G.W., Wyerman T.A. and Avanzino R.J. (1986) Determination of the components of stormflow using water chemistry and environmental isotopes, Mattole River Basin, California. *J. Hydrol.* 84 pp. 107–140.

Kennett-Smitha A., Cook P.G and Walkera G.R. (1994) Factors affecting groundwater recharge following clearing in the south western Murray Basin. *J. Hydrol.*, 154: 85-105.

Kinzelbach W., Aeschbach W., Alberich C., Goni I.B., Beyerle U., Brunner P., Chiang W. H., Rueedi J., and Zoellmann K. (2002) A survey of methods for groundwater recharge in arid and semi-arid regions. Early warning and assessment report series, UNEP/DEWA/RS.02-2. Nairobi, Kenya, pp. 101.

Kok TS (1992) Recharge of springs in South Africa. GH Report 3748. DWAF

Kotze J.C. (2002) Hydrogeology of the Table Mountain Sandstone aquifer –Klein Karoo. Unpub. PhD Thesis.

Kotze JC (2000) Modeling of Groundwater Flow in the Table Mountain Sandston Fractured Aquifer in the Little Karoo Region of South Africa. Current WRC Project No K5/729.

Kotze JC (2001) Towards a Management tool for Groundwater Exploitation in the Table Mountain Sandstone Fractured Aquifer. WRC Report No. 729/1/02.

Kotze JC and Rosewarne PN (1997) Little Karoo Scheme Hydrogeolgical Overview. SRK Report 230827/2 to DWAF.

Kuusisto E. (1984) Snow accumulation and snowmelt in Finland. Publications of the Water Research Institute, No. 55, National Board of Waters, Finland, Helsinki, 149 pp.

Lakey B.L. and Krothe N.C. (1996) Stable isotopic variation of storm discharge from a Perennial Karst spring, Indiana. *Water Resour. Res.* 32 (1996), pp. 721–731.

Lerner D. N., Issar A. and Simmers I. (1990) A guide to understanding and estimating natural recharge, Int. contribution to hydrogeology, I.A.H. Publ., Vol. 8, Verlag Heinz Heisse, pp. 345.

Liu B., Phillips F., Hoines S., Campbell A.R. and Sharma P. (1995) Water movement in desert soil traced by hydrogen and oxygen isotopes, chloride, and chlorine-36, southern Arizona. *J. Hydrol.* 168 , pp. 91–110.

Lloyd, J.W. (1986) A review of aridity and groundwater. Hydrological Processes 1, 63-78.

Lopes J., Braga B. and Conejo J. (1982) SMAP—a simplified hydrologic model, in: V. Singh (Ed.), Applied Modeling in Catchment Hydrology, Water Resources Publications, Littleton, CO, 1982.

Love A. J., A. L. Herczeg, Sampson L., Cresswell R. G. and Fifield L. K. (2000) Sources of chloride and implications for $^{36}C1$ dating of old groundwater, southwestern Great Artesian Basin, Australia. *Water Resour. Res.* 36: 1561-1574.

Maclear L.G.A. (1996) The geohydrology of the Swartkops River basin – Uitenhage Region, Eastern Cape. Unpublished MSc dissertation. University of Cape Town, Cape Town.

Maitre DC Le, Versfeld DB and Chapman RA (2000) The impact of invading alien plants on surface water resources in South Africa: A preliminary assessment. *Water SA* Vol. 26 No. 3. PP397-408.

Manabe, Syukuro (1969) Climate and the Ocean Circulation: I. The Atmospheric Circulation and the Hydrology of the Earth's Surface. *Monthly Weather Review*, 97, No. 11.

Mather J.R. (1972) *The Climatic Water Budget*, Lexington Books.

Mathieu R. and Bariac T. (1996) An isotopic study (^{2}H and ^{18}O) of water movements in clayey soils under a semiarid climate. *Water Resour. Rese*. 32, no. 4: 779-789.

Maule C.P., Chanasyk D.S and Muehlenbachs K. (1994) Isotopic determination of snow-water contribution to soil water and groundwater. *J. Hydrol.* 155. pp. 73–91.

Mayo A.L. and Loucks M.D. (1995) Solute and isotopic geochemistry and groundwater flow in the central Wasatch Range, Utah. *J. Hydrol.* 172, pp. 31–59.

Mazor E (1991) Applied Chemical and Isotopic Groundwater Hydrology. Printed in Great Britain by St Edmundsbury Press. ISBN 0-335-15212-0

Meyer PS (2002) Springs in the Table Mountain Group with special reference to fault controlled springs Kevin Pietersen and Roger Parsons (Editors). (2002) A synthesis of the Hydrogeology of the Table Mountain Group-Formation of a Research Strategy, WRC Report NO. TT 158/01, January 2002, (IBSN 1 86845 804 0). Water Research Commission.

Midgley DC, Pitman WV and Middleton BJ (1994) The surface water resources of South Africa 1990. Volumes 1 to 6. Report Numbers 298/1.1/94 to 298/6.1/94 (text) and 298/1.2/94 to 298/6.2/94 (maps), Water Research Commission, Pretoria. Also accompanied by a CD-ROM with selected data sets.

Mintz, Y., and G.K. Walker (1993) Global Fields of Soil Moisture and Land Surface Evapotranspiration Derived from Observed Precipitation and Surface Air Temperature. *J. Applied. Meteor*., 32, 1305-1334.

Mintz, Y., and Serafini, Y.V. (1992) A Global Monthly Climatology of Soil Moisture and Water Balance. *Climate Dynamics*, 8, 13-27.

Mook W.G., 2001. Environmental isotopes in the hydrological cycle, principles and applications. International hydrological Program, 39,? , IAEA, Vien.

Moore RE (1966) Interval Analysis, Prentice-Hall, Englewood Cliffs, New jersey.

Munnich, K.O., 1957. Messung des ^{14}C-Gehaltes von hartem Groundwasser. *Naturwissenshaften,* 44, p. 32.

Murphy E. M., Ginn T. R. and Phillips J. L. (1996) Geochemicale stimates of paleorecharge in the Pasco Basin: Evaluation of the chloride mass balance technique. *Water Resour. Res.* 32:2853:2868.

Murray EC (1996) Guidelines for Assessing Borehold Yields in Secondary Aquifers. Unpublished M.Sc.Thesis, Univ. of Rhodes, Grahamstown.

Neter J, Wasserman W and Whitmore GA. (1988) Applied Statistics. (Third Edition) Allyn and Bacon, INC. 21-89, 481-486.

Parajka J., Holko L.and Kostka Z. (2004) Distributed modelling of snow water equivalent - coupling a snow accummulation and melt model and GIS.

Pettyjohn W.A. (1987) Ground water contamination: Sources, effects and options to deal with the problem. In *Proceeding.v of the Third National Water Conference*, 117-132- Philadelphia, Pennsylvania: Academy of Natural Sciences.

Phillips F.M. (1994) Environmental Tracers for Water Movement in Desert Soils of the American Southwest. *Soil Sci. Soc. Am. J.*, 58,15-24.

Pitkänen P., Löfmana J., Koskinena L., Leino-Forsmana H. and Snellmanb M. (1999) Application of mass-balance and flow simulation calculations to interpretation of mixing at Äspö, Sweden. *Appl. Geochem.* Volume 14, Issue 7, September 1999, Pages 893-905.

Plummer L.N., Busby J.F., Lee R.W. and Hanshaw B.B. (1990) Geochemical modeling of the Madison aquifer in parts of Montana, Wyoming and South Dakota. Water Resour. Res. 26, pp. 1981–2014.

Prych EA (1998) Using chloride and chlorine-36 as soil-water tracers to estimate deep percolation at selected locations on the US Department of Energy Hanford Site, Washington. US Geol Surv Water-Supply Pap 2481:67.

Rosewarne PN (1984) Hydrogeology and Hydrogeochemistry of the Aquifer of the Hex River Valley. Unpubl. M.Sc. Thesis, Rhodes Univ.

Ross D. Brown1, Bruce Brasnett and David Robinson (2003) Gridded North American Monthly Snow Depth and Snow Water Equivalent for GCM Evaluation. Atmosphere-Ocean 41(1). Pp1-14.

Rust IC (1967) On the Sedimentation of the Table Mountain Group in the Western Cape Province. Unpubl. D.Sc. Thesis, Univ, Stellenbosch. 110pp.

Rust IC (1973) The evolution of the Palaeozoic Cape Basin, southern margin of Africa, In: Nairn AEM and Stehli FG (eds). *The Ocean Basins and Margins*, Vol. 1: The South Atlantic. Plenum Publishing Corporation, New York. 247-276.

SACS (South African Committee for Stratigraphy) (1980) Stratigraphy of South Africa, Part 1. (Compiled by Kent LE) Lithostratigraphy of the Republic of South

Africa, Southwest Africa/ Namibia, and the Republics of Bopgutha-tswana, Transkei and Venda. Handbook Geol, Surv, S.Afr. 8 515-534.

Sami K. and Hughes D.A. (1996) A comparison of recharge estimates to a fractured sedimentary aquifer in South Africa from a chloride mass balance and an integrated surface-subsurface model. *J. Hydrol.* 179 (1-4), 111-136.

Scanlon B.R. (1991) Evaluation of moisture flux from chloride data in desert soils. J. Hydrol., 128: 137-156.

Scanlon B.R. (1992) Evaluation of Liquid and Vapour Water Flow in Desert Soils Based on Chlorine 36 and Tritium Tracers and Non-isothermal Flow Simulations. *Water Resour. Res.*, 28(1), 285-297.

Scanlon B.R., Healy R.W. and Cook, P.G. (2002) Choosing appropriate techniques for quantifying groundwater recharge. In Theme issue on groundwater recharge (ed. B.R. Scanlon and P.G. Cook), *Hydrogeol J,* 10, 18-39.

Scanlon BR, Healy RW and Cook PG (2002) Choosing appropriate techniques for quantifying groundwater recharge *Hydrogeo. J.* 10:18-39.

Schlosser P., Stute M., Sonntag C., Munnich K.O. (1988) Tritiogenic ^{3}He in shallow groundwater. Earth and Planetary Science Letters 94, 245-256.

Scott DF, Maitre DC Le and Fairbanks DHK (1998) Forestry and streamflow reductions in South Africa: A reference system for assessing extent and distribution water SA Vol.24 No. 3. 187-200pp.

Selaolo E.T. (1998) Tracer studies and groundwater recharge assessment in the eastern fringe of the Botswana Kalahari - The Lethlakeng - Botlhapatlou area. Ph.D Thesis. Free University-Amsterdam, pp. 224.

Selaolo, E.T., Beekman, H.E., Gieske, A.S.M. and De Vries, J.J., 2003. Multiple tracer profiling in Botswana – Findings of the GRES Project, UNESCO IHP Series 64.

Sharma M.L. and Hughes M.W. (1985) Groundwatcr recharge estimation using chloride, deuterium and oxygen 18 profiles in the deep coastal sands of western Australia- *J. Hydrol.* 81, no, 1-2: 93-109.

Sheng Z, Liu G, Yang C, Sun S and Chen B. (1985) Hydrogeology, *Academic Press, PRC*. Pp 424-425.

Shiklomanov, A., and A.A. Sokolov (1983) Methodological Basis of World Water Balance Investigation and Computation. *New Approaches in Water Balance Computations* (Proceedings of the Hamburg Workshop), IAHS Publ. No. 148.

Simmers I. (ed.) Hendrickx J.M.H., Kmseman G.P. and Rushton, K.R. (1997) Recharge of phreatic aquifers in (semi)-arid areas. IAH Int Contrib Hydrogeol 19, AA Balkema, Rotterdam, pp.277.

Simpkins W.W. (1995) Isotopic composition of precipitation in central Iowa. *J. Hydrol.* 172 (1995), pp. 185–207.

Sloto RA and Crouse MY (1996) HYSEP: A computer program for streamflow hydrograph separation and analysis. U.S. Geological Survey, Water-Resources Investigations Report 96-4040.

Smart, M (2000) Personal Communication with Louis Carstens 2000-02-03.

Smit P.J. (1978) Groundwater recharge in the dolomite of the Gaap Plateau near Kuruman in the Northern Cape, Republic of South Africa. Water SA, 4(2), 81-92.

Söhnge APG and HÄlbich IW (1983) (eds) Geodynamics of the Cape Fold Belt. Spec. Publ. Geol.Soc. S.Afr. 12.184 pp.

Sophocleous Marios and Buchanan Rex C. (2003) Ground-water Recharge in Kansas. Web version August 15 http://www.kgs.ukans.edu/ Publications/ pic22/ pic22_1. html

Sukhija BS, Reddy DV, Nagabhushanam P and Chand R (1988) Validity of the environmental chloride method for recharge evaluation of coastal aquifers, India. *J. Hydrol.* 99, 349-366.

Tankard AJ, Jackson MPA, Erikson KA, Hobday DK, Hunter DR and Minter WEL (1982) 3.5 Billion Years of Crustal Evolution of Southern Africa. Springer-verlag, New York. 523pp.

Theron JIN and Loock JC (1988) Devonian deltas of the Cape Supergroup, South Africa. In: McMillan NJ, Embry AF and Glass DJ (eds). Devonian of the World, Volume 1, Mern. Can. Soc. Petr. Geol. 14 729-740.

Theron JN (1962) An analysis of the Cape Folding in the District of willowmore, C.P. Unpubl. D. Sc. Thesis, Univ. Stellenbosch.

Thorburn P.J. and Rose C.W. (1990) Interpretation of solute profile dynamics in irrigated soils. III. A simple model of bypass flow in soils. *Irrigation Science* 11, no, 4: 219-225.

Thornthwaite C.W. (1948) An Approach Toward a Rational Classification of Climate. *Geographical Review*, 38, 55-94.

Tóth J (1963) A theoretical analysis of groundwater flow in small drainage basins. *J Geophys Res* 68:4795–4812.

Tyner J. S., Brown G. O., Vogel J. R., and Garbrecht J. (2000) Chloride mass balance to determine water fluxes beneath KCI fertilized crops. *Trans. ASAE* 43(6): 1553-1559.

Tyner J. S., Brown G. O., Vogel J. R., Garbrecht J. (2002) Chloride mass balance to determine water fluxes beneath KCL-Fertilized crops. Transactions of ASAE, 2000 America Society of Agricultural Engineers Vol.43 (6): 553-1559.

USDA-SCS (1985) Hydrology. Section 4 in *Soil ConservationService National Engineering Handbook*. Washington D.C. USDA Soil Conservation Service

USGS (1994) Estimates of percolation rates and ages of water in unsaturated sediments at two Mojave Desert sites, California-Nevada. USGS Report No. 94-4160. Washington D.C.: USGS. Transactions of ASAE, 2003 America Society of Agricultural Engineers ISSN 0001-2351 Vol.46 (1):95-103.

Van der, Lee J. and Gehrels J.C. (1997) Modelling of groundwater recharge for a fractured dolomite aquifer under semi-arid conditions. In IAH-Recharge of Phreatic Aquifers in (Semi-) Arid Areas (ed. I. Simmers), A.A. Balkema/Rotterdam: 129-144.

Van Tonder G.J. and Xu Y. (2000) Recharge - Excel-based software to quantify recharge (unpublished). Short course, presented at the Department of Earth Sciences, University, Bellville, South Africa, 19-22 June 2002.

Van Tonder G.J., Kunstmann H. and Xu Y. (1998) *Estimation of the sustainable yield of a borehole including boundary information, drawdown derivatives and uncertainty propagation*, pumptest course notes, UWC.

Van Wligen BW, Little PM, Chapman RA, Gorgens AHM, Willems T and Marais (1997) The sustainable development of water resources: History, financial costs, and benefits of alien plant control programmes. *S. Afr. J. Sci.* 93 404-411.

Vandenschrick G., van Wesemael B., Frot E., Pulido-Bosch A., Molina L., Stiévenard M. and Souchez R. (2002) Using stable isotope analysis (δD, $\delta^{18}O$) to characterise the regional hydrology of the Sierra de Gador, south east Spain. *J. Hydrol.* Volume 265, Issues 1-4, 30 August 2002, Pages 43-55

Vegter JR (1995 a) An Explanation of a Set of National Groundwater Maps. WRC Report TT74/95, Water Research Commission, Pretoria.

Vegter JR (1995 b) Groundwater resources of South Africa. An explanation of a set of National Groundwater maps. WRC Report No. TT 74/95. Water Research Commission, Pretoria.

Vegter JR (2001) Groundwater development in South Africa and an Introduction to the Hydrogeology of Groundwater Regions. TT134/00, water research Commission.

Versfeld DB, LE Maitre DC and Chapman RA (1998) Alien Invading Plants and Water Resources in South Africa: A Preliminary Assessment. Report No. TT 99/98, Water Research Commission, Pretoria.

Walker GR, Jolly ID and Cook PG (1991) A new chloride leaching approach to the estimation of diffuse recharge following a change in land use. *J. Hydrol.* 128, 49-67.

Watson K.W. and Luxmoore R.J. (1986) Estimating macroporosily in a forest watershed by use of a tension infitrometer. *Soil Sci.Soc., Am.* 50. No. 3: 578-582.

Weaver J.M.C. and Talma A.S. (2002) Cumulative Rainfall Collectors - A Tool for Assessing Groundwater Recharge. Groundwater Division, Western Cape Conference: Tales of a hidden treasure; Somerset West, 16 Sept. 2002.

Weaver JMC and Talma AS (1999) Field Studies of Chlorofluorocarbons (CFCs) as Groundwater Dating Tool in Fractured Rock Aquifers. Report 731/1/99 Water Research Commission.

Weaver JMC, Talma AS and Cavé LC (1999) Geochemistry and Isotopes for Resource Evaluation in the Fractured Rock Aquifers of the Table Mountain Group. WRC Report 481/1/99, Water Research Commission, Pretoria.

White, K.L., Haggard, B.E., Chaubey, I., Green, W.R., Petersen, J.C. (2003) Water Quality Trends And Hydrograph Separation At The Buffalo National River, Arkansas, 1991-2001. Transactions Of The Asae. 47(2):407-417.

Willmott, C.J., C.M. Rowe, and Y. Mintz (1985) Climatology of the Terrestrial Seasonal Water Cycle. *J. Climatology*, 5, 589-606.

Wischmeier W.H. (1974) *New developments in estimating water erosion.* 29e Meeting Soil Cons. Soc. Amer. Syracuse, New York. pp. 179-186.

Wood WW (1999) Use and misuse of the chloride-mass balance method in estimating ground water recharge. *Ground Water*, 37, 1, 2-3 (Technical commentary).

Wood WW and Sanford WE (1995) Chemical and isotopic methods for quantifying groundwater recharge in a regional semiarid environment. *Ground Water*, 33, 3, 458-468.

Wood WW, Rainwater KA and Thompson DB. (1997) Quantifying Macropore Recharge : Examples from a Semi-Arid area. *Ground Water* Vol. 35 No. 6 pp. 1097-1106.

Woodford A. and Chevallier L. (1998) Regional characterisation and mapping of Karoo fractured aquifer systems - An integrated approach using a geographical information system and digital image processing. Water Research Commission Project report K5/653.

Woodford AC. (2002) Interpretation and applicability of pumping-tests in Table Mountain Group Aquifers. IN: A synthesis of the Hydrogeology of the Table Mountain Group-Formation of a Research Strategy. Kevin Pietersen and Roge Parsons (editors), 2002. ISBN 1 86845 804 0

Wu Y, Wang W, Xu Y, Liu H, Zhou X, Wang L and Titus R (2003) Radon concentration: A tool for assessing the fracture network at Guanyinyan study area, China. *Water SA* 29, 1 , 49-54.

Wu Y and Xu Y (2004) Recharge estimation with mixing model of chloride mass balance in Vermaaks River valley, South Africa (extended abstract). Groundwater flow understanding, from local to regional scales. XXXIII IAH Congress & ALHSUD Congress, Zacatecas City-Mexico, 2004.

Wu Y and Xu Y (2005) Snow Impact on Groundwater Recharge in Table Mountain Group Aquifer Systems with a Case Study of the Kommissiekraarivier Catchment South Africa. *Water SA*, 31, 3, 275-282.

Xu Y and Beekman HE (2003). A Box model for estimating recharge-The RIB Method. Yongxin Xu and Hans E. Beekman (Editors). Groundwater Recharge Estimation in Southern African. IBSN 92-9220-000-3. p83-88.

Xu Y and Van Tonder (2001) Estimation of recharge using a revised CRD method. *Water SA*, 27, 3, 341-343.

Xu Y, Titus R., Holness SD, Zhang J. and GJ van Tonder (2002) A hydrogeomorphological approach to quantification of groundwater discharge to streams in South Africa. *Water SA* vol.28, No.4, 375-380.

Xu Y, Wu Y and Beekman HE (2003) The Role of Interflow in Estimating Recharge in Mountainous Catchments. Yongxin Xu and Hans E. Beekman (Editors). Groundwater Recharge Estimation in Southern African. IBSN 92-9220-000-3. pp 135-145.

Xu Y, Wu Y and Titus R (2002) Influence of the Vermaaks Wellfield Abstraction on Groundwater Levels and Streams in Vicinity. Report prepared for Bellville Branch of the Department of Water Affairs and Forestry.

Ye W., Bates B., Viney N., Sivapalan M. and Jakeman A. (1997) Performance of conceptual rainfall–runoff models in low-yielding ephemeral catchments, *Water Resour. Res.* 33 (1997) 153–166.

Appendix I Fieldwork performed

Date	Fieldwork
2002-5-18-19	Stellenbosch-Franshhoek-Worcestrer-Montagu (Hydrogeological unit 5, 8 and 9)
2002-6-19-20	Vermaaks field work (Hydrogeological unit 14)
2002-7-13	Table Mountain (Hydrogeological unit 6)
2002-8-21	Western Coast (Hydrogeological unit 5)
2002-9-14-15	Hermanus-Stanford-Gansbaai (Hydrogeological unit 11)
2002-9-22	Jonkershoek catchment (Hydrogeological unit 8)
2002-9-28-29	West Coast, St. Helena Bay- Langebaan (Hydrogeological unit 5)
2002-10-18	Infiltrating process observed on campus at UWC
2002-10-29	Newlands spring research (Hydrogeological unit 6)
2002-12-15	Herdberg Somerset West (Hydrogeological unit 5)
2002-12-12	Borehole log: 3218A1731, 750m (Hydrogeological unit 2)
2002-12-25-26	Herdberg, Somerset West (Hydrogeological unit 5)
2003-1-28-30	Borehole log: 3218A1731, 750m (Hydrogeological unit 2)
2003-1-31	Cape Peninsula (Hydrogeological unit 6)
2003-4-27	Platteklip Gorge, Table Mountain (Hydrogeological unit 6)
2003-5-13-14	Sampling in the Vermaaks wellfield (Hydrogeological unit 14)
2003-5-31, 6-1	Stellenbosch-Suurbraak-Montagu (Hydrogeological unit 5, 8 and 9)
2003-6-14	Table Mountain (Hydrogeological unit 6)
2003-6-27-29	Infanta-De Hoop-Agulhas-Bredasdorp-Caledon (Hydrogeological unit 11)
2003-9-13-14	Calitzdorp - Prince Albert-Swartberg Pass (Hydrogeological unit 13,14 and 0)
2003-10-11	Strand-Rooiels Bay (Hydrogeological unit unit 8)
2003-11-8	Sir Lowry's Pass - Grabouw-Villiersdorp (Hydrogeological unit 8 and 5)
2003-11-9	Hermanus-Stanford-Gansbaai-Pearly Beach (Hydrogeological unit 11)
2003-11-12	Uniondale-Toorwater-Kamanassie South (Hydrogeological unit 14 and 16)
2003-11-15	Piketberg-Tulbagh-Ceres-Warmwaterberg (Hydrogeological unit 3, 7, 9 and 14)
2003-11-15	Ladismith-Swellendam-Ashton-Goudini-Brandvlei-Huguenot Pass (Hydrogeological unit 10, 12 and 14)
2003-11-17	George-Outeniqua Pass-Kamanassie Mountain (Hydrogeological unit 15 and 14)
2003-11-18	Setting up of rainfall station in Dysselsdorp (Hydrogeological unit 14)
2002-11-22	Infiltrating experiment in Franshhoek Pass (Hydrogeological unit 8)
2003-11-30	Piketberg-Pass-Citrusdal-Blikhuis (Hydrogeological unit 2 and 3)
2003-12-6	Wellington-Bain's Kloof-Ceres-Gouda (Hydrogeological unit 4 and 7)
2003-12-28,29	Greyton- Shaws Pass-Hermanus-Kleinmond-Strand (Hydrogeological unit 11)
2004-1-9	Riversdale-Stilbaai-Mossel Bay-George (Hydrogeological unit 12 and 15)
2004-1-10	Goeorge-Humansdorp-Port Elizabeth (Hydrogeological unit 15 and 17)
2004-1-12-14	Uitenhage-Hankey-Humansdorp (Hydrogeological unit 17 and 18)
2004-3-13	Mont Rochelle Nature Reserve (Hydrogeological unit 8)
2004-3-27-28	Clanwilliam-Graafwater-Lambert's Bay (Hydrogeological unit 1and 2)
2004-7-1-6	Hex River Valley-Koo Valley-Montagu-Barrydale-Beaufort West (Hydrogeological unit 9, 13 and 14)
2004-9-25-27	Vanrhynsdorp-Calvilia (Hydrogeological unit 0, 1 and 2)

Appendix II Summary of the production boreholes data in the Vermaaks area

Borehole	Depth (m)	Water Level (m)		Water Strike (m)*	Depth of pump (m)	Screen Depth (m)
		First	Now			
VG3	206.7	6.02	10	110-111(6.0), 190(3.0), 174 (3.0)	148	96.5-206.7
VR6	250	34.64	60	228-244(15)	165	108.7-230
VR7	177	63.3	90	78-81(8), 129-140(15)	159	53-177
VR8	251.3	100.5	125.4	113-117(5) 156-170(4) 234-240(4)	163	89.6-251.3
VR11	224.5	125.5	151	139(2) 183-194(8) 200-210(10)	180	18-224.5
DP10	210	114.07	90.2	183(7)	180	73-210
DP12	192	126.07	102.8	?(20)	180	66-192
DP29	240	120.6	97.09	160-170(2) 185-?(2)		
DP28	246	117.8	94.57	122-124(1.5) 151-160(10) 195-210(11)	170	121-207
DP15	224.5	103.8	86.04	110(3) 169(7) 187(11)	180	50-207
DP25	203	104.9	83.5	109, 166,201	170	9-203
DG110	212	110.6	107.57	114-117(1.5) 137 200-203(6)	200	92-212
DP18	17	3.6	3.2	4.2-9(15)	14	2-9.4

The first water strike (fracture zone) depth (m), followed by yield, e.g. 110 – 111(6.0), after Kotze, 2002.

Appendix III Information of unsuccessful production boreholes of the KKRWSS

Borehole	Depth (m)	Yield ($l \cdot s^{-1}$)	Geology	Water level (m)
WN101	243.5	>2.0	Baviaanskloof Quartzite, shale at 28m 188, 203 m, fractures at 120 m.	4.3 (1989)
VR5	215	15.0	0-12 boulders; 12-215 Baviaanskloof, shale at 37, 46, 57, 111 m, fractures at 82, 102, 169 and 184-186 m. *(75-215).*	4.3 (1989)
VG12	173	4.7	0-4 boulders; 4-230 Tchando Formation, fractures at 19, 78, 98, 14 and 171-173 *(40-173)*	2.93 (1992)
VG4	113	<2.0	0-2 scree, 2-113 Baviaanskloof	18.2 (1989)
DG107	210	4.1	0-22 boulders, 20-210 Kouga Formation	27 (1987)
DG104	250	5.7	0-8 Enon, 8-250 Kouga Formation	90 (1987)
DP27	249	135-140 (2) 140-195 (10) 240(8)	0-22 Enon 22-249 Baviaanskloof Formation, Fractures at 150 to 155 m, open joints with showing weathering at 241, 242 and 248 m	119 (1992)
DP20	220	0.9	0-18 Enon, 18-220 Baviaanskloof Formation	104.5 (1991)
DP14	167	12	0-6 Enon, 2-30 weathered sandstone, 30 to 167 sandstone	62.5 (1986)

DP13	184.6	30	Baviaanskloof with shale	112 (1990)

Appendix IV Information of some monitoring boreholes: Eastern Section

Borehole	Depth (m)	Depth of Water Strike#	Geology (depth in m)	Water Level (m)	Altitude (m)
G40171	50 *(34-40)*	?	0-17 boulders 17-50 Peninsula quarzite	5.085	660.516
G40172	16 *(0-16)*	(5.0)	Boulders	5.125	660.416
G40173	10 *(0-10)*	(3.0)	0-10 sandstone boulders and fragments in yellow sand matrix	4.925	660.216
G40174	147 *(129-135)*	127-133 (13)	0-12 sand and scree 92-147 sandstone and shale Fracture zone: 127 –133 with dark brown Fe staining	105.98	469.66
G40175	126	84(5.0)	0-23 Boulders 23-49 C/S layer 49-126 Peninsula quartzite		
G40175A	84 *(57-63)*	27 (11) 60(0.75)	0-19 Sand, boulders and scree 19-45 C/S layer 27-30 fractured with quartz vein 48-84 Quartzite, fractured, Fe stained, pyrite quartz veins	Artesian	652.031
G40176	150 *(39-45)* *(116-122)*		0-17 sand and boulders 17-150 sandstone and shale weathering visible up to 119 m, reddish to yellow brown stains	6.71	644.081
G40177	150	92(2.4)	0-17 Sand and boulders 17-150 Sandstone (water strike in quartz vein)	51.94	420.036
G40178	120 *(51-57)*	54(8.0)	0-11 weathered sandstone 11-120 sandstone 94-114 fault zone with quartz veins containing pyrite	10.22	535.691

#Water strike yield is indicated within brackets ($\ell \cdot s^{-1}$), screen, if present in italics.

Appendix V Summary of water quality in the Vermaaks area (mg·ℓ^{-1})

Name	TDS	pH	K	Na	Ca	Mg	F	Cl	HCO_3^-	NO_3^-	SO_4^{2-}	PO_4^{3-}	Si	NH_4-N	Mn	Fe	Source
Rainfall	136.5	6.5	6.89	1.92	20.15	5.98	nd	1.74	63.4	48.45	8.36	11.26	nd	25	0.21	0.03	1
VG3	86.8	5.48	0.76	24.08	2.18	2.98	0.13	39.40	5.1	0.89	10.40	0.01	9.75	0.04	0.44	0.0043	1,2,3
VR6	48.0	6.01	1.01	12.89	1.89	1.90	0.11	19.50	10.1	0.20	3.08	0.02	5.46	0.03	nd	0.01	1,2,3
VR7	58.3	6.30	0.75	13.29	2.40	2.20	0.15	21.65	9.7	0.31	7.49	0.02	4.76	0.05	0.0055	0.0265	1,2,3
VR8	60.4	6.19	0.89	15.68	2.14	2.58	0.25	28.26	8.0	0.11	7.44	0.05	5.08	0.01	nd	0.37	1,2,3
VR11	58.9	6.29	0.84	15.14	1.93	2.42	0.13	25.48	8.8	0.07	7.30	0.02	4.95	0.02	0.0005	0.0265	1,2,3
V-notch	79.0	6.71	1.04	23.27	2.93	2.33	0.10	32.90	13.2	0.03	7.80	0.02	10.24	0.03	0.00	0.07	3
VG16	71.4	5.50	0.80	23.63	1.60	2.30	nd	30.50	9.5	1.77	6.00	0.06	0.00	0.02	nd	0.03	1
G40171	64.0	6.59	0.59	14.30	3.80	2.10	0.08	20.60	19.3	0.32	5.60	0.03	8.78	0.01	0.001	0.136	3
G40172	64.0	6.45	0.74	15.60	2.50	2.30	0.08	21.60	14.1	0.39	8.30	0.05	8.80	0.02	0.001	0.136	3
G40173	56.0	6.31	0.74	14.60	2.20	2.00	0.07	20.50	12.3	0.17	5.60	0.02	8.06	0.00	0.157	0.248	3
G40175	52.0	5.20	0.90	13.00	3.00	2.00	0.10	23.00	6.0	0.08	8.00	0.04	9.20	0.04	0.167	0.005	3
G40175 51M	94.0	6.97	1.12	14.50	9.80	1.80	0.09	21.90	40.4	0.01	11.70	0.02	9.14	0.02	0.114	0.003	3
G40175A	57.0	6.18	0.99	13.60	2.40	2.40	0.09	19.70	7.6	0.10	10.80	0.01	9.18	0.01	0.186	0.003	3
G40175A 23M	96.0	7.06	1.06	15.20	9.70	1.60	0.10	22.50	37.8	0.01	14.80	0.02	8.92	0.02	0.139	0.306	3
G40175A 27M	78.0	6.78	1.43	13.50	3.20	2.30	0.11	22.00	31.2	0.20	8.70	0.02	8.88	0.31	0.093	0.003	3
G40175A 60M	73.0	6.71	2.55	11.90	3.50	1.50	0.08	16.90	32.3	0.01	9.80	0.01	4.54	0.02	0.309	0.003	3
G40175A 84M	67.0	6.55	1.82	12.70	3.50	2.10	0.08	21.30	15.8	0.02	12.10	0.01	8.32	0.02	0.507	0.003	3
G40175B 115M	57.0	6.20	1.08	13.80	2.00	1.60	0.07	20.90	10.6	0.01	8.60	0.02	8.86	0.03	0.17	0.003	3
G40175C 126M	60.0	6.63	1.15	13.40	2.30	1.70	0.07	20.80	13.0	0.02	9.60	0.03	9.10	0.03	0.196	0.068	3
G40176	58.0	6.37	0.80	13.70	2.90	2.40	0.09	19.10	13.5	0.22	7.00	0.03	9.26	0.04	0.013	0.003	3
G40176 42M	69.0	6.99	1.07	14.10	2.90	2.00	0.07	23.20	20.8	0.21	7.30	0.01	5.24	0.07	0.502	0.003	3
G40176A 119M	111.0	7.43	3.03	15.50	10.10	2.20	0.05	22.70	53.2	0.40	12.30	0.07	10.02	0.08	0.001	0.003	3
G40176B 150M	109.0	7.16	2.74	15.10	11.20	2.20	0.11	21.50	58.8	0.01	8.10	0.02	10.00	0.03	0.023	0.224	3
VS 1	266.8	6.90	6.51	56.56	20.88	13.49	nd	80.30	152.2	0.97	10.26	0.31	0.00	1.07	1.02	1.42	1
VS 2	172.9	6.20	1.35	55.21	2.90	6.67	nd	83.70	15.9	2.07	11.57	0.11	0.00	0.18	0.11	1.32	1
VS 3	144.4	6.10	1.03	45.97	2.66	5.15	nd	74.10	12.7	0.02	8.77	0.19	0.00	0.02	nd	0.18	1

1 This study (WRC K5/1329) 2 NGDB, 3 WRC 98 and Kotze, 2002 nd not detected

Appendix VI Constitutes of isotopes in the Kammanassie area

NAME	DATE	^{18}O(‰)	^{2}H (‰)	^{14}C (pmc)	T(TU)	^{13}C (PDB‰)
VR6	1996-1-31	-7.68	-48.1	79.4	0.4	-21.3
VR7	1997 7-1	-7.71	-52.7	80.6±2.5	1.0±0.2	
VR7	1996-1-31	-7.56	-45.2	83	0	-20.8
VR8	1997-7-1	-7.27	-49.7	79.3±2.5	0.4±0.1	
VR11	1996-1-31	-7.18	-51.1	74.6	0.3	-20.6
DP18	1996-1-31	-5.57	-35.1	114.2	3.2	-13.1
DP12	1996-1-31	-6.58	-47.3		0.3	
DP15	1996-1-31	-7.66	-47.8	52		-19.7
DP28	1996-1-31	-7.93	-48.6	62.3	0.4	-20.3
DP29	1996-1-31	-7.72	-48.9	41.2	0.1	-18.8
DP29	1997-7-1	-7.87	-50.8	40.6±2.0	0.0±0.2	
VG3	1997-7-1	-7.68	-57.1	78.1±2.5	1.3±0.2	
VG3	1998-6-1	-8.02	-55.1	65.7±2.3		
WN2	1996-1-31	-7.82	-50.4	72	0.3	-19.7
DG 110	1997-7-1	-7.7	-49.5	41.0±2.0	0.0±0.2	
G40171	1998-5-1	-7.2	-42			
G40172	1998-5-1	-7.3	-42			
G40173	1998-5-1	-7.7	-45			
G40175	1997-11-6	-7	-41			
G40175A	1998-5-1	-7.3	-42			
G40175A23M	1997-11-6	-7.1	-39			
G40175A 27M	1998-1-23	-7.2	-39			
G40175A 60M	1998-1-27	-7.2	-39			
G40175A84M	1998-2-3	-7	-38			
G40175B115M	1997-11-6	-7	-40			
G40175C126M	1997-11-12	-7	-40			
G40176	1998-5-1	-7.4	-44			
G40176 42M	1998-2-4	-7.5	-43			
G40176A 119M	1998-2-6	-7.3	-43			
G40176B150M	1998-2-7	-7.3	-46			
G40174147M	1997-9-18	-6.7	-38			
G40177 92M	1998-2-10	-7.3	-45			
G40177B150M	1998-2-18	-7.3	-40			
G40178 120M	1998-2-20	-7.3	-42			
G40178 54M	1998-2-19	-7	-41			
Marnewicks Notch	1997-7-1	-7.79	-54.8		1.6+0.2	
Marnewicks Notch	1996-1-31	-7.24	-45.8		0.5	
Rainfall in DP 25	1998-8-25	-4.25	-25.4			
Rainfall in Parshall	1998-8-25	-5.9	-30.7			
Rainfall in Parshall	1995-12-5	-4.5	-28			
Rainfall in V- keep	1998-8-25	-4.54	-22.4			
Rainfall in VG 3	1998-8-25	-4.21	-25.8			
Rainfall in Wildebeesvlakte	1998-8-25	-6.49	-29.8			
Vermaaks (Partial)	1997-7-1	-7.66	-51.2		0.5±0.1	
Vermaaks Notch	1997-7-1	-7.84	-55.3		1.6±0.2	
Vermaaks Notch	1996-1-31	-7.33	-46.2		0.5	
Calitzdorp hot spring	1996-1-31	-7.53	-46.6	13		-14.5
Calitzdorp hot spring	1997-7-1	-7.36	-49.7			
Toorwater	1996-1-31	-7.08	-48	25.6		-17.3
Warmwaterberg	1996-1-31	-7.57	-46	11		-14.6

Appendix VII(a) Recharge in m^3 based on two-component mixing model

BH	Year	1994	1995	1996	1997	1998	1999	2000	2001	2002	2003*
	P (mm)	411	601	714	430	380	316	446	299	432	188
VR6	Q_r	21642	0	1412	164	0	290	0	1326	4663	1413
	Q_v	1502	10148	4566	7044	10388	15591	23683	33239	19228	3990
VR7	Q_r	25345	7991	10778	0	0	0	0	833	4114	0
	Q_v	3891	31830	14318	26942	23666	33712	34824	37275	50500	12007
VR8	Q_r	10963	0	1621	1169	963	2114	0	1633	881	0
	Q_v	2550	5593	230	3863	6130	7032	26975	14421	9546	3604
VR11	Q_r	7442	0	3129	1056	571	0	59	2641	3101	113
	Q_v	1384	9507	1269	4996	8891	6247	5041	11075	14613	4858
? VR	? Q_r	65392	7991	16940	2388	1534	2405	59	6434	12759	1526
	? Q_v	9327	57078	20383	42845	49075	62582	90522	96010	93887	24460
	? ?	74719	65069	37323	45233	50609	64987	90581	102444	106645	25985
VG3	Q_r	20227	0	412	0	1958	5600	1438	18614	0	0
	Q_v	3447	4373	10190	46771	23796	13782	47374	36952	39948	8509
	?	23674	4373	10602	46771	25754	19382	48813	55565	39948	8509

* Only January to March.

Appendix VII(b) Recharge proportions of the scenarios from two-component model

Scenario	Ranges of ratio	VR6		VR7		VR8		VR11		VG3	
		Q_r/Q_p	Q_v/Q_p	Q_r/Q_p	Q_v/Q_p	Q_r/Q_p	Q_v/Qp	Q_r/Q_p	Q_v/Q_p	Q_r/Q_p	Q_v/Q_p
1	Max	0.380	0.685	0.381	0.388	0.346	0.586	0.354	0.488	0.612	1.473
	Min	0.038	0.009	0.006	0.000	0.002	0.007	0.010	0.018	0.020	0.024
2	Max	0.364	0.688	0.381	0.391	0.346	0.590	0.343	0.494	0.612	1.469
	Min	0.032	0.025	0.076	0.000	0.025	0.003	0.010	0.005	0.016	0.050
3	Max	0.380	0.563	0.381	0.321	0.346	0.489	0.354	0.405	0.612	1.066
	Min	0.038	0.008	0.006	0.000	0.002	0.006	0.010	0.015	0.020	0.017
4	Max	0.540	1.000	0.555	0.560	0.536	0.826	0.527	0.696	0.742	3.356
	Min	0.038	0.009	0.006	0.000	0.002	0.007	0.010	0.018	0.020	0.024
5	Max	0.370	1.000	0.370	0.560	0.335	0.826	0.344	0.696	0.602	3.356
	Min	0.037	0.014	0.006	0.000	0.002	0.009	0.010	0.025	0.020	0.056

Appendix VIII Recharge volumes (m^3) based on two-component model

Scenario 1

Year	VR6		VR7		VR8		VR11		VG3		Peninsula Formation			Nardouw
	Q_r	Q_v	Q_r	Q_v	Q_r	Q_v	Q_r	Q_v	Q_r	Q_v	? Q_r	? Q_v	??	? VG3
1994	21641.6	1502.3	25345.1	3890.5	10963.3	2550.3	7441.5	1384.0	20227.0	3446.6	65391.5	9327.1	74718.6	23673.5
1995	0.0	10036.7	8047.8	31645.1	0.0	5532.3	0.0	9427.7	0.0	4253.0	8047.8	56641.8	64689.6	4253.0
1996	1564.0	4300.3	11220.0	14116.8	1708.6	195.5	3351.5	1214.0	464.9	9945.6	17844.2	19826.7	37670.9	10410.5
1997	168.8	6579.7	593.7	26151.1	1435.2	3537.0	1564.0	4791.7	0.0	45852.5	3761.7	41059.5	44821.2	45852.5
1998	0.0	9572.9	1085.2	22104.6	1254.8	5786.9	936.4	8395.8	1994.8	22978.7	3276.4	45860.3	49136.7	24973.6
1999	434.4	14718.0	689.4	31913.4	2451.0	6547.6	0.0	6102.8	5742.6	13432.7	3574.8	59281.9	62856.7	19175.3
2000	0.0	22346.1	0.0	32175.3	0.0	26163.7	91.5	4847.8	1557.7	46526.9	91.5	85533.0	85624.5	48084.6
2001	1464.0	32056.4	1051.1	34637.3	2004.0	13597.9	2809.1	10487.7	19345.2	36780.5	7328.1	90779.2	98107.4	56125.7
2002	4874.1	18280.0	4343.8	47592.7	1407.5	8803.6	3840.5	13948.1	0.0	39238.7	14465.9	88624.3	103090.2	39238.7
2003	1759.8	3871.0	1105.6	11186.5	0.0	3372.2	142.5	4488.7	0.0	7883.5	3007.8	22918.3	25926.1	7883.5
Total	31906.6	123263.4	53481.7	255413.5	21224.4	76086.9	20177.1	65088.3	49332.2	230338.8	126789.8	519852.1	646641.8	279671.0

Scenario 2

Year	VR6		VR7		VR8		VR11		VG3		Peninsula Formation			Nardouw
	Q_r	Q_v	Q_r	Q_v	Q_r	Q_v	Q_r	Q_v	Q_r	Q_v	? Q_r	? Q_v	??	? VG3
1994	21641.6	1502.3	25345.1	3890.5	10963.3	2550.3	7441.5	1384.0	20227.0	3446.6	65391.5	9327.1	74718.6	23673.5
1995	0.0	10147.8	7990.8	31830.4	0.0	5592.9	0.0	9507.1	0.0	4373.4	7990.8	57078.2	65069.0	4373.4
1996	1412.1	4566.2	10777.7	14317.7	1621.0	230.0	3128.8	1269.2	411.7	10190.1	16939.6	20383.0	37322.7	10601.8
1997	164.0	7044.2	0.0	26941.8	1168.6	3863.2	1055.6	4995.8	0.0	46771.0	2388.1	42845.0	45233.1	46771.0
1998	0.0	10388.2	0.0	23666.1	962.9	6130.3	570.9	8890.8	1957.6	23796.4	1533.9	49075.4	50609.3	25754.0
1999	290.3	15591.3	0.0	33712.3	2114.4	7031.7	0.0	6247.0	5600.0	13781.6	2404.7	62582.2	64986.9	19381.6
2000	0.0	23682.9	0.0	34823.5	0.0	26974.5	59.3	5041.0	1438.3	47374.4	59.3	90521.8	90581.2	48812.7
2001	1326.1	33239.1	833.2	37275.3	1633.4	14421.0	2641.0	11074.7	18613.8	36951.5	6433.7	96010.2	102443.9	55565.3
2002	4662.9	19227.9	4113.8	50500.3	881.1	9545.6	3101.0	14612.7	0.0	39947.6	12758.8	93886.6	106645.4	39947.6
2003	1412.5	3990.4	0.0	12006.6	0.0	3604.3	113.3	4858.3	0.0	8508.6	1525.8	24459.6	25985.4	8508.6
Total	30909.4	129380.3	49060.5	268964.5	19344.8	79943.7	18111.6	67880.7	48248.3	235141.2	117426.3	546169.3	663595.5	283389.6

Appendix ? Recharge volumes (m^3) based on two-component model (continued)

Scenario 3

Year	VR6		VR7		VR8		VR11		VG3		Peninsula Formation			Nardouw
	Q_r	Q_v	Q_r	Q_v	Q_r	Q_v	Q_r	Q_v	Q_r	Q_v	? Q_r	? Q_v	??	?VG3
1994	21066.8	2182.7	24650.3	5604.3	10626.3	3579.8	7225.5	1966.4	19913.4	7763.6	63568.9	13333.2	76902.1	27677.1
1995	0.0	14595.0	7827.9	45621.2	0.0	7771.2	0.0	13404.9	0.0	9633.0	7827.9	81392.2	89220.1	9633.0
1996	1522.7	6259.0	10914.3	20367.7	1656.5	274.8	3254.9	1727.5	457.7	22652.2	17348.4	28628.9	45977.3	23109.9
1997	164.3	9585.4	577.6	37760.7	1391.5	4975.5	1519.1	6823.1	0.0	105026.3	3652.5	59144.7	62797.1	105026.3
1998	0.0	13958.8	1055.8	31943.2	1216.7	8146.4	909.6	11963.9	1964.2	52936.0	3182.2	66012.3	69194.5	54900.2
1999	423.0	21481.0	670.8	46154.8	2377.0	9223.9	0.0	8702.9	5654.6	31125.4	3470.8	85562.6	89033.4	36780.0
2000	0.0	32644.5	0.0	46571.2	0.0	36884.7	88.9	6918.3	1533.8	108448.1	88.9	123018.7	123107.6	109982.0
2001	1426.0	46873.3	1022.8	50175.3	1943.9	19183.9	2729.3	14978.0	19050.2	86245.8	7122.0	131210.5	138332.5	105296.0
2002	4747.9	26758.9	4227.5	69010.3	1365.4	12432.6	3731.9	19934.9	0.0	92695.2	14072.8	128136.7	142209.5	92695.2
2003	1714.4	5670.8	1076.1	16231.0	0.0	4764.5	138.5	6420.2	0.0	18713.9	2928.9	33086.5	36015.4	18713.9
Total	31065.2	180009.4	52023.0	369439.5	20577.4	107237.2	19597.7	92840.1	48574.0	535239.6	123263.3	749526.2	872789.5	583813.7

Scenario 4

Year	VR6		VR7		VR8		VR11		VG3		Peninsula Formation			Nardouw
	Q_r	Q_v	Q_r	Q_v	Q_r	Q_v	Q_r	Q_v	Q_r	Q_v	? Q_r	? Q_v	??	?VG3
1994	31117.8	2182.7	36980.9	5604.3	16971.6	3579.8	11167.9	1966.4	24539.3	7763.6	96238.2	13333.2	109571.4	32303.0
1995	0.0	14595.0	11725.7	45621.2	0.0	7771.2	0.0	13404.9	0.0	9633.0	11725.7	81392.2	93118.0	9633.0
1996	2242.3	6259.0	16324.4	20367.7	2634.4	274.8	5013.3	1727.5	563.4	22652.2	26214.5	28628.9	54843.4	23215.6
1997	241.6	9585.4	862.6	37760.7	2208.4	4975.5	2335.7	6823.1	0.0	105026.3	5648.3	59144.7	64793.0	105026.3
1998	0.0	13958.8	1574.5	31943.2	1927.0	8146.4	1396.2	11963.9	2415.3	52936.0	4897.7	66012.3	70910.0	55351.4
1999	620.1	21481.0	998.8	46154.8	3756.8	9223.9	0.0	8702.9	6949.8	31125.4	5375.8	85562.6	90938.4	38075.2
2000	0.0	32644.5	0.0	46571.2	0.0	36884.7	136.0	6918.3	1884.2	108448.1	136.0	123018.7	123154.7	110332.3
2001	2084.3	46873.3	1518.6	50175.3	3059.8	19183.9	4168.5	14978.0	23389.0	86245.8	10831.3	131210.5	142041.8	109634.8
2002	6929.8	26758.9	6267.6	69010.3	2145.1	12432.6	5687.5	19934.9	0.0	92695.2	21029.9	128136.7	149166.6	92695.2
2003	2498.6	5670.8	1593.1	16231.0	0.0	4764.5	210.8	6420.2	0.0	18713.9	4302.4	33086.5	37388.9	18713.9
Total	45734.6	180009.4	77846.1	369439.5	32703.2	107237.2	30116.0	92840.1	59741.0	535239.6	186399.9	749526.2	935926.1	594980.7

Appendix IX Recharge proportions from three-component model

scenario 1

Borehole	Component	1994	1995	1996	1997	1998	1999	2000	2001	2002	2003
VR6	Q_s'	0.823	0.823	0.934	0.915	0.913	0.914	0.827	0.738	0.602	0.763
	Q_r'	0.176	0.000	0.016	0.002	0.000	0.003	0.000	0.012	0.039	0.074
	Q_v'	0.001	0.177	0.050	0.083	0.087	0.082	0.173	0.251	0.146	0.164
VR7	S	0.177	0.177	0.066	0.085	0.087	0.086	0.173	0.262	0.185	0.237
	Q_s'	0.843	0.788	0.833	0.895	0.927	0.871	0.888	0.867	0.819	0.918
	Q_r'	0.135	0.050	0.074	0.002	0.003	0.002	0.000	0.004	0.017	0.011
	Q_v'	0.022	0.163	0.093	0.103	0.070	0.127	0.112	0.129	0.187	0.072
	S	0.157	0.212	0.167	0.105	0.073	0.129	0.112	0.133	0.204	0.082
VR8	Q_s'	0.852	0.851	0.926	0.942	0.910	0.907	0.722	0.851	0.719	0.811
	Q_r	0.148	0.000	0.073	0.016	0.017	0.025	0.000	0.021	0.015	0.000
	Q_v'	0.000	0.149	0.002	0.042	0.073	0.067	0.278	0.128	0.093	0.189
	S	0.148	0.149	0.074	0.058	0.090	0.093	0.278	0.149	0.107	0.189
VR11	Q_s'	0.875	0.801	0.912	0.933	0.919	0.706	0.833	0.807	1.083	0.896
	Q_r	0.104	0.000	0.062	0.016	0.009	0.000	0.004	0.041	0.055	0.005
	Q_v'	0.022	0.199	0.026	0.051	0.073	0.294	0.163	0.152	0.203	0.099
	S	0.125	0.199	0.088	0.067	0.081	0.294	0.167	0.193	0.259	0.104

Scenario 3

Borehole	Component	1994	1995	1996	1997	1998	1999	2000	2001	2002	2003
VR6	Q_s'	0.830	0.743	0.912	0.877	0.873	0.861	0.748	0.623	0.535	0.689
	Q_r'	0.170	0.000	0.016	0.002	0.000	0.011	0.000	0.011	0.038	0.072
	Q_v'	0.000	0.257	0.072	0.121	0.127	0.127	0.252	0.366	0.214	0.239
	S	0.170	0.257	0.088	0.123	0.127	0.139	0.252	0.377	0.252	0.311
VR7	Q_s'	0.837	0.717	0.794	0.849	0.896	0.815	0.837	0.809	0.736	0.886
	Q_r'	0.131	0.048	0.072	0.002	0.003	0.002	0.000	0.004	0.016	0.010
	Q_v'	0.031	0.234	0.134	0.148	0.101	0.183	0.163	0.187	0.271	0.104
VR8	S	0.163	0.283	0.206	0.151	0.104	0.185	0.163	0.191	0.287	0.114
	Q_s'	0.857	0.791	0.927	0.925	0.881	0.881	0.608	0.800	0.672	0.734
	Q_r'	0.143	0.000	0.070	0.015	0.016	0.025	0.000	0.020	0.019	0.000
	Q_v'	0.000	0.209	0.002	0.059	0.103	0.095	0.392	0.180	0.134	0.266
	S	0.143	0.209	0.073	0.075	0.119	0.119	0.392	0.200	0.154	0.266
VR11	Q_s'	0.869	0.717	0.903	0.912	0.888	0.581	0.764	0.743	0.998	0.853
	Q_r'	0.101	0.000	0.060	0.016	0.008	0.000	0.004	0.039	0.054	0.005
	Q_v'	0.031	0.283	0.037	0.073	0.104	0.419	0.233	0.217	0.291	0.142
	S	0.131	0.283	0.097	0.088	0.112	0.419	0.236	0.257	0.344	0.147

Appendix IX Recharge proportions from three-component model (continued)

Scenario 4

Borehole	Component	1994	1995	1996	1997	1998	1999	2000	2001	2002	2003
VR6	Q_s'	0.745	0.743	0.904	0.876	0.873	0.875	0.748	0.617	0.518	0.656
	Q_r'	0.254	0.000	0.023	0.003	0.000	0.005	0.000	0.017	0.056	0.105
	Q_v'	0.002	0.257	0.072	0.121	0.127	0.120	0.252	0.366	0.214	0.239
	S	0.255	0.257	0.096	0.124	0.127	0.125	0.252	0.383	0.269	0.344
VR7	Q_s'	0.772	0.693	0.758	0.848	0.894	0.814	0.837	0.807	0.728	0.881
	Q_r	0.197	0.073	0.107	0.004	0.005	0.003	0.000	0.006	0.024	0.016
	Q_v'	0.031	0.234	0.134	0.148	0.101	0.183	0.163	0.187	0.271	0.104
	S	0.228	0.307	0.242	0.152	0.106	0.186	0.163	0.193	0.295	0.119
VR8	Q_s'	0.771	0.791	0.885	0.916	0.872	0.866	0.608	0.788	0.673	0.734
	Q_r'	0.229	0.000	0.112	0.024	0.026	0.039	0.000	0.032	0.022	0.000
	Q_v'	0.000	0.209	0.002	0.059	0.103	0.095	0.392	0.180	0.131	0.266
	S	0.229	0.209	0.115	0.084	0.128	0.134	0.392	0.212	0.153	0.266
VR11	Q_s'	0.814	0.717	0.871	0.903	0.883	0.581	0.762	0.722	0.969	0.851
	Q_r'	0.155	0.000	0.092	0.024	0.013	0.000	0.005	0.060	0.082	0.007
	Q_v'	0.031	0.283	0.037	0.073	0.104	0.419	0.233	0.217	0.291	0.142
	S	0.186	0.283	0.129	0.097	0.117	0.419	0.238	0.278	0.373	0.149

Scenario 5

Borehole	Component	1994	1995	1996	1997	1998	1999	2000	2001	2002	2003
VR6	Q_s'	0.827	0.858	0.944	0.931	0.930	0.930	0.861	0.787	0.631	0.797
	Q_r'	0.172	0.000	0.016	0.002	0.000	0.003	0.000	0.011	0.038	0.072
	Q_v'	0.001	0.142	0.040	0.067	0.070	0.066	0.139	0.201	0.117	0.131
	S	0.173	0.142	0.056	0.069	0.070	0.070	0.139	0.213	0.156	0.203
VR7	Q_s'	0.851	0.820	0.853	0.915	0.940	0.896	0.909	0.892	0.856	0.932
	Q_r'	0.131	0.048	0.072	0.002	0.003	0.002	0.000	0.004	0.016	0.011
	Q_v'	0.018	0.131	0.075	0.083	0.056	0.102	0.091	0.104	0.151	0.058
	S	0.149	0.180	0.147	0.085	0.060	0.104	0.091	0.108	0.167	0.068
VR8	Q_s'	0.857	0.878	0.928	0.950	0.924	0.908	0.773	0.875	0.736	0.846
	Q_r'	0.143	0.000	0.070	0.015	0.016	0.034	0.000	0.020	0.014	0.000
	Q_v'	0.000	0.122	0.001	0.034	0.060	0.059	0.227	0.104	0.076	0.154
	S	0.143	0.122	0.072	0.050	0.076	0.092	0.227	0.125	0.090	0.154
VR11	Q_s'	0.882	0.838	0.919	0.943	0.932	0.761	0.864	0.837	1.123	0.915
	Q_r'	0.101	0.000	0.060	0.016	0.008	0.000	0.004	0.039	0.054	0.005
	Q_v'	0.018	0.162	0.021	0.041	0.059	0.239	0.133	0.124	0.165	0.081
	S	0.118	0.162	0.081	0.057	0.068	0.239	0.136	0.163	0.219	0.085

Appendix X Recharge in m^3 from three-component model

Scenario 1

Borehole	Component	1994	1995	1996	1997	1998	1999	2000	2001	2002	2003
VR6	Q_s	100932.1	54178.5	89171.7	77704.4	102124.9	114656.7	110993.7	91682.8	74788.0	18238.5
	Q_r	21614.9	1.5	1565.3	168.6	0.1	435.3	1.3	1465.2	4875.0	1760.5
	Q_v	141.0	11636.0	4738.0	7085.0	9778.0	10319.0	23204.0	31136.0	18163.0	3912.0
	S	21755.9	11637.5	6303.3	7253.6	9778.1	10754.3	23205.3	32601.2	23038.0	5672.5
VR7	Q_s	158148.9	127389.0	126736.8	212546.2	304418.0	271920.9	248041.7	222488.7	210318.5	94075.2
	Q_r	25346.1	8049.0	11221.2	593.8	1085.0	689.1	0.3	1051.5	4343.5	1105.8
	Q_v	4082.0	26285.0	14201.0	24388.0	22932.0	39524.0	31399.0	33204.8	48011.0	7348.0
	S	29428.1	34334.0	25422.2	24981.8	24017.0	40213.1	31399.3	34256.3	52354.5	8453.8
VR8	Q_s	77005.0	33945.7	21766.5	85416.4	68686.7	87366.6	74206.7	82260.0	69472.6	14609.7
	Q_r	13346.0	1.3	1708.5	1435.6	1254.3	2452.4	0.3	2005.0	1408.4	1.3
	Q_v	0.0	5947.0	40.0	3821.0	5518.0	6486.0	28643.0	12361.0	8942.0	3399.0
	S	13346.0	5948.3	1748.5	5256.6	6772.3	8938.4	28643.3	14366.0	10350.4	3400.3
VR11	Q_s	62850.9	44558.4	49501.6	90615.3	100012.5	16137.4	21057.8	55934.0	75066.2	26407.3
	Q_r	7442.1	1.6	3352.4	1565.7	936.5	0.6	91.2	2809.0	3840.8	143.7
	Q_v	1558.0	11050.0	1397.0	4952.0	7934.0	6726.0	4122.0	10560.0	14100.0	2932.0
	S	9000.1	11051.6	4749.4	6517.7	8870.5	6726.6	4213.2	13369.0	17940.8	3075.7

Scenario 3

Borehole	Component	1994	1995	1996	1997	1998	1999	2000	2001	2002	2003
VR6	Q_s	101876.0	48895.3	87070.7	74482.0	97657.7	108015.6	100332.0	77372.0	66521.5	16471.5
	Q_r	20812.0	0.7	1522.3	164.0	0.3	1426.4	1.0	1427.0	4747.5	1714.5
	Q_v	0.0	16920.0	6882.0	10312.0	14245.0	15969.0	33866.0	45485.0	26557.0	5725.0
	S	20812.0	16920.7	8404.3	10476.0	14245.3	17395.4	33867.0	46912.0	31304.5	7439.5
VR7	Q_s	157046.0	116002.0	120788.4	201763.1	294267.8	254347.4	234029.6	207661.2	188898.0	90799.6
	Q_r	24651.0	7828.0	10914.6	577.9	1055.2	670.6	0.4	1022.9	4227.0	1076.4
	Q_v	5880.0	37893.0	20456.0	35187.0	33112.0	57116.0	45411.0	48060.9	69548.0	10653.0
	S	30531.0	45721.0	31370.6	35764.9	34167.2	57786.6	45411.4	49083.8	73775.0	11729.4
VR8	Q_s	77415.3	31540.7	21802.9	83910.3	66481.0	84797.3	62498.2	77257.7	64980.9	13211.9
	Q_r	12935.7	0.3	1656.1	1391.7	1216.0	2377.7	0.8	1943.3	1866.1	0.1
	Q_v	0.0	8353.0	56.0	5371.0	7762.0	9130.0	40351.0	17425.0	12976.0	4798.0
	S	12935.7	8353.3	1712.1	6762.7	8978.0	11507.7	40351.8	19368.3	14842.1	4798.1
VR11	Q_s	62412.8	39898.2	49012.4	88568.9	96674.7	13280.0	19302.3	51504.0	69137.9	25154.0
	Q_r	7225.2	0.8	3254.6	1519.1	910.3	0.0	89.7	2729.0	3732.1	139.0
	Q_v	2213.0	15711.0	1984.0	7045.0	11298.0	9584.0	5879.0	15070.0	20137.0	4190.0
	S	9438.2	15711.8	5238.6	8564.1	12208.3	9584.0	5968.7	17799.0	23869.1	4329.0

Appendix X Recharge in m^3 from three-component model (continued)

Scenario 4

Borehole	Component	1994	1995	1996	1997	1998	1999	2000	2001	2002	2003
VR6	Q_s	91342.3	48894.9	86348.7	74404.9	97657.5	109745	100332	76715.7	64339.9	15687.2
	Q_r	31117.7	1.1	2243.3	241.1	0.5	620.4	1.5	2084.3	6929.1	2498.8
	Q_v	228.0	16920.0	6883.0	10312.0	14245.0	15046.0	33866.0	45484.0	26557.0	5725.0
	S	31345.7	16921.1	9126.3	10553.1	14245.5	15666.4	33867.5	47568.3	33486.1	8223.8
VR7	Q_s	144718	112104	115378	201478	2937478	254019	234029	207165	186855	90282.4
	Q_r	36980.3	11726.0	16324.8	863.0	1575.2	998.6	0.6	1518.7	6268.5	1593.6
	Q_v	5879.0	37893.0	20456.0	35187.0	33113.0	57116.0	45411.0	48060.9	69549.0	10653.0
	S	42859.3	49619.0	36780.8	36050.0	34688.2	58114.6	45411.6	49579.6	75817.5	12246.6
VR8	Q_s	69691.0	31540.6	20821.9	83093.3	65767.9	83417.0	62497.7	76138.9	65062.5	13211.8
	Q_r	20660.0	0.4	2636.1	2208.7	1928.1	3758.0	1.3	3061.1	2145.5	0.2
	Q_v	0.0	8353.0	57.0	5371.0	7763.0	9130.0	40351.0	17426.0	12615.0	4798.0
	S	20660.0	8353.4	2693.1	7579.7	9691.1	12888.0	40352.3	20487.1	14760.5	4798.2
VR11	Q_s	58470.6	39897.8	47251.1	87752.1	96187.8	13280.0	19254.8	50065.0	67182.3	25081.4
	Q_r	11167.4	1.2	5014.9	2335.9	1397.2	0.0	137.2	4168.0	5688.7	211.6
	Q_v	2213.0	15711.0	1985.0	7045.0	11298.0	9584.0	5879.0	15070.0	20136.0	4190.0
	S	13380.4	15712.2	6999.9	9380.9	12695.2	9584.0	6016.2	19238.0	25824.7	4401.6

Scenario 5

Borehole	Component	1994	1995	1996	1997	1998	1999	2000	2001	2002	2003
VR6	Q_s	101493	56441.5	90136.0	79088.6	104030	116686	115536	97826.8	78481.6	19054.9
	Q_r	21067.8	1.5	1522.0	164.4	1.6	423.2	1.3	1426.2	4748.4	1714.1
	Q_v	127.0	9373.0	3817.0	5705.0	7871.0	8302.0	18662.0	25031.0	14596.0	3142.0
	S	21194.8	9374.5	5339.0	5869.4	7872.6	8725.2	18663.3	26457.2	19344.4	4856.1
VR7	Q_s	159623	132642	129757	217237	308852	279541	254088	228925	219707	95525.0
	Q_r	24650.2	7828.9	10916.0	578.7	1055.0	670.3	0.6	1020.9	4228.2	1077.0
	Q_v	3301.0	21252.0	11486.0	19712.0	18528.0	31923.0	25352.0	26799.4	38738.0	5927.0
	S	27951.2	29080.9	22402.0	20290.7	19583.0	32593.3	25352.6	27820.3	42966.2	7004.0
VR8	Q_s	77415.3	35028.2	21825.0	86157.1	69732.7	87396.8	79452.3	84588.4	71157.7	15233.7
	Q_r	12935.7	1.8	1657.0	1391.9	1216.3	3250.2	1.7	1944.6	1366.3	2.3
	Q_v	0.0	4864.0	33.0	3124.0	4510.0	5658.0	23396.0	10093.0	7299.0	2774.0
	S	12935.7	4865.8	1690.0	4515.9	5726.3	8908.2	23397.7	12037.6	8665.3	2776.3
VR11	Q_s	63356.3	46621.4	49857.6	91588.1	101522	17397.0	21832.6	57997.6	77828.0	26965.6
	Q_r	7226.7	0.6	3256.4	1518.9	910.6	1.0	89.4	2729.4	3732.0	138.4
	Q_v	1268.0	8988.0	1137.0	4026.0	6450.0	5466.0	3349.0	8576.0	11447.0	2379.0
	S	8494.7	8988.6	4393.4	5544.9	7360.6	5467.0	3438.4	11305.4	15179.0	2517.4

Appendix XI Recharge rates of the scenarios based on two-component model

Scenario	Year	Rainfall (mm)	Annual recharge (%)		Cumulative recharge (%)	
			Catchment area	Window	Catchment	Window
			10.85 km^2	40.6 km^2	10.85 km^2	40.6 km^2
1	1994	411	1.67	0.45	1.67	0.45
	1995	601	0.99	0.27	1.27	0.34
	1996	714	0.49	0.13	0.95	0.25
	1997	430	0.96	0.26	0.95	0.25
	1998	380	1.19	0.32	0.98	0.26
	1999	316	1.83	0.49	1.08	0.29
	2000	446	1.77	0.47	1.17	0.31
	2001	299	3.02	0.81	1.33	0.35
	2002	432	2.2	0.59	1.42	0.38
	2003	188	1.27	0.34	1.41	0.38
	Average	421.7	1.54	0.41	-	-
2	1994	411	1.67	0.45	1.67	0.45
	1995	601	1	0.27	1.27	0.34
	1996	714	0.48	0.13	0.95	0.25
	1997	430	0.97	0.26	0.95	0.25
	1998	380	1.23	0.33	0.99	0.27
	1999	316	1.89	0.51	1.09	0.29
	2000	446	1.87	0.5	1.2	0.32
	2001	299	3.16	0.84	1.36	0.36
	2002	432	2.27	0.61	1.46	0.39
	2003	188	1.27	0.34	1.45	0.39
	Average	421.7	1.58	0.42	-	-
3	1994	411	1.72	0.46	1.72	0.46
	1995	601	1.37	0.37	1.51	0.4
	1996	714	0.59	0.16	1.13	0.3
	1997	430	1.35	0.36	1.17	0.31
	1998	380	1.68	0.45	1.25	0.33
	1999	316	2.6	0.69	1.4	0.37
	2000	446	2.54	0.68	1.55	0.42
	2001	299	4.26	1.14	1.78	0.48
	2002	432	3.03	0.81	1.91	0.51
	2003	188	1.76	0.47	1.91	0.51
	Average	421.7	2.09	0.56	-	-
4	1994	411	2.46	0.66	2.46	0.66
	1995	601	1.43	0.38	1.85	0.49
	1996	714	0.71	0.19	1.37	0.37
	1997	430	1.39	0.37	1.38	0.37
	1998	380	1.72	0.46	1.43	0.38
	1999	316	2.65	0.71	1.56	0.42
	2000	446	2.54	0.68	1.7	0.45
	2001	299	4.38	1.17	1.92	0.51
	2002	432	3.18	0.85	2.05	0.55
	2003	188	1.83	0.49	2.04	0.55
	Average	421.7	2.23	0.6	-	-

Appendix XII(a) Recharge estimates of the scenario 1 based on three-component model in the Vermaaks River Wellfield in 1994-2003

Borehole	Catchment		Peninsula Form. Window		Elongated zone		[1] Theis radius (Mean)		[1] Theis radius (Minimum)		[1] Cylinder radius	
	10.85 km^2		40.6 km^2		9×0.4 km^2		6375 ~ 40000 m		1368 ~ 4148 m		7959 ~ 24135 m	
	%	mm	%	mm	%	mm	%	mm	%	mm	%	mm
VR6	0.332	14.0	0.089	3.7	1.001	42.2	0.002	0.1	0.003	0.1	0.102	4.3
VR7	0.666	28.1	0.178	7.5	2.008	84.7	0.004	0.1	0.006	0.3	0.204	8.6
VR8	0.216	9.1	0.058	2.4	0.651	27.4	0.001	0.0	0.002	0.1	0.066	2.8
VR11	0.187	7.9	0.050	2.1	0.563	23.8	0.001	0.0	0.002	0.1	0.057	2.4
Total	1.401	59.1	0.374	15.8	4.223	178.1	0.007	0.3	0.013	0.5	0.428	18.1

[1] Xu *et al.* 2002

Appendix XII(b) Recharge estimates of the scenarios in the Vermaaks River Wellfield from 1994 to 2003 based on cumulative method

Model	Scenario	Catchment		Peninsula Form. Window		Elongated zone		[1] Theis radius (Mean)		[1] Theis radius (Min.)		[1] Cylinder radius	
		10.85 km^2		40.6 km^2		9×0.4 km^2		6375 ~ 40000 m		1368 ~ 4148 m		7959 ~ 24135 m	
		%	mm	%	mm	%	mm	%	mm	%	mm	%	mm
Three-component	1	1.401	59.1	0.374	15.8	4.223	178.1	0.007	0.3	0.013	0.5	0.428	18.1
	3	1.891	79.7	0.505	21.3	5.700	240.4	0.010	0.4	0.017	0.7	0.578	24.4
	4	2.027	85.5	0.542	22.8	6.110	257.6	0.011	0.5	0.018	0.8	0.620	26.1
	5	1.182	49.8	0.316	13.3	3.563	150.2	0.006	0.3	0.011	0.5	0.362	15.2
Two-component	1	1.413	59.6	0.378	15.9	4.259	179.6	0.007	0.3	0.432	18.2	0.013	0.5
	2	1.450	61.1	0.388	16.3	4.370	184.3	0.008	0.3	0.443	18.7	0.013	0.6
	3	1.907	80.4	0.510	21.5	5.748	242.4	0.010	0.4	0.583	24.6	0.017	0.7
	4	2.045	86.2	0.547	23.1	6.164	259.9	0.011	0.5	0.626	26.4	0.018	0.8
	5	1.216	51.3	0.325	13.7	3.666	154.6	0.006	0.3	0.372	15.7	0.011	0.5

[1] Xu *et al.* 2002

Appendix XIII Genetic types of groundwater regime

Type	Characteristics	Typical model
Climatic Rainfall-infiltration	Distribution: unconfined semiarid. There are good permeabilities in unsaturation zone. The water level fluctuation is in phase that of rainfall or slightly delayed. Methods: CRD, RIB (Xu amd Beekman, 2003) Case study: Karoo, G36441. (Kirchner et al., 1991) (Model from Fang et al. 1996)	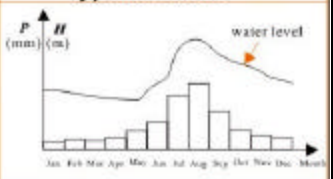
Evaportranpiration	Distribution: arid or semiarid plain. The water level is influenced by evapotranspiration. Groundwater flow is very slow. The range of water level is small. Method: Water Balance, Numerical Simulation. (Model from Fang et al. 1996)	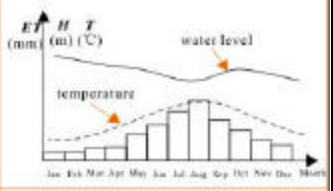
Abstraction	Distribution: water abstraction area. The water level is influenced by abstraction. The water level will slightly increase or decline with rainfall. Method : Numerical Simulation,CRD, RIB. (Model from Fang et al. 1996)	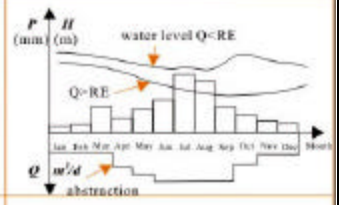
Runoff	Distribution: highly permeable aquifer. Recharge area is large. The low permeable layer occurs between unsatuated and saturated zones. Water level fluctuations is small. The peak water level occurs with a certain time lag of rainfall. Method: Water Balance,Numerical Simulation (Model from Fang et al. 1996)	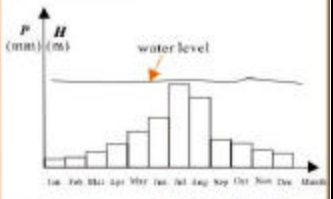
Hydrolic	Distribution: In vicinity of surface water. Groundwater and surface water are hydraulically connected. Surface water level is higher than that of groundwater. Groundwater level relates to level, flux of surface water. Method: Numerical Simulation (Model from, Fang et al. 1996)	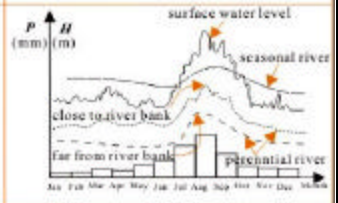
Irrigation	Distribution: Irrigation area. Soil cover with low permeability is thin. Water level relates to period and volume of irrigation. Method: Numerical Simulation (Model from Fang et al. 1996)	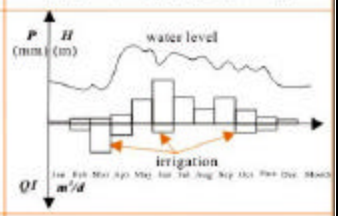
Frozen	Distribution: Frozen area. A large water fluctuation occurs in aquifer above frozen layer, small fluctuation in the lower aquifer. Method: Water balance, Numerical Simulation (Model from Fang et al. 1996)	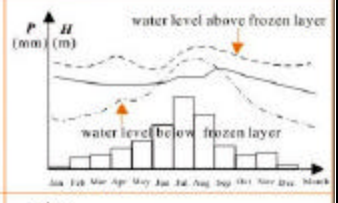
Leakage	Distribution: Aquifer and aquitard occur alternately. Leakage occurs when water level in production aquifer is lower than that of adjacent aquifer. Method: Numerical SimulationWater balance. (Model from Fang et al. 1996)	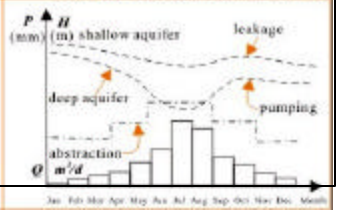

Appendix XIV (a) Recharge rate from the impact of preceding rainfall

Period	Date	P (mm)	WL (m)	? H (m)	? ? H (m)	$x_{a,t-1}$ (mm)	x_{s1} (mm)	RE (%)	RE (mm)
1	1998-11-30	30	5						
	1998-12-30	50	5.42	0.42		1.27			
	1999-1-30	9	5.99	0.57	0.99	2.17	12.45	7.95	7.08
2	1999-2-28	100	5.54						
	1999-3-30	31	5.62	0.08		4.24			
	1999-4-30	32	5.65	0.03		1.49			
	1999-5-30	45	5.66	0.01		1.42			
	1999-6-30	20	5.81	0.15		1.97	10.05		
	1999-7-30	28	6.29	0.48	0.75	0.93	38.05	1.97	5.05
3	1999-8-30	33	5.92						
	1999-9-30	37	5.98	0.06		1.4			
	1999-10-30	22	6.08	0.1		1.63			
	1999-11-30	18	6.17	0.09		1			
	1999-12-30	34	6.28	0.11		0.81	6.31		
	2000-1-30	40	6.36	0.08	0.44	1.48	46.31	0.95	1.75
4	2000-2-28	40	5.84						
	2000-3-30	69	6.09	0.25		1.7			
	2000-4-30	17	6.47	0.38		3	5.54		
	2000-5-30	5	6.56	0.09	0.72	0.85	10.54	6.87	9
5	2000-7-30	5	5.1						
	2000-8-30	8	5.27	0.17		0.21			
	2000-9-30	28	5.3	0.03	0.2	0.35	28.56	0.69	0.28
6	2000-11-30	150	4.2						
	2000-12-30	35	5.03	0.83		6.36			
	2001-1-30	15	5.13	0.1		1.75			
	2001-2-28	20	5.24	0.11		0.71			
	2001-3-30	10	5.34	0.1		0.88	10.16		
	2001-4-30	17	5.5	0.16	1.3	0.46	27.16	4.79	2.97
7	2001-5-30	7	5.17						
	2001-6-30	5	5.25	0.08		0.3			
	2001-7-30	40	5.32	0.07		0.22	2.23		
	2001-8-30	17	7.26	1.94	2.09	1.71	19.23	10.87	7.5
8	2001-9-30	60	6.95						
	2001-10-30	55	7.41	0.46		2.54			
	2001-11-30	53	7.46	0.05		2.44	7.33		
	2001-12-30	0	7.6	0.14	0.66	2.35	7.33	8.96	15.05

Appendix XIV (b) Recharge rate from the impact of preceding rainfall on spring flux

Period	Date	Flow ($\ell \cdot s^{-1}$)	Rainfall (mm)	Flow (mm)	? H (mm)	? ? H (mm)	$x_{a,t-1}$	x_{s1}	RE (%)
1	1997-2-28	5.6	13	1.25					
	1997-3-30	9.4	57	2.10	0.85		0.55		
	1997-4-30	10.3	87	2.30	0.20		2.44		
	1997-5-30	14.3	100	3.19	0.89		3.79		
2	1997-6-30	15.5	31	3.44	0.26	2.20	4.40	42.18	5.21
	1998-4-30	4.5	32	1.00					
	1998-5-30	5.6	45	1.25	0.25		1.36		
	1998-6-30	6.3	20	1.40	0.16		1.97		
	1998-7-30	7.0	28	1.56	0.16	0.56	0.93	32.25	1.73
3	1999-3-30	1.8	12	0.40					
	1999-4-30	3.4	26	0.76	0.36		0.51		
	1999-5-30	4.5	42	1.00	0.25	0.60	1.12	43.63	1.38
	1999-6-3	4.5	10	1.00	0.00		1.83		
	1999-7-30	4.5	37	1.00	0.00		0.50		
	1999-8-30	4.5	33	1.00	0.00		1.59		
	1999-9-30	5.6	37	1.25	0.25	0.85	1.47	44.02	1.92

Appendix XV The estimated recharge rate in the Kammanassie area

Initial order								Ascending order			
Item	Method	Scenario	Area (km^2)	S (‰)	Addition condition	RE (%)	RE (mm)	Item	RE (%)	Item	RE (mm)
1	Two-component	Scenario 1	10.85		Annual Average	1.54	6.49	39	0.24	39	1.07
2	Two-component	Scenario 2	10.85		Annual Average	1.58	6.66	36	0.27	36	1.21
3	Two-component	Scenario 3	10.85		Annual Average	2.09	8.81	33	0.30	33	1.45
4	Two-component	Scenario 4	10.85		Annual Average	2.23	9.40	26	0.32	30	1.94
5	Two-component	Scenario 1	10.85		Cumulative	1.41	5.95	22	0.33	27	2.88
6	Two-component	Scenario 2	10.85		Cumulative	1.45	6.11	23	0.37	13	4.98
7	Two-component	Scenario 3	10.85		Cumulative	1.91	8.05	18	0.38	9	5.13
8	Two-component	Scenario 4	10.85		Cumulative	2.04	8.60	19	0.39	40	5.46
9	Two-component	Scenario 5	10.85		Cumulative	1.22	5.13	14	0.41	10	5.91
10	Three-component	Scenario 1	10.85		Cumulative	1.40	5.91	15	0.42	5	5.95
11	Three-component	Scenario 3	10.85		Cumulative	1.89	7.97	24	0.51	6	6.11
12	Three-component	Scenario 4	10.85		Cumulative	2.03	8.55	20	0.51	37	6.13
13	Three-component	Scenario 5	10.85		Cumulative	1.18	4.98	25	0.54	1	6.49
14	Two-component	Scenario 1	40.60		Annual Average	0.41	17.3	21	0.55	2	6.66
15	Two-component	Scenario 2	40.60		Annual Average	0.42	17.7	16	0.56	34	7.27
16	Two-component	Scenario 3	40.60		Annual Average	0.56	23.6	17	0.60	48	7.69
17	Two-component	Scenario 4	40.60		Annual Average	0.60	25.3	30	0.61	77	7.7
18	Two-component	Scenario 1	40.60		Cumulative	0.38	16.02	27	0.76	76	7.8
19	Two-component	Scenario 2	40.60		Cumulative	0.39	16.45	73	0.81	11	7.97
20	Two-component	Scenario 3	40.60		Cumulative	0.51	21.51	13	1.18	75	8.0
21	Two-component	Scenario 4	40.60		Cumulative	0.55	23.19	9	1.22	7	8.05
22	Two-component	Scenario 5	40.60		Cumulative	0.33	13.70	40	1.22	12	8.55
23	Three-component	Scenario 1	40.60		Cumulative	0.37	15.80	37	1.37	8	8.60
24	Three-component	Scenario 3	40.60		Cumulative	0.51	21.30	10	1.40	3	8.81
25	Three-component	Scenario 4	40.60		Cumulative	0.54	22.80	5	1.41	4	9.40
26	Three-component	Scenario 5	40.60		Cumulative	0.32	13.30	6	1.45	31	9.69
27	CWD-CRD	G40171		0.1	V-notch	0.76	2.88	34	1.52	44	10.17
28	CWD-CRD	G40171		0.5	V-notch	3.78	14.31	1	1.54	45	10.31
29	CWD-CRD	G40171		1	V-notch	7.56	28.62	2	1.58	42	10.69
30	CWD-CRD	G40171		0.1	Purification	0.61	1.94	77	1.63	46	10.83
31	CWD-CRD	G40171		0.5	Purification	3.05	9.69	76	1.65	41	10.88
32	CWD-CRD	G40171		1	Purification	6.10	19.37	75	1.68	43	12.11
33	CWD-CRD	G40171		0.1	Wildebeevlakte	0.30	1.45	11	1.89	38	12.27
34	CWD-CRD	G40171		0.5	Wildebeevlakte	1.52	7.27	7	1.91	26	13.30
35	CWD-CRD	G40171		1	Wildebeevlakte	3.04	14.54	48	1.94	67	13.31
36	CWD-CRD	G40171		0.1	Parshall	0.27	1.21	12	2.03	22	13.70
37	CWD-CRD	G40171		0.5	Parshall	1.37	6.13	8	2.04	28	14.31
38	CWD-CRD	G40171		1	Parshall	2.74	12.27	3	2.09	63	14.35
39	CWD-CRD	VG15		0.1	Parshall	0.24	1.07	44	2.14	64	14.38
40	CWD-CRD	VG15		0.5	Parshall	1.22	5.46	45	2.17	35	14.54

Appendix XV The estimated recharge rate in the Kammanassie area (continued)

Initial order								Ascending order			
Item	Method	Scenario	Area (km^2)	S (‰)	Addition condition	RE (%)	RE (mm)	Item	RE (%)	Item	RE (mm)
41	CWD-CRD	VG15		1	Parshall	2.43	10.88	4	2.23	59	15.19
42	RIB	VR6	10.85	1		2.25	10.69	42	2.25	68	15.29
43	RIB	VR7	10.85	1		2.55	12.11	46	2.28	66	15.34
44	RIB	VR8	10.85	1		2.14	10.17	72	2.42	47	15.4
45	RIB	VR11	10.85	1		2.17	10.31	41	2.43	65	15.72
46	RIB	Mean		1		2.28	10.83	43	2.55	23	15.80
47	Preceding Rain	Vermaaks	10.85	1		3.88	15.39	38	2.74	74	15.80
48	Preceding Rain	Vermaaks	10.85	0.5		1.94	7.69	35	3.04	49	15.83
49	CTR-CTF	Vermaaks	10.85		Parshall	3.70	15.83	31	3.05	18	16.02
50	CTR-CTF	Vermaaks	10.85		Wildebeesvlakte	3.54	16.82	74	3.30	61	16.09
51	CTR-CTF	Vermaaks	10.85		V-notch	4.77	17.97	65	3.31	54	16.34
52	CTR-CTF	Vermaaks	10.85		Voorzorg	4.88	16.79	64	3.36	19	16.45
53	CTR-CTF	Vermaaks	10.85		Dorekloof	5.59	16.93	60	3.53	60	16.77
54	CTR-CTF	Marnewicks	25.3		Parshall	3.82	16.34	50	3.54	52	16.79
55	CTR-CTF	Marnewicks	25.3		Wildebeesvlakte	3.65	17.34	59	3.55	50	16.82
56	CTR-CTF	Marnewicks	25.3		V-notch	4.93	18.58	55	3.65	53	16.9
57	CTR-CTF	Marnewicks	25.3		Voorzorg	5.05	17.37	49	3.70	69	17.24
58	CTR-CTF	Marnewicks	25.3		Dorekloof	5.76	17.44	28	3.78	14	17.29
59	CTR-CTF	Before flood	10.85		Parshall	3.55	15.19	54	3.82	55	17.34
60	CTR-CTF	Before flood	10.85		Wildebeesvlakte	3.53	16.77	67	3.87	57	17.4
61	CTR-CTF	Before flood	10.85		V-notch	4.27	16.09	47	3.88	58	17.44
62	CTR-CTF	Before flood	10.85		Voorzorg	5.38	18.51	71	3.93	15	17.71
63	CTR-CTF	Before flood	10.85		Dorekloof	4.74	14.35	70	3.97	51	17.97
64	CTR-CTF	After foold	10.85		Parshall	3.36	14.38	69	4.03	62	18.5
65	CTR-CTF	After foold	10.85		Wildebeesvlakte	3.31	15.72	66	4.07	56	18.58
66	CTR-CTF	After foold	10.85		V-notch	4.07	15.34	61	4.27	71	18.67
67	CTR-CTF	After foold	10.85		Voorzorg	3.87	13.31	79	4.52	70	18.9
68	CTR-CTF	After foold	10.85		Dorekloof	5.05	15.29	78	4.72	32	19.4
69	CTR-CTF	Runoff removed	10.85		Parshall	4.03	17.24	63	4.74	72	20.98
70	CTR-CTF	Runoff removed	25.3		Wildebeesvlakte	3.97	18.86	80	4.75	73	21.0
71	CTR-CTF	Runoff removed	36.2		Wildebeesvlakte	3.93	18.7	51	4.77	24	21.30
72	Preceding Spring	Vermaaks	10.85			2.42	21.0	52	4.88	79	21.47
73	Preceding Spring	Vermaaks	10.85			0.81	21.0	56	4.93	20	21.5
74	WB					3.30	15.8	57	5.05	78	22.4
75	Integrated	Total factor				1.68	8.0	68	5.05	80	22.56
76	Integrated	Domination factors				1.65	7.8	62	5.38	25	22.80
77	Integrated	Integrated				1.63	7.7	53	5.59	21	23.19
78	Integrated	Total factor				4.72	22.4	58	5.76	16	23.6
79	Integrated	Domination factors				4.52	21.5	32	6.10	17	25.3
80	Integrated	Integrated				4.75	22.6	29	7.56	29	28.62

Appendix XVI Results based on water balance approach

Unit	Station	C_s	C_v	MAP (mm)	Runoff (mm)	Ev-Initial (mm)	Actual EV (mm)	Re $mm \cdot a^{-1}$	RE %
Unit1	0107 510	0.25	0.15	238.0	0.1	178.3	237.1	0.7	0.3
Unit1	0108 311	0.30	0.15	238.2	0.1	171.7	236.8	1.3	0.5
Unit1	0107 869	0.30	0.07	179.6	0.0	133.8	179.1	0.5	0.3
Unit2	0063 718	0.35	0.30	369.6	8.6	223.7	337.0	24.0	6.5
Unit2	0084 059	0.25	0.10	269.1	0.4	204.7	266.7	2.0	0.7
Unit2	0084 159	0.30	0.20	240.7	0.0	163.8	230.9	9.7	4.0
Unit3	0062 379	0.25	0.65	830.6	113.2	393.0	620.9	96.5	11.6
Unit3	0062 444	0.25	0.40	439.3	10.6	261.0	380.6	48.1	10.9
Unit4	0022 368	0.20	0.70	1002.7	203.2	486.6	756.1	43.4	4.3
Unit4	0022 440	0.20	0.35	780.7	95.5	477.8	662.2	23.0	2.9
Unit4	0022 038	0.20	0.45	752.6	78.5	455.0	652.5	21.7	2.9
Unit4	0022 521	0.20	0.40	593.5	51.4	363.0	511.7	30.5	5.1
Unit4	0041 836	0.20	0.30	461.3	20.3	315.3	429.1	11.9	2.6
Unit5	0021 621	0.20	0.35	704.2	66.6	432.7	599.6	38.0	5.4
Unit5	0021 778	0.20	0.60	1052.0	173.6	550.5	828.6	49.8	4.7
Unit5	0021 806	0.25	0.80	1536.4	316.8	663.4	1097.6	122.0	7.9
Unit5	0021 809	0.20	0.70	1488.9	399.0	649.9	1013.9	75.9	5.1
Unit5	0021 838	0.20	0.75	2063.0	531.5	897.2	1421.5	109.9	5.3
Unit5	0022 113	0.20	0.65	809.3	104.2	415.8	636.0	69.1	8.5
Unit5	0022 116	0.20	0.75	1842.1	450.0	795.3	1254.6	137.4	7.5
Unit5	0022 148	0.20	0.65	2020.7	542.2	878.9	1349.8	128.7	6.4
Unit5	0022 204	0.20	0.75	869.9	126.9	448.6	707.9	35.1	4.0
Unit5	0005 545	0.20	0.60	558.3	24.7	323.6	485.0	48.6	8.7
Unit5	0005 612	0.20	0.75	1264.2	261.2	577.8	911.5	91.5	7.2
unit6	0004 702	0.20	0.60	592.7	34.4	325.9	490.6	67.7	11.4
unit6	0004 723	0.20	0.60	922.7	139.0	491.6	740.0	43.8	4.7
unit6	0004 797	0.20	0.60	584.7	30.5	327.1	492.4	61.8	10.6
unit6	0004 826	0.20	0.60	710.9	65.5	396.3	596.6	48.8	6.9
unit6	0005 034	0.20	0.60	664.7	69.8	355.4	535.0	59.9	9.0
Unit7	0042 292	0.25	0.50	542.5	26.7	328.1	494.5	21.3	3.9
Unit7	0042 355	0.25	0.50	581.3	45.2	333.6	502.4	33.8	5.8
Unit7	0042 357	0.25	0.55	482.2	17.1	279.0	426.9	38.2	7.9
Unit7	0042 415	0.25	0.55	609.7	43.0	349.8	535.4	31.3	5.1
Unit7	0042 532?	0.25	0.65	1073.3	206.5	488.3	769.8	97.1	9.0
Unit7	0042 588	0.25	0.55	524.3	32.3	311.8	477.5	14.4	2.8
Unit7	0043 239	0.25	0.20	286.7	3.9	198.4	268.6	14.2	5.0
Unit8	0005 640	0.30	0.65	987.1	144.5	448.1	727.0	115.7	11.7
Unit8	0005 730	0.25	0.65	1095.6	176.5	497.3	783.6	135.5	12.4
Unit8	0005 771	0.25	0.65	1115.9	182.7	526.0	828.8	104.5	9.4
Unit8	0005 880	0.25	0.65	1079.1	192.8	489.8	771.8	114.5	10.6
Unit8	0006 065	0.25	0.75	1604.8	312.6	715.7	1162.1	130.0	8.1
Unit8	0006 214	0.20	0.50	792.5	108.5	420.2	612.2	71.9	9.1
Unit8	0022 504	0.20	0.30	735.8	83.9	428.0	582.7	69.2	9.4
Unit8	0022 539	0.30	0.50	611.3	41.8	321.0	498.1	71.3	11.7
Unit8	0022 792	0.35	0.25	287.0	0.4	192.2	283.7	2.9	1.0

Appendix XVI Results based on water balance approach (continued)

Unit	Station	C_s	C_v	MAP (mm)	Runoff (mm)	Ev-Initial (mm)	Actual EV (mm)	Re $mm \cdot a^{-1}$	RE %
Unit8	0022 803	0.30	0.25	237.3	0.0	165.6	236.4	0.9	0.4
Unit9	0007 311	0.25	0.20	367.1	0.5	267.4	364.0	2.7	0.7
Unit9	0008 136	0.20	0.20	387.4	0.3	287.1	376.7	10.4	2.7
Unit9	0008 782	0.25	0.40	682.8	18.4	451.5	658.1	6.3	0.9
Unit9	0023 070	0.25	0.25	235.0	0.0	169.8	234.1	0.9	0.4
Unit9	0023 218	0.25	0.25	261.9	0.0	187.8	258.9	3.0	1.2
Unit9	0023 602	0.30	0.20	274.5	0.0	192.3	271.1	3.5	1.3
Unit9	0023 611	0.25	0.40	494.2	9.5	322.5	470.4	14.3	2.9
Unit9	0023 706	0.25	0.35	392.1	0.0	266.7	382.4	9.8	2.5
Unit9	0024 684	0.30	0.20	293.3	0.0	205.5	289.8	3.5	1.2
Unit9	0025 162	0.45	0.05	132.4	0.0	88.7	131.2	1.2	0.9
Unit9	0025 270	0.15	0.45	764.4	39.5	489.7	678.9	46.0	6.0
Unit9	0025 414	0.30	0.20	280.9	0.0	196.8	277.5	3.4	1.2
Unit9	0025 599	0.20	0.50	999.0	94.6	606.5	885.3	19.0	1.9
Unit9	0026 240	0.20	0.40	643.1	14.7	408.3	575.9	52.5	8.2
Unit9	0026 510	0.20	0.50	635.6	11.8	403.6	589.1	34.7	5.5
Unit9	0026 824	0.30	0.10	232.0	0.0	170.3	230.7	1.3	0.6
Unit10	0007 699?	0.25	0.35	482.1	3.6	326.8	468.4	10.1	2.1
Unit10	0008 367	0.30	0.30	322.4	0.0	217.0	314.9	7.6	2.3
Unit10	0023 629	0.30	0.20	256.6	0.0	179.1	251.3	5.2	2.0
Unit10	0024 146	0.30	0.20	266.3	0.0	183.9	258.0	8.3	3.1
Unit11	0001 517	0.30	0.45	436.3	4.1	260.8	398.4	33.8	7.7
Unit11	0002 256	0.30	0.40	518.2	14.3	318.6	479.2	24.7	4.8
Unit11	0002 456	0.30	0.50	522.9	13.2	311.5	483.4	26.4	5.1
Unit11	0002 639	0.30	0.40	501.5	8.7	301.6	453.7	39.2	7.8
Unit11	0002 885	0.30	0.40	484.7	3.1	297.1	446.9	34.7	7.2
Unit11	0003 032	0.30	0.40	448.5	1.7	263.8	396.7	50.1	11.2
Unit11	0003 192	0.30	0.40	404.5	2.1	245.6	369.4	33.0	8.2
Unit11	0006 167	0.25	0.55	928.9	105.1	519.7	794.2	29.7	3.2
Unit11	0006 343	0.30	0.50	478.2	12.7	263.9	409.4	56.0	11.7
Unit11	0006 428	0.30	0.50	532.7	20.4	288.9	448.2	64.0	12.0
Unit11	0006 733	0.30	0.50	524.2	10.8	289.2	448.8	64.6	12.3
Unit12	0009 565	0.30	0.30	454.4	2.8	301.9	440.2	11.4	2.5
Unit12	0010 575	0.30	0.40	442.2	0.1	274.3	413.2	28.9	6.5
Unit12	0010 742	0.30	0.30	424.9	0.1	279.5	407.6	17.3	4.1
Unit12	0011 065	0.30	0.30	441.5	0.5	273.8	399.3	41.6	9.4
Unit12	0011 067	0.30	0.30	370.8	0.1	231.7	337.8	32.9	8.9
Unit12	0011 132	0.30	0.30	430.3	0.1	273.5	398.9	31.3	7.3
Unit12	0011 451	0.30	0.35	418.4	0.1	255.9	379.3	39.0	9.3
Unit12	0011 617	0.30	0.30	354.8	0.0	229.5	334.7	20.2	5.7
Unit13	0025 451	0.40	0.05	183.4	0.0	127.9	182.6	0.8	0.4
Unit13	0025 484	0.35	0.10	104.9	0.0	74.1	103.8	1.1	1.1
Unit13	0045 630	0.40	0.05	149.3	0.0	103.7	148.1	1.2	0.8
Unit13	0046 479	0.40	0.05	296.7	0.3	205.3	293.7	2.7	0.9
Unit13	0046 809	0.40	0.05	221.5	0.0	153.3	218.8	2.7	1.2

Appendix XVI Results based on water balance approach (continued)

Unit	Station	C_s	C_v	MAP (mm)	Runoff (mm)	Ev-Initial (mm)	Actual EV (mm)	Re $mm \cdot a^{-1}$	RE %
Unit13	0046 898	0.40	0.05	258.2	0.0	178.0	254.1	4.2	1.6
Unit13	0047 205	0.40	0.10	258.4	0.0	175.9	255.2	3.1	1.2
Unit13	0047 567	0.40	0.10	265.1	0.0	181.9	264.0	1.1	0.4
Unit13	0047 716	0.30	0.20	421.5	0.5	288.1	404.2	16.8	4.0
Unit13	0048 043	0.40	0.10	163.5	0.0	112.2	162.8	0.7	0.4
Unit13	0048 083	0.40	0.10	415.2	0.4	280.3	407.6	7.2	1.7
Unit13	0048 406	0.40	0.15	224.5	0.0	147.2	217.1	7.5	3.3
Unit13	0048 564	0.35	0.15	506.2	1.8	343.2	490.1	14.3	2.8
Unit13	0048 624	0.35	0.15	553.5	4.0	375.2	535.9	13.6	2.5
Unit13	0049 060	0.40	0.15	316.2	0.0	202.0	298.4	17.8	5.6
Unit13	0049 868	0.40	0.05	197.7	0.0	136.2	194.5	3.2	1.6
Unit13	0050 058	0.40	0.05	235.2	0.0	162.1	231.4	3.8	1.6
Unit13	0050 205	0.40	0.10	233.1	0.0	158.7	230.3	2.8	1.2
Unit13	0050 745	0.40	0.10	270.8	0.0	184.4	267.6	3.3	1.2
Unit14	0026 215	0.35	0.10	165.7	0.0	117.5	164.6	1.1	0.7
Unit14	0027 302	0.35	0.10	188.7	0.0	132.1	185.2	3.5	1.8
Unit14	0028 055	0.20	0.45	806.8	42.9	503.1	721.9	42.0	5.2
Unit14	0028 083	0.25	0.45	769.5	36.6	476.3	706.2	26.7	3.5
Unit14	0028 415	0.20	0.45	992.8	97.1	594.0	852.5	43.2	4.4
Unit14	0028 536	0.25	0.40	642.5	12.7	402.1	586.4	43.4	6.8
Unit14	0029 168	0.25	0.15	260.0	0.0	193.7	257.1	2.9	1.1
Unit14	0029 211	0.30	0.15	243.2	0.0	169.6	233.5	9.7	4.0
Unit14	0029 258	0.25	0.35	495.6	0.4	332.2	474.1	21.1	4.3
Unit14	0029 556	0.25	0.25	414.3	0.9	275.6	380.0	33.4	8.1
Unit14	0029 821	0.30	0.20	339.0	0.0	226.2	317.3	21.7	6.4
Unit14	0030 073	0.30	0.20	385.2	0.4	259.0	363.4	21.5	5.6
Unit14	0030 088	0.20	0.50	1049.3	87.8	634.7	926.5	35.0	3.3
Unit14	0030 219	0.30	0.15	298.5	0.0	214.9	295.7	2.8	0.9
Unit14	0030 493	0.30	0.30	419.5	0.0	275.9	400.4	19.1	4.5
Unit14	0030 764	0.30	0.30	407.9	0.0	269.3	390.9	17.0	4.2
Unit14	0047 359	0.35	0.10	190.9	0.0	132.1	185.1	5.8	3.0
Unit14	Wildebeevlakte.)	0.25	0.45	479.5	20.1	308.8	448.2	15.8	3.3
Unit15	0012 220	0.35	0.50	460.6	0.5	251.5	402.2	57.9	12.6
Unit15	0028 407	0.25	0.15	243.8	0.0	181.0	240.7	3.1	1.3
Unit15	0028 748	0.25	0.35	756.0	33.1	478.9	686.3	36.6	4.8
Unit15	0028 771	0.25	0.35	490.3	1.8	332.4	476.7	11.8	2.4
Unit15	0028 775	0.30	0.55	950.4	83.7	491.9	774.9	91.8	9.7
Unit15	0030 090	0.30	0.55	892.9	58.5	470.6	741.5	92.9	10.4
Unit15	0030 265	0.30	0.65	1099.3	124.6	568.9	923.4	51.3	4.7
Unit16	0030 584	0.30	0.30	437.5	0.7	288.8	421.2	15.6	3.6
Unit16	0031 361	0.30	0.15	256.0	0.6	178.5	246.2	9.1	3.6
Unit16	0031 782	0.30	0.15	286.7	0.0	200.8	276.8	9.8	3.4
Unit16	0032 275	0.30	0.15	301.7	0.1	213.8	296.3	5.3	1.8
Unit16	0032 408	0.30	0.25	444.0	0.7	297.6	426.9	16.4	3.7
Unit16	0032 503	0.30	0.20	602.3	7.1	411.3	580.0	15.2	2.5

Appendix XVI Results based on water balance approach (continued)

Unit	Station	C_s	C_v	MAP (mm)	Runoff (mm)	Ev-Initial (mm)	Actual EV (mm)	Re $mm \cdot a^{-1}$	RE %
Unit16	0032 640	0.30	0.10	325.7	0.0	235.4	320.6	5.1	1.6
Unit16	0032 894	0.30	0.35	554.5	5.6	356.2	527.7	21.2	3.8
Unit17	0016 484	0.25	0.55	941.3	81.4	503.3	769.1	90.8	9.6
Unit17	0016 782	0.30	0.65	865.6	55.9	459.5	745.8	63.9	7.4
Unit17	0017 452	0.25	0.50	669.7	15.3	411.0	619.5	34.9	5.2
Unit17	0017 582	0.25	0.60	646.1	20.0	364.7	566.1	60.1	9.3
Unit17	0017 723	0.25	0.40	511.8	1.9	339.7	495.1	14.9	2.9
Unit17	0030 283	0.25	0.40	423.0	0.3	278.2	405.8	16.9	4.0
Unit17	0030 297	0.20	0.40	1120.7	132.8	675.4	952.8	35.1	3.1
Unit17	0030 323	0.20	0.45	779.4	33.7	498.8	715.3	30.4	3.9
Unit17	0030 390	0.20	0.40	882.6	57.1	560.4	790.4	35.0	4.0
Unit17	0030 446	0.20	0.40	839.3	47.1	525.2	740.8	51.4	6.1
Unit17	0030 775	0.20	0.45	840.0	48.8	523.8	751.6	39.6	4.7
Unit17	0031 197	0.20	0.40	557.9	5.6	372.6	525.5	26.9	4.8
Unit17	0031 237	0.20	0.45	990.8	89.6	597.1	857.0	44.2	4.5
Unit17	0031 438	0.20	0.40	533.4	5.6	357.5	504.2	23.5	4.4
Unit17	0031 507	0.20	0.45	1091.7	122.4	645.0	926.0	43.4	4.0
Unit17	0031 619	0.20	0.45	471.4	2.2	317.2	455.2	14.1	3.0
Unit17	0031 680	0.20	0.35	415.9	2.0	280.9	389.3	24.7	5.9
Unit17	0031 688	0.15	0.40	1208.4	166.7	730.9	995.9	45.7	3.8
Unit17	0031 810	0.15	0.45	1126.3	135.4	686.2	952.1	38.8	3.4
Unit17	0032 173	0.20	0.45	628.1	13.3	401.9	576.4	38.4	6.1
Unit17	0032 209	0.15	0.45	1122.2	133.6	681.3	945.2	43.4	3.9
Unit17	0032 507	0.20	0.45	759.6	29.5	477.1	684.6	45.4	6.0
Unit17	0033 384	0.20	0.40	543.2	3.1	372.3	525.1	14.9	2.7
Unit18	0033 224	0.30	0.25	362.1	0.0	244.3	350.4	11.7	3.2
Unit18	0033 283	0.30	0.25	404.1	0.3	265.7	381.1	22.7	5.6
Unit18	0033 526	0.30	0.20	387.5	0.6	263.5	371.5	15.4	4.0
Unit18	0033 613	0.30	0.25	523.0	4.6	344.0	493.3	25.1	4.8
Unit18	0033 680	0.30	0.25	426.2	0.4	287.8	412.8	13.0	3.1
Unit18	0033 774	0.30	0.20	434.9	0.3	298.1	420.3	14.2	3.3
Unit18	0034 047	0.30	0.35	833.3	49.5	504.3	747.5	36.3	4.4
Unit18	0034 052	0.30	0.25	522.9	3.4	355.8	510.2	9.2	1.8
Unit18	0034 231	0.25	0.35	728.5	25.0	462.7	663.3	40.2	5.5
Unit18	0034 405	0.30	0.40	619.0	13.5	384.4	578.8	26.7	4.3
Unit18	0034 581	0.30	0.40	649.1	20.2	397.0	597.7	31.3	4.8
Unit18	0034 659	0.30	0.30	818.4	44.7	496.8	724.6	49.1	6.0
Unit18	0034 706	0.30	0.30	447.3	1.6	297.5	433.9	11.8	2.6
Unit18	0034 762	0.30	0.30	481.6	1.8	315.5	460.1	19.7	4.1
Unit18	0035 148	0.30	0.30	667.4	16.2	435.0	634.1	17.1	2.6
Unit18	0035 334	0.30	0.35	404.7	0.2	257.0	380.9	23.6	5.8

Appendix XVII Recharge rates for the quaternary catchment in the outcrop of the TMG

Unit No	Quaternary Catchment	Min ($mm \cdot a^{-1}$)	Max ($mm \cdot a^{-1}$)	Mean ($mm \cdot a^{-1}$)	Unit No	Quaternary Catchment	Min ($mm \cdot a^{-1}$)	Max ($mm \cdot a^{-1}$)	Mean ($mm \cdot a^{-1}$)
1	E10H	15	25	20	4	H10K	15	30	22.5
1	E10J	5	15	10	4	H10L	15	20	17.5
1	E10K	0.5	10	5.3	5	G10A	55	130	92.5
1	E21K	20	25	22.5	5	G10B	25	45	35
1	E24A	15	25	20	5	G10C	50	75	62.5
1	E24B	10	15	12.5	5	G22F	20	85	52.5
1	E24J	0.5	10	5.3	6	G22A	45	70	57.5
1	E24K	0.5	5	2.8	6	G22B	35	50	42.5
1	E23L	0.5	20	10.3	6	G22D	40	55	47.5
1	E24M	0.5	10	5.3	7	E10A	15	25	20
1	E32E	0.5	5	2.8	7	E10B	20	30	25
1	E33F	0.5	5	2.8	7	E10C	25	40	32.5
1	E33G	0.5	5	2.8	7	E10D	30	40	35
1	E40C	0.5	5	2.8	7	E21A	15	20	17.5
1	E40D	0.5	5	2.8	7	E21D	15	25	20
2	E10B	20	30	25	7	E22C	10	20	15
2	E10C	25	35	30	7	G10E	25	40	32.5
2	E10D	30	40	35	7	G10G	20	30	25
2	E10E	30	45	37.5	7	G10H	25	40	32.5
2	E10F	25	45	35	7	H10A	10	20	15
2	E10G	15	35	25	7	H10B	20	70	45
2	E10H	15	20	17.5	7	H10C	15	80	47.5
2	E10J	5	25	15	7	H10D	40	75	57.5
2	E10K	0.5	10	5.3	7	H10F	50	55	52.5
2	E21D	15	25	20	7	H20C	10	25	17.5
2	E21F	20	25	22.5	7	H20D	15	30	22.5
2	E21G	25	35	30	7	H20E	15	40	27.5
2	E21H	20	35	27.5	8	G22J	75	90	82.5
2	E21J	20	30	25	8	G22K	75	95	85
2	E21K	20	30	25	8	G40A	75	100	87.5
2	G30C	20	50	35	8	G40B	85	100	92.5
2	G30E	0.5	30	15.3	8	G40C	30	85	57.5
2	G30F	5	35	20	8	G40D	45	100	72.5
2	G30G	5	20	12.5	8	G40E	40	65	52.5
2	G30H	0.5	10	5.25	8	H10K	10	25	17.5
3	G10H	50	60	55	8	H10L	10	20	15
3	G10K	50	95	72.5	8	H40D	0.5	35	17.75
3	G30A	35	55	45	8	H40E	10	30	20
3	G30B	55	80	67.5	8	H40F	0.5	10	5.25
3	G30D	25	95	60	8	H40G	5	15	10
4	G10C	25	35	30	8	H60A	65	95	80
4	G10E	15	30	22.5	8	H60B	35	50	42.5
4	G10F	15	25	20	8	H60C	15	70	42.5
4	G10J	20	25	22.5	8	H60D	25	70	47.5
4	H10E	25	40	32.5	8	H60E	10	25	17.5
4	H10F	20	45	32.5	9	H20A	5	10	7.5
4	H10G	35	50	42.5	9	H20B	5	15	10
4	H10J	20	40	30	9	H20F	5	20	12.5

Appendix XVII Recharge rates for the quaternary catchment in the outcrop of the TMG (continued)

Unit No	Quaternary Catchment	Min ($mm \cdot a^{-1}$)	Max ($mm \cdot a^{-1}$)	Mean ($mm \cdot a^{-1}$)	Unit No	Quaternary Catchment	Min ($mm \cdot a^{-1}$)	Max ($mm \cdot a^{-1}$)	Mean ($mm \cdot a^{-1}$)
9	H20G	10	20	15	11	G40L	30	50	40
9	H30A	0.5	10	5.3	11	G40M	20	40	30
9	H30B	0.5	10	5.3	11	G50A	25	30	27.5
9	H30C	0.5	10	5.3	11	G50B	20	30	25
9	H30D	10	15	12.5	11	G50C	30	40	35
9	H40A	5	10	7.5	11	G50D	15	45	30
9	H40B	5	10	7.5	11	G50E	35	45	40
9	H70C	5	15	10	11	G60G	20	40	30
9	H70D	5	20	12.5	12	G50K	5	10	7.5
9	H70E	5	15	10	12	H70H	10	20	15
9	H80A	20	50	35	12	H70K	5	10	7.5
9	H80B	15	30	22.5	12	H80F	15	20	17.5
9	H90A	25	35	30	12	J40E	30	40	35
9	H90B	35	50	42.5	13	J11H	0.5	10	5.3
9	J12A	5	15	10	13	J11J	0.5	10	5.3
9	J12B	0.5	10	5.3	13	J12F	0.5	5	2.8
9	J12D	0.5	10	5.3	13	J12G	0.5	10	5.3
9	J12F	0.5	5	2.8	13	J23E	5	15	10
9	J12J	0.5	5	2.8	13	J23F	5	10	7.5
9	J12K	0.5	10	2.8	13	J23J	0.5	5	2.75
9	L12L	5	25	15	13	J24F	0.5	5	2.8
9	J12M	20	45	32.5	13	J25A	0.5	10	5.3
9	J13A	5	15	10	13	J25B	0.5	10	5.3
9	J13B	20	30	25	13	J31A	5	10	7.5
9	J13C	20	30	25	13	J31C	0.5	10	5.3
9	J40A	20	25	22.5	13	J32E	0.5	10	5.3
9	J40B	25	35	30	13	J33C	10	15	12.5
9	J40C	25	40	32.5	13	J33D	5	15	10
10	H40G	0.5	15	7.8	13	J35A	5	15	10
10	H40J	5	10	7.5	13	L30D	0.5	10	5.3
10	H40K	0.5	15	7.8	13	L32A	0.5	10	5.3
10	H50A	0.5	15	7.8	13	L50A	0.5	5	2.8
10	H50B	5	10	7.5	14	J11J	0.5	5	2.8
10	H60E	5	25	15	14	J11K	0.5	5	2.8
10	H60F	0.5	10	5.3	14	J12G	0.5	5	2.8
10	H60H	0.5	5	2.8	14	J12H	0.5	5	2.8
10	H60J	0.5	5	2.8	14	J13A	0.5	5	2.8
10	H60K	5	10	7.5	14	J13B	0.5	5	2.8
10	H60L	5	10	7.5	14	J13C	0.5	10	5.3
10	H70H	15	20	17.5	14	J25A	0.5	5	2.8
11	G40B	85	100	92.5	14	J25B	0.5	5	2.8
11	G40D	45	95	70	14	J25C	0.5	5	2.8
11	G40E	35	65	50	14	J25E	0.5	10	5.3
11	G40F	35	65	50	14	J31A	5	10	7.5
11	G40G	35	70	52.5	14	J31B	5	10	7.5
11	G40H	40	60	50	14	J31D	0.5	5	2.8
11	G40J	35	50	42.5	14	J33A	0.5	25	12.8
11	G40K	20	45	32.5	14	J33B	5	20	12.5

Appendix XVII Recharge rates for the quaternary catchment in the outcrop of the TMG

(continued)

Unit No	Quaternary Catchment	Min ($mm \cdot a^{-1}$)	Max ($mm \cdot a^{-1}$)	Mean ($mm \cdot a^{-1}$)	Unit No	Quaternary Catchment	Min ($mm \cdot a^{-1}$)	Max ($mm \cdot a^{-1}$)	Mean ($mm \cdot a^{-1}$)
14	J33E	10	15	12.5	17	L82B	15	30	22.5
14	J34A	0.5	15	7.8	17	L82C	15	30	22.5
14	J34B	0.5	30	15.3	17	L82D	15	35	25
14	J34C	15	40	27.5	17	L82E	15	30	22.5
14	J34D	5	35	20	17	L82F	10	20	15
14	J34E	0.5	15	7.8	17	L82G	10	25	17.5
14	J34F	10	45	27.5	17	L82H	5	15	10
14	J35B	5	40	22.5	17	L82J	5	25	15
14	J35C	5	30	17.5	17	L90A	10	25	17.5
14	J35E	10	20	15	17	L90B	10	15	12.5
14	J35F	10	20	15	17	K50A	25	40	32.5
14	J40A	20	30	25	17	K60A	20	30	25
14	J40B	25	35	30	17	K60B	20	35	27.5
15	K10A	40	60	50	17	K60C	25	45	35
15	K10B	40	50	45	17	K60D	25	40	32.5
15	K10C	30	40	35	17	K60E	35	45	40
15	K10E	15	35	25	17	K70A	35	45	40
15	K20A	5	25	15	17	K70B	25	45	35
15	K30A	5	35	20	17	K80A	20	35	27.5
15	K30B	35	70	52.5	17	K80B	30	45	37.5
15	K30C	20	65	42.5	17	K80C	35	55	45
15	K30D	20	35	27.5	17	K80D	40	80	60
15	K40A	25	40	32.5	17	K80E	60	85	72.5
15	K40B	30	40	35	17	K80F	65	80	72.5
15	K40C	35	45	40	17	K90A	25	45	35
15	K40E	30	70	50	17	K90B	25	80	52.5
15	K50A	30	45	37.5	17	K90C	15	45	30
15	K50B	50	75	62.5	17	K90D	35	70	52.5
15	K60A	30	35	32.5	17	K90E	55	65	60
15	K60E	35	45	40	17	K90F	15	30	22.5
15	K60F	35	50	42.5	17	K90G	10	20	15
16	L50A	5	10	7.5	18	L70C	0.5	10	5.3
16	L70A	0.5	10	5.25	18	L70D	10	15	12.5
16	L70C	0.5	5	2.8	18	L70F	5	30	17.5
16	L70G	5	10	7.5	18	L70G	0.5	30	15.3
16	L81A	5	15	10	18	L82H	5	15	10
16	L81B	5	15	10	18	L90A	25	30	27.5
16	L81C	0.5	15	7.8	18	L90B	30	35	32.5
16	L81D	0.5	15	7.8	18	L90C	15	30	22.5
16	L82A	10	15	12.5	18	M10A	25	35	30
16	L82B	10	25	17.5	18	M10B	15	35	25
16	L82C	10	20	15	18	M10C	10	25	17.5
16	L82D	10	20	15	18	M10D	10	20	15
16	L82E	10	20	15	18	M20A	15	20	17.5
16	L82F	5	20	12.5	18	M20B	15	25	20
16	L82G	5	15	10	18	M30A	20	30	25
16	L82H	5	10	7.5	18	N40B	25	35	30
17	L82A	10	25	17.5	18	N40E	25	35	30